Increasing the capacity of Australian raw sugar factory milling units

Thesis submitted by

Geoffrey Alan KENT

BE (Mech Hons) *UQ*

MIEAust CPEng RPEQ

in September 2003

for the degree of Doctor of Philosophy

in the School of Engineering (Mechanical Engineering)

James Cook University

Statement of access

I, the undersigned, author of this work, understand that James Cook University will make this thesis available for use within the University Library and, via the Australian Digital Theses network, for use elsewhere.

I understand that, as an unpublished work, a thesis has significant protection under the Copyright Act and;

I wish the following restrictions to be placed on this work:

- I wish this work to be embargoed until 30 April 2006.
- I wish access to this work to be restricted until 30 April 2009. During this time, the thesis may be made available for use within the University Library but not for use elsewhere.

Signature Date

Electronic copy

I, the undersigned, the author of this work, declare that the electronic copy of this thesis provided to the James Cook University Library is an accurate copy of the print thesis submitted, within the limits of the technology available.

Signature

Date

Statement of sources

DECLARATION

I declare that this thesis is my own work and has not been submitted in any form for another degree or diploma at any university or other institution of tertiary education. Information derived from the published or unpublished work of others has been acknowledged in the text and a list of references is given.

Signature Date

Acknowledgements

Firstly, the author wishes to thank the late Dr Rod Murry and Dr Vic Mason and Dr Ray Scott, both formerly of the Sugar Research Institute, for their encouragement to commence this investigation. The author also thanks Dr Terry Dixon and Dr Graeme Bullock of the Sugar Research Institute for their ongoing support throughout the investigation.

Secondly, Mr Rod Cullen, formerly of Bundaberg Sugar Limited, is acknowledged for suggesting the topic for this investigation.

Thirdly, the author sincerely thanks the Sugar Research and Development Corporation and the member mills of the Sugar Research Institute; in particular, CSR Limited, Mackay Sugar Co-operative Association Limited, Mulgrave Central Mill Company Limited, Tully Sugar Limited, Proserpine Co-operative Sugar Milling Association Limited, Maryborough Sugar Factory Limited, NSW Sugar Milling Co-operative Limited, Mossman Central Mill Company Limited and Isis Central Mill Company Limited; for their financial support of this project.

Fourthly, the author wishes to thank those who assisted in the experimental investigations that formed part of this investigation. Mr Neil McKenzie of the Sugar Research Institute, Dr Con Doolan, Mrs Linda Dixon-Kelso and Miss Lyn Forsell, formerly of the Sugar Research Institute and the staff of Mulgrave, South Johnstone, Invicta, Inkerman, Plane Creek and Isis factories are acknowledged for their assistance in the factory effectiveness survey. Mr Neil McKenzie, Mr John Williams and the late Mr Allan Connor of the Sugar Research Institute are acknowledged for their assistance in the permeability investigation. Mr Neil McKenzie and Mr John Williams of the Sugar Research Institute, Miss Kristine Strohfeldt and Mr Andrew Zammit formerly of the Sugar Research Institute and Mr Dave Kauppila and Mr Arasu Kannapiran of James

Cook University are acknowledged for their assistance with the two-roll mill experiment. Mr Neil McKenzie of the Sugar Research Institute, Miss Letitia Langens formerly of the Sugar Research Institute and Mr Kevin Wardrop, Mr Bob Watters, Mr Jeff King Koi and the staff of Mulgrave Central Mill Company Limited for their assistance with the factory mill experiment.

Fifthly, the author thanks his supervisors A/Prof Jeff Loughran of James Cook University and Dr Vic Mason formerly of the Sugar Research Institute, along with Dr Mac Kirby of CSIRO, Dr Floren Plaza and Dr Matt Schembri of the Sugar Research Institute, Dr Chris Downing formerly of the Sugar Research Institute, Dr Clayton Adam formerly of Queensland University of Technology and Mr Tom Davis, Mr John Sawyer and Mr John Li of Worley FEA for the fruitful discussions and advice received throughout this investigation.

Lastly, the author thanks his wife Karen and children Natasha and Christopher for their support and encouragement throughout this long investigation.

Abstract

This thesis reports on an investigation to identify methods to increase the capacity or throughput of the six-roll roller mills used in Australia to extract sugar from sugarcane. The approach taken was to gain an understanding of the factors affecting mill throughput through the application of the computational milling model, developed in recent years at James Cook University. The computational milling model is based on general equations of force equilibrium and continuity and a general description of sugarcane material behaviour.

The development of the throughput model was conducted in stages. Firstly, an experiment was conducted on a laboratory two-roll mill to gain an understanding of the factors affecting throughput on this simple milling geometry. A two-roll computational model was constructed to predict the observed behaviour, accounting for all mechanisms identified from the experimental results. Secondly, a three-roll computational model was constructed which was sufficient to describe the throughput behaviour of the factory six-roll mill. An experiment was conducted on a factory six-roll mill to provide data to validate the model. The three-roll computational model was tested across the range of geometries and operating conditions known to exist in Australian factories and its throughput predictions were tested against throughput measurements.

The three-roll computational model was used to identify the main factors affecting mill throughput and was used to construct a data set across a wide range of parameter values. The data set was used in a multiple regression analysis to develop an empirical model that could readily be used to identify conditions for maximum throughput.

The computational and empirical models developed during this investigation were shown to predict throughput better than existing models. Conditions for maximum

throughput were identified and involved the openings between rolls, the speed of the rolls and the amount of water in the sugarcane material being processed.

As part of the investigation, further development of the computational milling model was undertaken in order to advance the model to a sufficient standard for this investigation. A material parameter was introduced to define the hardening rule for the plastic material model following established soil mechanics methodology. Darcy's law, describing fluid flow through porous media, was shown to adequately describe the flow of water through bagasse for a wide range of fluid velocities. Greater confidence in the measured magnitude of the permeability factor in Darcy's law was gained through improved experimental and parameter estimation procedures. One of the experimental and parameter estimation procedures was found to significantly reduce the time involved in measuring both the hardening rule for the plastic material model and the permeability for Darcy's law.

Contents

Tables

Figures

Symbols

A	Cross-sectional area
A_T	Total cross-sectional area
C_0	Compression ratio
D	Mean roll diameter
D'	Outside roll diameter
D_i	Inside diameter
D_p	Pressure feeder roll mean diameter
D_p'	Pressure feeder roll outside diameter
E	Effectiveness
F	Total frictional force
F	Yield surface
F_F	Tangential force component
F_H	Horizontal force component
F_N	Normal force component
F_V	Vertical force component
F_{b0}	Initial force at bottom of sample
F_c	Cap yield surface
F_s	Shear yield surface
F_{t0}	Initial force at top of sample
G	Plastic potential surface
$\hat{G}$	Shear modulus
G_c	Cap plastic potential surface
G_p	Pressure feeder torque
G_s	Shear plastic potential surface
G_u	Underfeed roll torque
H	Height of a strip of bagasse in the feed chute

H_1	Height of bagasse in the feed chute
H_2	Total height of feed chute
K	Bulk modulus
K_0	Ratio of transverse to axial pressure
L	Roll length
M	Slope of the critical state line
P	Pressure of fluid
P_a	Bagasse feed pressure
P_b	Pressure in bagasse
P_d	Bagasse pressure in feed chute
P_{dH1}	Bagasse pressure in feed chute at height H_1
P_{do}	Bagasse pressure at the feed chute exit
P_{sp}	Hydraulic pressure on pressure feeder drive
P_{su}	Hydraulic pressure on underfeed roll drive
p_t	Intercept of shear surface on p axis
p_t^e	Elastic tensile limit
$P_{v\theta}$	Vertical pressure in bagasse at an angle θ from the nip
Q	Total mass rate
Q_c	Cane rate
Q_{cf}	Cane fibre rate
Q_f	Fibre rate
Q_f^*	Theoretical maximum fibre rate for a pressure feeder
R	Cap eccentricity parameter
S	Roll surface speed (based on mean diameter)
S'	Roll surface speed (based on outside diameter)
S_F	Bagasse feed speed at entry plane
S_p	Top pressure feeder roll surface speed
S_p'	Top pressure feeder surface speed at outside diameter
U	Feed chute position offset
V	Volume
V_0	No-void volume

V_E	Escribed volume
V_g	Volume of solid
V_v	Volume of voids
W	Nip work opening
W_p	Pressure feeder nip work opening
W_s	Nip setting
W_{sp}	Pressure feeder nip setting
W_{su}	Underfeed nip setting
W_{su}^*	Underfeed nip setting for maximum throughput
W_{sua}	Underfeed nip setting relative to setting for maximum throughput
W_{sup}	Setting between underfeed roll and bottom pressure feeder roll
W_u	Underfeed nip work opening
Z	Level of cane preparation
a	Regression constant
b	Regression constant
c_i	Regression constants where i is a positive integer
d	Related to material cohesion
d_g	Roll groove depth
e	Void ratio
e_0	Void ratio at reference volume
f	Fibre fraction
f_c	Fibre fraction in cane
f_d	Fibre content of bagasse in feed chute (accounting for imbibition)
g	Acceleration due to gravity
h	Chute setting
h^*	Theoretical feed chute setting for maximum throughput of pressure feeder rolls
h_d	Feed chute setting
h_{do}	Feed chute exit setting
h_{do}^*	Feed chute exit setting for maximum throughput
h_{doa}	Feed chute exit setting relative to setting for maximum throughput
k	Intrinsic permeability

k_i, $i = 1, 2$	Permeability parameter
l	Length of bagasse mat
m	Mass
n	Porosity
n_R	Number of rolls in a milling train
p	Pressure stress
p_a	Pressure stress at maximum cap height
p_b	Hydrostatic compression yield strength
q	Deviator stress
r_M	Murry's feed speed ratio
t	Time
v_i, $i = x, y$ or z	Velocity component of fluid
w	Material coordinate
x	Cartesian coordinate
y	Cartesian coordinate
α	Contact angle (based on mean diameter)
α'	Contact angle (based on outside diameter)
α_{do}'	Contact angle between feed chute and rolls forming underfeed nip
β	Related to material angle of friction
ε_a	Axial strain component
ε_{ij}, $i, j = x, y$ or z	Strain component
ε_p	Volumetric strain
ε_q	Deviatoric strain
ε^e	Elastic strain
ε^p	Plastic strain
γ	Compaction
γ_α	Compaction of bagasse at entry plane
γ_d	Compaction in feed chute
γ_{do}	Compaction at the feed chute exit
η	Ratio of deviatoric to mean stress components

φ	Angle of nip
κ	Logarithmic bulk modulus
λ	Hardening rule size parameter
λ_1	Hardening rule size parameter
μ	Coefficient of friction
μ'	Ratio of tangential force to normal force
μ_v	Absolute or dynamic viscosity
ν	Poisson's ratio
θ	Angle
ρ	Bulk density
ρ_α	Bulk density at entry plane
ρ_f	Density of fibre
ρ_j	Density of juice
ρ_w	Density of fluid
σ_a	Axial stress component
σ_{ao}	Initial axial stress component
σ_{ij}, $i, j = x, y$ or z	Total stress component
σ'_{ij}, $i, j = x, y$ or z	Effective stress component
σ'_{zz0}	Initial axial effective stress component
ω	Roll angular velocity
ψ	Chute angle
z	Cartesian coordinate
z_0	Initial height

1 Introduction

1.1 Introductory remarks

The continuing decline in the price of sugar has forced continual productivity improvements upon the Australian sugar industry, resulting in an increasing crop size to be processed. To process this crop, factories have had to increase their throughput. The high capital cost of milling units, used to extract sugar from sugarcane, is an impediment to further growth. The work contained in this thesis is aimed at providing the technical knowledge to enable the raw sugar factories to increase the throughput of their existing milling units.

This chapter provides a general overview of the milling process and provides a description of a milling unit and its associated terminology. It describes the motivation for the work reported in this thesis. Finally, this chapter describes the overall layout of the thesis.

1.2 Overview of the milling process and milling equipment

1.2.1 Description of sugarcane

Sugarcane is a perennial grass belonging to family Gramineae tribe Andropogoneae and is classified in the genus Saccharum (Julien, Irvine & Benda 1989). Sorghum is a close relative (Alexander 1973).

Six species of sugarcane exist (Julien, Irvine & Benda 1989). The commercial sugarcanes used to produce raw sugar are complex hybrids of two or more species of Saccharum. The development of new hybrids or varieties is an ongoing activity. Within Australia, there are over 100 varieties approved for sugarcane production (Bureau of Sugar Experiment Stations 2003). Of those varieties, the 10 most widespread varieties constitute approximately 83% of the total crop (Australian Sugar Year Book 2002 c. 2002).

Raw sugar is produced from the stem of the sugarcane. The sugar is stored in parenchyma storage cells that constitute the majority of the stem (Payne 1968). The other major component of the stem consists of fibrovascular bundles that encase the conducting vessels that transport water and food from the roots to the other parts of the plant. A thin rind surrounds the stem. A cross-section of the stem showing the major components is displayed in Figure 1.1.

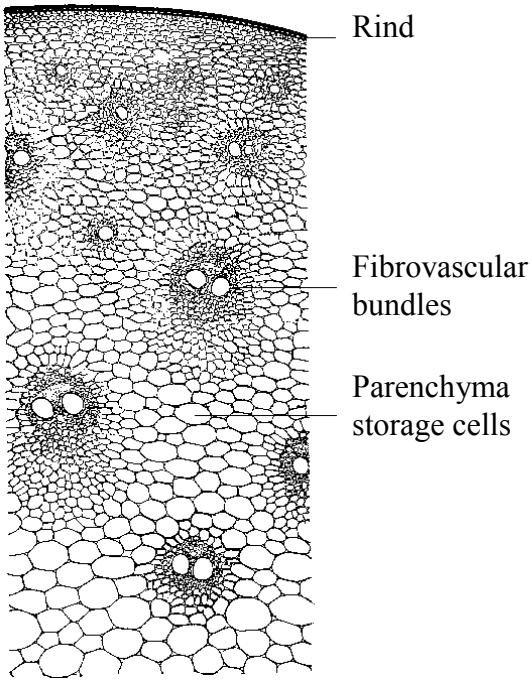

Figure 1.1 Cross-section of a cane stem (after Payne 1968)

Within the Australian sugar industry, the constituents of sugarcane are generally described on a macroscopic level. Sugarcane consists of fibre, brix and water. The relative quantity of each constituent is usually stated as a mass fraction of the total cane.

Fibre is the dry, water-insoluble matter in the cane (Bureau of Sugar Experiment Stations 2001). It typically constitutes about 14% of the cane. The density of the fibre is approximately 1530 kg/m^3 (Pidduck 1955).

The mixture of brix and water constitutes the juice of the sugarcane. Brix refers to the water-soluble solids in the cane and includes the sugar. Technically, brix is the concentration of a solution of pure sucrose in water having the same density as a sample of juice at the same temperature (Bureau of Sugar Experiment Stations 1984). It typically constitutes about 17% of the cane. The density of the juice is a function of the brix fraction of the juice and is approximately 1080 kg/m^3 for a juice with a typical brix fraction of 0.2 (Bureau of Sugar Experiment Stations 2001).

A proportion of the water in the sugarcane, known as *hygroscopic* water, is absorbed into the fibre. Hygroscopic water is generally assumed to amount to 25% of the fibre mass (Bureau of Sugar Experiment Stations 2001).

1.2.2 Description of the milling process

Around the world, there are two major processes used to extract sugar from cane: milling and diffusion. In Australia, almost all sugar is extracted using the milling process. Only three Australian factories use the diffusion process and none of those use it exclusively. Even where diffusers are used, the milling process is required to dewater the bagasse after it leaves the diffuser. Since the milling process is widely used, the milling process is the focus of this work and only the milling process is discussed in this section.

The milling process essentially involves the removal of juice from sugarcane by squeezing the cane between pairs of large cylindrical rolls in a series of milling units

collectively called a milling train. The first milling unit in the milling train is generally identified as #1 mill, the second milling unit is generally identified as #2 mill, and so on. The last milling unit is generally called the final mill. The milling units between the first and final mills are collectively known as the intermediate mills.

Before entering the milling train, the sugarcane is first pulverised by pounding it with hammers rotating at high speed in a hammer mill known as a shredder. The shredder ruptures the cell walls of many of the parenchyma storage cells making the juice in the cane easier to extract. The pulverised material is known as prepared cane. Prepared cane typically consists of 15% fibre, 70% water and 15% brix.

After passing through a pair of rolls and expressing juice, the remaining sugarcane material is known as bagasse. Only the first milling unit in the milling train processes prepared cane. The remaining milling units process bagasse. After being processed by a mill, bagasse typically consists of 30% to 50% of fibre, 45% to 60% of water and a diminishing quantity of brix as subsequent milling units process the bagasse. Although prepared cane and bagasse are defined as different materials, this thesis uses bagasse as a general term to collectively refer to both prepared cane and bagasse.

To aid in the extraction of juice from the much drier bagasse, water or diluted juice is added to the bagasse before it enters the milling unit in a process called imbibition. The water or juice added to the bagasse is called imbibition water or imbibition juice. The common version of the imbibition process, called compound imbibition, is shown in Figure 1.2. Imbibition water is added to the bagasse entering the final milling unit at a rate that is typically 200% to 300% of the rate of fibre passing through the milling train. The juice expressed from the final milling unit is used as imbibition juice for the second last milling unit. The juice from the second last milling unit is then used as imbibition juice for the third last milling unit. This process continues back to the second milling unit. After first passing through a juice screen to remove most of the fibre in the juice, the juice from the first and second milling units, called *mixed juice*, is taken away for processing into sugar. The fibre removed in the juice screen is returned to the milling train, usually before the second milling unit. The bagasse from the final milling unit is used as fuel for the boilers.

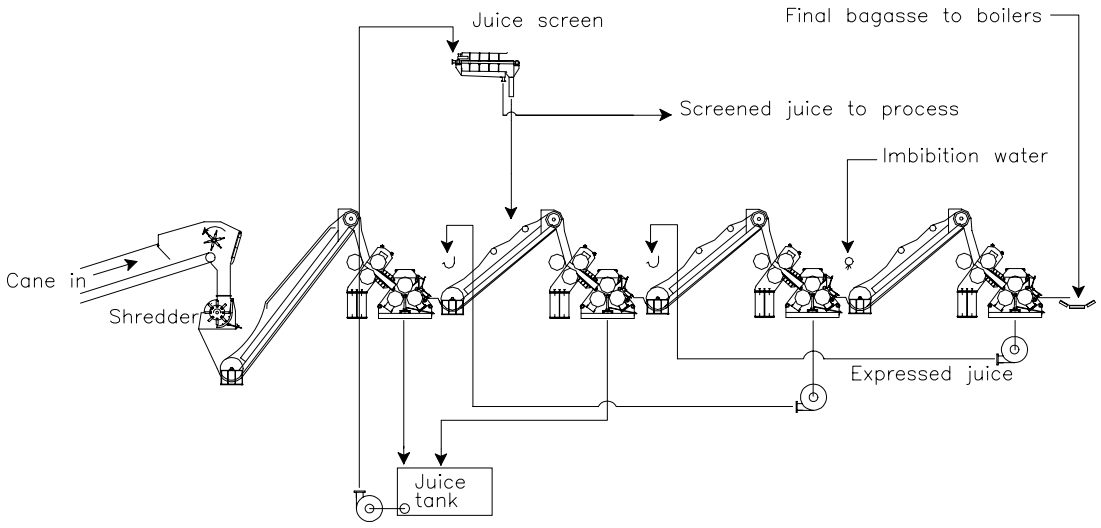

Figure 1.2 Typical layout of a milling train with four milling units (from Neill, McKinnon & Garson 1996)

1.2.3 Description of a milling unit

A typical Australian milling unit is shown in Figure 1.3. There are six rolls arranged so that the prepared cane or bagasse passes through four squeezes or *nips* between the entry and the exit of the milling unit. The six-roll mill is the focus of this thesis.

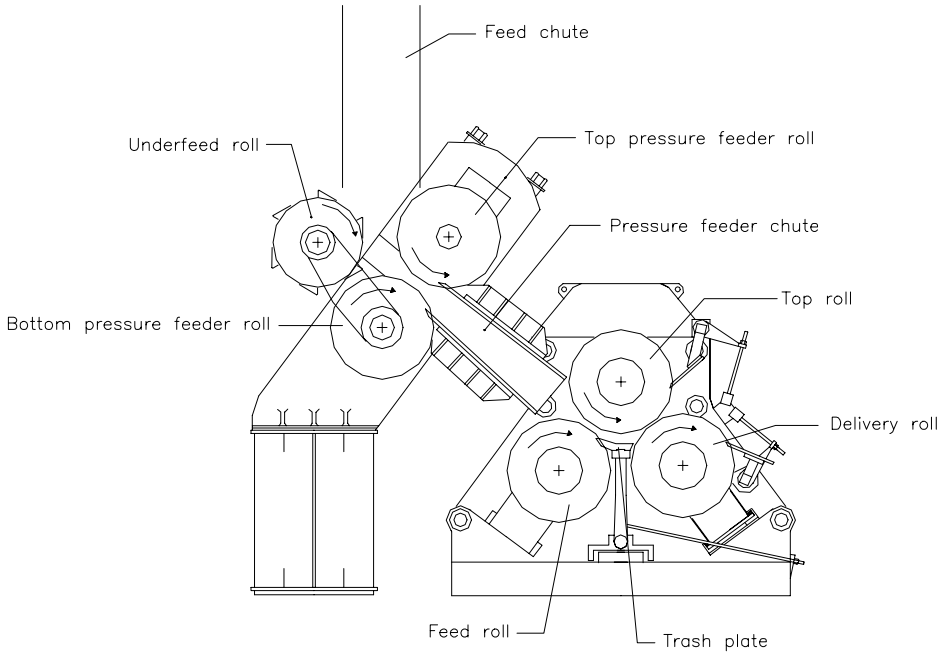

Figure 1.3 Typical layout of a milling unit (from Neill, McKinnon & Garson 1996)

The main crushing part of the milling unit consists of three rolls shown in the bottom right hand side of Figure 1.3. These rolls are named the top roll, the feed roll and the delivery roll and are collectively called the mill rolls. There are two nips in this part of the milling unit known as the *feed nip* and the *delivery nip*. A *trash plate* scrapes the bagasse away from the feed roll and helps to feed the bagasse into the delivery nip.

A *pressure feeder* consists of two rolls known as the top pressure feeder roll and the bottom pressure feeder roll. The pressure feeder feeds bagasse through the *pressure feeder nip* along a *pressure feeder chute* into the main crushing part of the milling unit.

Over 95% of Australian milling units also contain a sixth roll known as the underfeed roll. The underfeed roll forms a nip with the top pressure feeder roll that is known as the *underfeed nip*. Bagasse exiting the underfeed nip is fed into the pressure feeder. Because of the widespread use of underfeed rolls on Australian milling units, the term pressure feeder is often extended to include the underfeed roll.

A vertical or nearly vertical closed feed chute feeds the bagasse into the underfeed nip (or pressure feeder nip if there is no underfeed roll).

Most rolls have circumferential V-shape grooves to assist with gripping the bagasse blanket and the drainage of juice away from the bagasse blanket. About one-fifth of the pressure feeder rolls have large teeth to assist feeding rather than the circumferential grooves. Approximately one-third of underfeed rolls have similar teeth. Another one-third of underfeed rolls have neither grooves nor teeth and are virtually flat.

1.2.4 Definition of milling terms

Introductory remarks

This section describes specific terminology used in the Australian raw sugar factories to describe milling unit geometry and operation.

Crushing rate and fibre rate

The *crushing rate* (Q_c) is the rate at which cane is processed by the milling train based on mass. It is the ultimate measure of throughput.

The cane *fibre rate* (Q_{cf}) is the rate at which the fibre component of the cane is processed by the milling train. For cane with a fibre fraction of f_c, the fibre rate is given by:

$$Q_{cf} = f_c \, Q_c \qquad \textbf{(1.1)}$$

When describing the milling train, it is common to talk in terms of fibre rate rather than crushing rate. Due to the expression of some of the juice fraction in the cane, the total mass rate is quite variable between milling units depending on the amount of juice expressed by the milling units and the amount of imbibition water added to the process. The fibre rate, however, is relatively constant between milling units. Only a small

fraction of the fibre is expressed with the juice and this fraction is ignored in conventional milling theory.

Roll length and diameter

A grooved roll showing length and diameter dimensions is presented in Figure 1.4.

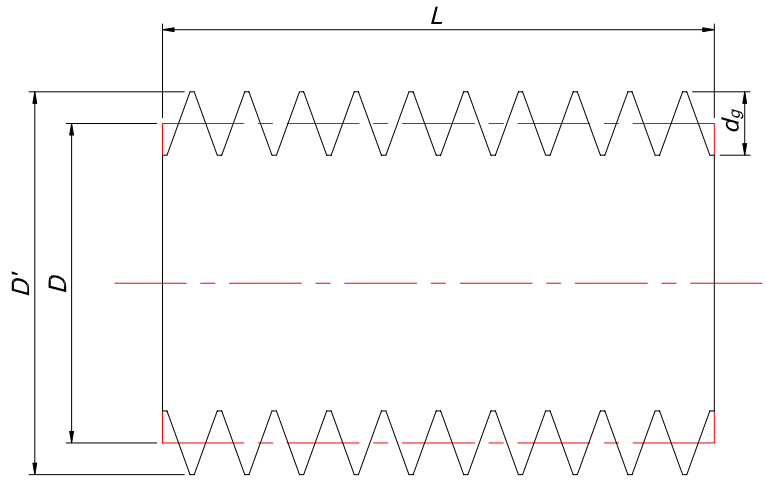

Figure 1.4 Roll dimensions

L is the roll length.

D' is the outside diameter of the roll and is measured to the tips of the grooves.

D is the mean diameter of the roll. The mean diameter represents an average diameter taking into account the variation due to the grooves. It is defined by

$$D = D' - d_g \qquad \textbf{(1.2)}$$

where d_g is the depth of the grooves. For rolls without grooves, the groove depth is zero and both diameter measurements are the same.

Mill settings

The mill settings are the openings between various rolls, chutes and plates.

Figure 1.5 shows the opening between a pair of rolls and the entry or exit to a chute.

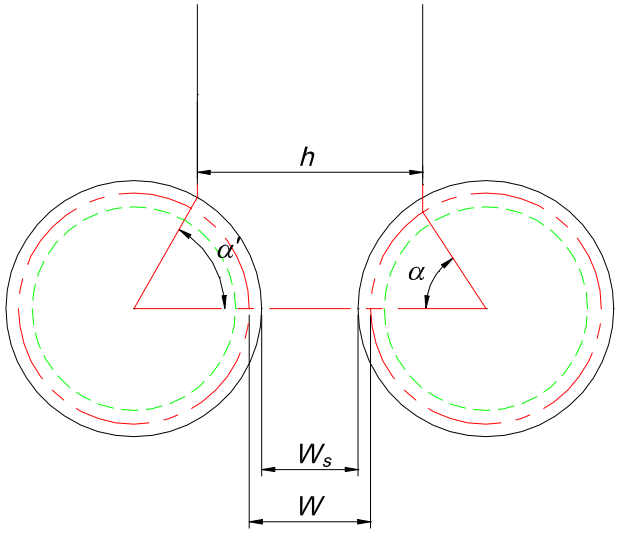

Figure 1.5 Nip and chute settings and contact angles

The nip setting (W_s) is the minimum opening between two rolls forming a nip and is defined relative to the outside diameter.

The work opening (W) is an alternative measure of the opening between two rolls and is defined relative to the mean diameter. The two measures are related by

$$W = W_s + d_g \qquad \textbf{(1.3)}$$

If the two rolls have different groove depths, equation **(1.3)** needs a slight modification.

The chute setting (h) is the minimum opening of a chute and is usually measured at its entry or exit.

Contact angles

The contact angle (α) between a chute and a roll is the angle between a line joining the centres of the two rolls and a line from the centre of a roll to the point where an extension of the chute contacts the roll as shown in Figure 1.5. The point of contact between the chute and the roll is usually taken to be at the mean diameter. On occasions, however, the contact angle is defined at the outside diameter (and denoted α').

The contact angle is given by:

$$\cos\alpha = \frac{D + W - h}{D} \qquad \textbf{(1.4)}$$

If the two rolls have different diameters, the diameter used in equation **(1.4)** is the mean of the two diameters.

Roll surface speed

The surface speed of a roll (S) is usually defined at the mean diameter:

$$S = \frac{\omega\, D}{2} \qquad \textbf{(1.5)}$$

where ω is the angular velocity of the roll.

On occasion, however, the surface speed is defined at the outside diameter (and denoted S').

Escribed volume

The escribed volume (V_E) is the volume passing a given section of the milling unit in unit time.

At the nip between a pair of rolls, the escribed volume is given by:

$$V_E = L\,W\,S \qquad \textbf{(1.6)}$$

At the entry or exit of a chute adjacent to a pair of rolls, it is assumed that the appropriate speed is the component of the roll speed in the direction perpendicular to a line between the centres of the rolls. The escribed volume is given by:

$$V_E = L\,h\,S\cos\alpha \qquad \textbf{(1.7)}$$

For all calculations involving the three mill rolls, escribed volume is defined using the top roll surface speed. For all calculations involving the pressure feeder rolls, escribed volume is defined using the top pressure feeder roll surface speed.

Compaction and other volumetric measures

Compaction (γ) is a measure of the bulk density of fibre at a point in the milling unit. It is the parameter used in the Australian factories as a measure of the volumetric compression of the cane or bagasse. It is defined by

$$\gamma = \frac{Q_{cf}}{V_E} \qquad \textbf{(1.8)}$$

While compaction is the volumetric measure commonly used in industry, there are other measures that feature regularly in the literature.

Compression ratio (C_0) was defined by Bullock (1957) to be:

$$C_0 = \frac{V_0}{V_E} \qquad (1.9)$$

where V_0 is the *no-void* volume. The no-void volume is the sum of the fibre and juice volumes in the cane before expression of juice. Because of its definition relating to the juice volume before expression, compression ratio is only used in association with milling units processing prepared cane. Compression ratio is related to compaction by

$$\gamma = \frac{f_c}{\frac{f_c}{\rho_f} + \frac{1-f_c}{\rho_j}} C_0 \qquad (1.10)$$

where ρ_f is the density of fibre and ρ_j is the density of juice.

Underfeed nips

While the mean diameter and work opening definitions are generally used to describe contact angles and escribed volumes, underfeed nip conditions are described in terms of outside diameter and nip setting. The logic behind this discrepancy is that the light pressures exerted on the bagasse in the underfeed nip are not expected to press the bagasse into the grooves substantially, unlike other nips where bagasse is expected to penetrate close to the bottom of the grooves.

1.3 The need to increase milling unit capacity

1.3.1 The Australian raw sugar industry

Australia produces about 5 Mt of raw sugar annually, about 4% of the world sugar production (Hildebrand 2002; United States Department of Agriculture 2002). Approximately 80% of that sugar is exported, representing about 10% of the total global

free sugar trade. Sales of Australian raw sugar are worth about A$1500 million annually.

All of Australia's sugar is manufactured from sugarcane. Most of Australia's sugarcane is grown along the east cost of Australia from Mossman in North Queensland to Grafton in northern New South Wales. The remainder of the crop is grown in the Ord River district of Western Australia. Thirty factories located within the sugarcane growing areas process or *crush* the crop. Twenty-nine of the factories are on the east coast. The remaining factory is in the Ord River district.

The raw sugar factories operate in the latter part of each year. The part of the year in which the factories operate is known as the *crushing season*. The crushing season for the east cost factories is generally from June or July to November or December. The crushing season for the Ord River factory is from April to December.

1.3.2 Maintaining industry viability

While Australia has long been recognised as a low cost producer of raw sugar, Brazil is now the lowest cost producer (Hildebrand 2002) and largest exporter (United States Department of Agriculture 2002). With 80% of its raw sugar sold on the world market, Australia is dependent on the world sugar price and needs to maintain its sugar production costs below the world sugar price.

Remaining a low cost producer of sugar requires ongoing productivity improvements. In real terms, the price of sugar is reducing at an annual rate of about 2% (Fry 1997). McMaster (2003) stated that overtaking Brazil as the lowest cost producer of raw sugar will require increases in cane productivity and production, an increase in asset utilisation and a reduction in production costs.

1.3.3 The path to processing larger crops

The task of processing a larger crop and reducing production costs can most readily be achieved by processing the larger crop through the same equipment to minimise capital expenditure. While there is some scope for processing the larger crop by increasing the length of the crushing season, any substantial increase in crop size requires an increase in crushing rate.

This thesis focuses on the task of achieving higher crushing rates through the milling train: one of the two highest capital cost factory stations.

1.3.4 Increasing milling unit capacity

The desire to increase milling unit capacity to accept higher crushing rates is not new. The throughput of the original three-roll milling units was increased by the introduction of the pressure feeder (Scriven 1941), the underfeed roll and the closed vertical feed chute (Donnelly 1958). Many other devices have also been used at times with less success (Murry & Shann 1969). The net result of milling unit development over much of the 20th century is that the three-roll mill was converted into a six-roll mill, and the capacity of the mill was more than doubled in the process.

The need to minimise capital and maintenance costs means it is unlikely that the industry will accept further add-ons (more rolls or moving parts) as the mechanism for achieving higher mill throughput. Consequently, understanding the milling process better and using that knowledge to set up and control milling units to achieve higher throughput is considered the means by which higher throughput will be achieved.

1.4 Overview of the thesis

The overall objective of this study was to identify the means by which the conventional six-roll Australian milling unit can achieve a higher throughput. The approach taken

was to gain an understanding of the throughput aspects of the milling process through the development of mathematical models and then to use the models to identify avenues to achieve higher throughput.

Chapter 2 reviews the various models that have been used to predict mill throughput in both sugarcane and other industrial applications. It identifies that the model currently used by the Australian sugarcane factories is the best throughput model currently available for the purpose.

Chapter 3 shows that the state-of-the-art model does not predict observed differences in throughput behaviour well. Model predictions are compared to throughput measurements made in Australian sugarcane factories and found to be deficient. The need for an improved model is identified.

Chapter 4 presents the underlying theory behind an improved throughput model. Unlike the existing theory that is essentially a geometric model, the new model is based on general equations of force equilibrium and continuity and a general description of bagasse material behaviour. Chapter 5 describes the processes used to quantify the material parameters required by the model.

Chapters 6, 7 and 8 compare new model results against experimental data and show that the new model is capable of reproducing all identified experimental trends. In chapter 6, an experiment carried out in a two-roll experimental mill at low pressures without juice expression is studied and the results are used to refine the requirements for the new model. Hypotheses are presented for the mechanisms causing the observed behaviour and those hypotheses are tested through the use of the developed model. Chapter 7 studies an experiment at similar conditions but with juice expression. In chapter 8, a three-roll experimental pressure feeder and the factory six-roll mill are studied. The experimental results are compared to model results and similar behaviour is observed.

The new model is explored in chapters 9 and 10. In chapter 9, the model is compared against the best available model and its usefulness in predicting throughput is explored.

The model is used to develop a simple empirical model that will replace the existing best available model for everyday use. In chapter 10, hypotheses for the observed behaviour in the factory milling unit are presented. Opportunities for achieving increases in milling unit capacity are discussed and the avenues are explored in order to gain greater understanding of the underlying mechanisms.

1.5 Concluding remarks

To maintain its competitiveness in the world market, Australia needs to increase its cane productivity and production and reduce its production costs. This task requires processing higher rates through existing plant to avoid excessive capital costs.

One of the areas of the factory where capital costs are highest is the milling train. If methods could be devised to substantially increase the capacity of existing milling units, increases in factory capacity will become more attractive.

This study focuses on the development of a satisfactory model of milling unit throughput and its subsequent use to predict avenues for increasing the throughput of existing milling units. Laboratory and factory experimentation, followed by modelling of the experimental conditions, are used to gain understanding of the underlying mechanisms affecting milling unit throughput. The developed models are shown to capture the main influences on milling unit throughput and to provide a substantial contribution to knowledge in understanding mill behaviour.

2 Mill throughput literature review

2.1 Introductory remarks

This chapter reviews the throughput models that have been developed for sugarcane milling units and for roller mills used in other industries. The model currently used in the Australian sugar factories is shown to be the most advanced model available for the prediction of throughput in six-roll mills. Previous experimental investigations into factors affecting milling unit throughput are also identified but are reviewed in detail in later chapters. Finally, the milling computational model, a recent development that describes the milling process in terms of more fundamental material behaviour, is introduced. The fundamental nature of the milling computational model provides the potential for a considerably enhanced throughput model.

2.2 Review of sugarcane milling unit throughput research

2.2.1 Introductory remarks

The sugar industry has had an interest in defining and expanding the capacity of its milling units for over a century (Alonso 1949 refers to work by E. Pimienta in 1881 to define milling unit capacity). The models that have been developed broadly fit into three classes:

1. Empirical models that provide information for the design of milling trains,
2. Simple two-roll models that provide some understanding about milling behaviour,
3. Extensions to the two-roll models that cater for more complex milling geometries.

The throughput or capacity models are generally called *feeding* models since it is the process of feeding the bagasse into the mill that largely determines its throughput.

2.2.2 Empirical models

Empirical models were developed by many industry technologists to define milling unit capacity. Perk (1957), Mittal (1969) and Chauhan (1988) reviewed many of these models. The approach taken to develop these models was to fit an equation to historical crushing rate data from many factories. The following factors were identified as having a considerable influence on milling train capacity:

- roll length,
- roll diameter,
- roll surface condition (groove profile and surface roughness),
- number of milling units, compressions or rolls,
- roll speed,
- cane fibre content,
- cane preparation.

For example, the model of Hugot (1986) assumes:

$$Q_{cf} \propto \sqrt{n_R}\ L\ D\ S \qquad \textbf{(2.1)}$$

where n_R is the number of rolls in the milling train, L is the roll length, D is the roll diameter and S is the roll surface speed. Hugot's model also adjusts the fibre rate to

account for cane preparation and the coefficient of friction between the cane and the roll surface.

Many other factors are understood to influence capacity but are not explicitly included in any of the empirical models. The Mackay Institute of Milling Engineers (1937) presented what is arguably the most well known discussion of these factors.

While most of the factors in the list above relate to the throughput of an individual milling unit, the number of milling units, compressions or rolls is included to account for the requirement of a milling train to achieve satisfactory sugar extraction performance. There is a belief within some parts of the sugar industry that the extraction performance of a milling train reduces as crushing rate increases and that longer milling trains, either with more milling units or more rolls per milling unit, can make up for that reduction. This belief is not necessarily correct. Kent, McKenzie and Downing (2000) demonstrated in a controlled factory experiment that crushing rate could be varied by over 30% without significant change in extraction provided delivery nip compactions were maintained. Milling train extraction models developed by Murry and Russell (1969) and by Kent, McKenzie and Downing based on factory extraction data do not explicitly consider crushing rate as a factor affecting extraction. The Australian industry grew considerably in crushing rate in the 1960s and 1970s while simultaneously improving extraction.

The empirical models are useful for the purpose of milling train design. Provided a designer is content to construct a new milling train that will perform similarly to existing milling trains, the empirical models will provide useful information. However, the models provide little information to assist in the task of improving the capacity of a milling unit.

2.2.3 The two-roll mill

The two-roll mill is the simplest roller mill and is, consequently, the ideal milling unit on which to build a capacity theory.

Murry (1960b) is understood to have first developed a theory to calculate the crushing rate for a two-roll cane mill. His theory assumes that there is no slip between the cane blanket and the roll surface and that the average speed of the cane blanket is the speed of the cane blanket at the roll surface. This second assumption implies there is no internal shearing within the cane blanket causing a non-constant velocity profile. The assumptions imply that the average speed of the cane blanket (S_F) at the *entry plane* (plane of first contact with the rolls) is $S \cos \alpha$ (Figure 2.1). Using these assumptions, the volume rate of cane passing the entry plane is equal to the escribed volume (V_E) given in equation **(1.7)**:

$$V_E = L\, h\, S \cos\alpha \qquad \textbf{(2.2)}$$

where h is the chute setting and α is the contact angle.

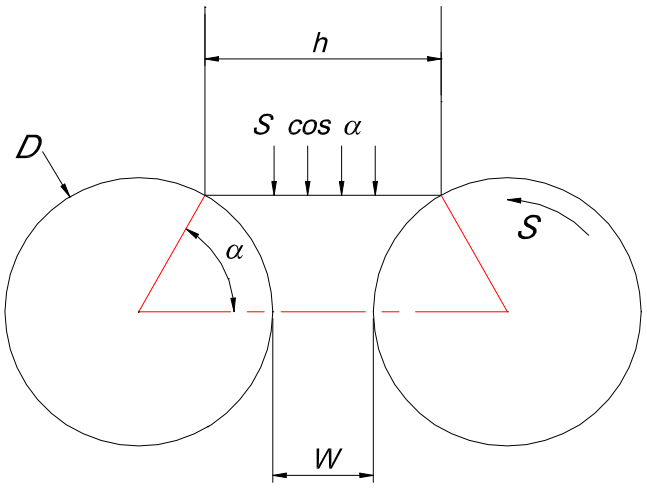

Figure 2.1 Two-roll mill geometry

Rearranging equation **(1.4)** to eliminate h from equation **(2.2)**,

$$V_E = L\, D\, S \left(1 + \frac{W}{D} - \cos\alpha\right)\cos\alpha \qquad \textbf{(2.3)}$$

where W is the work opening.

If the bulk density of the cane at the entry plane is ρ_α, the crushing rate (mass flow rate at the entry plane, Q, and hence through the mill) is:

$$Q = \rho_\alpha \; L \; D \; S \left(1 + \frac{W}{D} - \cos\alpha \right) \cos\alpha \qquad \textbf{(2.4)}$$

By differentiating equation **(2.4)** with respect to cos α, the contact angle resulting in the maximum crushing rate can be identified:

$$\cos\alpha = \frac{1 + \frac{W}{D}}{2} \qquad \textbf{(2.5)}$$

The chute exit setting corresponding to this optimum contact angle can be found from equation **(1.4)**:

$$h = \frac{W + D}{2} \qquad \textbf{(2.6)}$$

While crushing rate is a parameter of great significance to the performance of a milling train, fibre rate (Q_f) is generally more relevant (section 1.2.4). To convert equation **(2.4)** to a fibre rate equation, a relationship is required between bulk density of bagasse (ρ) and bulk density of only the fibre component of bagasse (compaction, γ):

$$\gamma = f \; \rho \qquad \textbf{(2.7)}$$

where f is the fibre content.

Substituting equations **(1.1)** and **(2.7)** into equation **(2.4)**, the fibre rate for a two-roll mill, based on Murry's assumptions as discussed above, is:

$$Q_f = \gamma_\alpha \, L \, D \, S \left(1 + \frac{W}{D} - \cos\alpha \right) \cos\alpha \qquad \textbf{(2.8)}$$

where γ_α is the compaction at the entry plane.

Since Murry's entire theory is based on the assumption that $S_F = S \cos \alpha$, the ratio $\frac{S_F}{S\cos\alpha}$ is a logical measure of the validity of the assumption. This ratio is called *Murry's feed speed ratio* (r_M) throughout this thesis.

Solomon (1967) carried out the only known experiments to investigate Murry's theory. Solomon carried out four independent experiments on a small-scale two-roll mill. He concluded that $S_F = S \cos \alpha$ was not an adequate model for feed speed. His experiments are discussed in detail in section 7.2.

If, as Solomon concluded, Murry's theory does not adequately describe milling practice, one or both of Murry's two assumptions must be invalid: either there is slip between the cane blanket and the roll surface or there must be some internal shear in the cane blanket so that the bagasse speed in the feed direction through the depth of the blanket is not constant. No attempt has been made to modify Murry's theory to address either of these alternatives. However, the conditions for slip between the cane blanket and the roll surface have been examined in some detail.

The University of Queensland and the Sugar Research Institute devoted considerable resources to the development of a theory known as the *frictional theory of mill feeding*. This theory did not estimate mill throughput. Instead, it determined whether it was likely that cane or bagasse would feed into a mill at all by analysing the force system that the mill imposed on the cane or bagasse. Figure 2.2 shows the forces acting on a strip of bagasse at an angle θ from the nip. Bullock (1957) was first to examine this force system.

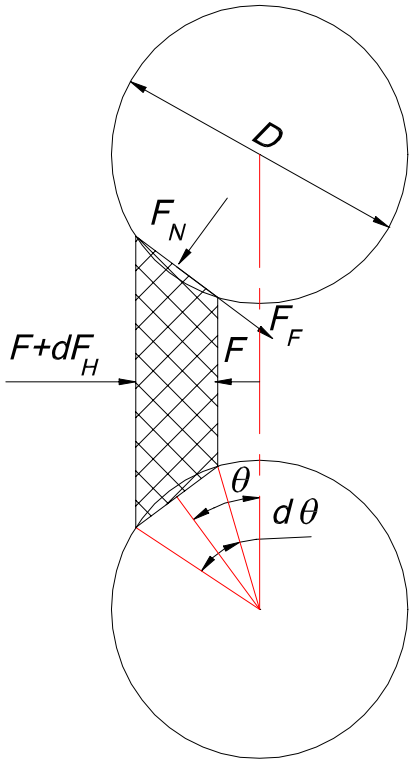

Figure 2.2 Forces acting on a strip of bagasse in a two-roll mill

Equilibrium of forces in the horizontal direction gives:

$$dF_H = 2\left(F_N \sin\theta - F_F \cos\theta\right) \qquad \textbf{(2.9)}$$

where dF_H is the component of a feed force acting on the strip of bagasse, F_N is the normal force generated by the roll in compressing the strip and F_F is the frictional force acting on the strip to feed it into the nip.

If the ratio of frictional force to normal force is μ', then

$$dF_H = 2\,F_N \cos\theta\left(\tan\theta - \mu'\right) \qquad \textbf{(2.10)}$$

Equation **(2.10)** shows that, for self feeding (no feed force),

$$\mu' = \tan\theta \qquad \textbf{(2.11)}$$

Since the highest value for μ' is the coefficient of friction, μ, the equation also defines the largest possible contact angle for which cane will feed without the application of a feeding force. This contact angle is known as the angle of nip, φ. Substituting the coefficient of friction and the angle of nip into equation **(2.11)**,

$$\tan\varphi = \mu \qquad \textbf{(2.12)}$$

This equation is known as the *angle of nip* theory. It was originally developed for stone-crushing mills and was applied to cane mills by Jenkins (1953).

Equation **(2.10)** also shows that the application of a feeding force allows the contact angle to exceed the angle of nip.

To solve equation **(2.10)**, Bullock (1957) found it convenient to convert the normal force, F_N into a vertical force, F_V. A relationship between vertical force and the vertical displacement of the strip of bagasse was available from uniaxial compression tests (of the type described in section 5.2). To relate F_N to F_V, equilibrium of forces in the vertical direction in Figure 2.2 was examined:

$$F_N = \frac{F_V}{\cos\theta\,(1+\mu'\tan\theta)} \qquad \textbf{(2.13)}$$

Substituting equation **(2.13)** into equation **(2.10)**:

$$dF_H = 2\,\frac{\tan\theta - \mu'}{1+\mu'\tan\theta}\,F_V \qquad \textbf{(2.14)}$$

Bullock (1957) did not state this equation correctly. He corrected his error in Bullock (1958) and his theory was fully explained by Murry (1960b).

Rather than state the feed force equation in terms of the vertical force as in equation **(2.14)**, Bullock stated the equation in terms of the vertical feed pressure, $P_{v\theta}$, where $F_v = \frac{1}{2} P_{v\theta} \; L \; D \cos\theta \; d\theta$. Consequently, equation **(2.14)** was restated as:

$$dF_H = L \; D \; P_{v\theta} \frac{\tan\theta - \mu'}{1 + \mu' \tan\theta} \cos\theta \; d\theta \qquad \textbf{(2.15)}$$

Since no feeding force is required to feed the mill up to an angle equal to the angle of nip, the feed force is only required from the angle of nip to the contact angle. The minimum feed force required is calculated by substituting the coefficient of friction into equation **(2.15)** and integrating from the angle of nip to the contact angle.

The frictional theory highlights the importance of the coefficient of friction between the cane blanket and the roll surface. There was considerable effort to determine the coefficient of friction and identify the factors that affect its value. Bullock and Murry (1957) and Cullen (1965) carried out the most comprehensive studies and found that the coefficient of friction decreased with increasing normal pressure, increasing rubbing speed and coarser preparation.

While the frictional theory gives an indication that there are conditions that will cause slip between the cane blanket and the roll surface and identifies factors that will affect the feeding of a mill, it does not link the frictional behaviour to feed speed. This fact is seen as a significant shortcoming in the frictional theory.

2.2.4 Extending the two-roll mill theory to more complex milling geometry

Murry's theory for the two-roll mill, described in section 2.2.3 has been applied to mills with three or more rolls (Sugar Research Institute 1957; Russell 1968; de Boer 1972; Júnior & Delfini 1988). The approach taken has been to apply the theory to the first pair of rolls in the milling unit.

Jenkins and Murry (1981) provided the only known experimental results that could be used to evaluate Murry's theory on milling units with more than two rolls. Jenkins and Murry experimented with a small-scale pressure feeder with an underfeed roll. They aimed to identify underfeed roll arrangements that would maximise throughput. Jenkins and Murry carried out two series of tests. These experiments are reviewed in detail in section 8.4.

2.2.5 The six-roll mill

Jenkins and Murry (1981) extended the theory of Murry (1960b) for the purpose of modelling the throughput of the Australian six-roll mill. Whereas Murry's theory has previously been applied to the first pair of rolls in a milling unit (section 2.2.4), Jenkins and Murry applied the theory to the pressure feeder rolls: the second pair of rolls in the six-roll mill.

If equation **(2.5)** is substituted into equation **(2.8)**, the maximum theoretical throughput of the pressure feeder nip (Q_f^*) is calculated:

$$Q_f^* = \gamma_{do} \frac{L\left(D_p + W_p\right)^2}{4\,D_p} S_p \qquad \textbf{(2.16)}$$

where γ_{do} is the compaction at the feed chute exit, D_p is the mean of the two pressure feeder roll mean diameters, W_p is the pressure feeder nip work opening and S_p is the top pressure feeder roll surface speed.

Jenkins and Murry defined a parameter called *effectiveness* (E) to account for the difference between the actual fibre rate (Q_f) and Q_f^*.

$$E = \frac{Q_f}{Q_f^*} \qquad \textbf{(2.17)}$$

Substituting equation **(2.17)** into equation **(2.16)**,

$$Q_f = E\,\gamma_{do}\,\frac{L\left(D_p + W_p\right)^2}{4\,D_p}\,S_p \qquad \textbf{(2.18)}$$

Jenkins and Murry also defined effectiveness in terms of the feed speed, S_F. If S_F, the actual feed speed at the feed chute exit, is used instead of $S_p' \cos \alpha_{do}'$ (using the outside diameter definitions for the underfeed nip as discussed in section 1.2.4), the compaction at the feed chute exit is defined by:

$$\gamma_{do} = \frac{Q_f}{L\,h_{do}\,S_F} \qquad \textbf{(2.19)}$$

Substituting equation **(2.19)** into equation **(2.18)**, the effectiveness can be expressed as:

$$E = \frac{S_F}{S_p'}\,\frac{2\,D_p'}{D_p + W_p}\,\frac{2\,h_{do}}{D_p + W_p} \qquad \textbf{(2.20)}$$

From equation **(2.6)**, $\frac{D_p + W_p}{2}$ is the theoretical chute setting for maximum throughput of the pressure feeder nip. Defining:

$$h^* = \frac{D_p + W_p}{2} \qquad \textbf{(2.21)}$$

equation **(2.20)** can be expressed as:

$$E = \frac{S_F}{S_p'}\,\frac{D_p'}{h^*}\,\frac{h_{co}}{h^*} \qquad \textbf{(2.22)}$$

$\frac{S_F}{S_p'}$ can be calculated from equation **(2.22)**.

Jenkins and Murry measured the effectiveness of 59 six-roll mills in Australian factories. From the data, they developed an empirical relationship to define Murry's feed speed ratio:

$$\frac{S_F}{S_p' \cos\alpha_{do}'} = 4.63 - 0.88\frac{W_{su}}{h^*} - 1.58\frac{D_p'}{h^*} \qquad \textbf{(2.23)}$$

where W_{su} is the underfeed nip setting. Substituting equations **(2.23)** and **(1.4)** into equation **(2.22)** gives an empirical relationship to estimate effectiveness:

$$E = \frac{h_{do}}{h^*}\left(\frac{D_p'}{h^*} + \frac{W_{su}}{h^*} - \frac{h_{do}}{h^*}\right)\left(4.63 - 0.88\frac{W_{su}}{h^*} - 1.58\frac{D_p'}{h^*}\right) \qquad \textbf{(2.24)}$$

This empirical relationship is discussed further in section 3.3.

Jenkins and Murry differentiated equation **(2.24)** to determine the conditions for maximum throughput:

$$W_{su}^* = 3.508\, h^* - 1.53\, D_p' \qquad \textbf{(2.25)}$$

$$h_{do}^* = \frac{W_{su} + D_p'}{2} \qquad \textbf{(2.26)}$$

These maximum throughput conditions remain widely used in the Australian industry today.

In addition to the effectiveness measurements used to define equation **(2.23)**, Jenkins and Murry carried out an experiment on a six-roll mill where deliberate changes to mill settings were made. This experiment is discussed in section 8.5.

2.2.6 Concluding remarks

A throughput model for the Australian six-roll milling unit exists (Jenkins & Murry 1981) and has been used by the Australian sugar factories for over 20 years.

The model is based on a simple throughput model for two-roll mills (Murry 1960b). The key assumption in the two-roll model is that the feed speed of bagasse in the feed chute (S_F) is equal to $S \cos \alpha$ where S is the roll surface speed and α is the contact angle between the feed chute and the rolls.

To extend the two-roll model to the six-roll mill, Jenkins and Murry applied the two-roll model to the pressure feeder rolls and developed a parameter called effectiveness to account for the difference between the theoretical maximum throughput of the pressure feeder and the actual throughput of the mill. An empirical relationship was developed from factory measurements to provide a value for effectiveness.

There are three substantial sets of experimental data that are available to test the throughput models. Solomon (1967) carried out experiments on a small-scale two-roll mill. Jenkins and Murry (1981) carried out experiments on a small-scale pressure feeder with underfeed roll. Jenkins and Murry also carried out experiments on a factory six-roll mill.

2.3 Review of milling unit throughput research outside the sugarcane industry

2.3.1 Introductory remarks

In this section, roller mills used for applications other than the expression of juice from sugarcane are reviewed. A general description is provided for the various applications for roller mills in industry. Throughput issues for these roller mills are described.

2.3.2 Roller mill applications

The Australian raw sugar factory milling unit is a type of roller mill. Roller mills are used in industry for many other applications beside the expression of juice from sugarcane. There are three main application classes: forming, crushing and expression.

The forming process is associated with the production of plates, strips and sections from metals and plastics. Roller mills are generally used in the production of long sections. They are used to plastically work the materials to cause a change in the cross-section.

The crushing process involves the reduction of materials to a suitable size for their intended uses. Materials that are crushed in roller mills include coal, oil shale, powder, sorghum, wheat and corn.

The expression process involves the separation of liquid from a solid-liquid mixture by compression. Roller mills are used in the dewatering of paper and textiles and the expression of juice from sweet sorghum. Sugarcane mills also fit into this category.

2.3.3 Throughput models for roller mills

The materials processed by roller mills can be separated into two distinct classes: continuum materials and discrete particle mats. Continuum materials include the metals and plastics processed for forming applications. The woven paper and textile mats also fit best within this class. Materials such as coal, powder, wheat and sorghum, like prepared sugarcane and bagasse, consist of discrete particles.

The roller mills that process continuum materials invariably produce relatively small changes in cross-section as the materials pass through the nips of the roller mills. Based on the geometry of one such paper mill (Roux & Vincent 1991), it appears that contact angles are typically only about 2°. Compared to typical sugar mill contact angles of 30° to 40°, these contact angles are quite small. Since cos 2° is 0.999 to three significant figures, assuming Murry's theory and the angle of nip theory (section 2.2.3) to be

applicable, it is likely that the roll surface speed provides a satisfactory indication of the feed speed. If so, the calculation of throughput based on roll surface speed is most likely quite reliable. This may explain the seeming lack of throughput literature in this field.

Throughput does appear to be a significant research issue for milling units in other industries processing discrete particles. Adamski (1964) discussed the application of a tall chute as a method of increasing the capacity of a grinding mill. Sander and Schönert (1999) discussed the application of a screw feeder for a similar purpose.

Throughput models for roller mills processing discrete particles for the purpose of size reduction do exist and generally assume that the volumetric throughput is equal to the escribed volume at the nip as defined by equation **(1.6)**. The challenge appears to be to fill the escribed volume with particles and still perform the function of size reduction. Some extensions to the simple model have been proposed. Sander and Schönert (1999) added a *slip factor* to the equation to account for slip on the roll surface. They do not appear to have developed any theory to quantify the slip factor, however.

For the pressing of powders, expression of gas from the feed appears to be a factor limiting capacity and models have been developed to incorporate this limitation into a capacity theory (Katrus 1997). The theory appears to be an empirical extension to Darcy's law (presented in section 4.8) and is concerned with the *fluidisation* of the powder mat, the situation where the gas pressure is sufficient to cause the particles to *float* in the gas. Although air expression is considered an issue for the modelling of throughput in a sugarcane mill (section 6.3.6), the air pressures are not expected to be high and the fibrous nature of the bagasse is likely to minimise fluidisation. Some fluidisation of the finer bagasse particles may occur but this is unlikely to have a substantial effect on the bulk bagasse behaviour. While the use of Darcy's law is considered relevant, it is unlikely that Katrus' theory is of much value to sugarcane mill throughput modelling.

The process of crushing sweet sorghum is the rolling process that is most similar to the crushing of sugarcane. Three-roll mills like the early sugarcane mills are used. Recent

literature for crushing sweet sorghum (Bryan, Monroe & Gascho 1985) suggests that sugarcane crushing research is well in advance of sweet sorghum crushing research.

2.3.4 Concluding remarks

While roller mills are used for many applications in industry, the sugarcane crushing process is quite different to most. The throughput models developed for sugarcane mills (section 2.2) are quite advanced compared to most. It is not believed that models for other applications provide any substantial information for the further development of sugarcane milling unit throughput models.

2.4 The milling computational model

The milling unit throughput models described in section 2.2 are based on simplistic models of bagasse behaviour. They assumed that there is no slip between the bagasse mat and the roll surface and that there is no shearing within the bagasse mat affecting the average speed of the mat (Murry 1960b). Although Jenkins and Murry (1981) developed an empirical model to account for variations from Murry's assumptions, the model provides little additional understanding of the behaviour of bagasse in the milling unit.

In recent years, a model of milling behaviour based on more fundamental physical principles has been developed (Owen, Zhao & Loughran 1995; Owen et al 1998, Adam & Loughran 1998; Loughran & Kannapiran 2002). In this model, a constitutive sub-model for bagasse behaviour is included that allows internal shear to occur. In addition, contact between the bagasse mat and the roll surface is modelled. Preliminary efforts to use this model to simulate a pressure feeder have been made (Adam 1997, Kannapiran 2002, Plaza 2003).

Since the milling computational model has the features required to investigate deficiencies in Murry's simple theory and since it is based on more fundamental

principles, the milling computational model provides an obvious avenue to pursue in order to develop an improved throughput model for the six-roll mill.

2.5 Concluding remarks

Published literature regarding throughput models for roller mills were reviewed in this chapter. While there are many applications for roller mills throughout industry, there appear to be no relevant throughput models that offer superior understanding of the factors affecting throughput to the models previously developed for sugarcane milling units.

Jenkins and Murry (1981) discussed the development of a throughput model for the Australian six-roll milling unit. This model has been widely used within the Australian raw sugar factories to determine mill settings for achieving the desired throughput. The model represents the current state of knowledge.

The Jenkins and Murry model contains an empirical component to account for discrepancies believed to originate from Murry's assumptions that the bagasse mat does not slip on the roll surface and that there is no internal shear within the bagasse mat affecting the feed speed. No attempt has been made to investigate which of these assumptions is not valid.

A computational model has been developed to better understand the crushing process. The model contains a constitutive sub-model that allows shearing in the bagasse mat and a friction law to model the contact between the mat and the roll surface. These features will allow Murry's assumptions to be explored in detail and so provide an avenue to develop an improved throughput model for the six-roll mill.

3 Evaluation of the Jenkins and Murry feeding model

3.1 Introductory remarks

In chapter 2, the throughput model of Jenkins and Murry (1981) was identified as the most advanced throughput model for the raw sugar factory six-roll milling unit. The Australian raw sugar factories have used the Jenkins and Murry model for the past 20 years to determine mill settings to maximise throughput.

The Jenkins and Murry model of throughput uses a parameter called effectiveness to account for discrepancies between the theoretical maximum throughput of the pressure feeder rolls and the actual throughput of the milling unit. Jenkins and Murry developed an empirical equation to predict effectiveness from measurements of effectiveness of 59 six-roll milling units.

In this chapter, the ability of the Jenkins and Murry model to satisfactorily predict the throughput of Australian raw sugar factory six-roll milling units is assessed. From the Jenkins and Murry theory, if effectiveness is well predicted, then throughput will be well predicted. Consequently, this examination of the Jenkins and Murry throughput model focuses on the prediction of effectiveness. The Jenkins and Murry theory is tested by comparing its predictions to measurements of effectiveness made by Jenkins and Murry and against further measurements of effectiveness made as part of this study.

3.2 Measuring the effectiveness of factory milling units

The procedure used by Jenkins and Murry to measure effectiveness (E) was based on equation **(2.18)**. Rearranging this equation,

$$E = \frac{Q_f}{\gamma_{do}\, S_p} \frac{4\, D_p}{L \left(D_p + W_p\right)^2} \qquad \textbf{(3.1)}$$

where Q_f is the fibre rate, γ_{do} is the compaction at the feed chute exit, S_p is the top pressure feeder roll surface speed, D_p is the mean of the top and bottom pressure feeder roll mean diameters, L is the roll length and W_p is the pressure feeder nip work opening.

The measurement of S_p, D_p, L and W_p is straightforward.

The fibre rate for each milling unit in a milling train was assumed to be equal to the fibre rate entering the first mill.

The feed chute exit compaction cannot easily be directly measured. Jenkins and Murry modelled the forces on the bagasse in the feed chute in order to estimate γ_{do}. The model used was extended from the earlier work of Crawford (1955), Murry and Hutchinson (1958) and Shann (1962). The model uses an incremental method to satisfy equilibrium of forces in the flow direction for the bagasse in the feed chute. Figure 3.1 shows the feed chute geometry and the forces included in the model.

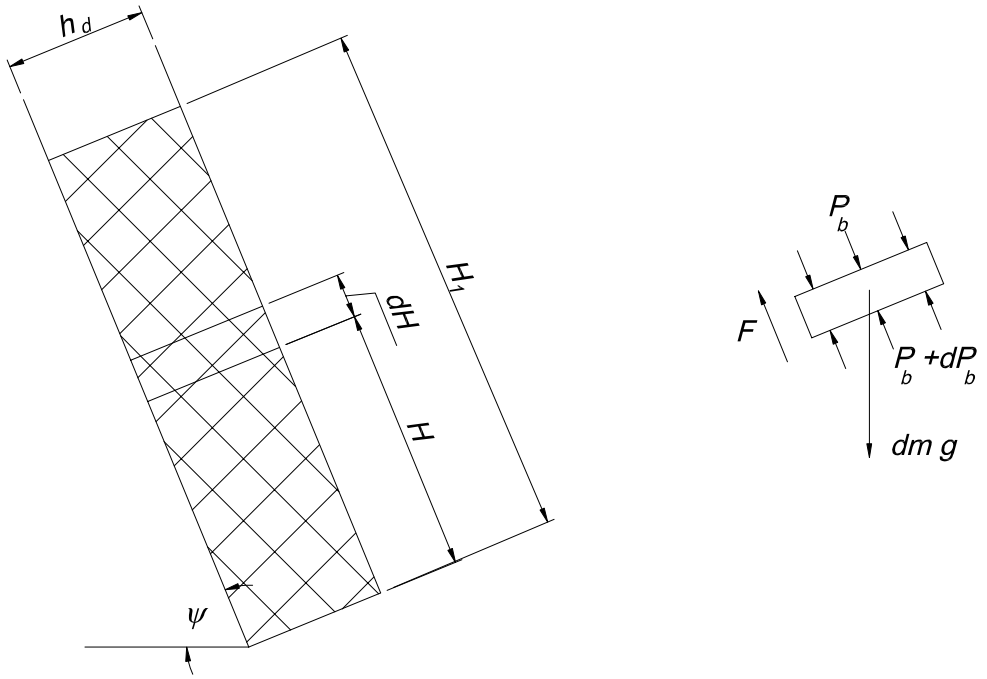

Figure 3.1 Feed chute dimensions

From force equilibrium in the axial direction of a strip across the chute of length *dH*,

$$dm\ g \sin\psi = dP_b\ L\ h_d + F \qquad \textbf{(3.2)}$$

where *dm* is the mass of the strip, *g* is the acceleration due to gravity, dP_b is the increment in pressure across the strip and *F* is the total frictional force between the strip and the chute walls. *L* is the width of the chute (into the page in Figure 3.1).

The mass of the strip is calculated from:

$$dm = \frac{\gamma_d\ L\ h_d}{f_d}\ dH \qquad \textbf{(3.3)}$$

where γ_d is the compaction of the strip and f_d is the fibre content of the bagasse in the chute.

The total frictional force is the sum of the frictional forces on the four chute walls:

$$F = \mu \left[dm\, g \cos\psi + 2\, K_0\, P_b \left(L + h_d \right) dH \right] \qquad \textbf{(3.4)}$$

where μ is the coefficient of friction between the bagasse and the chute wall and K_0 is the ratio of transverse pressure to axial pressure in the strip.

Substituting equations **(3.3)** and **(3.4)** into equation **(3.2)**, the equilibrium equation for the strip is

$$dP_b = \left[\frac{\gamma_d\, g}{f_d} \left(\sin\psi - \mu \cos\psi \right) - 2\, \mu\, K_0\, P_b \frac{L + h_d}{L\, h_d} \right] dH \qquad \textbf{(3.5)}$$

The pressure in the bagasse at the chute exit, P_{do}, was found by integrating from the top surface of the bagasse in the chute ($H = H_1$) to the bottom of the chute ($H = 0$). The position in the chute at the top surface of the bagasse is known as the chute *level*. The pressure at this height (P_{dH1}) was assumed to be zero.

To solve equation **(3.5)**, a relationship between pressure (P_b) and compaction (γ_d) was required. A suitable relationship was determined from measurements of force and displacement during compression of a sample of bagasse in a confined uniaxial test cell. The same relationship was used to calculate the compaction at the feed chute exit (γ_{do}) from P_{do}.

3.3 Factory effectiveness measurements

This section describes the data sets used to test the throughput model of Jenkins and Murry (1981). The first data set was the data set compiled by Jenkins and Murry (1981) on which the empirical model for effectiveness was based. The second data set was compiled in 1997 in a similar factory survey.

Jenkins and Murry (1981) presented a series of 109 effectiveness measurements from 59 milling units in 15 factories. The individual effectiveness measurements are listed in Appendix A.

In 1997, as part of this project, a second series of effectiveness measurements were made. In this series, a total of 63 measurements were made from 29 milling units in six factories. The individual effectiveness measurements are listed in Appendix B.

3.4 Performance of the Jenkins and Murry model

The Jenkins and Murry (1981) model was stated in equation **(2.24)**:

$$E = \frac{h_{do}}{h^*}\left(\frac{D_p'}{h^*} + \frac{W_{su}}{h^*} - \frac{h_{do}}{h^*}\right)\left(4.63 - 0.88\frac{W_{su}}{h^*} - 1.58\frac{D_p'}{h^*}\right) \qquad \textbf{(3.6)}$$

where h_{do} is the feed chute exit setting, D_p' is the mean of the two pressure feeder roll outside diameters, W_{su} is the underfeed nip setting and h^* is the theoretical chute setting for maximum throughput of the pressure feeder nip.

Figure 3.2 compares the 109 individual measurements of effectiveness reported by Jenkins and Murry (1981) against the effectiveness predicted using equation **(3.6)**. It also compares the measurements made as part of this project (section 3.3) against equation **(3.6)**. The figure shows that the model does not predict effectiveness particularly well, even using the Jenkins and Murry measurements upon which the model was based.

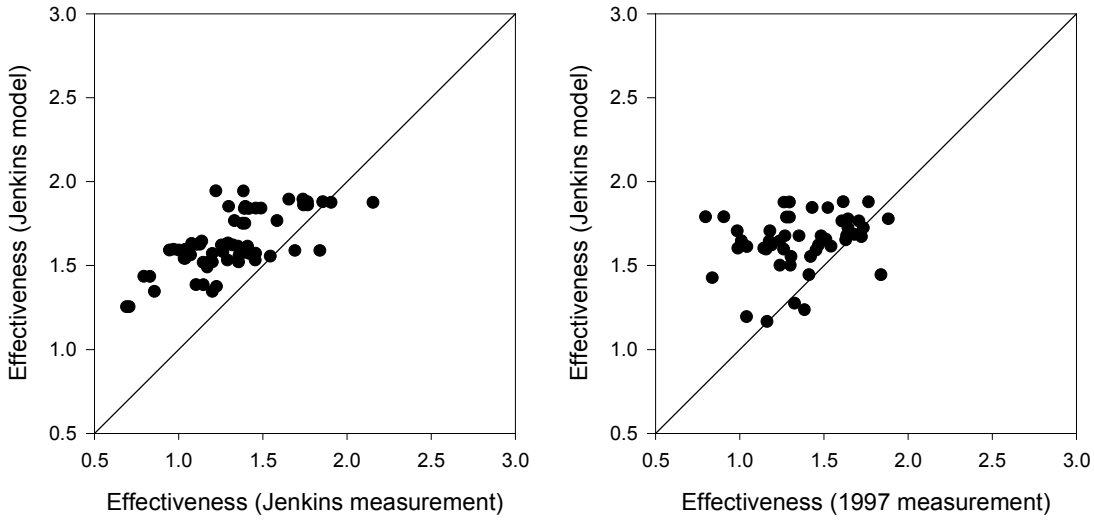

Figure 3.2 Comparison of the Jenkins and Murry and 1997 effectiveness measurements with Jenkins and Murry model predictions

To determine whether the model can discriminate between a milling unit with high effectiveness and a milling unit with low effectiveness, a further test was conducted.

For each milling train where effectiveness was measured more than once, an analysis of variance was undertaken to determine whether a statistically significant effectiveness difference at a significance level better than 5% could be found between milling units. For those milling trains where statistically significant effectiveness differences were found, a multiple comparison test known as Tukey's method (Mathsoft 1999) was carried out to identify the pairs of milling units with effectiveness values that were significantly different based on a 95% confidence interval. For each pair of milling units that were identified by this process, the difference in effectiveness between the milling unit with high effectiveness and the milling unit with low effectiveness was calculated and compared against the predicted difference using the Jenkins and Murry model. Figure 3.3 shows the results for the 54 pairs of milling units that were identified from the Jenkins and Murry measurements and the 18 pairs of milling units that were identified from the 1997 measurements.

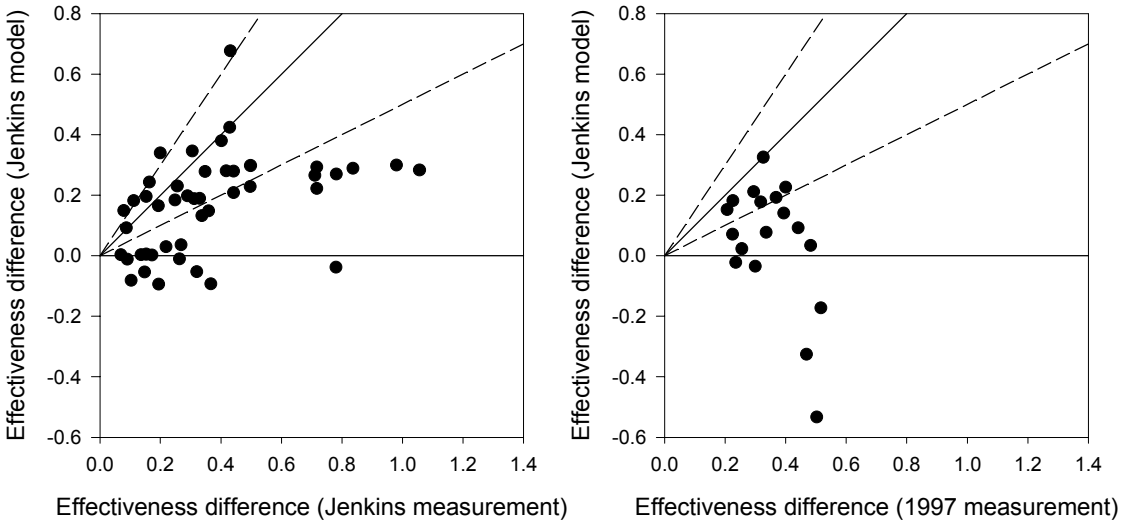

Figure 3.3 Comparison of the difference in effectiveness of pairs of milling units with the predicted difference using the Jenkins and Murry model

In Figure 3.3, points below the horizontal axis represent situations where an increase in effectiveness was measured between two milling units while the model predicted a decrease. The dashed lines represent boundaries where the magnitude of the predicted difference was 50% different from the magnitude of the measured difference. Table 3.1 shows the percentage of data points below the horizontal axis and within the 50% error bands for the graphs in Figure 3.3. In summary, on only about 40% of occasions did the Jenkins and Murry model predict the effectiveness difference within 50% of the measured difference.

Table 3.1 Comparison of Jenkins and Murry model results from Figure 3.3

Data set	Percentage with wrong sign	Percentage with error less than 50%
Jenkins & Murry	18	36
1997	28	39

3.5 Concluding remarks

While the throughput model of Jenkins and Murry (1981) is considered to be the best model currently available to predict the throughput of the raw sugar factory six-roll milling units, it does not appear to make accurate predictions.

The model is based on an empirical equation to predict effectiveness. The empirical equation was developed from the factory effectiveness measurements made by Jenkins and Murry. Comparing the original effectiveness measurements to the predicted effectiveness using the empirical equation, the empirical equation performed poorly. The model performance was not significantly different when compared against recent measurements of factory effectiveness made as part of this project.

Given the concerns with the model identified in this chapter, it is unlikely that the Jenkins and Murry throughput model is adequate for the task of identifying the means to make further increases in milling unit throughput. Consequently, a need exists for a superior throughput model if further increases in milling unit throughput are to be made. The development of the improved throughput model is the focus of the remainder of this thesis.

4 Foundations of a new feeding model

4.1 Introductory remarks

In chapter 3, the state-of-the-art throughput model of Jenkins and Murry (1981) was assessed and found to be inadequate for the purpose of identifying means of increasing mill throughput. In this chapter, the foundations of a new throughput model are presented.

The new throughput model is based on the milling computational model briefly described in section 2.4. Unlike the Jenkins and Murry model that is essentially a function of mill geometry, the milling computational model is based on general equations of force equilibrium and continuity and a general description of bagasse material behaviour. The throughput model itself is a specific application of the more general model.

This chapter describes the general model. Chapter 5 describes the material parameters that are required for use in the model. The specific throughput models are described in chapters 6 and 8.

4.2 Overview of the model

The milling computational model is based on theory describing the behaviour of porous media. Owen, Zhao and Loughran (1995) provided the equations in a general form.

Adam and Loughran (1998) documented a subset of the general equations applicable to saturated porous media. Adam and Loughran's subset of the equations, with some modifications, have been adopted here.

The milling computational model is solved using the ABAQUS/Standard finite element analysis software (Hibbitt, Karlsson & Sorensen 2000). The ABAQUS/Standard solver was considered the most appropriate and least limiting general-purpose solver available for the task.

4.3 A porous media description for bagasse

Bagasse was assumed to consist of a deformable solid structure containing voids. While the structure was assumed to be deformable, the individual solid particles that construct the solid structure were assumed to be incompressible. Deformation of the solid structure, therefore, required a change in the volume of the voids. An incompressible fluid was assumed to fill the voids. These incompressibility assumptions are considered valid for the pressure range examined in this study (up to 2 MPa) where relatively large increments in deformation of the solid structure still occur under relatively small increments in pressure.

For an elemental volume δV, containing a volume of solid δV_g and a volume of voids δV_v,

$$\delta V = \delta V_g + \delta V_v \qquad \textbf{(4.1)}$$

Since the fluid was assumed to fill the voids in the elemental volume, the volume of the fluid was the same as the volume of the voids.

Porosity (n) is defined as the ratio of the volume of voids to the total volume:

$$n = \frac{\delta V_v}{\delta V} \qquad \textbf{(4.2)}$$

Void ratio (e) is defined as the ratio of the volume of voids to the volume of solid:

$$e = \frac{\delta V_v}{\delta V_g} \qquad \textbf{(4.3)}$$

Porosity and void ratio are related by:

$$n = \frac{e}{1+e} \qquad \textbf{(4.4)}$$

4.4 Force equilibrium

The equations of force equilibrium were applied to an elemental volume of the bagasse mat (Figure 4.1). The elemental volume has dimensions δx, δy and δz in the three Cartesian coordinate directions.

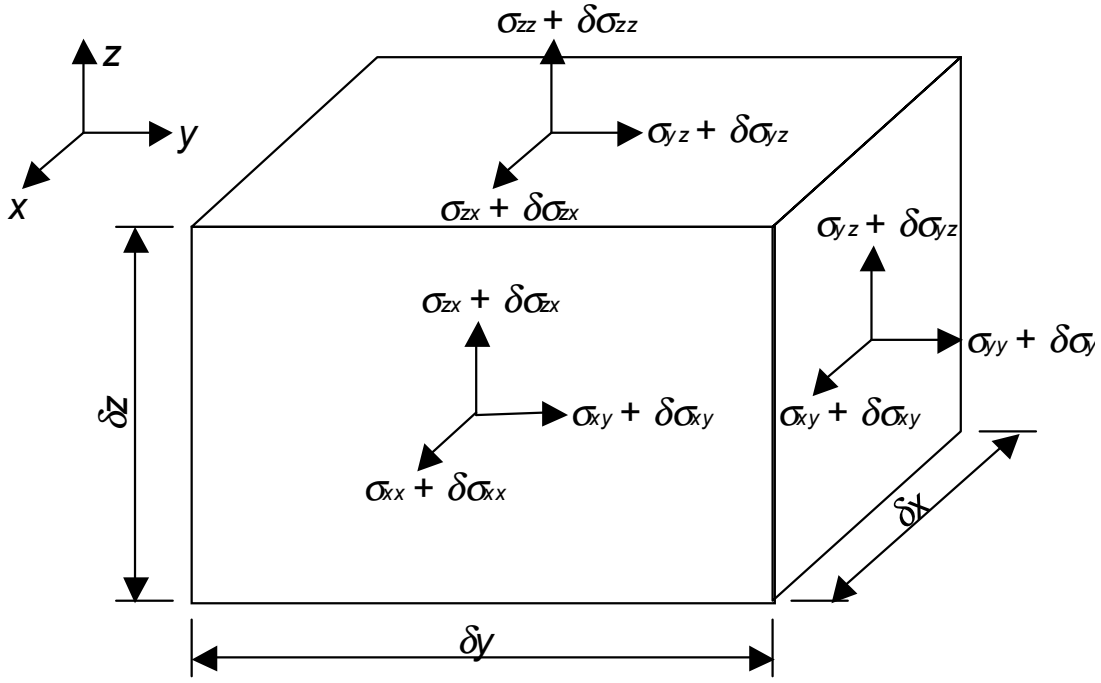

Figure 4.1 Stresses acting on an elemental volume

The analysis was assumed to be quasi-static so that dynamic effects could be neglected. Since the rolling process is essentially steady state with typical speeds of the order of 200 mm/s and accelerations largely resulting only from changes in direction imposed by the roll surface (perhaps 50 mm/s^2), this assumption was considered quite reasonable.

Although substantially larger than the accelerations associated with dynamic effects, gravitational acceleration was also neglected. Compared to the forces involved in the compaction of the bagasse mat, gravitational forces were calculated to be quite small.

Considering the forces acting in the *x* direction, the volume is subjected to a normal stress on the back face acting into the page, a normal stress on the front face acting out of the page and shear stresses acting along the other four surfaces of the volume (Figure 4.1). There is a stress gradient across the element. Considering the normal stress in the *x* direction, a stress of magnitude σ_{xx} acts on the back face (not shown in Figure 4.1) and a stress of magnitude $\sigma_{xx} + \delta\sigma_{xx}$ acts on the front face. Similar stress differences exist for the shear stress components. Tensile stresses are defined positive.

Equating forces in the *x* direction,

$$-\sigma_{xx}\,\delta y\,\delta z+(\sigma_{xx}+\delta\sigma_{xx})\,\delta y\,\delta z-\sigma_{xy}\,\delta z\,\delta x+(\sigma_{xy}+\delta\sigma_{xy})\,\delta z\,\delta x-\sigma_{zx}\,\delta x\,\delta y+(\sigma_{zx}+\delta\sigma_{zx})\,\delta x\,\delta y=0$$

Simplifying and dividing both sides of the equation by $\delta x\,\delta y\,\delta z$,

$$\frac{\delta\sigma_{xx}}{\delta x}+\frac{\delta\sigma_{xy}}{\delta y}+\frac{\delta\sigma_{yz}}{\delta z}=0$$

At the limit,

$$\frac{\partial\sigma_{xx}}{\partial x}+\frac{\partial\sigma_{xy}}{\partial y}+\frac{\partial\sigma_{zx}}{\partial z}=0 \qquad \textbf{(4.5)}$$

Equating forces in the *y* and *z* directions and following the same procedure, equations similar to **(4.5)** can be developed:

$$\frac{\partial\sigma_{yy}}{\partial y}+\frac{\partial\sigma_{yz}}{\partial z}+\frac{\partial\sigma_{xy}}{\partial x}=0 \qquad \textbf{(4.6)}$$

$$\frac{\partial\sigma_{zz}}{\partial z}+\frac{\partial\sigma_{zx}}{\partial x}+\frac{\partial\sigma_{yz}}{\partial y}=0 \qquad \textbf{(4.7)}$$

4.5 Fluid continuity

The continuity equation was applied to the fluid flowing through the elemental volume described in section 4.4 (Figure 4.2). The continuity equation ensures that fluid mass is conserved. The rate of increase in fluid mass in the elemental volume must equal the difference between the mass flow rate into elemental volume and the mass flow rate out of the elemental volume. The fluid was assumed to be incompressible so that the fluid density, ρ_w, was constant.

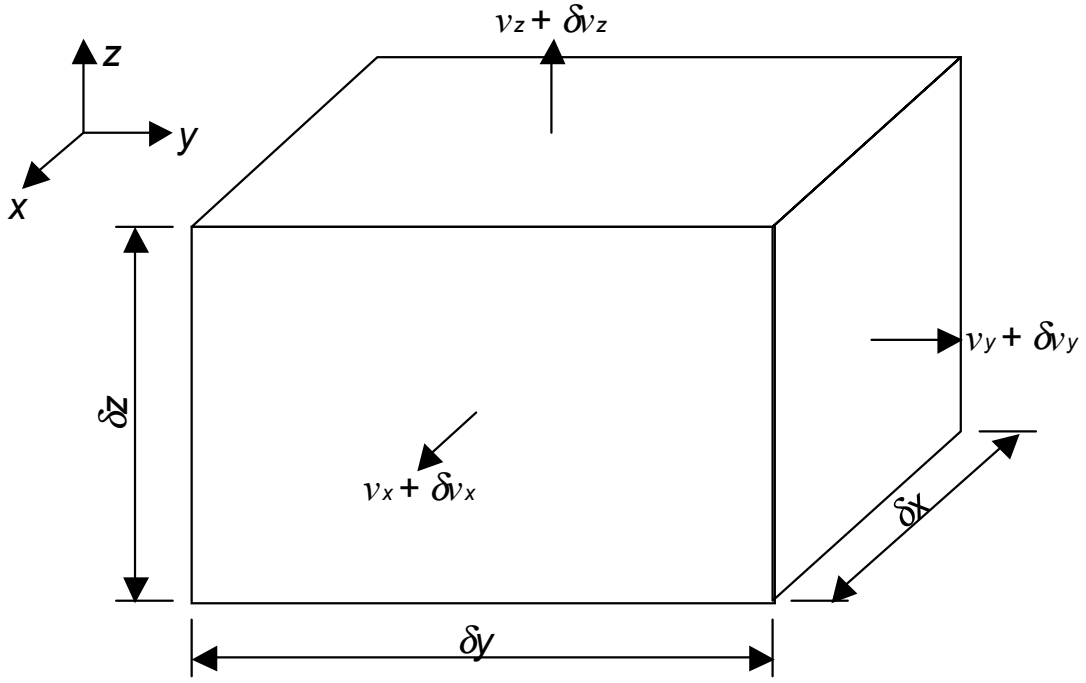

Figure 4.2 Fluid flowing through the elemental volume

Consider first the flow into the back surface of the volume (not shown in Figure 4.2). The fluid velocity vector can be split into three component vectors in the three coordinate directions, respectively. For this particular flow, the vector components in the *y* and *z* directions are aligned with the surface and do not cause any fluid flow into the volume. Only the *x* component of the velocity vector causes fluid flow into the elemental volume. The symbol v_x is used to define the mean or *superficial* velocity of this vector component. The mass flow rate into the back surface of the elemental volume is, then, $\rho_w\, v_x\, \delta y\, \delta z$. Similarly, the mass flow rate out of the front surface of the elemental volume is $\rho_w\, (v_x + \delta v_x)\, \delta y\, \delta z$ where δv_x is the difference in magnitude of the velocity vector between the back and front faces of the elemental volume. Mass flows can similarly be defined for each of the other four surfaces of the elemental volume.

The rate of increase in fluid mass is defined by $\rho_w \dfrac{d(\delta V_v)}{dt}$ where *t* is time. Substituting equation **(4.3)** into the expression, the rate of increase in fluid mass becomes $\rho_w \dfrac{d(e\,\delta V_g)}{dt}$. For the elemental volume, δV_g is constant (section 4.3) and so does not

vary with time. The rate of increase in fluid mass can then be expressed as $\rho_w \, \delta V_g \, \frac{de}{dt}$.

The solid component of the elemental volume, δV_g, can be expressed as δV - δV_v and, using equation **(4.2)**, δV_v can be expressed as $n \, \delta V$ so that δV_g can be expressed as $(1-n)\delta V$. Substituting equation **(4.4)** into the expression, $\delta V_g = \frac{1}{1+e} \delta V$. Defining the volume by $\delta x \, \delta y \, \delta z$, the rate of increase in fluid mass is defined by $\rho_w \, \delta x \, \delta y \, \delta z \, \frac{1}{1+e} \frac{de}{dt}$.

Equating the rate of increase in fluid mass to the difference between the inflow and the outflow,

$$\rho_w \, \delta x \, \delta y \, \delta z \, \frac{1}{1+e} \frac{de}{dt} = \rho_w \, v_x \, \delta y \, \delta z - \rho_w \, (v_x + \delta v_x) \delta y \, \delta z + \rho_w \, v_y \, \delta z \, \delta x - \rho_w \, (v_y + \delta v_y) \delta z \, \delta x + \rho_w \, v_z \, \delta x \, \delta y - \rho_w \, (v_z + \delta v_z) \delta x \, \delta y$$

Simplifying and dividing throughout by $\rho_w \, \delta x \, \delta y \, \delta z$,

$$\frac{1}{1+e} \frac{de}{dt} + \frac{\delta v_x}{\delta x} + \frac{\delta v_y}{\delta y} + \frac{\delta v_z}{\delta z} = 0$$

At the limit,

$$\frac{1}{1+e} \frac{de}{dt} + \frac{\partial v_x}{\partial x} + \frac{\partial v_y}{\partial y} + \frac{\partial v_z}{\partial z} = 0 \qquad \textbf{(4.8)}$$

Equation **(4.8)** defines the rate of increase in mass differently (but no less correctly) to Adam and Loughran (1998). Adam and Loughran define the rate of increase in mass in terms of volumetric strain rather than void ratio.

4.6 Principle of effective stress

The total stress was assumed to be a function of stress components due to the solid and fluid phases. The principle of effective stress describes the relationship between these stress components:

$$\sigma_{xx} = \sigma'_{xx} - P \qquad (4.9)$$

where σ'_{xx} is called the *effective stress* and P is the *pore pressure*. While the total and effective stresses are defined so that the tensile direction is positive, the pore pressure is defined so that a compressive stress is positive. Similar equations can be defined for the other two coordinate directions:

$$\sigma_{yy} = \sigma'_{yy} - P \qquad (4.10)$$

$$\sigma_{zz} = \sigma'_{zz} - P \qquad (4.11)$$

Since fluids do not support shear stresses, the total shear stress and the effective shear stress in the solid phase are equal:

$$\sigma_{xy} = \sigma'_{xy} \qquad (4.12)$$

$$\sigma_{yz} = \sigma'_{yz} \qquad (4.13)$$

$$\sigma_{zx} = \sigma'_{zx} \qquad (4.14)$$

While the principle of effective stress was assumed to apply, no tests have been carried out to determine whether it is applicable to bagasse. The principle of effective stress assumes point contact between solid particles that may not be quite true for the fibre particles. These particles have some capacity to deform resulting in contact across a finite area rather than a point. Adam (1997) discussed this issue in some detail but considered the principle of effective stress to be an adequate assumption. It is also more likely to be adequate at the lower pressure range considered in this report (up to 2 MPa) compared to the pressure range considered by Adam (up to 20 MPa).

4.7 Constitutive behaviour of the solid phase

4.7.1 Introductory remarks

The computational milling model, as described by Adam and Loughran (1998), employed the linear elasticity material model and a simplified version of the critical state model known as the Drucker-Prager cap plasticity model (defined by Hibbitt, Karlsson & Sorensen 2000) to describe the constitutive behaviour of the solid phase. Loughran and Adam (1998) and Downing, Loughran and Domanti (1999) recognised that the porous elasticity model (also defined by Hibbitt, Karlsson & Sorensen 2000) described the elastic behaviour of prepared cane better than the linear elasticity model. Consequently, the porous elasticity model was chosen to describe the elastic behaviour here. Following Adam and Loughran (1998), the Drucker-Prager cap model was chosen to describe the plastic behaviour.

Following the usual convention with critical state models, the stress state was defined in terms of two components: the mean stress, p, and the deviator stress, q, where:

$$p = -\frac{\sigma'_{xx}+\sigma'_{yy}+\sigma'_{zz}}{3} \qquad \textbf{(4.15)}$$

$$q = -\sqrt{\frac{\left(\sigma'_{yy}-\sigma'_{zz}\right)^2+\left(\sigma'_{zz}-\sigma'_{xx}\right)^2+\left(\sigma'_{xx}-\sigma'_{yy}\right)^2}{2}+3\left(\sigma_{yz}^2+\sigma_{zx}^2+\sigma_{xy}^2\right)} \qquad \textbf{(4.16)}$$

Strain, likewise was defined in terms of two components: the volumetric strain, ε_p, and the deviatoric strain, ε_q, where, in incremental form,

$$d\varepsilon_p = -\left(d\varepsilon_{xx}+d\varepsilon_{yy}+d\varepsilon_{zz}\right) \qquad \textbf{(4.17)}$$

$$d\varepsilon_q = -\frac{1}{3}\sqrt{2\left[\left(d\varepsilon_{yy}-d\varepsilon_{zz}\right)^2+\left(d\varepsilon_{zz}-d\varepsilon_{xx}\right)^2+\left(d\varepsilon_{xx}-d\varepsilon_{yy}\right)^2\right]+3\left(d\varepsilon_{yz}^2+d\varepsilon_{zx}^2+d\varepsilon_{xy}^2\right)} \qquad \textbf{(4.18)}$$

Volumetric strain was related to void ratio as follows:

$$\varepsilon_p = -\ln\left(\frac{1+e}{1+e_0}\right) \qquad \textbf{(4.19)}$$

where e_0 is the void ratio at the reference volume where volumetric strain is defined to be zero.

4.7.2 General description of a constitutive model

As discussed in section 4.7.1, the constitutive model defines both elastic and plastic behaviour. It was assumed that

$$\begin{bmatrix}\varepsilon_p \\ \varepsilon_q\end{bmatrix} = \begin{bmatrix}\varepsilon_p^e \\ \varepsilon_q^e\end{bmatrix} + \begin{bmatrix}\varepsilon_p^p \\ \varepsilon_q^p\end{bmatrix} \qquad \textbf{(4.20)}$$

The *e* superscript refers to the elastic strain increment. The *p* superscript refers to the plastic strain increment.

In differential form, equation **(4.20)** becomes:

$$\begin{bmatrix}d\varepsilon_p \\ d\varepsilon_q\end{bmatrix} = \begin{bmatrix}d\varepsilon_p^e \\ d\varepsilon_q^e\end{bmatrix} + \begin{bmatrix}d\varepsilon_p^p \\ d\varepsilon_q^p\end{bmatrix} \qquad \textbf{(4.21)}$$

Muir Wood (1990) defined a general constitutive relationship for an elastic model:

$$\begin{bmatrix}d\varepsilon_p^e \\ d\varepsilon_q^e\end{bmatrix} = \begin{bmatrix}\frac{1}{K} & 0 \\ 0 & \frac{1}{3\hat{G}}\end{bmatrix}\begin{bmatrix}dp \\ dq\end{bmatrix} \qquad \textbf{(4.22)}$$

where K is the bulk modulus and $\hat{G}$ is the shear modulus. K and $\hat{G}$ are related as follows:

$$\hat{G} = \frac{3(1-2\nu)}{2(1+\nu)} K \qquad \textbf{(4.23)}$$

where ν is Poisson's ratio.

The definition of a plastic model requires the definition of a yield surface and a plastic potential surface. The yield surface defines the boundary in stress space between elastic and plastic behaviour. The plastic potential surface defines the relative amounts of volumetric and deviatoric strain that occur during plastic deformation.

Muir Wood (1990) defined a general constitutive relationship for a plastic model:

$$\begin{bmatrix} d\varepsilon_p^p \\ d\varepsilon_q^p \end{bmatrix} = \frac{-1}{\left[\frac{\partial F}{\partial p_b}\left(\frac{\partial p_b}{\partial \varepsilon_p^p}\frac{\partial G}{\partial p} + \frac{\partial p_b}{\partial \varepsilon_q^p}\frac{\partial G}{\partial q}\right)\right]} \begin{bmatrix} \frac{\partial F}{\partial p}\frac{\partial G}{\partial p} & \frac{\partial F}{\partial q}\frac{\partial G}{\partial p} \\ \frac{\partial F}{\partial p}\frac{\partial G}{\partial q} & \frac{\partial F}{\partial q}\frac{\partial G}{\partial q} \end{bmatrix} \begin{bmatrix} dp \\ dq \end{bmatrix} \qquad \textbf{(4.24)}$$

where F and G define the shape of the yield and plastic potential surfaces respectively (section 4.7.4) and p_b defines the size of the yield and plastic potential surfaces (section 4.7.5).

In summary, the definition of the elastic behaviour involves the definition of the bulk modulus, K (equation **(4.23)** can then be used to define the shear modulus, $\hat{G}$) and Poisson's ratio, ν; and the definition of the plastic behaviour involves the definition of the shape of the yield and plastic potential surfaces, F and G, and the size of the yield and plastic potential surfaces, p_b.

4.7.3 Elastic behaviour

The specific model chosen to describe the elastic behaviour was the porous elastic model (Hibbitt, Karlsson and Sorensen 2000). In this model, the volumetric component of the elastic strain is determined from:

$$de^e = -\kappa \, d\left[\ln\left(p - p_t^e\right)\right] \qquad \textbf{(4.25)}$$

where κ is a material constant called the logarithmic bulk modulus and p_t^e is the elastic tensile limit of the solid material.

The elastic volumetric strain is defined like equation **(4.19)**:

$$\varepsilon_p^e = -\ln\left(\frac{1+e^e}{1+e_0}\right) \qquad \textbf{(4.26)}$$

where e^e is the void ratio from the elastic volume change.

Differentiating equation **(4.26)** and substituting equation **(4.25)** into it:

$$d\varepsilon_p^e = \frac{\kappa}{\left(1+e^e\right)\left(p - p_t^e\right)} dp \qquad \textbf{(4.27)}$$

Comparing **(4.27)** to the first equation in **(4.22)**,

$$K = \frac{\left(1+e^e\right)\left(1-\dfrac{p_t^e}{p}\right)p}{\kappa} \qquad \textbf{(4.28)}$$

Substituting **(4.28)** in **(4.23)**,

$$\hat{G} = \frac{3\left(1-2\nu\right)\left(1+e^e\right)\left(1-\dfrac{p_t^e}{p}\right)p}{2\left(1+\nu\right)\kappa} \qquad \textbf{(4.29)}$$

In summary, three parameters are required to define the elastic behaviour: κ to define the volumetric behaviour, ν to define the deviatoric behaviour and p_t^e to define the elastic tensile limit.

4.7.4 Shape of the yield and plastic potential surfaces

The Drucker-Prager cap material model was chosen to define the plastic behaviour (Hibbitt, Karlsson & Sorensen 2000). The yield surface includes two regions: a shear failure surface and a cap (Figure 4.3).

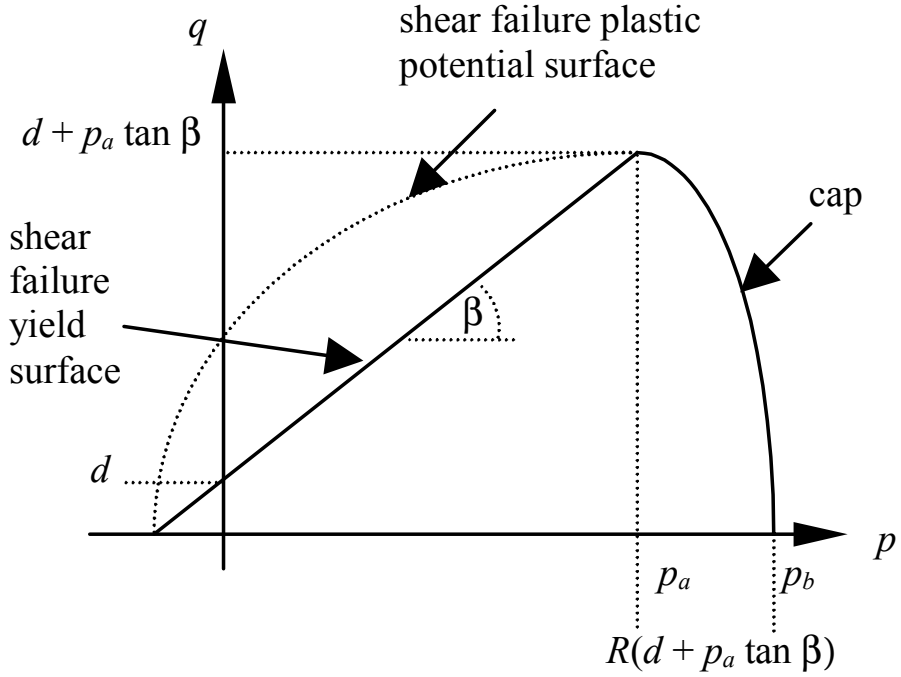

Figure 4.3 The yield surface for the simplified Drucker-Prager cap material model

The shear surface (F_s) is defined by:

$$F_s = q - p \tan\beta - d = 0 \qquad \textbf{(4.30)}$$

where β and d are material parameters representing the material angle of friction and the material cohesion respectively.

The cap is defined by:

$$F_c = (p - p_a)^2 + (R\,q)^2 - [R\,(d + p_a \tan\beta)]^2 = 0 \qquad \textbf{(4.31)}$$

where R is also a material parameter called the cap eccentricity factor. The pressure, p_a is defined by:

$$p_a = \frac{p_b - R\,d}{1 + R\tan\beta} \qquad \textbf{(4.32)}$$

where p_b is the pressure used to define the size of the yield surface.

The model uses associated flow in the cap region and nonassociated flow in the shear failure region. The plastic potential for the shear surface is:

$$G_s = \left[\left(p - p_a\right)\tan\beta\right]^2 + q^2 - \left(d + p_a\tan\beta\right)^2 = 0 \qquad \textbf{(4.33)}$$

Since the cap region uses associated flow, equation **(4.31)** defines the plastic potential surface, as well as the yield surface, for the cap region.

In summary, three parameters are required to define the yield and plastic potential surfaces as defined above: d, the intercept of the shear failure surface on the q axis; β, the angle of the shear failure surface from the p axis; and R, the ratio of the width of the cap ellipse to the height of the cap ellipse.

Adam (1997) describes a further simplifying assumption, adopted here, that eliminates one of the parameters required to define the yield and plastic potential surfaces.

$$R = \frac{1}{\tan\beta} \qquad \textbf{(4.34)}$$

This assumption sets the width of the cap ellipse on the p axis to the same width as the shear failure surface ellipse on the plastic potential surface. The assumption makes the cap region of the yield surface the same shape as the equivalent modified Cam clay (Muir Wood 1990) yield surface, one of the simplest critical state model yield surfaces.

While d and β are described above and are the parameters described by Hibbitt, Karlsson & Sorensen (2000) for the Drucker-Prager cap model, two alternative parameters were defined and used throughout this thesis: M, the slope of the shear surface; and p_t, the intercept of the shear surface on the p axis. These two parameters are more widely used by soil mechanics analysts. These parameters are defined by:

$$\mathrm{M} = \tan\beta \qquad \textbf{(4.35)}$$

$$p_t = \frac{-d}{\tan\beta} \qquad \textbf{(4.36)}$$

In summary, two parameters, M and p_t are used throughout this thesis to describe the shape of the yield and plastic potential surfaces.

Redefining the yield and plastic potential surfaces in terms of M and p_t (substituting equations **(4.32)**, **(4.34)**, **(4.35)** and **(4.36)** into equations **(4.30)**, **(4.31)** and **(4.33)**,

$$F_s = q - \mathrm{M}\left(p - p_t\right) = 0 \qquad \textbf{(4.37)}$$

$$F_c = G_s = G_c = \left(2\,p - p_b - p_t\right)^2 + \left(\frac{2\,q}{M}\right)^2 - \left(p_b - p_t\right)^2 = 0 \qquad \textbf{(4.38)}$$

4.7.5 Size of the yield and plastic potential surfaces

In section 4.7.4, two parameters were chosen to define the shape of the yield and plastic potential surfaces. There is a need for a further parameter to fully define the yield and plastic potential surfaces: a size parameter. The size of the yield and plastic potential surfaces are defined by the parameter p_b, the intercept of the cap on the p axis (Figure 4.3). It is interesting to note that only the cap is associated with the size parameter. If the yield surface is reached on the shear surface, the cap must reduce in size (p_b decreasing) until the cap intersects the shear surface at the stress state. Consequently, even under this condition, the cap defines the size of the yield and plastic potential surfaces.

For the Drucker-Prager cap model, the ABAQUS software package requires that a hardening rule, defining the growth of the yield and plastic potential surfaces, be defined such that p_b is a function of ε_p^p, the volumetric component of the plastic strain. It places no further restrictions on the form of the hardening rule. The hardening rule is provided to ABAQUS as a list of ε_p^p, p_b points.

Adam (1997) described two approaches to the development of a hardening rule. The first approach, common with critical state models, was to assume that $de = -\lambda\, d(\ln p)$ where λ is a constant. Examination of most compression data for bagasse over a wide pressure range shows that λ decreases with pressure (Loughran & Adam 1998). The constant λ approach has, however, been used where the pressure range is relatively small (Plaza, Harris & Kirby 2001, for example). Adam's second approach, that he subsequently adopted, was to *inverse-calibrate* by using the computational model to reproduce the load / displacement curve produced in a uniaxial compression test. Since the hardening rule was defined as a series of points, the calibration procedure consisted of a trial and error approach to adjust these points to match the load / displacement curve. While this approach achieved a good match to the load / displacement data, it was a laborious procedure and did not specifically define an alternative function for the hardening rule.

Downing, Loughran and Domanti (1999) refined the inverse-calibration procedure developed by Adam and applied a functional form to the hardening rule: $p_b = a \exp(b\, \varepsilon_p^p)$ where a and b are constants. The function was chosen for its ability to match the inverse-calibrated hardening rule developed by Adam.

A more fundamental approach was adopted here for the selection of a hardening rule. Butterfield (1979) argued that, for highly compressible soils,

$$d[\ln(1+e)] = -\lambda_1\, d(\ln p) \qquad \textbf{(4.39)}$$

is a more appropriate form for a hardening rule than $de = -\lambda\, d(\ln p)$, the classical soil model hardening rule. Butterfield's approach has been adopted here.

Figure 4.4 compares the suitability of the constant λ and constant λ_1 hardening rules. Models using both hardening rules were fitted to sample height and top platen pressure measurements from a uniaxial compression test of the type described in section 5.2. The experimental and constant λ_1 model data are the test 1 data presented in Figure 5.3. An equivalent model was developed using the constant λ model (Kent 2001) for comparison. The constant λ_1 hardening rule is better able to match the curvature of the experimental data over the entire pressure range. While Figure 4.4 shows the constant λ hardening rule to be quite adequate for matching the pressure range up to 100 kPa, it is not satisfactory when the pressure range extends to about 2 MPa, typical pressure feeder pressures. The constant λ_1 hardening rule is considered more suitable over the wider pressure range.

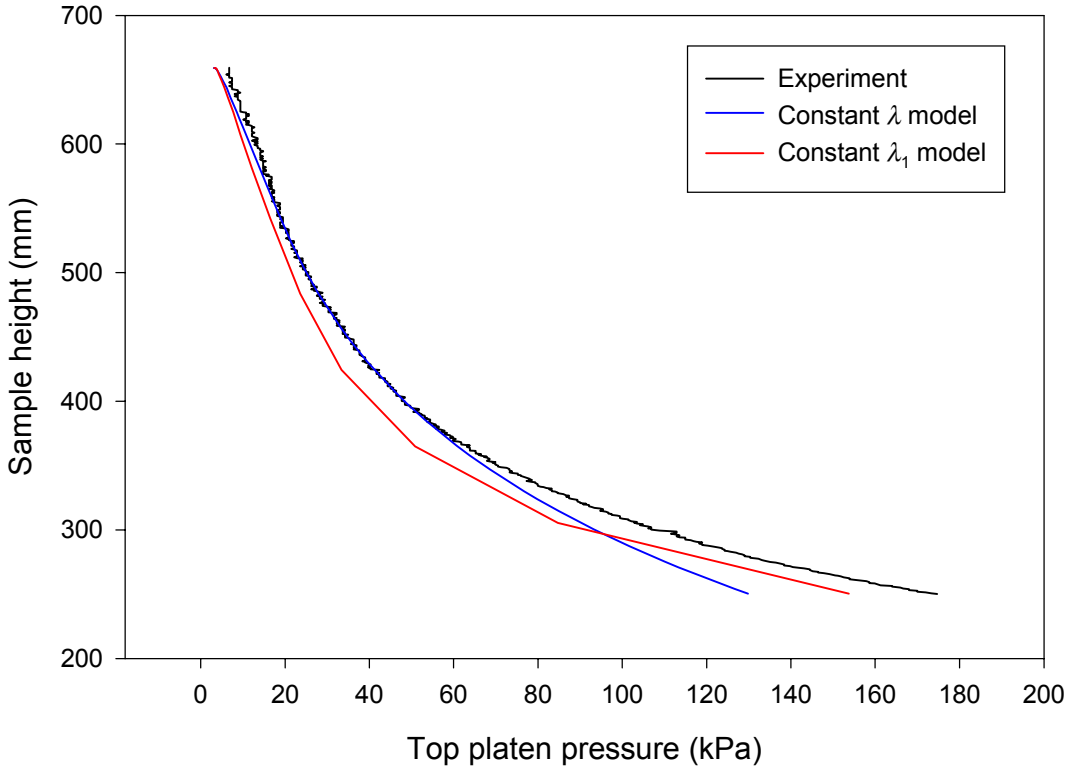

Figure 4.4 A comparison of constant λ and constant λ_1 hardening rules for modelling uniaxial compression

The suitability of the λ_1 model is discussed at greater length by Kent (2003).

Differentiating equation **(4.19)** and substituting equation **(4.39)** into it:

$$d\varepsilon_p = \frac{\lambda_1}{p} dp \qquad \textbf{(4.40)}$$

Substituting equation **(4.27)** and equation **(4.40)** into equation **(4.21)** to calculate $d\varepsilon_p^p$,

$$d\varepsilon_p^p = \frac{\left[\lambda_1 - \dfrac{\kappa}{\left(1+e^e\right)\left(1-\dfrac{p_t^e}{p}\right)}\right]}{p} dp \qquad \textbf{(4.41)}$$

Rearranging and substituting $p = p_b$, equation **(4.41)** becomes:

$$dp_b = \frac{p_b}{\left[\lambda_1 - \dfrac{\kappa}{\left(1+e^e\right)\left(1-\dfrac{p_t^e}{p_b}\right)}\right]} d\varepsilon_p^p \qquad \textbf{(4.42)}$$

From equations **(4.19)** and **(4.20)**,

$$1 + e^e = \frac{1+e}{\exp\left(-\varepsilon_p^p\right)} \qquad \textbf{(4.43)}$$

Substituting equation **(4.43)** into equation **(4.42)**,

$$dp_b = \frac{p_b}{\left[\lambda_1 - \dfrac{\kappa \exp\left(-\varepsilon_p^p\right)}{\left(1+e\right)\left(1-\dfrac{p_t^e}{p_b}\right)}\right]} d\varepsilon_p^p \qquad \textbf{(4.44)}$$

Integrating equation **(4.39)**,

$$1 + e = \left(1+e_0\right)\left(\frac{p_b}{p_{b0}}\right)^{-\lambda_1} \qquad \textbf{(4.45)}$$

Substituting equation **(4.45)** into equation **(4.44)**,

$$dp_b = \frac{p_b}{\left[\lambda_1 - \dfrac{\kappa \exp\left(-\varepsilon_p^p\right)}{\left(1+e_0\right)\left(\dfrac{p_b}{p_{b0}}\right)^{-\lambda_1}\left(1-\dfrac{p_t^e}{p_b}\right)}\right]} d\varepsilon_p^p \qquad \textbf{(4.46)}$$

Equation **(4.46)** defines the hardening rule in differential form. In summary, only one additional parameter is required to define the hardening rule: λ_1.

4.8 Constitutive behaviour of the fluid phase

Darcy's law was used to describe the constitutive behaviour of the fluid phase:

$$\boldsymbol{v} = -\frac{k}{\mu_v}\boldsymbol{\nabla} P \qquad \textbf{(4.47)}$$

where $\boldsymbol{v} = \begin{bmatrix} v_x & v_y & v_z \end{bmatrix}^T$ and $\boldsymbol{\nabla} = \begin{bmatrix} \dfrac{\partial}{\partial x} & \dfrac{\partial}{\partial y} & \dfrac{\partial}{\partial z} \end{bmatrix}^T$. The symbol k represents the *intrinsic permeability* of the bagasse mat and μ_v is the *absolute* or *dynamic* viscosity.

Darcy's law is commonly used to describe fluid flow through porous media. Murry (1960a) was the first to test Darcy's law for prepared sugarcane and found it to be generally applicable, particularly at lower void ratios.

The ABAQUS software package allows permeability to be defined as a function of void ratio. A permeability equation of the following form was used (based on the relationship used by Adam and Loughran 1998):

$$k = k_1 \left(1+e\right)^{k_2} \qquad \textbf{(4.48)}$$

where k_1 and k_2 are constants. Downing (1999a) used a similar relationship, $k = k_1 (e)^{k_2}$. While both relationships were considered equally suitable, equation **(4.48)** was chosen for compatibility with the solid phase constitutive model where the $1 + e$ term was extensively used.

4.9 Concluding remarks

The preceding sections detail the governing equations for the computational feeding model used throughout this study. While previous researchers largely defined the governing equations, this study introduced the constitutive equation defining the hardening rule as a function of the hardening parameter, λ_1.

To use the model, parameter values were required in order to define the constitutive behaviour of both the solid and fluid phases. The solid phase behaviour was defined by three elastic parameters (κ, ν and p_t^{el}), two parameters to define the shape of the yield and plastic potential surfaces (M and p_t) and one parameter to define the size of the yield and plastic potential surfaces (λ_1). The fluid phase behaviour was defined by three parameters: two intrinsic permeability parameters (k_1 and k_2) and the absolute viscosity (μ_v).

The methods used to determine the parameter values for the model are presented in chapter 5.

5 Determination of material parameters for the new feeding model

5.1 Introductory remarks

In chapter 4, the framework for a new throughput model was developed based on the elementary principles of equilibrium of forces and conservation of mass. In order to use the model, however, the physical behaviour of the bagasse feed material needs to be quantified in terms of material parameters for the selected constitutive models. In this chapter, the techniques used to determine the material parameters are described.

The new throughput model contains two constitutive models: one for the solid phase and one for the fluid phase. As summarised in section 4.9, the solid phase behaviour is defined by three elastic parameters (κ, v and p_t^e), two parameters to define the shape of the yield and plastic potential surfaces (M and p_t) and one parameter to define the size of the yield and plastic potential surfaces (λ_1). The fluid phase behaviour is defined by three parameters: two intrinsic permeability parameters (k_1 and k_2) and the absolute viscosity (μ_v).

This chapter presents the material testing methods used to provide the experimental data to determine the material parameters and the numerical techniques used to extract the material parameters from the experimental data. While only one method was used to measure the solid phase material parameters, two methods were used on different occasions to measure the fluid phase material parameters. Both methods are described and a comparison between the two methods is made.

5.2 Material parameters for the solid phase

5.2.1 Introductory remarks

As part of the work undertaken to validate the throughput models described in chapters 6 and 8, experiments were conducted with prepared sugarcane and bagasse of different sugarcane varieties and levels of preparation at different sites throughout Queensland. Since quarantine laws make it difficult to transport sugarcane between cane growing areas and since prepared sugarcane, in particular, deteriorates quickly, it was impractical to transport samples of the sugarcane used in the experiments to a single site for material property determination. Consequently, it was necessary for the apparatus used to determine the material parameters to be sufficiently portable to transport to the experimental sites. Since the material property tests were a relatively small component of the entire experimental programme, it was also necessary for the material property tests to require only a short period of time to complete.

Material parameters for critical state models are traditionally obtained from triaxial apparatus where the entire stress state of a sample is well defined. Cullen (1965) and Leitch (1996) carried out triaxial tests on prepared sugarcane and bagasse with limited success using conventional soil and rock testing apparatus. One of the limitations of the available triaxial apparatus was that they were not designed for the large deformations experienced by bagasse. In addition, the equipment was not portable and the tests were time consuming.

Plaza, Harris and Kirby (2001) experienced considerably more success at obtaining material parameters using a direct shear apparatus. While the information available from the direct shear test is more limited than that available from a triaxial apparatus, Plaza's apparatus was specifically designed for the large deformations experienced by bagasse. Once again, however, the equipment was not portable and considerable time was required to carry out sufficient tests to fully define the material behaviour.

A uniaxial compression test was chosen as the most suitable material property test for the experimental programme. A portable apparatus was relatively cheap to construct and required only a short time to complete a test. Adam (1997) and Downing, Loughran and Domanti (1999) previously used uniaxial compression tests to determine material parameters. Although the number of parameters that can be determined from a uniaxial compression test is less than from a direct shear test, the loss of information was a necessary compromise to obtain experimental data rapidly at the experimental sites.

5.2.2 Apparatus

The uniaxial test cell consisted of a 200 mm diameter, 800 mm high stainless steel cylinder (Figure 5.1). The size of the cylinder was selected to be large compared to the fibre length of prepared cane but not so large that the required sample size was difficult to handle. The height of the cylinder was chosen so that, at the maximum applied load, the sample height was still reasonably large (about 100 mm). The cylinder was designed for a maximum vertical pressure on the sample of 2 MPa.

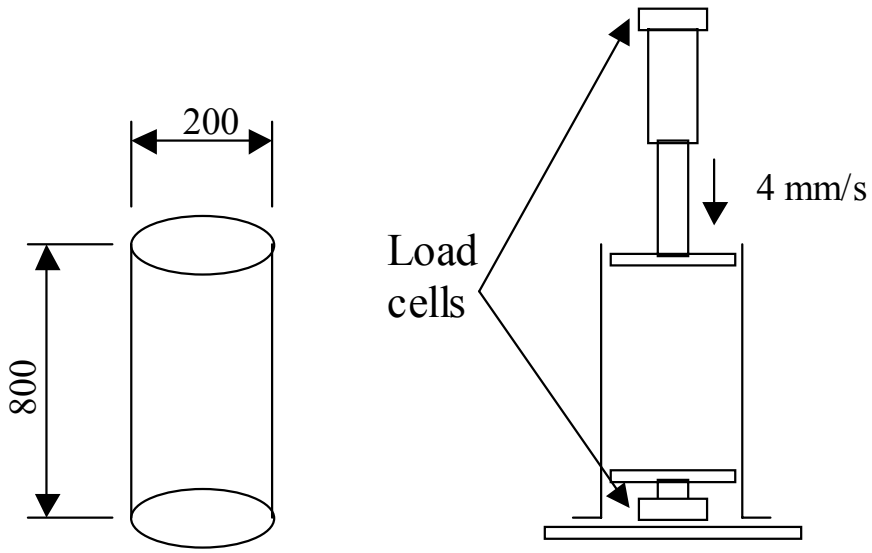

Figure 5.1 Uniaxial compression test cell used to provide experimental data for material parameter determination

The load was applied to the sample through a porous top platen. The porous platen allowed expressed fluids to escape the cell while maintaining low fluid pressure. The top platen was attached to a hydraulic cylinder that was controlled to achieve constant piston speed. A load cell was attached to the hydraulic cylinder to measure the applied load. A pressure sensor was fitted to the top platen to measure the pore pressure at the top of the sample.

The cell was used in two configurations.

In the first configuration (Figure 5.1), a porous bottom platen was used to contain the sample and allow the free flow of expressed fluids from the cell. A second load cell was attached to the bottom platen to measure the proportion of the applied load that reached the platen. The difference between the top and bottom platen force provided a measurement of the load transmitted to the cylinder from the sample through friction. A pressure sensor was also fitted to the bottom platen to measure the pore pressure at the bottom of the sample. Speeds in the order of 4 mm/s were used to determine the material parameters for the solid phase directly. Only results up to the point of juice expression were used for material parameter determination so that juice expression and its resulting build up of pore pressure had negligible effect on the results.

In the second configuration (Figure 5.2), the bottom platen was removed and an impermeable plate was fixed to the bottom of the cylinder. The plate was strain gauged to measure the sample pressure at the bottom of the cylinder. A pressure sensor was used to record the pore pressure at the bottom of the cylinder as well. In this configuration, all expressed fluid escaped the cylinder through the top platen only. Speeds from 1 mm/s to 100 mm/s were used to determine material parameters for the solid phase indirectly. The technique used for accounting for the build up of pore pressure is described in section 5.4.

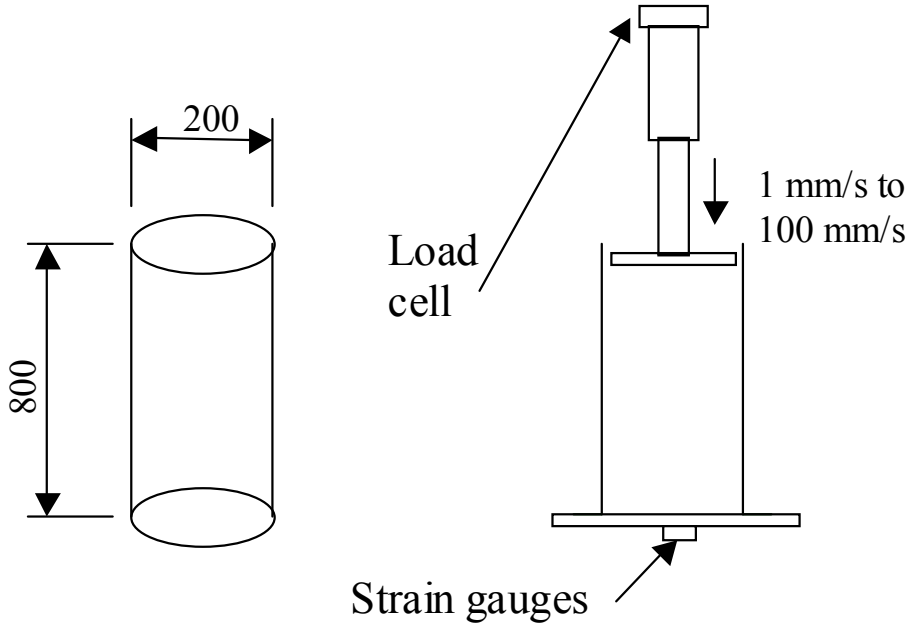

Figure 5.2 Uniaxial compression test cell used to provide experimental data for material parameter determination (second configuration)

In both configurations, the sample height was recorded to provide a deformation measurement.

5.2.3 Experimental method

A typical test involved the compression of a sample at constant speed until the ultimate pressure of 2 MPa was reached.

For some tests, the compression was halted part of the way through the test. The piston was then reversed until the load was completely removed. Once the load was removed, the compression resumed. This alternative method provided some information to determine the elastic parameters.

5.2.4 The parameter estimation process

To estimate the material parameters, a parameter estimation software package called PEST (Watermark Numerical Computing 2000) was used to match a series of selected top and bottom platen loads from the experimental data to the equivalent loads determined from a model of the test cell. The parameter estimation software adjusted the material parameters until an objective function, essentially the sum of squared deviations between model and test results, was minimised.

The model of the test cell was constructed within the ABAQUS finite element analysis software (Hibbitt, Karlsson & Sorensen 2000). The model consisted of eight four-node axisymmetric elements. Frictional contact on the cylinder sidewall was modelled assuming a constant coefficient of friction. The position and speed of the top platen were modelled closely by applying a velocity boundary condition on the top surface of the sample. Consequently, the model's time scale matched the time scale in the experimental data quite closely.

The model was used to estimate four of the six material parameters: two elastic parameters, κ and v; a yield surface and plastic potential surface shape parameter, M[1]; and the yield surface and plastic potential surface size parameter, λ_1. No attempt was made to quantify the remaining two parameters, p_t^e and p_t, from the experimental data. These parameters were set to zero. This assignment was not expected to alter the estimated values for the other parameters.

---

[1] Because of the specific constraint on the model that $R = \frac{1}{\tan\beta}$ (equation **(4.34)**) where $\tan\beta = \mathrm{M}$ (equation **(4.35)**), M is the parameter that, in uniaxial compression, is strongly linked to the ratio of radial to axial stress. Since the coefficient of friction on the sidewall was defined for this exercise, M was the parameter that had most influence on the ratio of bottom platen pressure to top platen pressure. Consequently, M could be determined from the test but what was measured was not the true slope of the shear surface.

No attempt was made to measure the coefficient of friction on the cylinder sidewall. Coefficient of friction measurements have been made previously for bagasse on steel surfaces at low pressures with quite variable results. Bernhardt (1996) reported values less than 0.5. Plaza and Kent (1998) reported values close to 1.0. It is also well established that coefficient of friction is a function of pressure. To account for the lack of a known coefficient of friction, material parameters were estimated for two constant coefficient of friction values: 0.5 and 1.0.

Initially, the void ratio and the stress state were assumed constant throughout the test cell.

The initial void ratio, e_0, was determined from:

$$e_0 = \frac{\pi\, D_i^2\, z_0\, \rho_f}{4\, f\, m} - 1 \qquad \textbf{(5.1)}$$

where D_i is the internal diameter of the cylinder, z_0 is the initial height of the sample, ρ_f is the density of fibre (1530 kg/m^3), f is the fibre content of the sample (expressed as a fraction) and m is the initial sample mass. The initial height was the height of the sample at an arbitrarily chosen time near the start of the test when load first started to register on the load cells.

The initial stress in the axial direction, σ_{a0}, was calculated as the average stress from the two load cell force measurements corresponding to the initial height:

$$\sigma_{a0} = \frac{2\left(F_{t0} + F_{b0}\right)}{\pi\, D_i^2} \qquad \textbf{(5.2)}$$

where F_{t0} and F_{b0} are the top and bottom load cell measurements respectively.

Since the radial stress was not measured, the initial stress in the radial direction needed to be determined from the constitutive equation **(4.21)**. The constitutive equation is somewhat simplified for the test cell. Only two direct stress components are required

(axial and radial). There are no shear stresses. There is only one direct strain component (axial). There is no radial or shear strain. Based on these simplifications, equations **(4.15)**, **(4.16)**, **(4.17)** and **(4.18)** reduce to:

$$p = -\frac{1 + 2\,K_0}{3}\,\sigma_a \qquad \textbf{(5.3)}$$

$$q = -(1 - K_0)\,\sigma_a \qquad \textbf{(5.4)}$$

$$d\varepsilon_p = -d\varepsilon_a \qquad \textbf{(5.5)}$$

$$d\varepsilon_q = -\frac{2}{3}\,d\varepsilon_a \qquad \textbf{(5.6)}$$

where σ_a is the axial stress, $d\varepsilon_a$ is the axial strain increment and K_0 is the ratio of the radial to the axial stress.

For $\eta = \frac{q}{p}$,

$$q = \eta\; p \qquad \textbf{(5.7)}$$

Dividing equation **(5.4)** by equation **(5.3)** and substituting equation **(5.7)** into the result:

$$K_0 = \frac{3 - \eta}{2\,\eta + 3} \qquad \textbf{(5.8)}$$

The elastic behaviour was defined by equation **(4.22)**. Substituting equations **(4.28)** and **(4.29)** into equation **(4.22)**:

$$\begin{bmatrix} d\varepsilon_p^e \\ d\varepsilon_q^e \end{bmatrix} = \frac{1}{(1+e^e)p} \begin{bmatrix} \dfrac{\kappa}{1-\dfrac{p_t^e}{p}} & 0 \\ 0 & \dfrac{2(1+\nu)\kappa}{9(1-2\nu)\left(1-\dfrac{p_t^e}{p}\right)} \end{bmatrix} \begin{bmatrix} dp \\ dq \end{bmatrix} \qquad \textbf{(5.9)}$$

During the initial compression in the test cell, the sample is continuously deforming plastically. Consequently, the stress state must be on the yield surface. The plastic deformation is defined by equation **(4.24)**. Since growth of the yield surface (defined by p_b) requires the stress state to be on the cap (section 4.7.5), the yield and plastic potential surfaces for the cap, equation **(4.38)**, was used to define the plastic behaviour.

Substituting equation **(5.7)** into equation **(4.38)** and rearranging,

$$p_b = \frac{1+\dfrac{\eta^2}{\mathrm{M}^2}-\dfrac{p_t}{p}}{1-\dfrac{p_t}{p}}\, p \qquad \textbf{(5.10)}$$

Substituting equation **(5.10)** into equation **(4.42)** and rearranging,

$$\frac{\partial p_b}{\partial \varepsilon_p^p} = \frac{(1+e^e)\left[1-\dfrac{\dfrac{p_t^e}{p}\left(1-\dfrac{p_t}{p}\right)}{1+\dfrac{\eta^2}{\mathrm{M}^2}-\dfrac{p_t}{p}}\right]\dfrac{1+\dfrac{\eta^2}{\mathrm{M}^2}-\dfrac{p_t}{p}}{1-\dfrac{p_t}{p}}\, p}{\lambda_1 (1+e^e)\left[1-\dfrac{\dfrac{p_t^e}{p}\left(1-\dfrac{p_t}{p}\right)}{1+\dfrac{\eta^2}{\mathrm{M}^2}-\dfrac{p_t}{p}}\right]-\kappa} \qquad \textbf{(5.11)}$$

A parameter, c_1, was defined to simplify equation **(5.11)** where:

$$c_1 = \frac{\lambda_1 \left(1+e^e\right)\left[1-\dfrac{\dfrac{p_t^e}{p}\left(1-\dfrac{p_t}{p}\right)}{1+\dfrac{\eta^2}{\mathrm{M}^2}-\dfrac{p_t}{p}}\right]-\kappa}{\left[1-\dfrac{\dfrac{p_t^e}{p}\left(1-\dfrac{p_t}{p}\right)}{1+\dfrac{\eta^2}{\mathrm{M}^2}-\dfrac{p_t}{p}}\right]\left(1+\dfrac{\eta^2}{\mathrm{M}^2}-\dfrac{p_t}{p}\right)} \qquad \textbf{(5.12)}$$

Substituting equation **(5.12)** into equation **(5.11)**:

$$\frac{\partial p_b}{\partial \varepsilon_p^p} = \frac{\left(1+e^e\right)\ p}{c_1\left(1-\dfrac{p_t}{p}\right)} \qquad \textbf{(5.13)}$$

Differentiating equation **(4.38)** with respect to p and substituting equation **(5.10)** into the result,

$$\frac{\partial F}{\partial p} = \frac{\partial G}{\partial p} = \frac{4\ p\left[1-\dfrac{\eta^2}{\mathrm{M}^2}-2\dfrac{p_t}{p}+\left(\dfrac{p_t}{p}\right)^2\right]}{1-\dfrac{p_t}{p}} \qquad \textbf{(5.14)}$$

A parameter, c_2, was defined to simplify equation **(5.14)** where:

$$c_2 = \frac{1-\dfrac{\eta^2}{\mathrm{M}^2}-2\dfrac{p_t}{p}+\left(\dfrac{p_t}{p}\right)^2}{1-\dfrac{p_t}{p}} \qquad \textbf{(5.15)}$$

Substituting equation **(5.15)** into equation **(5.14)**:

$$\frac{\partial F}{\partial p} = \frac{\partial G}{\partial p} = 4\ p\ c_2 \qquad \textbf{(5.16)}$$

Differentiating equation **(4.38)** with respect to q and substituting equation **(5.7)** into the result,

$$\frac{\partial F}{\partial q} = \frac{\partial G}{\partial q} = \frac{8\,\eta\ p}{\mathrm{M}^2} \qquad \textbf{(5.17)}$$

Differentiating equation **(4.38)** with respect to p_b:

$$\frac{\partial F}{\partial p_b} = -4\ p\left(1 - \frac{p_t}{p}\right) \qquad \textbf{(5.18)}$$

Substituting equations **(5.13)**, **(5.16)**, **(5.17)** and **(5.18)** into equation **(4.24)**:

$$\begin{bmatrix} d\varepsilon_p^p \\ d\varepsilon_q^p \end{bmatrix} = \frac{1}{\left(1+e^e\right)p} \begin{bmatrix} c_1\ c_2 & \dfrac{2\,c_1\,\eta}{\mathrm{M}^2} \\ \dfrac{2\,c_1\,\eta}{\mathrm{M}^2} & \dfrac{4\,c_1\,\eta^2}{\mathrm{M}^4\ c_2} \end{bmatrix} \begin{bmatrix} dp \\ dq \end{bmatrix} \qquad \textbf{(5.19)}$$

Substituting equations **(5.9)** and **(5.19)** into equation **(4.21)**:

$$\begin{bmatrix} d\varepsilon_p \\ d\varepsilon_q \end{bmatrix} = \frac{1}{\left(1+e^e\right)p} \begin{bmatrix} \dfrac{\kappa}{1-\dfrac{p_t^e}{p}} + c_1\ c_2 & \dfrac{2\,c_1\,\eta}{\mathrm{M}^2} \\ \dfrac{2\,c_1\,\eta}{\mathrm{M}^2} & \dfrac{2\left(1+\nu\right)\kappa}{9\left(1-2\,\nu\right)\left(1-\dfrac{p_t^e}{p}\right)} + \dfrac{4\,c_1\,\eta^2}{\mathrm{M}^4\ c_2} \end{bmatrix} \begin{bmatrix} dp \\ dq \end{bmatrix} \qquad \textbf{(5.20)}$$

For uniaxial compression, equations **(5.5)**, **(5.6)** and **(5.7)** can be substituted into equation **(5.20)**. Dividing the equation for $d\varepsilon_p$ in equation **(5.20)** by the equation for $d\varepsilon_q$ in equation **(5.20)** and rearranging:

$$\left[\frac{\eta(1+\nu)}{3(1-2\nu)}-1\right]\frac{\kappa}{1-\frac{p_t^e}{p}}+c_1\left(\frac{6\eta^3}{M^4 c_2}+\frac{3\eta}{M^2}-\frac{2\eta^2}{M^2}-c_2\right)=0 \qquad \textbf{(5.21)}$$

Equation **(5.21)** can be solved for η. The value for η can then be substituted into **(5.8)** to calculate K_0. Multiplying K_0 by the initial axial stress σ_{a0} gives the initial radial stress.

The use of porous top and bottom platens and the selection of low platen speeds were designed to minimise the effect of fluid expression on the test results. Consequently, the ABAQUS model used to estimate the solid phase material parameters did not include a fluid phase.

5.2.5 An example of the parameter estimation process

To illustrate the results of the parameter estimation process, two tests from the same batch of prepared cane were examined. The tests were carried out as part of the series described in section 6.4.2. The tests were carried out using the cane variety Q124 and were prepared with a shredder speed of 1200 r/min in the Sugar Research Institute small-scale shredder (section 6.3.2). One of these tests simply involved compressing the cane at nominally constant platen speed (test 17) while the other test involved stopping the test before the final pressure was reached and reversing the platen to remove the load before continuing to compress the sample (test 18).

Figure 5.3 shows the pressure and sample height results from the uniaxial compression tests and the equivalent predictions from the model using the estimated parameters. Although the uniaxial compression tests were conducted up to a top platen pressure of 2 MPa, the parameter estimation process was only conducted on the first portion of the experimental data where sample height was greater than 250 mm (top platen pressure less than about 200 kPa). At the range of pressures examined, little juice expression occurred and the assumption that the fluid phase could be ignored in the model was considered valid. The parameters estimated from this data were used to model milling

tests where juice was not expressed (6.3), so the range of pressures examined was also the range of pressures of interest.

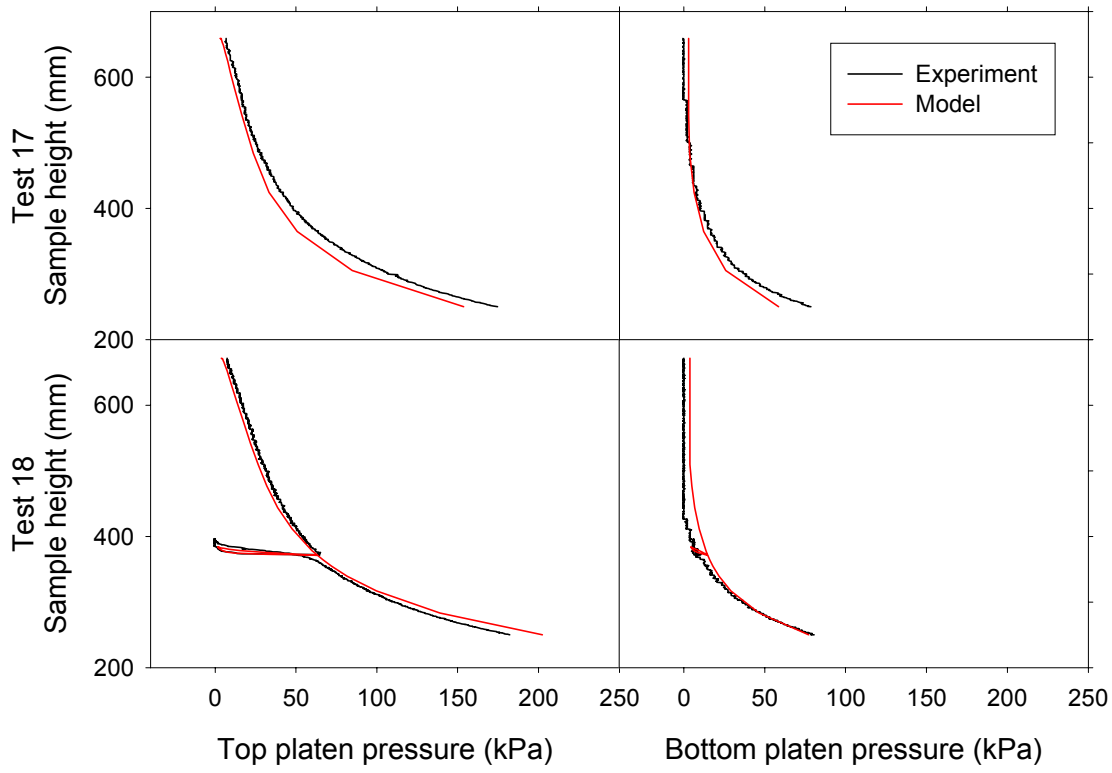

Figure 5.3 Typical experimental and model results for uniaxial compression tests obtained from parameter estimation process for solid phase material parameters

Figure 5.3 shows the effect of friction on the results. The bottom platen pressure was typically half the magnitude of the top platen pressure indicating that about half the top platen pressure was transmitted to the cylinder wall through friction. As discussed in section 5.2.4, no attempt was made to determine the coefficient of friction. Instead, the parameter estimation process was carried out twice assuming coefficients of friction of 0.5 and 1.0 respectively. Only one model prediction is shown in Figure 5.3 because the model predictions were virtually identical.

Table 5.1 shows the estimated parameters for each assumed value of coefficient of friction (μ). Large differences in the predicted values of v and M were found for the

different values of coefficient of friction while the values for λ_1 were identical. The relationship between coefficient of friction and v and M is well established (Plaza, Harris & Kirby 2001). From the solid phase material model definition, based on the assumptions in equations **(4.23)** and **(4.34)**, the parameters v and M are closely linked to K_0, the ratio of the radial to the axial stress. The frictional force on the sidewall is a function of the product μK_0 (using an equation like equation **(3.5)**). As explained by Plaza, Harris and Kirby (2001), it is really K_0 rather than v and M that is defined by the parameter estimation procedure although v and M are the parameters being used to achieve a particular value for K_0.

Table 5.1 Results of the parameter estimation process for the two assumed values of coefficient of friction

μ	κ	ν	M	λ_1
0.5	0.49	0.30	2.0	0.28
1.0	0.56	0.17	2.8	0.28

To assess the success of the parameter estimation process in identifying the correct solid phase material parameter values, a sensitivity analysis was conducted in which the objective function (described in section 5.2.4) was determined over a range of parameter values. The results of the sensitivity analysis for a coefficient of friction of 0.5 are presented in Figure 5.4. The contours in Figure 5.4 show the ratio of the difference between the objective function at particular parameter values and the objective function at the estimated parameters to the objective function at the estimated parameters. Figure 5.4 shows that λ_1 was particularly well defined with the objective function increasing by 10% (0.10 in Figure 5.4) for a change in λ_1 of less than 0.01 in 0.28. The other plastic parameter, M, was also quite well defined, although as discussed earlier, was dependent on the assumed coefficient of friction. The elastic parameters κ and v, however, were quite poorly defined, giving little confidence in their value.

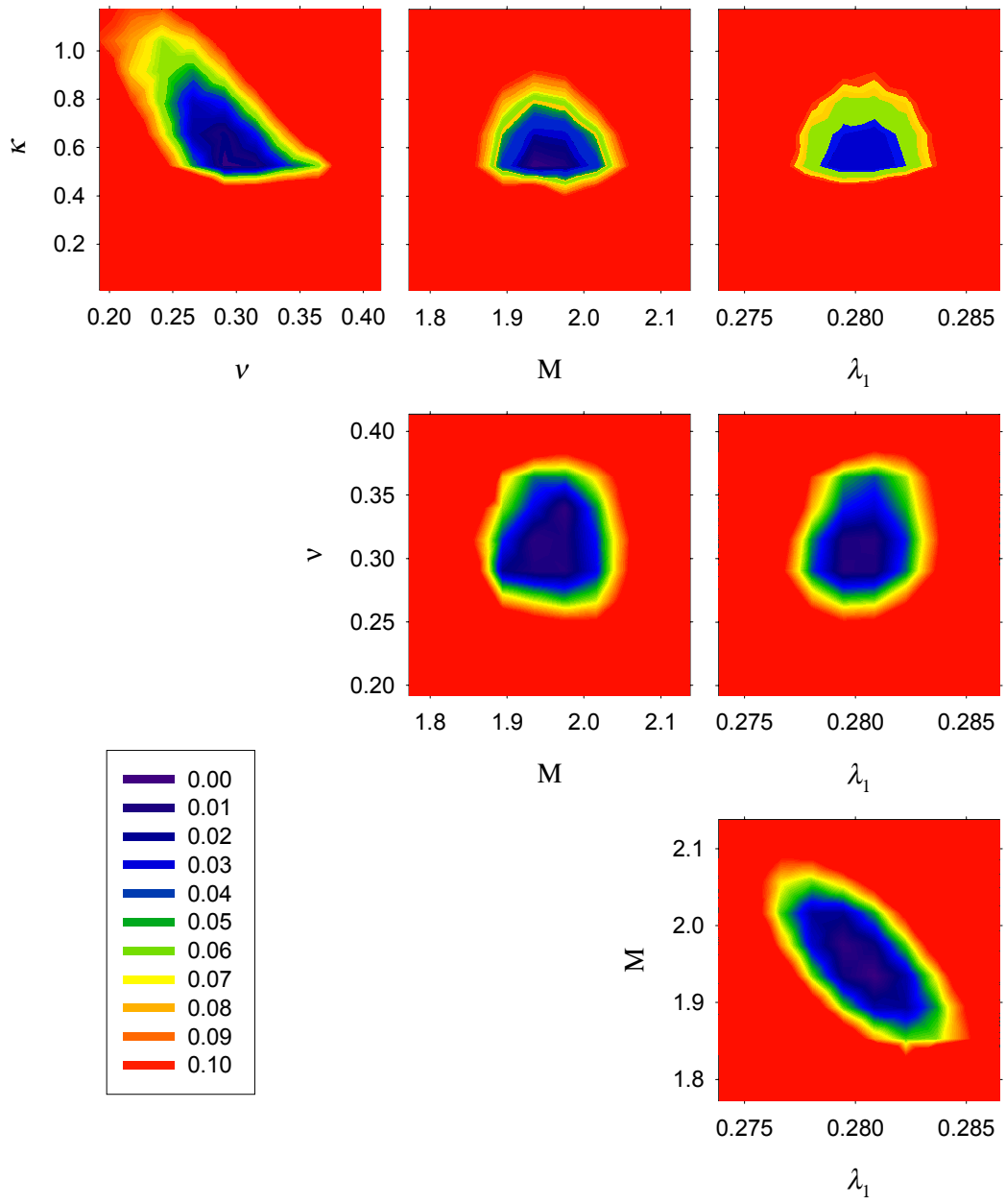

Figure 5.4 **Results of sensitivity analysis for solid phase material parameters showing the relative change in the objective function for a change in the material parameters**

5.2.6 Concluding remarks

A procedure has been defined for determining material parameter values to use in the solid phase constitutive model defined in section 4.7.

The procedure uses a simple uniaxial compression test to rapidly gain some information with which to determine the parameters. The test apparatus measures the force on the bagasse at the top and bottom of the sample and the sample height.

The parameter estimation process involves matching a series of force measurements from the uniaxial compression test to equivalent force values determined from a model of the test. Material parameters are adjusted to minimise the differences between the experimental and model results.

The procedure estimates four parameters: two elastic parameters, κ and ν; a yield surface and plastic potential surface shape parameter, M; and the yield surface and plastic potential surface size parameter, λ_1. The remaining two parameters, p_t^e and p_t, were assumed to be zero during the parameter estimation process. Of the four parameters, λ_1, was best defined. The parameter, M, was also reasonably well defined in the estimation process but was affected by the assumed coefficient of friction. The two elastic parameters, κ and ν, were not well defined.

5.3 Material parameters for the fluid phase – steady state method

5.3.1 Introductory remarks

As discussed in section 5.1, the material parameters required to describe the fluid phase constitutive behaviour were the intrinsic permeability parameters and the absolute viscosity. No attempt was made to measure the absolute viscosity. Known values were used from other sources. The focus of the tests carried out to measure the material

parameters for the fluid phase was the measurement of intrinsic permeability as a function of void ratio.

As discussed in section 5.2.1, the tests required for the determination of material parameters were performed at several sites in Queensland requiring the test apparatus to be relatively portable. The tests were carried out as part of much larger experimental programmes and needed to be carried out relatively quickly so that they did not take too many resources away from the main programme.

This section describes the *steady state* method used to determine permeability. Bullock (1957), Holt (1960), Holt (1961), and Downing (1999a) previously used steady state tests to define permeability as a function of void ratio or compression ratio.

5.3.2 Apparatus

Downing (1999a) described the test cell used for the material property tests (Figure 5.5). A measured mass of bagasse was placed in the specimen chamber and, through the use of appropriately sized spacers, compressed to the desired void ratio. Water was then pumped through the cell and exited the specimen chamber through either the centre section, identified in Figure 5.5 as the outlet manifold, or the outer section, identified in Figure 5.5 as the waste flow. The need for the isolated centre section arose from the known low-resistance path for the water flow at the bagasse / cell wall interface (Holt 1960). Proportionally more water flows around the sides of the cell than passes through the bagasse. By assuming the flow through the cell was largely in the vertical direction (from the inlet to the outlet), it was assumed that the flow through the centre section originated from a centre section of the same area at the top of the sample.

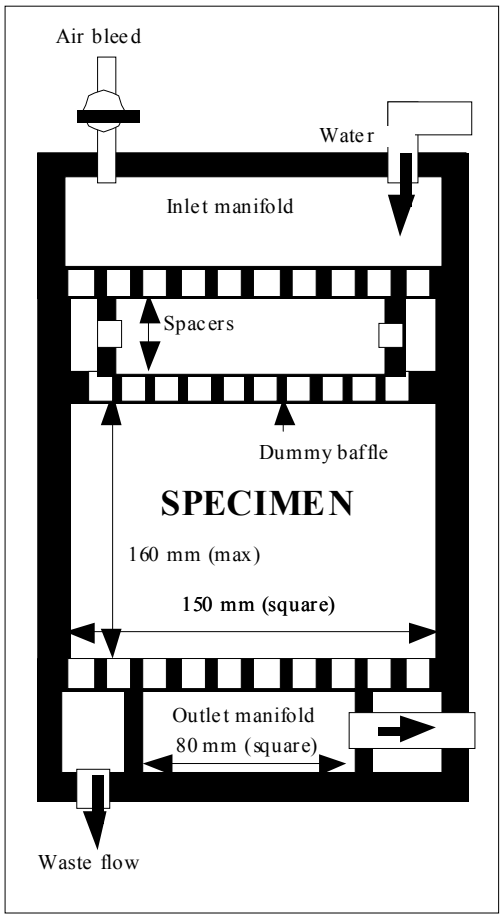

Figure 5.5 Steady state permeability test apparatus (Downing 1999)

While the cell instrumentation was changed for different test series, the measurement requirements were met in each case. The main instrumentation requirements were for the measurement of the pressure drop in the water across the sample and the flow rate through the outlet manifold. A pressure gauge or transducer was fitted to either the inlet manifold or the pipe leading to the inlet manifold to measure the inlet pressure. In some cases, the outlet pressure was assumed to be atmospheric pressure while in other cases, the pressure in the outlet manifold was measured using a pressure transducer. The flow through the outlet manifold was either measured using a flow meter or measured from the time taken to fill a container holding a known volume.

5.3.3 Experimental method

A typical test involved a gradual increase in water pressure to a maximum inlet pressure of about 2 MPa while measuring the flow through the outlet manifold. In some cases, the pressure was increased in steps and maintained constant at each step until a steady flow rate was achieved. For some tests, the pressure was then reduced. In some cases, the pressure cycle was repeated many times.

5.3.4 The parameter estimation process

Permeability has traditionally been calculated directly using equation **(4.47)** (Bullock 1957, Holt 1960, Holt 1961, and Downing 1999a). Rearranging equation **(4.47)** and using ΔP to represent the pressure drop across the cell and Δx to represent the height of the sample in the specimen chamber,

$$k = \frac{\mu_v \, \Delta x}{A} \frac{Q}{\Delta P} \qquad \textbf{(5.22)}$$

where the superficial flow velocity $v = \frac{Q}{A}$ and Q is the water flow rate through the outlet manifold, A is the cross-sectional area of the outlet manifold (6439 mm^2) and μ_v is the absolute viscosity of the fluid. To determine the constitutive parameters, k_1 and k_2, the steady state permeability test was repeated at different void ratios. The constitutive parameters were determined from a regression fit of the permeability / void ratio results to the permeability equation (equation **(4.48)**). The void ratio used in the regression equation was the average void ratio calculated from:

$$e = \frac{A_T \, \Delta x \, \rho_f}{f \, m} - 1 \qquad \textbf{(5.23)}$$

where A_T is the total cross-sectional area of the test cell, ρ_f is the density of fibre, f is the fibre content of the sample and m is the sample mass.

Loughran and Adam (1998) recognised that the constitutive parameters calculated using the above method were in error at higher void ratios due to *seepage-induced consolidation*. Depending on the relative magnitudes of the effective stress imposed on the sample during compression to the required void ratio and the pore pressure used to impose a water flow, the void ratio will increase on the water inlet side of the sample and may decrease on the water outlet side of the sample. This void ratio gradient will cause a permeability gradient that may not be well represented by the average void ratio and average permeability calculated using equations **(5.22)** and **(5.23)**. Loughran and Adam (1998) used a model of the test cell to match the pressure drop and flow rate conditions in order to determine appropriate constitutive parameters. A modified version of that procedure was used in this study to determine the permeability constitutive parameters from the steady state test cell results. A comparison of the results of the traditional, direct, method of calculation and the method used here is presented in section 5.3.5.

The estimation process adopted for determination of the permeability parameters from the steady state test was similar to that used to determine the solid phase material parameters (section 5.2.4).

The parameter estimation package, PEST (Watermark Numerical Computing 2000) was used to match the measured flow rates from the experimental data to the equivalent values determined from a model of the test cell. As discussed in section 5.2.4, PEST minimises an objective function that is essentially the sum of squared deviations between the experimental data and the model predictions.

The model of the test cell was constructed within the ABAQUS finite element analysis software (Hibbitt, Karlsson & Sorensen 2000). The test cell was modelled using two-dimensional, plane strain, four-node elements. Unlike the model used to determine the solid phase material parameters (section 5.2.4), the effect of sidewall friction was assumed negligible. Due to the one-dimensional nature of the flow behaviour and the assumption of no sidewall friction, the transverse dimensions of the test cell were of no consequence and the model was constructed using a single column of elements in the direction of the water flow. Each element was approximately square with a typical

dimension of 10 mm. The model was used to simulate the initial compression of the sample into the permeability cell and the water pressure loading.

The model was used only to estimate the two permeability parameters, k_1 and k_2. Values for the six solid phase material parameters were assumed. Like the solid phase material parameter estimation procedure, the tensile parameters, p_t^e and p_t, were set to zero. Because the model was essentially a one-dimensional model, the two parameters that describe the behaviour in the transverse dimension, v and M, had no effect on the model results. The important parameters were κ and λ_1. Estimates for these parameters were obtained from the results of compression tests.

5.3.5 An example of the parameter estimation process

To illustrate the results of the parameter estimation process, three tests from the same batch of prepared cane are discussed here. The tests were carried out as part of the series described in section 5.5.3. The tests were carried out using cane prepared in the Sugar Research Institute's Waddell hammer mill (section 5.5.2) at a speed of 750 r/min for 10 s with a sample thickness of 104 mm at average void ratios of approximately 9, 7 and 5, respectively. The tests were identified as tests 7, 9 and 4 for the three void ratios respectively.

Figure 5.6 shows a pressure cycle (described in section 5.5.3) for each of the three tests and a regression line forced to go through the origin for each test. The slope of the regression line for each plot provides $\frac{Q}{\Delta P}$ for the permeability calculation (equation **(5.22)**). Of the several pressure cycles carried out for each test, the cycle for each test shown in Figure 5.6 is the first cycle for which the regression analysis returned a positive R^2 value (the second cycle for test 7 and the first cycle for tests 9 and 4). Negative R^2 values occurred where the best fit through the data should not have passed through the origin. The absolute viscosity of the fluid used in the permeability calculation was 0.894 mPa.s, the tabulated value for water at a temperature of 25°C (Streeter & Wiley 1981).

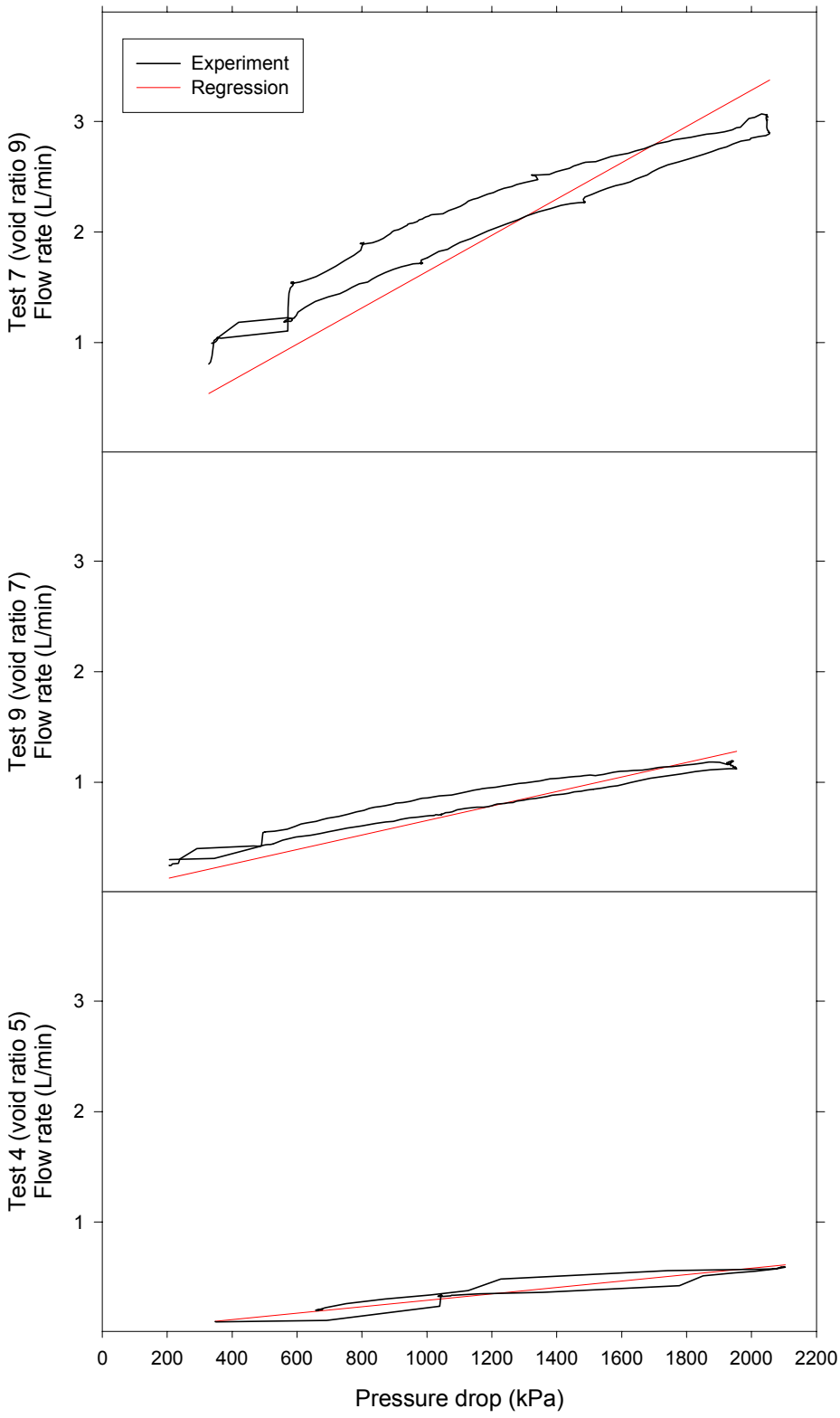

Figure 5.6 Typical experimental results for the steady state permeability tests

To determine permeability as a function of void ratio, the three tests were modelled as discussed in section 5.3.4. A single parameter estimation process was used to match the flow rate at the start of the loading cycle (the initial low water pressure), at the peak load (the highest water pressure) and at the end of the loading cycle (the final low water pressure) for all three tests simultaneously. The parameter values obtained from the parameter estimation process were $k_1 = 3.9 \times 10^{-18}$ m^2 and $k_2 = 5.9$.

Figure 5.7 shows the three permeability values calculated directly from the slopes of the regression lines shown in Figure 5.6 using equation **(5.22)** at the nominal void ratio (equation **(5.23)**) and a line representing the void ratio versus permeability relationship determined from the estimated k_1 and k_2 values. The discrepancy between the permeability values calculated directly and the permeability curve determined by the parameter estimation procedure represents the error in the directly calculated values. The directly calculated permeability was quite close to the estimated permeability at the nominal void ratio of 4 while it was approximately one order of magnitude in error at the nominal void ratio of 9. The discrepancy between the directly calculated permeability and the estimated permeability measurements is believed to be caused by the relative magnitudes of the initial confining pressure and the pore pressure used to provide the water flow. At a void ratio of 9, the initial confining pressure was about 100 kPa, only 5% of the maximum pore pressure of 2 MPa. At a void ratio of 4, the initial confining pressure was about 500 kPa, 25% of the maximum pore pressure. With low confining pressure at the higher nominal void ratio, the maximum pore pressure caused considerable further deformation of the sample, changing the sample void ratio substantially from the conditions assumed to exist within the cell. As the initial confining pressure increased towards the maximum pore pressure, the pore pressure caused less deformation and the conditions in the cell were much closer to those assumed in the direct analysis, resulting in a closer match between the directly calculated permeability and the estimated permeability.

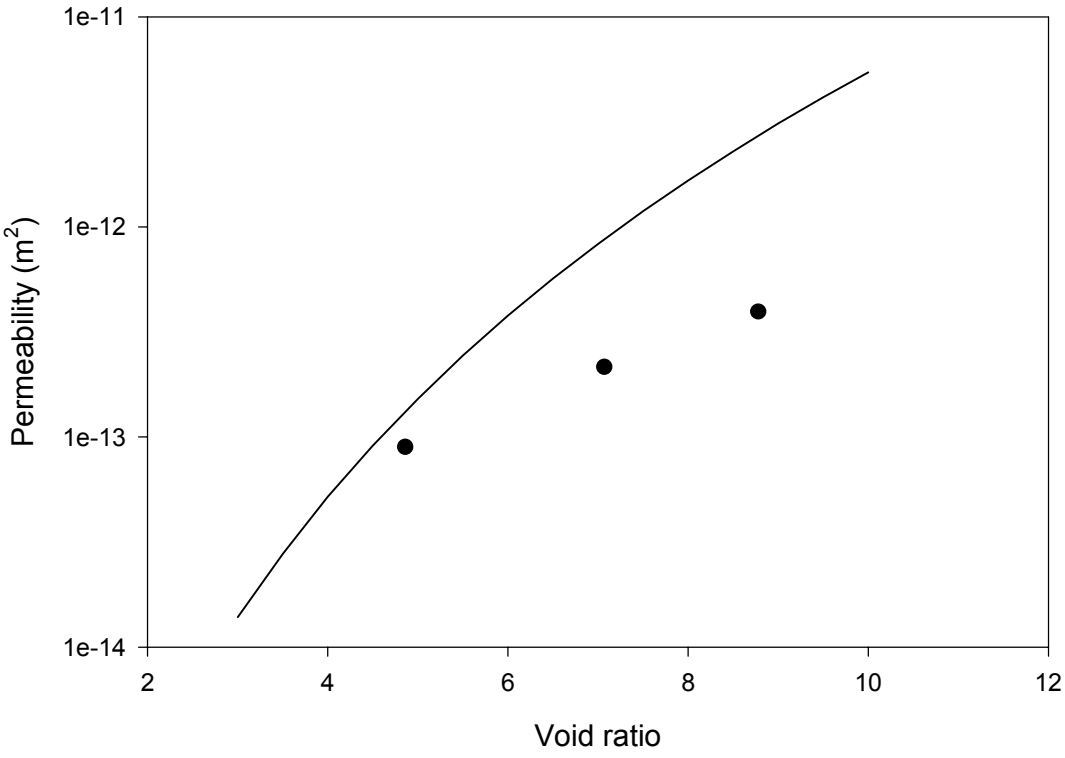

Figure 5.7 Regression fit to determine the permeability parameters for typical experimental results for the steady state permeability tests

The deformation of the sample resulting from the applied water pressure also provides an explanation for the slight nonlinearity of the pressure drop versus flow rate data shown in Figure 5.6. As the pressure increases, the void ratio in the cell decreases. It is likely that it is the reduction in void ratio that causes the decrease in the gradient of the pressure drop versus flow rate curve, rather than a deviation from Darcy's law.

5.3.6 Concluding remarks

The steady state permeability test provided a method of determining the permeability constitutive parameters, k_1 and k_2. Permeability was calculated directly from the constitutive equation for fluid flow (equation **(4.47)**) based on measurements of the pressure drop across the test cell and the flow rate through the outlet manifold. The directly measured permeability values, however, were previously found to be in error at

higher void ratios due to the difference between the initial confining pressure and the water pressure used to induce the water flow. To overcome this error for this study, a model of the permeability test was used in association with a parameter estimation process that involved matching the measured flow rates to those determined from the model. The permeability parameters were adjusted to minimise the difference between the measured flow rates and those predicted by the model.

5.4 Material parameters for the fluid phase – indirect method

5.4.1 Introductory remarks

The steady state method of determining material parameters for the fluid phase, described in section 5.3, is quite time consuming. An alternative, *transient*, test was explored and used on some occasions. The transient tests were uniaxial compression tests where the material parameters were indirectly determined from the platen load, pore pressure and platen displacement data.

The focus of the transient test was on the determination of the permeability parameters. As for the steady state test, no attempt was made to measure the absolute viscosity.

Holt (1960), Adam (1997) and Downing (1999a) all previously used transient tests to determine permeability as a function of void ratio or compression ratio.

5.4.2 Apparatus

The transient permeability tests were conducted using the same uniaxial compression test cell used to determine the solid phase constitutive parameters (section 5.2.2). The configuration of the test cell, as used for permeability determination, was shown in Figure 5.2.

The test apparatus differs from that used by Holt (1960), Adam (1997) and Downing (1999a). Holt and Adam had grooved top and bottom platens and porous side plates so that juice flow was in the transverse direction and also, to some extent, in the axial direction. Downing used porous top and bottom platens but impermeable side plates so that the juice flow was in both axial directions only. The test apparatus shown in Figure 5.2 has a porous top platen but an impermeable base on the cylinder so that the juice flows in only one axial direction.

The test cell in Figure 5.2 is similar in concept to that described by Znidarčić et al (1986). With juice flow in only one direction, the flow behaviour is as simple as possible.

A detailed description of the test cell is presented in section 5.2.2.

5.4.3 Experimental method

The test method used for the transient permeability tests was virtually identical to the compression-only uniaxial compression test described in section 5.2.3. The main differences were that the cell was filled with water before compression so that it was always fully saturated and that the speed of compression was varied between tests, up to a maximum of 100 mm/s, to increase or decrease the effect of juice flow on the measured behaviour as desired.

5.4.4 The parameter estimation process

The estimation process used to determine the fluid phase material parameters was similar to that used to determine the solid phase material parameters (section 5.2.4).

The parameter estimation package, PEST (Watermark Numerical Computing 2000) was used to match a series of bottom pore pressures and platen displacements from the experimental data to the equivalent values determined from a model of the test cell.

Rather than use the ABAQUS (Hibbitt, Karlsson & Sorensen 2000) package to build the model like in the solid phase material parameter estimation procedure (section 5.2.4), a special purpose model, based on the model of Banks (1984), was constructed to reduce solution time.

Since both compression and fluid flow occur in the same direction, the special purpose model was developed as a one-dimensional model. This assumption simplified the governing equations (chapter 4).

Taking the axial direction as the z direction, a material coordinate, w, was introduced where $dw = \frac{dV_g}{A}$ and A is the cross-sectional area of the test cell. The advantage of the material coordinate is that dw does not change in size during compression, unlike dz.

Now $A = \frac{dV}{dz}$ so $dw = \frac{dV_g}{dV} dz$. Substituting equations **(4.1)** and **(4.3)** into the expression for dw,

$$dw = \frac{1}{1+e} dz \qquad \textbf{(5.24)}$$

Equation **(5.24)** was used to restate the governing equations in terms of the material coordinate.

While considerable frictional behaviour was observed in the tests carried out to determine the solid phase material parameters (section 5.2.5), no frictional effects were observed in these tests (section 5.4.5). The most likely explanation for the difference is that the test cell walls were well lubricated in these tests where the cell was filled with water, unlike the tests to determine the solid phase material parameters where there was relatively little liquid flow. Since friction could be ignored, no frictional term was included in the force equilibrium equation **(4.7)**. Substituting equation **(5.24)** into the force equilibrium equation **(4.7)** and simplifying,

$$\frac{\partial \sigma_{zz}}{\partial w} = 0 \qquad \textbf{(5.25)}$$

Substituting equation **(5.24)** into the fluid continuity equation **(4.8)** and simplifying,

$$\frac{\partial e}{\partial t} + \frac{\partial v_z}{\partial w} = 0 \qquad \textbf{(5.26)}$$

Equation **(4.11)** provided the principle of effective stress:

$$\sigma_{zz} = \sigma'_{zz} - P \qquad \textbf{(5.27)}$$

A simplified version of the solid phase constitutive model was adopted. Since the compression test involved only increases in compressive stress, there was no need to model the elastic recovery. Equation **(4.39)** provided a relationship between void ratio and pressure stress. After evaluating the differentials,

$$\frac{1}{1+e} de = -\lambda_1 \frac{dp}{p} \qquad \textbf{(5.28)}$$

From equation **(5.3)**,

$$p = -\frac{1+2\,K_0}{3}\,\sigma_{zz} \qquad \textbf{(5.29)}$$

$$dp = -\frac{1+2\,K_0}{3}\,d\sigma_{zz} \qquad \textbf{(5.30)}$$

Substituting equations **(5.29)** and **(5.30)** into equation **(5.28)**,

$$\frac{1}{1+e} de = -\lambda_1 \frac{d\sigma'_{zz}}{\sigma'_{zz}} \qquad \textbf{(5.31)}$$

In integrated form,

$$1+e=(1+e_0)\left(\frac{\sigma'_{zz}}{\sigma'_{zz0}}\right)^{-\lambda_1} \qquad \textbf{(5.32)}$$

where e_0 and σ'_{zz0} are the initial void ratio and axial stress respectively.

Substituting equation **(5.24)** into the fluid phase constitutive equation **(4.47)** and simplifying,

$$v_z=-\frac{k}{\mu_v(1+e)}\frac{\partial P}{\partial w} \qquad \textbf{(5.33)}$$

where, from equation **(4.48)**,

$$k=k_1(1+e)^{k_2} \qquad \textbf{(5.34)}$$

Equations **(5.25)**, **(5.26)**, **(5.27)**, **(5.31)**, **(5.33)** and **(5.34)** define the model used to determine the permeability parameters. The six equations were simplified into a single equation as shown below.

Substituting equation **(5.27)** into equation **(5.25)**,

$$\frac{\partial P}{\partial w}=\frac{\partial \sigma'_{zz}}{\partial w} \qquad \textbf{(5.35)}$$

Substituting equation **(5.35)** into equation **(5.33)**,

$$v_z=-\frac{k}{\mu_v(1+e)}\frac{\partial \sigma'_{zz}}{\partial w} \qquad \textbf{(5.36)}$$

Substituting equation **(5.36)** into equation **(5.26)**,

$$\frac{\partial e}{\partial t} = \frac{\partial}{\partial w}\left[\frac{k}{\mu_v (1+e)}\frac{\partial \sigma'_{zz}}{\partial w}\right] \qquad \textbf{(5.37)}$$

Substituting equations **(5.31)** and **(5.34)** into equation **(5.37)**,

$$\frac{\partial e}{\partial t} = \frac{\partial}{\partial w}\left[-\frac{k_1 \sigma'_{zz} (1+e)^{k_2-2}}{\mu_v \lambda_1}\frac{\partial e}{\partial w}\right] \qquad \textbf{(5.38)}$$

Substituting equation **(5.32)** into equation **(5.38)**,

$$\frac{\partial e}{\partial t} = \frac{\partial}{\partial w}\left[-\frac{k_1 \sigma'_{zz0} (1+e_0)^{-\frac{1}{\lambda_1}} (1+e)^{k_2-2-\frac{1}{\lambda_1}}}{\mu_v \lambda_1}\frac{\partial e}{\partial w}\right] \qquad \textbf{(5.39)}$$

Equation **(5.39)** was then solved to determine the void ratio distribution through the sample using the following boundary conditions:

- At the top of the sample, the top platen pressure was specified as a function of time. Since the top platen was porous with $P = 0$, the top platen pressure was equal to the top platen effective pressure. Using equation **(5.32)**, the top platen effective pressure was converted to a void ratio boundary condition.
- At the bottom of the sample, $v_z = 0$ since there was no flow through the impermeable base. Using equations **(5.33)**, **(5.35)** and **(5.31)**, this boundary condition was converted into $\frac{\partial e}{\partial w} = 0$.

Once the void ratio distribution was determined, the sample height and the pore pressure at the bottom of the test cell were determined for each time increment. Equation **(5.24)** was integrated to determine the sample height. Equation **(5.27)** was used to determine the pore pressure. The total stress term in the equation came from the top platen boundary condition since the effective stress was equal to the total stress at the top platen and the total stress was constant throughout the test cell. The effective

stress term in the equation came from equation **(5.32)** using the calculated void ratio at the bottom of the test cell.

Equation **(5.39)** shows that the model contains three material parameters: one solid phase material parameter, λ_1, and the two permeability material parameters, k_1 and k_2. The parameter estimation process estimated all three parameters.

The initial void ratio was determined from the approximate initial height of the material in the test cell using equation **(5.1)**. At this height, the effective stress in the axial direction was given a nominal value of 1 kPa. The initial pore pressure was assumed to be zero.

Tests were typically carried out in sets of three, each with a different platen speed, in order to capture the rate-dependent effect of the fluid flow on the compression behaviour. The parameter estimation software was used to minimise the objective function for all three tests simultaneously.

5.4.5 An example of the parameter estimation process

To illustrate the results of the parameter estimation process, three tests from the same batch of prepared cane were examined. The tests were carried out as part of the series described in section 5.5.4. The tests were carried out using cane prepared in the Sugar Research Institute's Waddell hammer mill (section 5.5.2) at a speed of 750 r/min for 10 s with an initial sample mass of 4 kg at compression speeds of nominally 1 mm/s, 20 mm/s and 100 mm/s, respectively. The tests were identified as tests 4, 6 and 12 for the three compression speeds respectively.

Figure 5.8 shows the top platen total pressure, the bottom pore pressure and sample height results from the uniaxial compression tests and the equivalent predictions from the model. The estimated parameters were $\lambda_1 = 0.33$, $k_1 = 2.0 \times 10^{-17}$ m^2 and $k_2 = 5.3$. Only the total pressure at the top platen is presented in Figure 5.8 since the bottom total pressure was quite similar in magnitude, indicating that, unlike the uniaxial tests

conducted to determine the solid phase material parameters (section 5.2), friction was negligible. Only the pore pressure at the bottom of the test cell is presented in Figure 5.8 since the pore pressure at the top platen was small (typically less than 10 kPa).

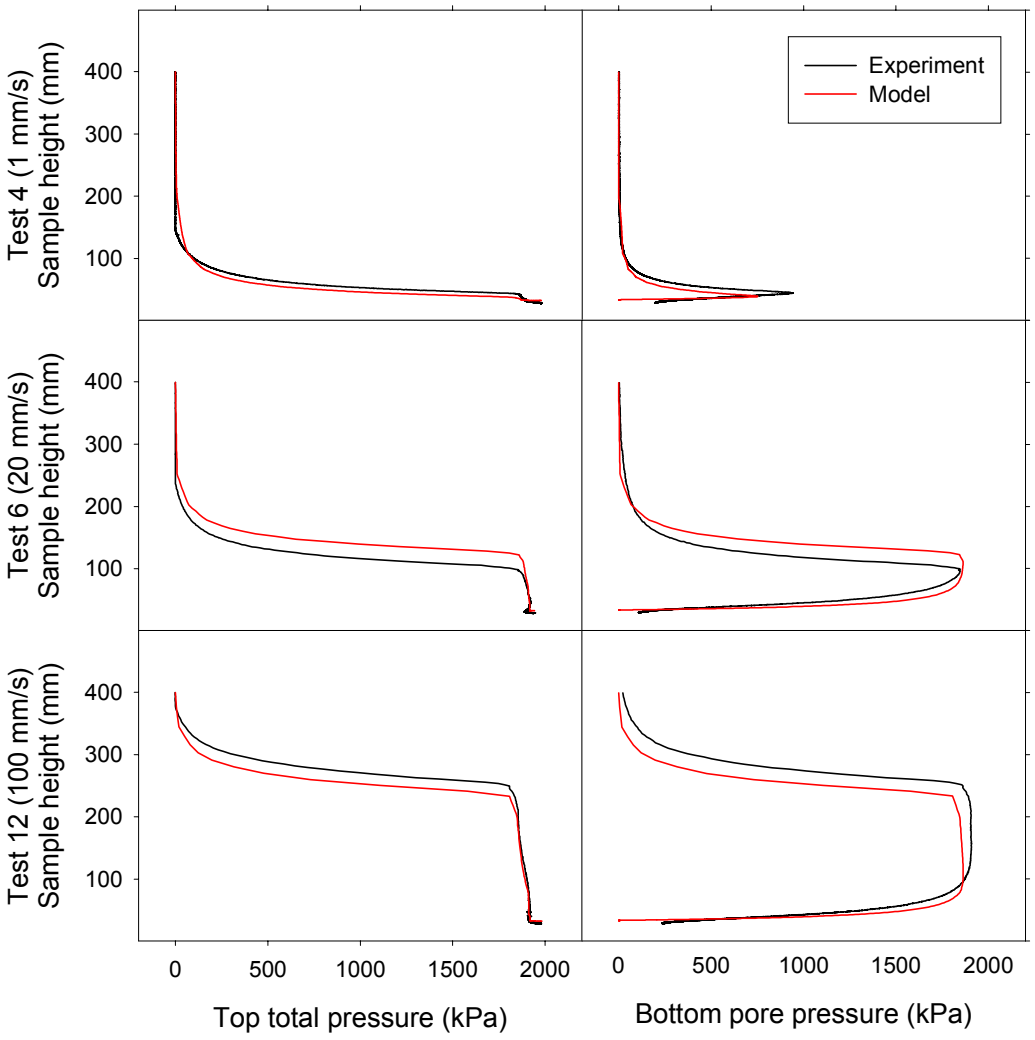

Figure 5.8 Typical experimental and model results for indirect permeability tests obtained from parameter estimation process for fluid phase material parameters

The graphs in Figure 5.8 all show an initial period where the top platen has compressed the prepared cane with relative ease since there was little build up of pressure. For each compression speed, there is a subsequent section where the pressure rises rapidly for little further compression. Comparing the total pressure graphs to the bottom pore

pressure graphs, it is clear that the build up in pressure comes from the build up in pore pressure rather than mechanical resistance. As compression speed increases, the pressure builds up earlier during the compression. When the total pressure reaches 2000 kPa (the maximum pressure applied), another section of compression commences. This section corresponds to the expression of juice from the cell. There is then a final section where the pore pressure drops, indicating that the mechanical resistance has finally increased to a sufficient level to support the applied load.

To assess the success of the parameter estimation process in identifying the correct parameter values, a sensitivity analysis was conducted over a range of parameter values and the objective function was determined. This sensitivity analysis was similar to that carried out for the process to determine material parameters for the solid phase (section 5.2.5). The results of the sensitivity analysis are shown in Figure 5.9. The solid phase material parameter, λ_1, and the two permeability parameters, k_1 and k_2, were all quite well defined. The solid phase parameter was predicted within about 5%. The two permeability parameters were also well defined although the bottom graph in Figure 5.9 shows a relationship between them. The true parameters appear to lie between the values $k_1 = 3.0 \times 10^{-17}$ m^2 and $k_2 = 5.1$ and the values $k_1 = 1.5 \times 10^{-17}$ m^2 and $k_2 = 5.3$. The parameter, k_2, appears predicted within about 5%. The parameter, k_1, appears predicted within a factor of two. Considering the non-linear nature of the permeability relationship (equation **(5.34)**), this prediction is also considered good.

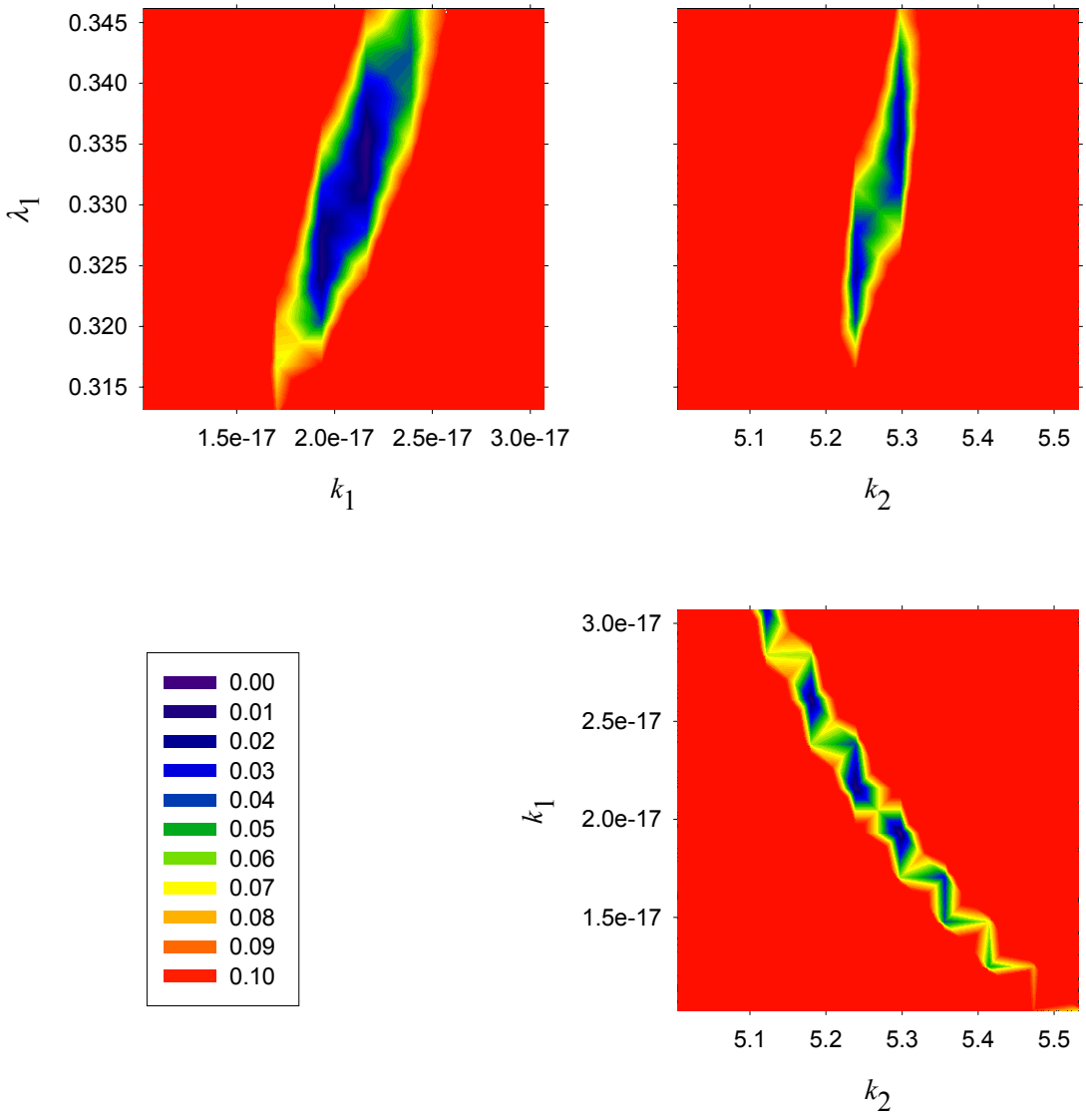

Figure 5.9 Results of sensitivity analysis for permeability parameters showing the relative change in the objective function for a change in material parameters

5.4.6 Concluding remarks

The transient permeability test provided an indirect method of determining the permeability material parameters, k_1 and k_2. In addition to the two permeability material parameters, the test also provided an estimate of the solid phase material parameter, λ_1.

The test is a uniaxial compression test that, in addition to the measurements made to determine the solid phase material parameters, requires only the pore pressure at the bottom of the cell to be known.

The parameter estimation process involves matching the sample height and bottom pore pressure measurements to equivalent values determined from a model of the test. Material parameters are adjusted to minimise the differences between the experimental and model results.

The transient test requires substantially less experimental testing time to complete than the steady state test. Consequently, the transient test was concluded to be the more appropriate test for the determination of permeability.

5.5 Effect of test method on permeability

5.5.1 Introductory remarks

In sections 5.3 and 5.4, two different methods for determining permeability parameters were introduced. The steady state method, conceptually the simpler method, was used in the earlier experiments (section 6.4.3) but was found to be quite laborious. Consequently, an alternative method, the transient method, was explored and used in later experiments (section 8.6.7).

This section presents experiments with both methods, using the same prepared cane material, designed to compare the permeability parameter estimates.

5.5.2 Experimental materials

The experiments were carried out using prepared sugarcane of variety Q124 with a fibre content of typically 11%. The sugarcane was prepared using the Sugar Research Institute's small hammer mill known as the Waddell hammer mill (Waddell 1953).

Two preparation levels were used in the experiments. For both preparation levels, the hammer mill was operated at a speed of 750 r/min. For the coarse level of preparation, the hammer mill was run for 10 s (designated 750/10). For the fine level of preparation, the hammer mill was run for 30 s (designated 750/30).

5.5.3 The steady state permeability measurement experiment

An experiment consisting of 12 tests was conducted to measure permeability using the steady state method (section 5.3). The experiment explored the effect of three factors on permeability: average void ratio, sample thickness and preparation. Three average void ratios were explored: nominally 9, 7 and 5. The desired void ratio was achieved by controlling the mass of cane placed into the test cell. Two sample thicknesses were explored: 43 mm and 104 mm. Sample thickness was adjusted through the selection of the desired spacer for the test cell (section 5.3.2). The two levels of preparation used in the experiment were described in section 5.5.2. The experiment was conducted in a randomised factorial design.

For each test, water was pumped through the sample. The pressure drop across the sample was slowly but continuously increased from typically 300 kPa (tap pressure) to a maximum value of approximately 2 MPa and then continuously decreased back to 300 kPa. The pressure cycle was repeated several times. One pressure cycle was chosen for a linear regression analysis to determine $\frac{Q}{\Delta P}$ for a direct permeability calculation. The pressure cycle chosen was the first one that returned a positive R^2

value from the linear regression analysis. An example of the data used to determine $\frac{Q}{\Delta P}$ is presented in Figure 5.6. Further details of the tests are presented in Appendix C.

To estimate the parameters, the tests were grouped into series with the same sample thickness and same preparation. Each group consisted of three tests with different void ratios. For each group of three tests, the parameter estimation process described in section 5.3.4 was carried out to determine the permeability parameters, k_1 and k_2. For this process the elastic material parameter, κ, was assumed to be 0.56 and the plastic material parameter, λ_1, was determined from the parameter estimation process for the transient test (Table 5.3). The directly measured results and the corresponding curve from the parameter estimation process are presented in Figure 5.10. The calculated permeability parameters are presented in Table 5.2.

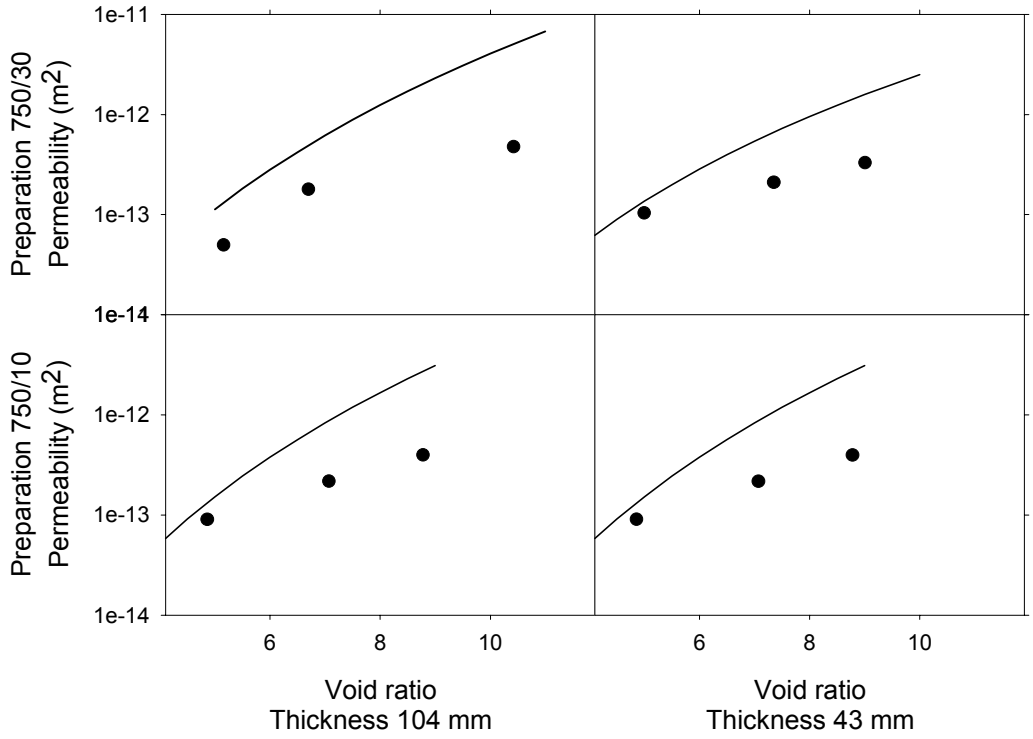

Figure 5.10 Results from the steady state permeability experiment

Table 5.2 Estimated parameters from the steady state permeability experiment

Preparation	Sample thickness (mm)	k_1 (m^2)	k_2
750/30	104	2.9×10^{-18}	5.9
	43	25.0×10^{-18}	4.8
750/10	104	3.9×10^{-18}	5.9
	43	5.2×10^{-18}	5.7

An analysis of variance was conducted on the data contained in Table 5.2 to determine if there were any differences in the parameter values between the two levels of cane preparation. No statistically significant differences were identified.

5.5.4 The transient permeability measurement experiment

An experiment consisting of 12 tests was conducted to measure permeability using the transient method (section 5.4). The experiment explored the effect of three factors on permeability: platen speed, sample mass and preparation. Three platen speeds were explored: nominally 1 mm/s, 20 mm/s and 100 mm/s. Two sample masses were explored: 8 kg and 4 kg. The two levels of preparation used in the experiment were described in section 5.5.2. The experiment was conducted in a randomised factorial design.

The physical test procedure was described in section 5.4.3. The bottom total pressure was recorded to ensure that friction between the prepared cane and the test cell wall was negligible. The top platen pore pressure was recorded to ensure that it was close to zero. The three measurements of interest were the top platen total pressure, the bottom pore pressure and the sample height. Further details of the tests are presented in Appendix C.

The results were grouped into series with the same sample mass and same preparation. Each group consisted of three tests with different nominal platen speeds. For each group of three tests, the parameter estimation process described in section 5.4.4 was carried out to determine the solid phase material parameter, λ_1 and the two permeability

parameters, k_1 and k_2. The calculated parameters are presented in Table 5.3. The void ratio and permeability relationships based on the parameter values are shown in Figure 5.11.

Table 5.3 Estimated parameters from the transient permeability experiment

Preparation	Sample mass (kg)	λ_1	k_1 (m^2)	k_2
750/30	8	0.41	5.8×10^{-18}	6.17
	4	0.34	1.8×10^{-18}	6.05
750/10	8	0.29	1.2×10^{-18}	6.20
	4	0.33	20.5×10^{-18}	5.27

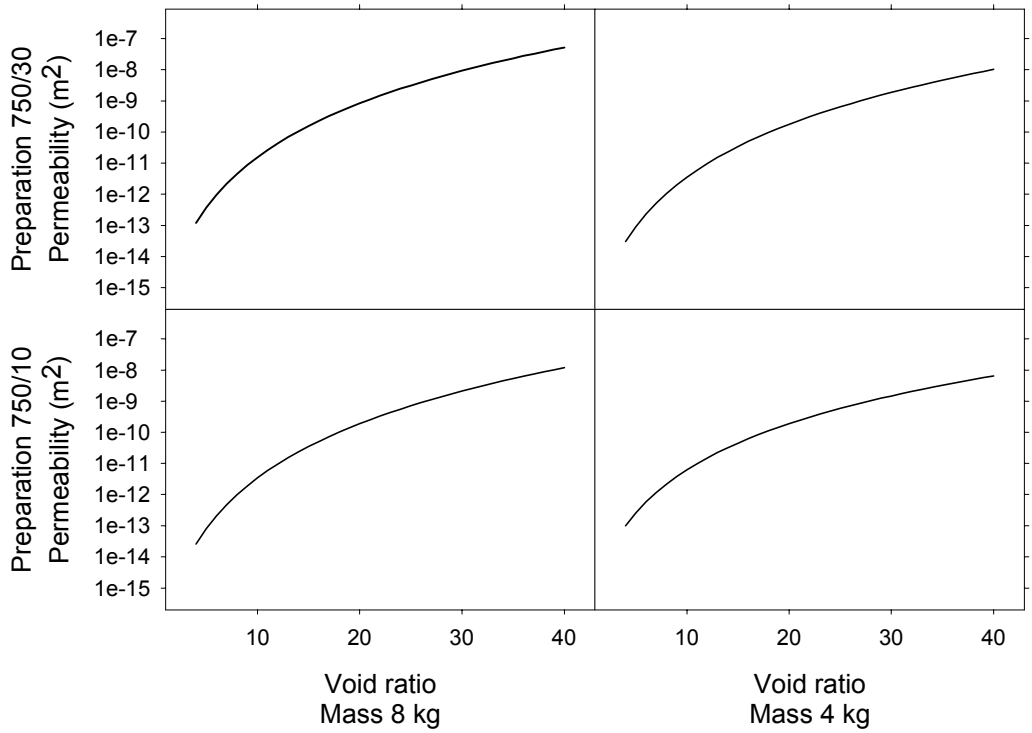

Figure 5.11 Void ratio and permeability relationships from the transient permeability experiment

An analysis of variance was conducted on the data contained in Table 5.3 to determine if there were any differences in the parameter values between the two levels of cane preparation. No statistically significant differences were identified.

5.5.5 Comparison of results

To compare the permeability relationship derived from the steady state measurement technique to the permeability relationship derived from the transient measurement technique, the four curves in Figure 5.10 from steady state permeability measurements were compared to the four curves in Figure 5.11 from transient permeability measurements. Figure 5.12 shows all eight curves.

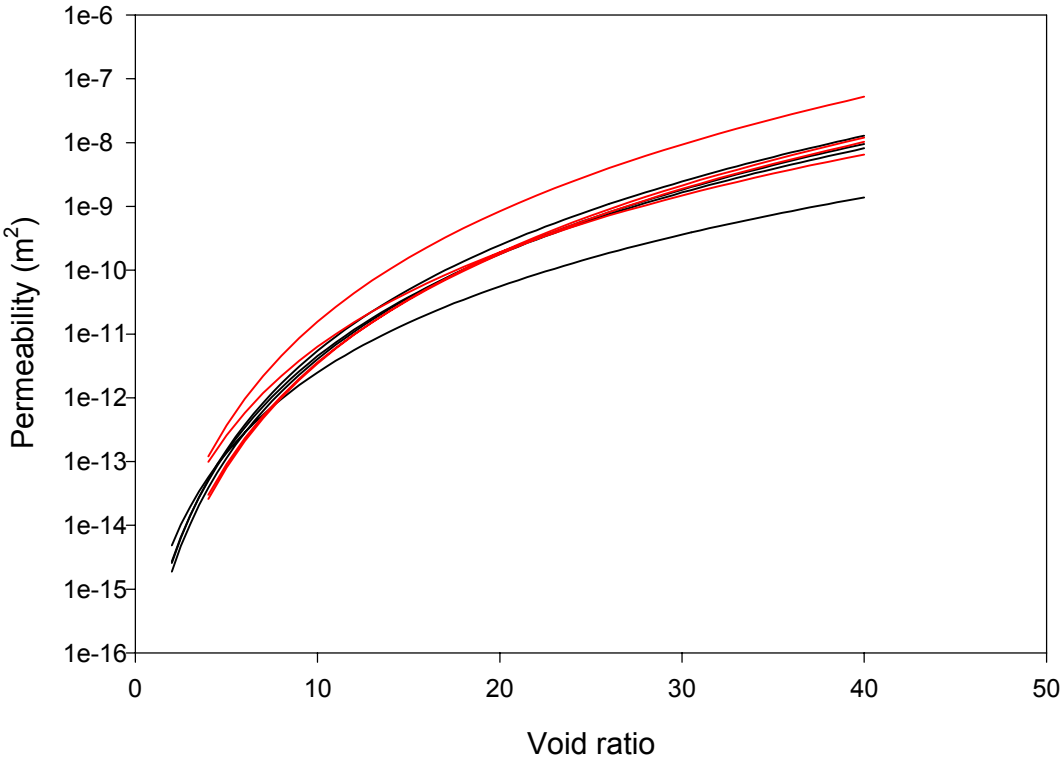

Figure 5.12 Comparing permeability measurements between steady state (black curves) and transient (red curves) testing methods

Figure 5.12 shows that the permeability estimates from the two testing methods were quite similar. One permeability estimate using each test method was approximately one order of magnitude from the other three at high void ratios. The results show that the error in measurement using one test method is greater than the error in measurement found between the testing methods. There was no evidence to suggest that one test method gave substantially more accurate measurements of permeability than the other.

5.5.6 Concluding remarks

The steady state method and the transient method provide permeability predictions of similar magnitude. For each method, the error in the permeability estimate at high void ratio of about 40 was about one order of magnitude. The error reduced as the void ratio reduced.

Although both methods were found to produce similar permeability estimates, the transient method was preferred due to the simplicity of the physical test procedure and the relatively short testing time.

5.6 Concluding remarks

This chapter presents the techniques used in the following chapters for the determination of material parameters for use in the computational feeding models. Three techniques are presented: one technique for determining material parameters for the solid phase and two techniques for determining material parameters for the fluid phase.

All three techniques make use of the parameter estimation software, PEST, to estimate the material parameters. PEST provides a systematic method for determining parameter values and a means for quantifying the adequacy of the match between experimental results and model predictions. The introduction of this systematic method is considered a significant improvement on the trial and error approach used previously.

To estimate the solid phase material parameters, uniaxial compression tests were carried out in a cylindrical test cell. The pressures at the top platen and at the bottom of the cell were measured, along with the sample height. A model of the test cell was developed and a parameter estimation technique was used to vary the material parameters in the model to match the pressures at the top platen and at the bottom to the equivalent pressures from the compression tests. Of the six solid phase material parameters in the

model, one was well defined (λ_1) and another was well defined but dependent on the assumed value of coefficient of friction between the bagasse and the test cell wall (M). The elastic parameters (κ, v) were not as well defined. No attempt was made to define the remaining two parameters (p_t^e and p_t). These tests are the first known tests where the pressure at the top and bottom of the sample were both measured, providing valuable information on the effect of side-wall friction on the results.

Two techniques, identified as steady state and transient methods, are presented to measure the permeability parameters (k_1 and k_2) that define the relationship between permeability and void ratio. The steady state method involves compressing a sample of bagasse to a desired void ratio in a test cell and then pumping water through the cell. The transient method involves a uniaxial compression test similar to that used to define the solid phase material parameters. For permeability measurement, the pore pressure at the bottom of the test cell was also measured. This transient method is considered a significant improvement on the transient methods used previously since it involves one-directional, one-dimensional, saturated flow only. For this simpler test arrangement, a one-dimensional model was developed with substantially shorter solution times than the comparable ABAQUS model, enabling the parameter estimation process to be completed much quicker. For both test methods, a parameter estimation process similar to that used to derive the solid phase material parameters was used. For the steady state test method, the parameter estimation process matched water flow rates between the model and test results. For the transient method, the parameter estimation procedure matched the pore pressure and the sample height results between the model and the test results. For both techniques, the two permeability parameters were well defined. The transient method also provided an estimate for a solid phase material parameter (λ_1). No attempt was made to estimate a value for the absolute viscosity (μ_v).

An experiment was conducted to compare the permeability parameters estimated using the two techniques. The comparison showed that the two techniques gave similar permeability estimates. At higher void ratios of about 40, both methods gave permeability estimates with an error of about one order of magnitude. The permeability estimates improved as the void ratio reduced.

The new transient method for determining the permeability parameters is considered the better method since it involves substantially less experimental effort and also estimates the solid phase material parameter, λ_1, eliminating the need for separate compression tests to define this parameter.

6 Mill feeding in a two-roll mill without juice expression

6.1 Introductory remarks

In chapter 4, the governing equations for a new throughput model were described. The new throughput model was considered necessary to achieve the aim of this study to identify the means of increasing the throughput of six-roll milling units since the existing model of Jenkins and Murry (1981) was found in chapter 3 to be inadequate.

The governing equations described in chapter 4 are general equations that describe the response of bagasse to applied loads and displacements and the associated fluid flows. In this chapter and in chapter 8, the general equations are applied to specific milling unit geometries to develop the required throughput model of six-roll milling units.

This chapter describes the first step towards the development of the improved throughput model: the development of a throughput model for a two-roll mill. The two-roll mill is the simplest milling geometry. Consequently, it is the milling geometry that can provide the clearest experimental results and is considered the easiest milling geometry to model.

An experiment to determine the factors affecting the throughput of a two-roll mill was carried out on a small-scale two-roll mill. For simplicity, the experiment was carried out at nip compactions that did not cause juice expression. These compactions are representative of conditions in the underfeed nip, the first pair of rolls in the six-roll

mill. An effort was made to thoroughly examine the results of the experiment to identify the mechanisms that resulted in the observed behaviour. The conclusions from this work were used to refine the requirements for the computational feeding model.

Tests were also carried out to determine material parameters to describe the prepared sugarcane processed in the two-roll mill experiment using the methods described in chapter 5. A throughput model for a two-roll mill was developed using the governing equations of chapter 4 and tested by assessing its ability to reproduce the two-roll mill experiment.

The work in this chapter shows that the simple throughput model for a two-roll mill developed by Murry (1960b) identifies the factors affecting the throughput of a two-roll mill but does not accurately predict their effect. In particular, the effects of contact angle, nip setting, roll speed and feed pressure are not adequately represented. The newly developed throughput model, on the other hand, captures all of these effects.

6.2 Features of the two-roll mill

Figure 6.1 shows the general layout of a two-roll mill as used throughout this chapter. The size of the rolls (length L and diameter D, not shown in Figure 6.1), the work opening between the rolls (W) and the feed blanket depth (h) define the mill geometry. The contact angle is defined by equation **(1.4)** to be:

$$\cos\alpha = \frac{D + W - h}{D} \qquad \textbf{(6.1)}$$

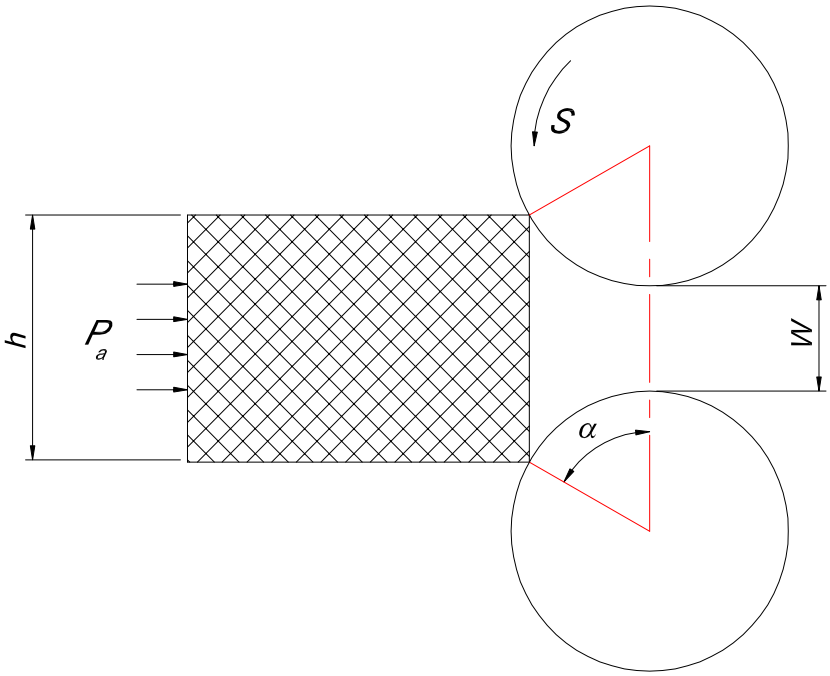

Figure 6.1 Two-roll mill layout

The surface speed of the rolls is *S*. A small feed pressure (P_a) is applied to the trailing edge of a pre-compressed block of prepared sugarcane.

The existing throughput theory for a two-roll was developed by Murry (1960b) and was more fully described in section 2.2.3. According to Murry's theory, the average speed of the prepared cane block (S_F) is equal to $S \cos \alpha$ and the mill throughput, in terms of fibre rate, is given by equation **(2.8)**:

$$Q_f = \gamma_\alpha \, L \, D \, S \left(1 + \frac{W}{D} - \cos\alpha\right) \cos\alpha \qquad \textbf{(6.2)}$$

Since feed speed is clearly affected by roll speed and contact angle according to Murry's theory, feed speed results were normalised by dividing by $S \cos \alpha$. The ratio $\frac{S_F}{S\cos\alpha}$ is named *Murry's feed speed ratio* throughout this thesis. Any variation in

Murry's feed speed ratio away from a value of 1 is an indication of weakness in Murry's theory.

6.3 An experiment without juice expression

6.3.1 Introductory remarks

As discussed in section 2.2.4, the two-roll mill throughput model of Murry (1960b) has been used for more complex milling geometry by applying it to the first pair of rolls in a milling unit. The first pair of rolls in the six-roll mill form the underfeed nip. The underfeed nip compaction for a six-roll milling unit in the #1 mill position is typically 90 kg/m^3. Since juice is not typically expressed until compaction reaches 160 kg/m^3, the underfeed nips of six-roll mills do not generally express juice. While it is desirable to commence the study of mill throughput without the complication of juice expression, the lack of juice expression in the first nip of the six-roll mill makes the study of throughput without juice expression quite relevant to the ultimate six-roll mill throughput investigation.

This section presents the results of an experiment undertaken to quantify the influence of mill geometry, roll speed, feed pressure and feed material on mill throughput. The experiment was undertaken to provide validation data with which to test the new throughput model. Section 6.4 presents the material parameters necessary for modelling the experiment. Section 6.5 presents the results of testing the model against the experimental data from this section.

6.3.2 Apparatus

The cane for the experiments was prepared in the Sugar Research Institute's hammer mill known as the shredder (Loughran & Murry 1984). Adjusting the speed of the

shredder controlled the degree of preparation. Consequently, the shredder speed was used as the measure of preparation.

The experiment was carried out on the James Cook University two-roll mill (known as the CR Murry Milling Facility). Loughran and Kauppila (1999) provided a description of the mill. The roll dimensions are presented in Table 6.1.

Table 6.1 Roll dimensions for the two-roll mill experiments

Parameter	Value (mm)
Length	225
Outside diameter	782
Groove depth	32
Groove pitch	25

Instead of using the mill's 'live' feeder (Loughran & Kauppila 1999), a pneumatic ram was fitted to provide a constant pressure feed to the mill. The constant pressure feed was designed to simulate the effect of a constant feed height in a factory feed chute. The speed of the ram provided a measure of the feed speed. Since the feed speed was the required output of the experiment, the ram was considered a more appropriate feeding device than the live feeder that effectively sets the feed speed. The mill layout presented in Figure 6.1 describes the mill layout for this experiment.

The milling facility's pre-compression apparatus (Loughran & Kauppila 1999), designed to form the cane block for feeding into the mill, was not considered suitable for this experiment. The pre-compression apparatus compresses the feed blanket in the direction normal to the feed direction. Since the feed in a factory feed chute is compressed (by the action of prepared cane or bagasse above it) in the direction of the feed, it was decided that a pre-compressor that would compress the feed in the feed direction was required. A special pre-compressor was constructed for the purpose.

6.3.3 Experimental design

Since Murry's theory assumes that the feed speed (S_F) is equal to $S \cos \alpha$, S and α were selected as experimental factors. The other parameters in Murry's throughput model as described by equation **(6.2)**, work opening and feed compaction, were also considered desirable as experimental factors. Following the convention for underfeed nips (section 1.2.4), work opening was replaced by nip setting as an experimental factor. Because feed compaction is difficult to control it was not used directly as an experimental factor. Instead, three factors known to influence feed compaction were selected: cane variety, cane preparation and feed pressure. In all, six factors were explored at two levels as shown in Table 6.2.

Table 6.2 Levels of each factor explored in the two-roll mill experiment

Factor	Level 0	Level 1
Nip setting (W, mm)	240	120
Cane variety (V)	Q124	Q117
Cane preparation (Z, rpm)	1200	2000
Feed pressure (P_a, kPa)	3	7
Roll speed (S, mm/s)	100	500
Contact angle on outside diameter (α, °)	16	40

To keep the experiment to a manageable size, the experiment was conducted as a 2^{6-1} fractional factorial experiment. Because of the difficulties associated with changing the nip setting and the contact angle, the experiment was conducted in a split-split-plot arrangement (Mathsoft 1999) so that the nip setting and contact angle were changed less frequently than in the fully randomised experimental design. The testing order is presented in Appendix D.

6.3.4 Procedure

The cane for the entire experiment was cut at one time and stored as whole stalks in a refrigerator (5ºC). Each cane variety came from a single block. At the start of each day, the day's cane was billeted, shredded, mixed and, again, stored in the refrigerator.

For each test, the cane was taken from the refrigerator and placed in the pre-compressor. An appropriate mass of cane was chosen so that, once the sample was compacted, the length of the feed block was the same (900 mm). The samples were compacted to approximately the feed pressure for the test so that there was minimal compaction of the feed during the experiment.

Once the feed block was formed in the pre-compressor, it was transferred to the milling facility. A grid was then painted on the side of the block so that the deformation of the blanket would be visible from a video recording of the test.

Once the rolls were brought up to the required operating speed, logging of the roll speed, feed pressure and ram head position commenced. Although of less interest, roll load and roll torque were also logged (the roll load and roll torque load cells were calibrated for delivery nip loads, so the signals at underfeed nip loads were small and quite noisy). Each parameter was logged at a frequency of 10 Hz. The video recording also commenced. The ram was then operated. The recording ended once the end of the stroke on the ram was reached.

6.3.5 Results

Feed speed results

Appendix D presents the detailed experimental results. Two measures of roll speed and feed speed were available: one from the logged data as described in section 6.3.4 and one from the video recording. An analysis of variance of the data showed that the roll speed measurement from the video recording had lower error variance than the roll speed measurement from the logged data while the feed speed measurement from the logged data had lower error variance than the feed speed measurement from the video recording. Consequently, the roll speed measurement from the video recording and the feed speed measurement from the logged data were used in the subsequent analysis and were recorded in Appendix D.

Table 6.3 presents the analysis of variance of Murry's feed speed ratio. The symbols used in Table 6.3 were defined in Table 6.2. Second order interaction terms were combined to form the *Residuals* in order to identify significant effects. Three main effects (nip setting, roll speed and feed pressure) and three first order interactions (nip setting / roll speed, contact angle / roll speed and cane variety / cane preparation) were identified with a level of significance less than 0.1.

Table 6.3 Analysis of variance of Murry's feed speed ratio for the two-roll mill experiment

Source	Degrees of freedom	Mean square	Variance ratio	Significance level
W	1	0.670	26.5	0.007
α:Z	1	0.009	0.4	-
S:V	1	0.021	0.8	-
Residuals	4	0.025		
α	1	0.027	0.4	-
Z	1	0.007	0.1	-
W:α	1	0.121	1.6	-
W:Z	1	0.004	0.1	-
S:P_a	1	0.086	1.1	-
V: P_a	1	0.051	0.7	-
Residuals	2	0.076		
S	1	0.279	15.9	0.02
V	1	0.002	0.1	-
P_a	1	0.293	16.6	0.02
W:S	1	0.122	7.0	0.06
W:V	1	0.008	0.4	-
W:P_a	1	0.068	3.9	-
α:S	1	0.127	7.2	0.06
α:V	1	0.002	0.1	-
α:P_a	1	0.036	2.0	-
S:Z	1	0.001	0.1	-
V:Z	1	0.149	8.5	0.04
Z:P_a	1	0.000	0.0	-
Residuals	4	0.018		

Figure 6.2 shows the mean levels for each of the experimental factors. Murry's feed speed ratio was higher at the higher levels of nip setting and feed pressure and at the lower level of roll speed.

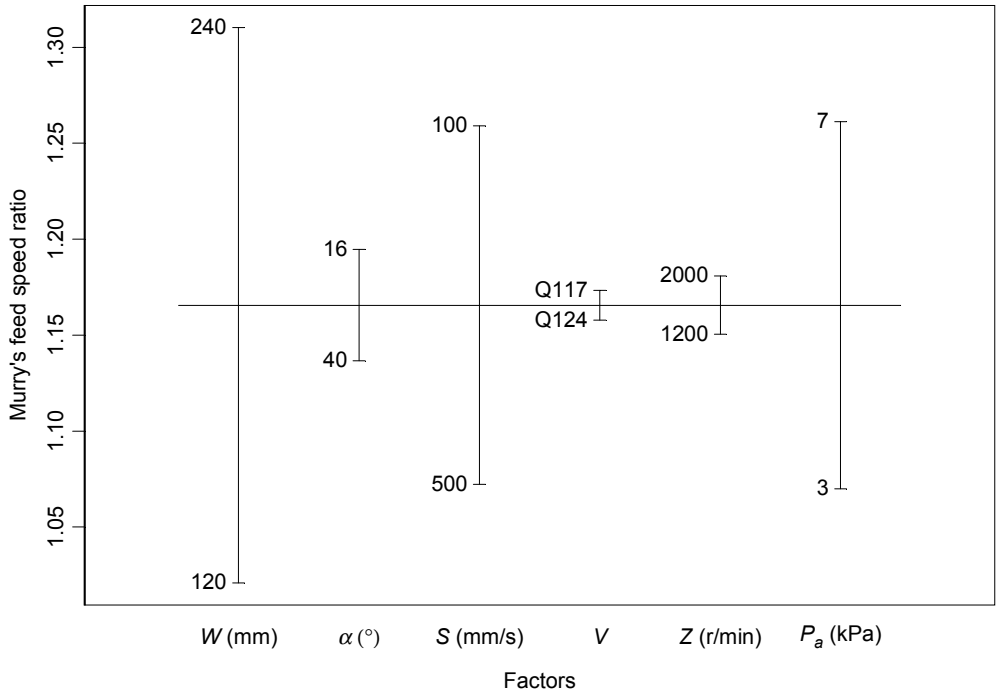

Figure 6.2 Mean values of Murry's feed speed ratio for each level of each factor for the two-roll mill experiment with all results included

Figure 6.3 shows the effect of each of the significant interaction terms from Table 6.3 on Murry's feed speed ratio. Nip setting had a much greater influence on Murry's feed speed ratio at low speed than at high speed although, for both speeds, the trend to higher values of Murry's feed speed ratio at larger nip setting exists. Murry's feed speed ratio was largely independent of contact angle at the higher roll speed of 500 mm/s. At 100 mm/s, however, Murry's feed speed ratio increased with reducing contact angle. At both contact angles, Murry's feed speed ratio was higher at the lower roll speed. Murry's feed speed ratio was higher for Q124 at coarse preparation and for Q117 at fine preparation.

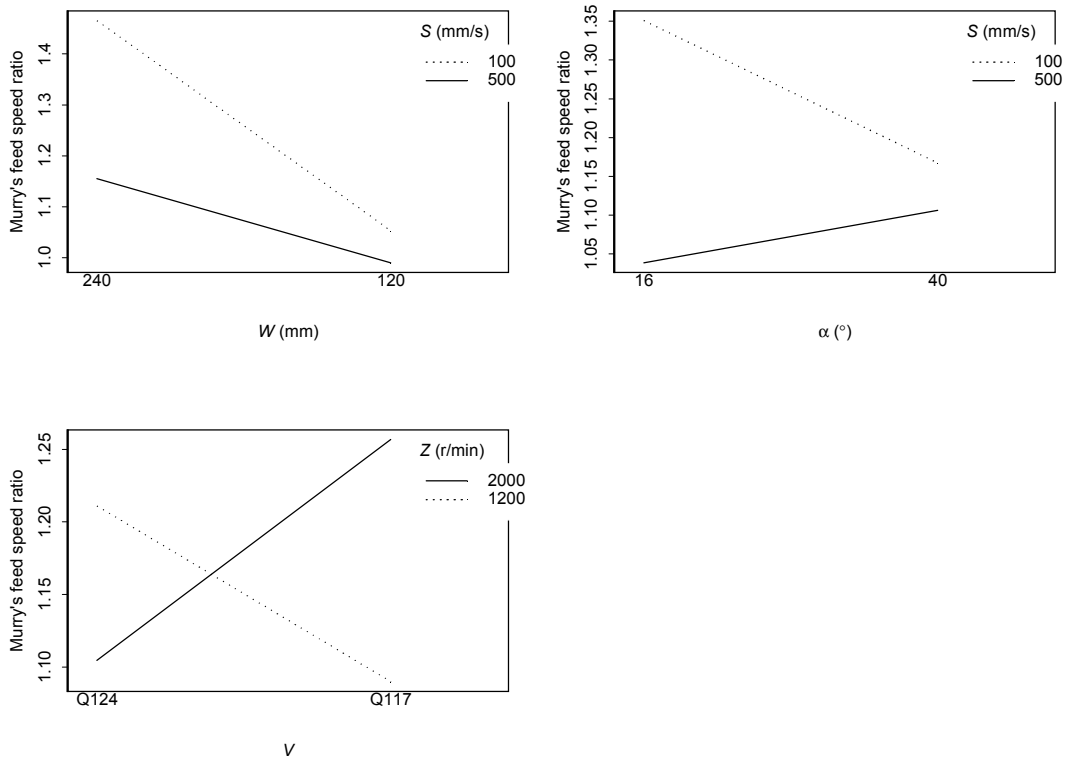

Figure 6.3 Significant interactions identified in the analysis of variance of Murry's feed speed ratio for the two-roll mill experiment

Feed speed results after allowing for slip on the roll surface

An examination of the video footage of the tests shows that, in test 13 and test 19 (as described in Appendix D), a substantial amount of forward slip occurred where the bagasse blanket travelled forward at a higher speed than the rolls, resulting in very high values of Murry's feed speed ratio. In test 3, a small amount of slip was suspected from the video footage and Murry's feed speed ratio was quite high for this test, too. In terms of the force system acting on the prepared cane mat, the feed pressure was sufficiently high to overcome the frictional force available between the prepared cane and the roll surface and enable the mat to accelerate forward through the nip. All of the three tests occurred at the larger nip setting of 240 mm, the smaller contact angle of 16º and the lower roll speed of 100 mm/s. Tests 13 and 19 occurred at the higher feed pressure of 7 kPa. While test 3 occurred at the lower pressure setting of 3 kPa, the recorded data

showed that the average pressure was, in fact, 4.5 kPa, considerably higher than desired. Tests 3 and 13 occurred with Q124 cane prepared with a shredder speed of 1200 r/min. Test 19 occurred with Q117 cane prepared with a shredder speed of 2000 r/min. An explanation for why these three tests were affected by slip to a much greater degree than the other tests is presented in section 6.3.6. A summary of the mean values of the experiment without tests 3, 13 and 19 is presented in Figure 6.4.

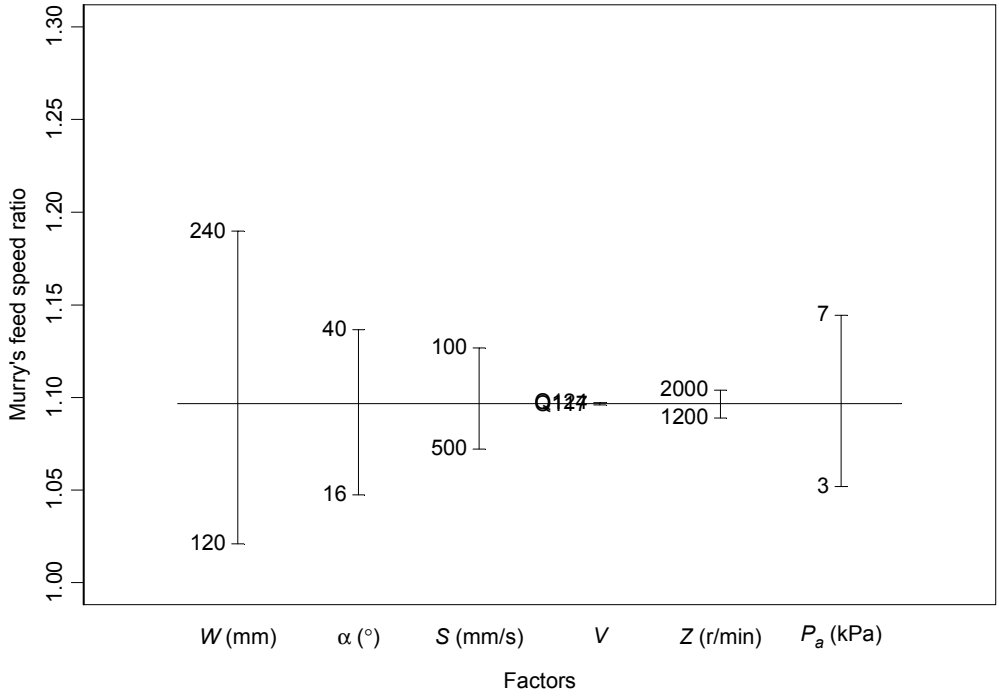

Figure 6.4 Mean values of Murry's feed speed ratio for the two-roll mill experiment with tests 3, 13 and 19 removed

The three tests affected by slip provide an explanation for the three significant interactions identified previously and presented in Figure 6.3. The three tests are three of the eight tests providing the high value of Murry's feed speed ratio at a nip setting of 240 mm and a roll speed of 100 mm/s. The three tests are also three of the eight tests providing the high value of Murry's feed speed ratio at a contact angle of 16º and a roll speed of 100 m/s. The three tests also explain why Q124 cane prepared with a shredder speed of 1200 r/min and Q117 cane prepared with a shredder speed of 2000 r/min

should have higher values of Murry's feed speed ratio than Q124 cane prepared with a shredder speed of 2000 r/min and Q117 cane prepared with a shredder speed of 1200 r/min.

Treating the three tests affected by slip as missing values, the analysis of variance of the experiment was redone. According to Hicks (1964), missing values can be replaced by values that minimise the sum of squares of the residuals, provided the number of degrees of freedom for the residuals are reduced by the number of missing values. For this case, the sum of squares of the residuals was minimised by setting the feed speed ratios for tests 3, 13 and 19 to 1.0, 1.3 and 1.6 respectively. The resulting analysis of variance is shown in Table 6.4. The analysis of variance found very few significant effects. The main cause of the lack of significant effects was the removal of three degrees of freedom from the *Residuals* row at the bottom of the table to account for the missing values, leaving only one degree of freedom for hypothesis testing. Since this approach yielded little information, an alternative approach of analysing half the experiment without the slip-affected tests was adopted.

Table 6.4 Analysis of variance of Murry's feed speed ratio for the two-roll mill experiment treating results from tests 3, 13 and 19 as missing values

Source	Degrees of freedom	Mean square	Variance ratio	Significance level
W	1	0.287	144.1	0.0003
α:Z	1	0.014	7.2	0.05
S:V	1	0.028	14.1	0.02
Residuals	4	0.002		
α	1	0.014	0.7	-
Z	1	0.012	0.6	-
W:α	1	0.004	0.2	-
W:Z	1	0.007	0.4	-
S:P_a	1	0.017	0.8	-
V: P_a	1	0.017	0.8	-
Residuals	2	0.020		
S	1	0.061	4.5	-
V	1	0.005	0.3	-
P_a	1	0.143	10.5	-
W:S	1	0.005	0.3	-
W:V	1	0.012	0.9	-
W:P_a	1	0.010	0.7	-
α:S	1	0.005	0.4	-
α:V	1	0.004	0.3	-
α:P_a	1	0.001	0.1	-
S:Z	1	0.003	0.2	-
V:Z	1	0.011	0.8	-
Z:P_a	1	0.011	0.8	-
Residuals	1	0.014		

From a consideration of geometry, it was considered likely that the 16º contact angle tests were affected by slip to a greater degree than halves of the experiment based on any other experimental factor. At a contact angle of 16º, the prepared cane mat undergoes very little deformation. Consequently, little opportunity exists for the development of a normal force large enough to provide the frictional resistance to withstand the feed pressure. By removing the 16º contact angle tests from the experiment, a 16-test split-plot experiment remained for analysis that was considered unlikely to be affected by slip. The analysis of variance of this reduced experiment is shown in Table 6.5. From this analysis, only two main effects (nip setting and feed pressure) were identified with a level of significance less than 0.1. No significant first order interactions were identified.

Table 6.5 Analysis of variance of Murry's feed speed ratio for the 40º contact angle tests from the two-roll mill experiment

Source	Degrees of freedom	Mean square	Variance ratio	Significance level
W	1	0.111	22.1	0.04
Z	1	0.000	0.0	-
W:Z	1	0.003	0.7	-
S:P_a	1	0.009	1.7	-
V: P_a	1	0.010	2.0	-
Residuals	2	0.005		
S	1	0.015	18.3	-
V	1	0.000	0.0	-
P_a	1	0.062	76.3	0.07
W:S	1	0.001	0.8	-
W:V	1	0.001	1.8	-
W:P_a	1	0.004	4.9	-
Z:P_a	1	0.019	22.9	-
Residuals	1	0.001		

Figure 6.5 shows the mean levels for each of the experimental factors. Murry's feed speed ratio was higher at the higher levels of nip setting and feed pressure. While Figure 6.5 shows that Murry's feed speed ratio was higher for the 100 mm/s roll speed tests than for the 500 mm/s roll speed tests, the analysis of variance showed that this result was not significant.

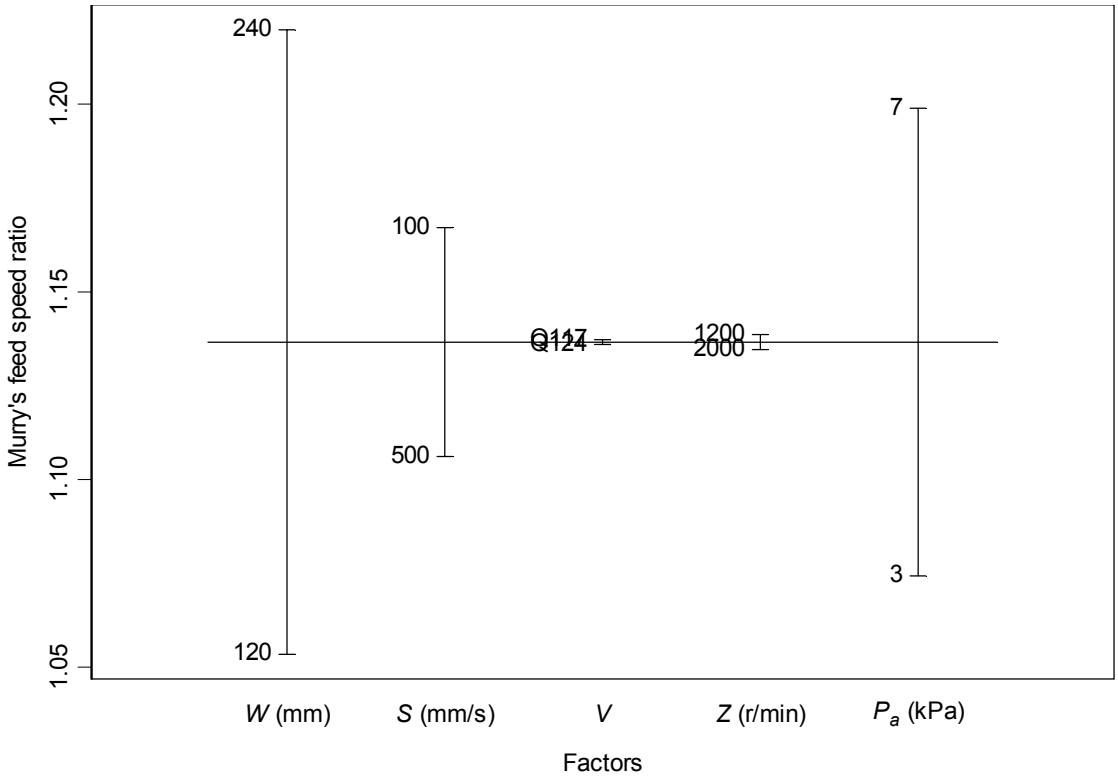

Figure 6.5 Mean values of Murry's feed speed ratio for each level of each factor for the 40º contact angle tests from two-roll mill experiment

By analysing only the 40º contact angle tests, it was not possible to explore a contact angle effect on Murry's feed speed ratio. To look for a contact angle effect, a different half of the experiment was required. The 120 mm nip setting tests were chosen for this purpose. As discussed above, the video footage only provided clear evidence that the 240 mm nip setting tests were affected by roll slip. The analysis of variance of this reduced experiment is shown in Table 6.6. From this analysis, only one main effect was identified with a level of significance less than 0.1: contact angle. Although feed pressure had the next highest variance ratio, and, in fact, a higher mean square value, it was not sufficient for the analysis to select feed pressure as a significant effect, in contrast to the analysis shown in Table 6.5. The residual term used for the significance test for feed pressure was substantially greater than the residual term used for the significance test for contact angle.

Table 6.6 Analysis of variance of Murry's feed speed ratio for the 120 mm nip setting tests from the two-roll mill experiment

Source	Degrees of freedom	Mean square	Variance ratio	Significance level
α	1	0.017	9.1	0.09
Z	1	0.000	0.1	-
α:Z	1	0.001	0.6	-
S:P_a	1	0.002	0.8	-
V: P_a	1	0.001	0.7	-
Residuals	2	0.002		
S	1	0.016	2.3	-
V	1	0.001	0.1	-
P_a	1	0.039	5.6	-
α:S	1	0.000	0.1	-
α:V	1	0.000	0.0	-
α:P_a	1	0.000	0.0	-
Z:P_a	1	0.001	0.1	-
Residuals	1	0.007		

Figure 6.6 shows the mean levels for each of the experimental factors. Figure 6.6 shows that Murry's feed speed ratio was higher for a contact angle of 40º than for a contact angle of 16º. It is worth noting that Figure 6.6 shows that the feed pressure effect was measured to be greater than the contact angle effect and the roll speed effect of similar magnitude to the contact angle effect, although the analysis of variance found these two effects to not be significant because of the higher residual error term used for testing these effects.

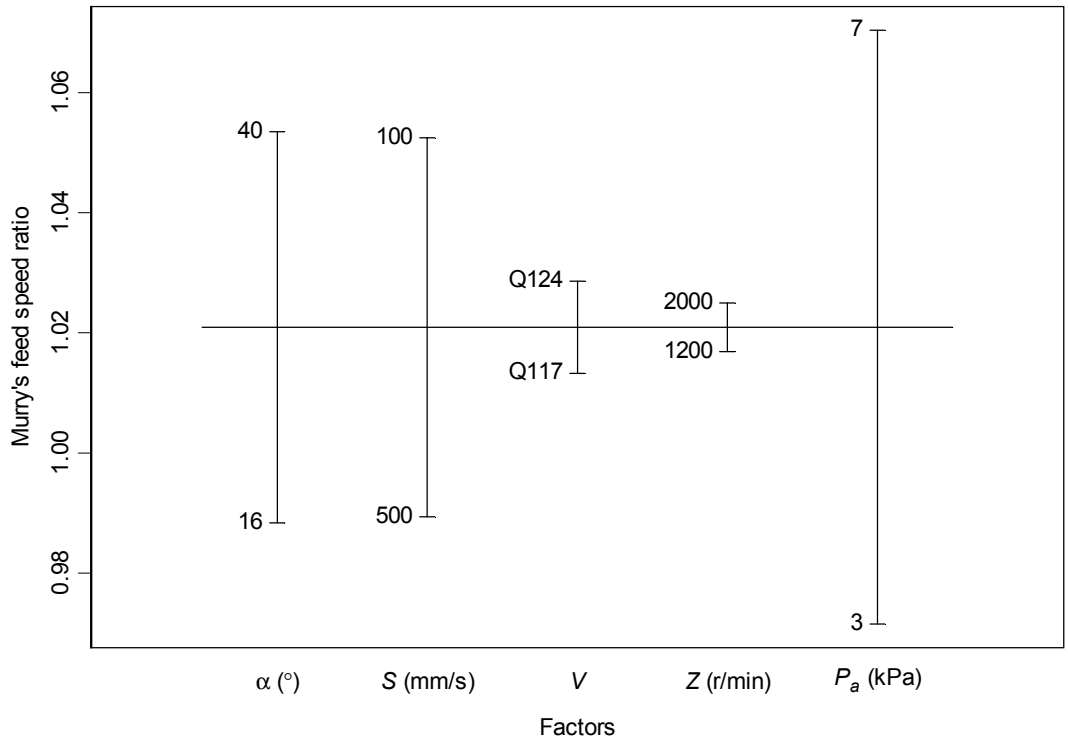

Figure 6.6 Mean values of Murry's feed speed ratio for each level of each factor for the 120 mm nip setting tests from two-roll mill experiment

Even though the analysis of variance of the two half experiments in Table 6.5 and Table 6.6 failed to show a significant roll speed effect on Murry's feed speed ratio, there is evidence that roll speed has some impact on Murry's feed speed ratio. It seems reasonable to conclude that the two significant first-order interactions from the analysis of variance of the whole experiment (Figure 6.3) show the importance of the higher roll speed for preventing slip. In addition, Figure 6.5 and Figure 6.6 show that, for both half experiments, the mean value for Murry's feed speed ratio for the 100 mm/s tests was higher than the mean value for the 500 mm/s tests, indicating a possible roll speed effect, even though its level of significance from the analysis of variance was greater than 0.1.

Roll load results

In addition to the feed speed results documented above, roll load measurements were also made, although they were of secondary interest. The roll load measurements were of relatively poor quality since the load cells used were calibrated for delivery nip loads (pressures up to 20 MPa) while the pressures generated in this experiment were from underfeed nip loads (typically up to 100 kPa). While the smaller contact angle tests generated little observable roll load signal, the larger contact angle tests generated an observable trace. A typical result (test 6) is shown in Figure 6.7. While Figure 6.7 indicates the prepared cane passed through the mill roughly from the 5 s mark to the 15 s mark, the roll load trend shows a gradual increase in roll load to a peak around the 13 s mark. This trace is in contrast to the expected result where roll load typically rises quite fast to a maximum value and maintains that value before falling quite fast towards the end of the test. This issue is discussed further in section 6.3.7.

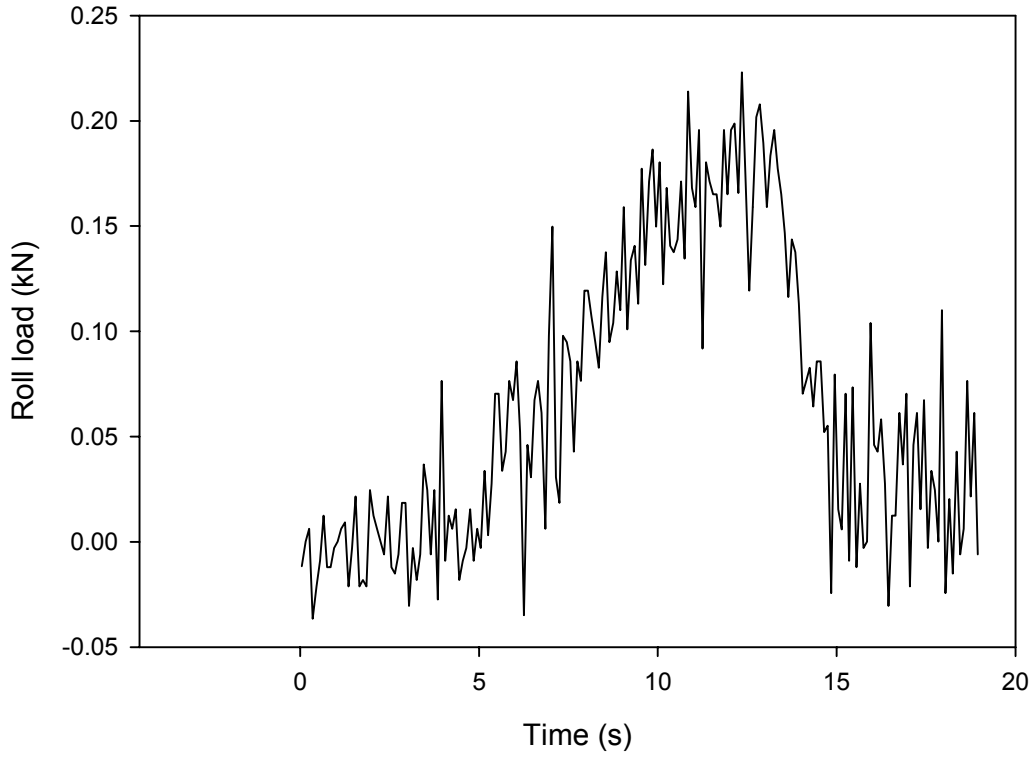

Figure 6.7 Roll load history for the two-roll mill experiment's test 6

6.3.6 Discussion of feed speed results

Introductory remarks

For Murry's feed speed ratio to vary from a value of 1, the assumption that the feed speed (S_F) is equal to $S \cos \alpha$ (section 2.2.3) must be invalid. The expression, $S \cos \alpha$, describes the component of the roll speed in the feed direction. For the feed speed to vary from $S \cos \alpha$, there are three possible explanations:

1. The mat does not make contact with the roll surface at the contact angle α,
2. The mat slips on the roll surface so that the speed of the mat on the roll surface is not equal to S cos α,
3. The mat deforms in the feed direction so that the speed of the centre of the mat remote from the roll surface differs from the speed of the mat at the roll surface.

The true contact angle

Murry's theory assumes that the bagasse at the surface of the mat is following the wall of a chute up until the prepared cane makes contact with the roll surface. Immediately upon contact with the roll surface, the prepared cane is assumed to suddenly change direction and follow the roll surface. This ideal behaviour is unlikely to occur in practice. The action of one part of the prepared cane mat changing direction is going to result in the immediately adjacent part of the prepared cane mat also moving to follow the roll surface and consequently not make contact with the roll surface until closer to the nip. This more realistic behaviour is shown in Figure 6.8. While Murry's theory uses the contact angle α, the true contact angle has the smaller value α'. Since α' is smaller than α, cos α' is greater than cos α. If the feed speed was actually equal to S cos α', Murry's feed speed ratio would be higher than one.

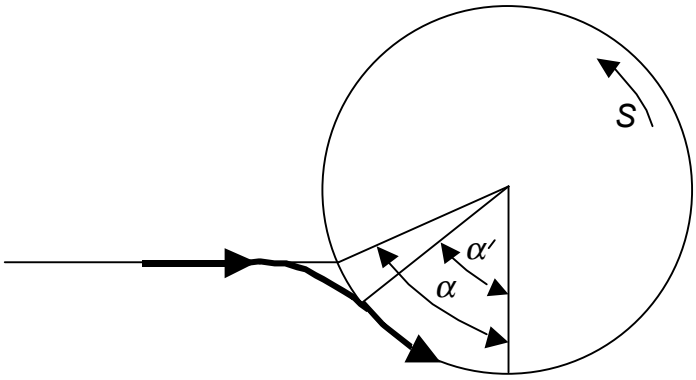

Figure 6.8 More realistic flow path for the surface of the bagasse mat

In addition to the effect on the contact angle, the more realistic flow path shown in Figure 6.8 may also affect the speed of the mat. It is likely that the act of pulling the prepared cane mat into the nip before the nominal contact point also pulls the mat forward towards the nip, causing the speed of the prepared cane mat to increase. Under these circumstances, Murry's feed speed ratio would again be greater than one.

Intuitively, the contact angle modification will be greater when contact angle is large than when contact angle is small. Consequently, α will be overestimated and S will be underestimated to a greater extent when the contact angle is large, meaning Murry's feed speed ratio is expected to be overestimated to a greater extent at large contact angles than at small contact angles. This expected result matches the experimental trend that shows Murry's feed speed ratio to be greater at larger contact angles.

Slip on the roll surface

Slip could potentially occur either backwards (with the blanket speed less than the roll speed) or forwards (with the blanket speed greater than the roll speed) depending on the direction of the tangential force at the roll surface. Backwards slip would result in lower values for Murry's feed speed ratio. Forwards slip would result in higher values for Murry's feed speed ratio, as observed in section 6.3.5.

Backwards slip was addressed in the frictional theory of mill feeding developed by Bullock (1957) and discussed in section 2.2.3. For backwards slip to occur, the contact angle must be greater than the angle of nip (section 2.2.3). In addition, the tangential frictional force developed from the pressure the roll surface exerts on the bagasse mat between the contact angle and the angle of nip, coupled with the feed pressure, must be insufficient to cause the bagasse mat to feed past the angle of nip. Under these conditions, the bagasse mat would not feed into the mill. Since the bagasse mat did feed into the mill in the experiments, it is unlikely that backwards slip occurred.

If the feed pressure was sufficiently large that the tangential frictional force changed directions to oppose the feed pressure, forward slip may occur. As discussed in section 6.3.5, substantial forward slip was observed in two tests and one other test experienced forward slip to a limited extent.

The forces acting on the bagasse mat under conditions of forward slip are shown in Figure 6.9. The only difference between this force diagram and the diagram for backwards slip presented in Figure 2.2 is the direction of the frictional force, F_F. Equation **(6.3)** was developed for forward slip in the same way that equation **(2.15)** was developed for backwards slip:

$$dF_H = L\ D\ P_{v\theta}\ \frac{\tan\theta + \mu'}{1 - \mu'\tan\theta}\cos\theta\ d\theta \qquad \textbf{(6.3)}$$

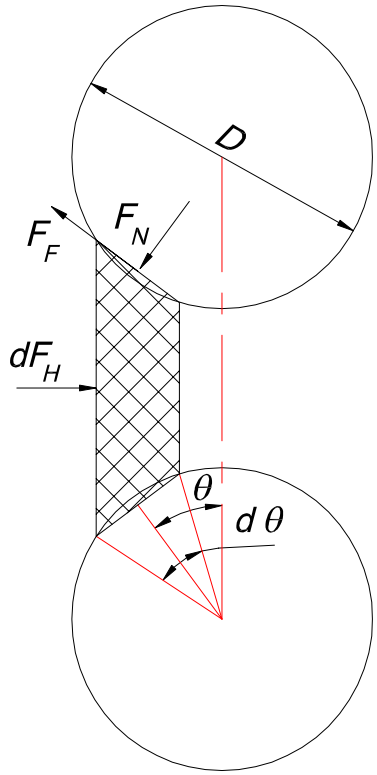

Figure 6.9 Forces acting on a strip of bagasse in a two-roll mill under conditions of forward slip

Forward slip will occur when the left hand side of equation **(6.3)** exceeds the right hand side with μ' equal to the coefficient of friction. For this condition to occur, either $P_{v\theta}$ must be small or θ must be small (as shown in Figure 6.10, $\frac{\tan\theta + \mu'}{1 - \mu' \tan\theta} \cos\theta$ is small when θ is small) for the right hand side of the equation to be small or the feed pressure must be large for the left hand side of the equation to be large.

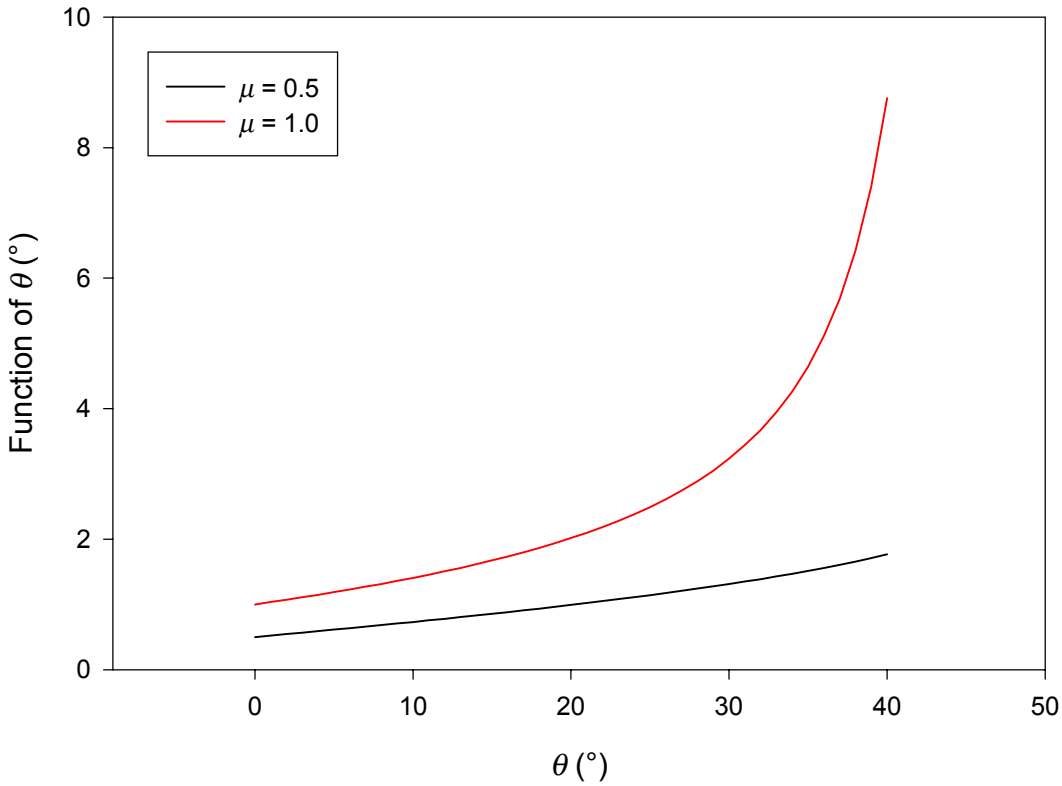

Figure 6.10 The effect of the angle from the nip on the function of the angle in equation (6.3)

For θ to be small for all possible values, the contact angle must be small. At small contact angles, the amount of compression undertaken by the bagasse mat will be small and the pressure resulting from that compression, $P_{v\theta}$, will also be small. Consequently, small contact angles will result in low values for both θ and $P_{v\theta}$, increasing the likelihood of forward slip.

While the contact angle defines the amount of compression that will take place in the bagasse mat, the thickness of the bagasse mat also has an impact on the pressure resulting from the compression. Since the nip setting defines the thickness of the blanket, nip setting also has an impact on the value of $P_{v\theta}$. Larger values of nip setting result in lower values of $P_{v\theta}$ for a given contact angle, indicating that larger nip settings are also likely to favour forward slip.

As discussed in section 6.3.5, forward slip was detected during tests involving the larger feed pressure, smaller contact angle and larger nip setting values. Forward slip was also only detected at the smaller roll speed values. In this section, three possible mechanisms are explored to explain why forward slip should be more likely at low roll speed: changes to the coefficient of friction, rate dependent solid phase behaviour and rate dependent fluid phase behaviour.

To achieve forward slip at the lower roll speed value, the coefficient of friction between the bagasse mat and the roll surface would have to be lower at low roll speed than at high roll speed. Bullock and Murry (1957) and Cullen (1965) found that coefficient of friction decreased as rubbing speed increased (section **2.2.3**). It is unlikely that, prior to the onset of forward slip, rubbing speed could be higher at low roll speed than at high roll speed, making it unlikely that coefficient of friction differences could be responsible for forward slip at low roll speed.

Rate dependent solid phase behaviour, known as creep (Muir Wood 1990), is certain to occur to some extent. This behaviour would result in a lower compression pressure, $P_{v\theta}$, at lower roll speed. As discussed above, the lower compression pressure would reduce the frictional force available to resist the feed pressure, resulting in a greater likelihood of forward slip. The analysis of the compression tests described in section **5.5.4** found a good match to the experimental data with a single set of material parameters at compression speeds from 1 mm/s to 100 mm/s and compression times from seconds to hundreds of seconds without a rate dependent solid phase model. Since the compression speeds varied by only a factor of five between the lower roll speed and the higher roll speed and the compression times from fractions of a second to several seconds, it was considered unlikely that creep could have contributed substantially to the likelihood of forward slip.

Rate dependent fluid phase behaviour is built into the new throughput model through the fluid phase constitutive model (section 4.8). Adam and Loughran (1998) show model predictions of maximum fluid pressure just before the nip with a pressure gradient back towards the feed side, an effect capable of providing a further force to resist the feed pressure and prevent forward slip. Since the resisting force would be

greater at higher roll speed, forward slip would be more likely at low roll speed. While Adam and Loughran's prediction was based on the flow of juice, the same trend is expected for the flow of air, the only fluid expressed in this experiment, although the effect would be less since the viscosity of air is less than the viscosity of juice. The statistically significant feed pressure effect was achieved with a 4 kPa difference in feed pressure. It is reasonable to assume that a difference in juice pressure resistance resulting from the different roll speeds would also need to be of this order to affect the feed speed. Assuming the juice velocity to be 0.5 m/s, the same as the roll speed in the higher speed tests; a flow length of 0.1 m, about half of the nip setting; and using an absolute viscosity of 0.02 mPa.s for air (Streeter & Wiley 1981); equation **(4.47)** predicts a permeability of about 10^{-9} m^2 would be required to cause a sufficiently large pressure drop (section 6.5.2 discusses the validity of equation **(4.47)** for compressible fluids like air). As shown in Figure 6.14, the permeability was measured to be less than 10^{-9} m^2 for void ratios less than about 20. Since the void ratio at the nip was typically about 20, air pressure could well be responsible for resisting forward slip at higher roll speeds.

Of the three potential mechanisms for explaining why forward slip should be more likely at low roll speed than at high roll speed, one has effectively been ruled out (lower coefficient of friction) and one is considered unlikely (creep). The remaining mechanism, that the expression of air creates a larger resisting force at higher roll speed, appears, from a simple calculation, to have sufficient ability to provide the required explanation for why forward slip was only observed at the lower roll speed value where the resisting force from the fluid is less.

In summary, it is considered unlikely that slip on the roll surface has contributed substantially to the variation in Murry's feed speed ratio. It is unlikely that backwards slip occurred to any degree since no feeding problems were experienced in any of the tests. The most likely impact of slip was during the tests where forward slip was identified. Credible explanations have been found to explain why forward slip should have occurred during the high feed pressure, low contact angle, large nip setting and low roll speed tests. High feed pressure is expected to overcome the forces preventing forward slip. Low contact angles and large nip settings are expected to reduce the

frictional force available to prevent roll slip. Low roll speeds are expected to develop insufficient air pressure to resist the feed pressure and prevent forward slip.

Non-uniform speed distribution

If Murry's feed speed ratio is not equal to 1.0 and there is no slip at the roll surface, it is likely that there is a non-uniform speed distribution through the mat with the centre of the mat either travelling faster than the material at the surface of the roll (Murry's feed speed ratio greater than 1.0) or slower than the material at the surface of the roll (Murry's feed speed ratio less than 1.0). Considering a strip of bagasse through the mat such as the vertical strip shown in Figure 6.9, if the material at the centre of the mat is travelling faster than the material at the roll surface, the material at the centre of the mat must be shearing forward. Forces must be present to enable this forward shear to occur.

To explore conditions likely to result in a non-uniform speed distribution through the mat, the strip of bagasse in Figure 6.9 has been considered to be a thick beam, supported at the roll surfaces and deformed by the forces present. The forces acting on the strip are the feed pressure and the fluid resistance.

If feed pressure increases, the centre of the strip of bagasse will move towards the nip, increasing the speed at the centre of the mat and increasing Murry's feed speed ratio. Increasing the nip setting increases the length of the strip, increasing the deflection of the strip for a given feed pressure and increasing Murry's feed speed ratio. As discussed above, air pressure is expected to provide a fluid resistance force acting in the opposite direction to feed pressure. Since the resisting force is expected to be larger at higher roll speed, it will reduce the deflection more at high roll speed, reducing Murry's feed speed ratio.

In summary, higher average speeds and, consequently, higher values of Murry's feed speed ratio, are expected with higher feed pressure, larger nip setting and lower roll speed. These expectations match the experimental trends.

Concluding remarks

The results of a two-roll mill experiment to explore the effect of various factors on Murry's feed speed ratio have been interpreted in order to identify mechanisms to explain the observed behaviour.

It is considered likely that the prepared cane mat is pulled towards the rolls before the nominal contact point, making the true contact angle on the rolls smaller than the theoretical contact angle and the speed of the mat leading to the contact point higher. These two effects combine to result in the feed speed being higher than $S \cos \alpha$. The difference between the feed speed and $S \cos \alpha$ is expected to be greater at larger contact angles. As a consequence, Murry's feed speed ratio is expected to be higher when contact angle is higher.

A non-uniform speed distribution through the bagasse mat is expected to result in changes to Murry's feed speed ratio. Higher values for Murry's feed speed ratio are expected for higher feed pressures, larger nip settings and lower roll speeds. The higher feed pressure and larger nip settings are expected to enable the centre of the bagasse mat to shear forwards through the nip at a faster rate than the surface of the bagasse mat. Higher roll speeds are expected to provide a greater air pressure to resist the forward shear, resulting in higher values for Murry's feed speed ratio at lower roll speeds.

Forward slip is expected to occur at lower contact angles, higher feed pressures, larger nip settings and lower roll speeds. The higher feed pressure is expected to exceed the frictional resistance available. The lower contact angle and larger nip setting are expected to reduce the frictional resistance available. The lower roll speed is expected to reduce the air pressure resistance to the flow of bagasse.

6.3.7 Discussion of roll load results

As discussed in section 6.3.5, the roll load trace throughout a test was quite unusual with roll load slowly rising towards a peak near the end of the test. Since roll load is

strongly correlated with nip compaction (Bullock 1955), it seems likely that the nip compaction was increasing throughout the test. Since the escribed volume was constant throughout the test, the fibre rate must have increased. The most likely cause of an increasing fibre rate is an increase in feed compaction caused by an increase in the effective feed pressure acting on the prepared cane mat.

The test results showed that the applied feed pressure at the back of the prepared cane block was constant throughout each test. It seems likely that, if the effective feed pressure acting on the prepared cane mat at the mill did increase as concluded above, some of the applied feed pressure must have dissipated through frictional contact with the wooden board on which the block slid into the mill. Assuming a coefficient of friction between the prepared cane block and the wooden board of μ_b, the effective feed pressure at the roll surface, P_a', is given by:

$$P_a' = P_a - \frac{\mu_b \, m \, g}{h \, L} \qquad \textbf{(6.4)}$$

where P_a is the applied feed pressure measured at the back of the block, m is the mass of cane in the block applying force to the board, g is the acceleration due to gravity, h is the feed setting and L is the roll length.

As the block leaves the wooden board and passes into the nip between the two rolls, the mass of the block remaining on the board reduces and the effective feed pressure increases until it equals the applied feed pressure at the end of the test.

6.3.8 Concluding remarks

A 32 test experiment was carried out on a small scale two-roll mill to explore the effect of mill geometry, roll speed, feed pressure and feed material on Murry's feed speed ratio.

Nip setting was found to be the factor with the greatest effect on Murry's feed speed ratio. Larger nip settings resulted in larger values for Murry's feed speed ratio. The contact angle and feed pressure factors also affected Murry's feed speed ratio. The larger contact angle and larger feed pressure settings gave larger values for Murry's feed speed ratio. A reasonably large roll speed effect was also identified but this effect was not found to have a level of significance less than 0.1 in any of the analyses of variance. No evidence of a cane variety or preparation effect on Murry's feed speed ratio was found.

From video footage taken of the experiment and the calculated values for Murry's feed speed ratio, three of the tests were found to have experienced forward slip of the prepared cane mat through the mill nip. Forward slip was identified by comparing the motion of specific points on the roll surface with the motion of adjacent points within the prepared cane mat. This forward slip occurred at the low contact angle, large nip setting, low roll speed and high feed pressure conditions. Roll speed, while not found to have a statistically significant effect, was most likely an important factor in causing forward slip.

Probable explanations were found for the experimental results. Murry's feed speed ratio is believed to be underestimated at large contact angles since it is likely that the true contact angle is somewhat less than the theoretical contact angle. Forward shear is expected to occur to a greater degree when the feed pressure is high, the nip setting is high and the roll speed is low, causing higher values for Murry's feed speed ratio. Forward slip was expected at high feed pressure conditions since the high feed pressure exceeded the frictional resistance, low contact angle and large nip setting conditions since the frictional resistance was reduced and low roll speed conditions since the air pressure resistance was reduced.

An examination of the roll load results suggests that feed pressure increased throughout a test. The most likely cause of increasing feed pressure was a change in the frictional force between the prepared cane block and the wooden board underneath. As the test progressed and the remaining prepared cane block became smaller, the frictional force reduced, allowing a greater proportion of the feed pressure applied to the back of the

block to reach the rolls. This feed pressure variation was considered unlikely to have significantly affected the conclusions of this work but was considered to have reduced the effective feed pressure acting on the prepared cane mat.

6.4 Material parameters for modelling the experiment without juice expression

6.4.1 Introductory remarks

The experiment to explore the factors affecting mill throughput (section 6.3) involved the use of prepared sugarcane from two cane varieties (Q124 and Q117) and two levels of preparation (using shredder speeds of 1200 r/min and 2000 r/min) as listed in Table 6.2. This section describes the tests that were conducted to define material parameters for the solid and fluid constitutive equations within the new throughput model.

6.4.2 Material parameters for the solid phase

Uniaxial compression tests and subsequent parameter estimation techniques were used to determine the material parameters for the solid phase as described in section 5.2.

The test cell was in the configuration shown in Figure 5.1. Although the compression tests were conducted up to a maximum pressure of 2 MPa (corresponding to pressure feeder nip compactions), only the first stage of this compression where no juice was expressed, corresponding to the mill experimental conditions, was analysed to determine material parameters. The criterion used to determine the end point of the experimental data was when the sample height reduced to 250 mm. At this height, the top platen pressure was in the order of 200 kPa.

A complete list of the uniaxial compression tests undertaken is presented in Appendix D. Kent and McKenzie (2000) provided a more complete presentation of the experimental data.

The parameter estimation process involved matching model results to data from all tests for a particular cane variety and preparation level combination simultaneously. The parameters obtained from this process, using two different values for coefficient of friction between the prepared cane and the cell wall in the models, are shown in Table 6.7.

Table 6.7 Results of the solid phase material parameter estimation process

Cane variety	Shredder speed (r/min)	μ	κ	ν	M	λ_1
Q124	1200	0.5	0.49	0.30	2.0	0.2802
		1.0	0.56	0.17	2.8	0.2780
	2000	0.5	0.74	0.24	2.1	0.3029
		1.0	0.72	0.14	2.9	0.3007
Q117	1200	0.5	1.49	0.13	2.4	0.3029
		1.0	1.60	0.04	3.1	0.3012
	2000	0.5	0.65	0.28	2.0	0.3092
		1.0	0.64	0.16	2.9	0.3070

To assess whether the differences in parameters between the different cane varieties, levels of preparation and assumed coefficient of friction represent true differences in material behaviour or limitations in the estimation process, an analysis of variance was conducted on the data in Table 6.7. An analysis of variance was carried out for each of the four material parameters (elastic parameters, κ and ν and plastic parameter, M and λ_1). The data for each material parameter was treated as a 2^3 factorial experiment with cane variety (V), preparation (Z) and coefficient of friction (μ) as the factors. The results of the analysis of variance for all material parameters are shown in Table 6.8. The mean levels for each experimental factor for each of the material parameters is shown in Figure 6.11. The effect of each of the significant interaction terms identified in Table 6.8 is shown in Figure 6.12.

Table 6.8 Analysis of variance of the four estimated solid phase material parameters

Parameter	Source	Degrees of freedom	Mean square	Variance ratio	Significance level
κ	V	1	0.4371	3885	0.01
	Z	1	0.2415	2146	0.01
	μ	1	0.0028	25	-
	V:Z	1	0.6105	5427	0.009
	V: μ	1	0.0003	3	-
	Z: μ	1	0.0055	49	0.09
	Residuals	1	0.0001		
ν	V	1	0.0072	16	-
	Z	1	0.0041	9	-
	μ	1	0.0242	54	0.09
	V:Z	1	0.0162	36	-
	V: μ	1	0.0001	0	-
	Z: μ	1	0.0000	0	-
	Residuals	1	0.0005		
M	V	1	0.045	9	-
	Z	1	0.020	4	-
	μ	1	1.280	256	0.04
	V:Z	1	0.080	16	-
	V: μ	1	0.000	0	-
	Z: μ	1	0.005	1	-
	Residuals	1	0.005		
λ_1	V	1	0.00042778	13689	0.005
	Z	1	0.00041328	13225	0.006
	μ	1	0.00000861	276	0.04
	V:Z	1	0.00013861	4436	0.01
	V: μ	1	0.00000003	1	-
	Z: μ	1	0.00000003	1	-
	Residuals	1	0.00000003		

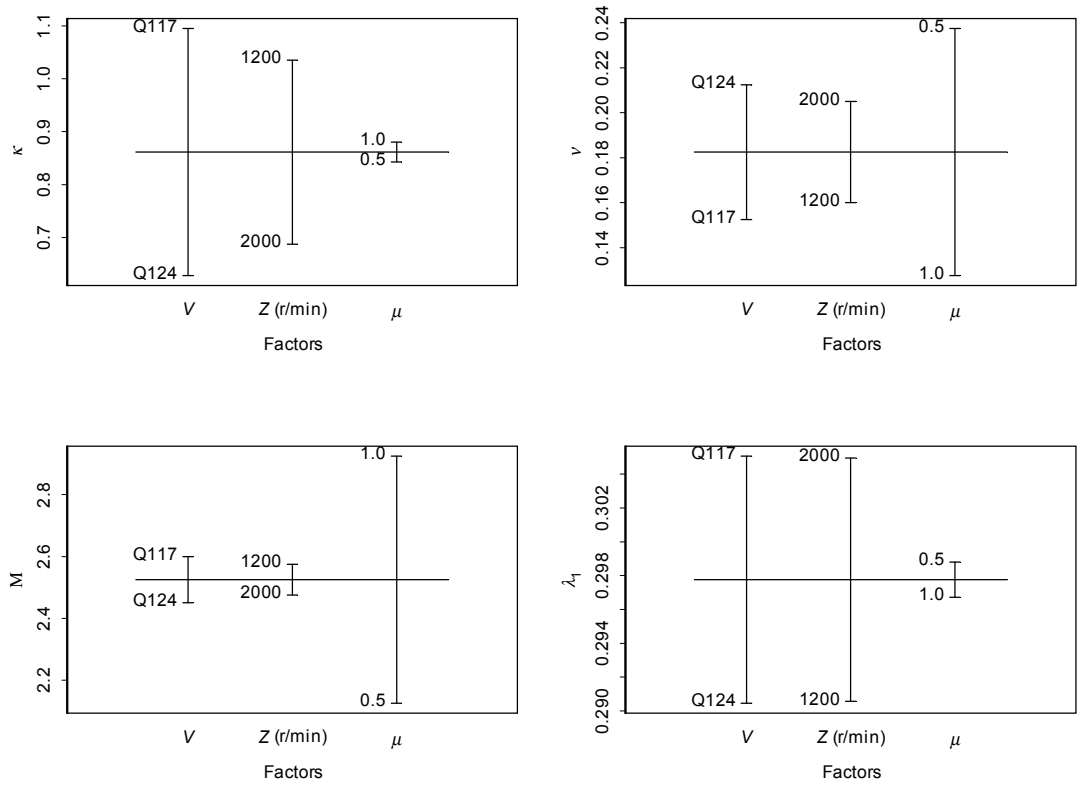

Figure 6.11 Mean values of estimated material parameters for each level of each factor from the material parameter estimation process

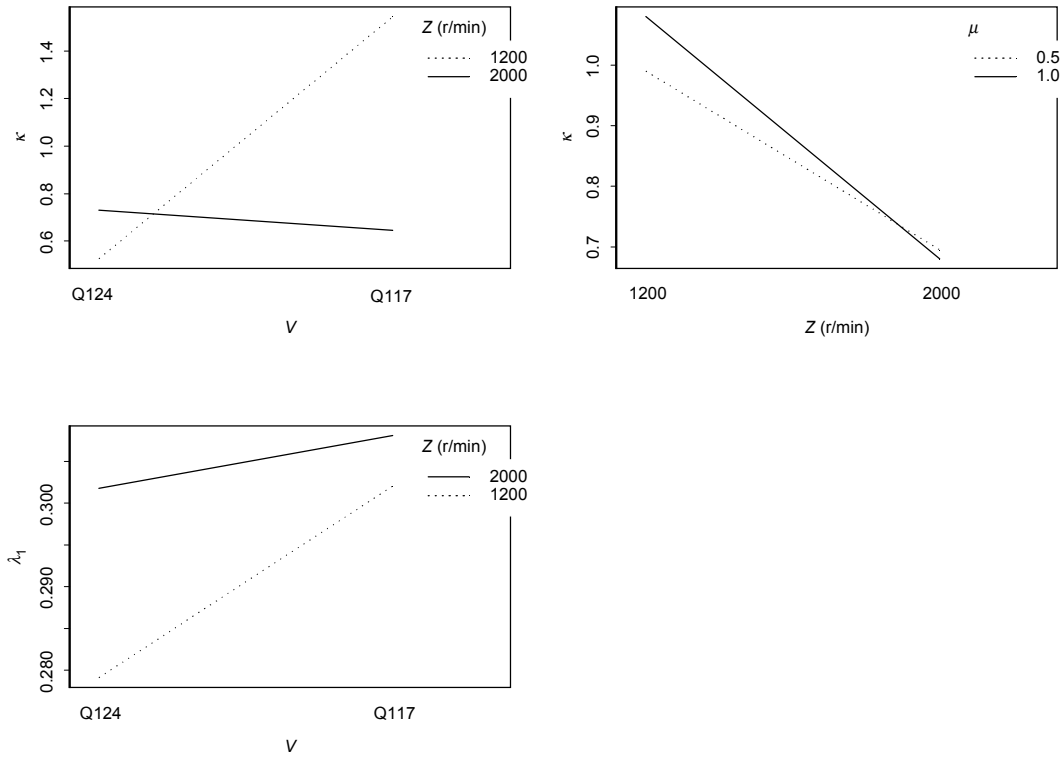

Figure 6.12 Significant interactions identified in the analysis of variance of the estimated material parameters

The analysis of variance for κ identified four significant effects: main effects for cane variety and preparation and first-order interactions between cane variety and preparation and between preparation and coefficient of friction. Referring back to the raw data in Table 6.7, it is evident that the estimated value for κ was much higher for cane variety Q117 prepared with the shredder speed of 1200 r/min than for any other combination. This difference is also shown in the cane variety and preparation interaction plot in Figure 6.12 and is responsible for three of the four significant effects: the two main effects and the first-order interaction between cane variety and preparation. Table 6.7 also shows that, for cane variety Q117 prepared with the shredder speed of 1200 r/min, ν is smaller than for any other combination. As discussed in section 5.2.5, the parameter estimation process does not define the elastic parameters, κ and ν, particularly well. A sensitivity analysis for the elastic parameters estimated for cane variety Q117 prepared with the shredder speed of 1200 r/min and using a coefficient of friction of 0.5,

similar to that shown in Figure 5.4, is shown in Figure 6.13. The sensitivity analysis shows that there is a range of suitable κ and ν combinations that achieve low objective functions. If the value for ν was known to be about 0.25, similar to the other cane variety and preparation combinations, a suitable value for κ to minimise the objective function would be 0.8, a value of similar magnitude to the remaining cane variety and preparation combinations. In light of the range of possible values for κ that provide reasonably low objective functions, the remaining significant interaction, between cane preparation and coefficient of friction, is unlikely to yield much information. In summary, the parameter estimation process has not provided any strong guidance to suggest any cane variety or preparation effect on the value for κ. A median value of about 0.7 from the values presented in Table 6.7 was considered appropriate.

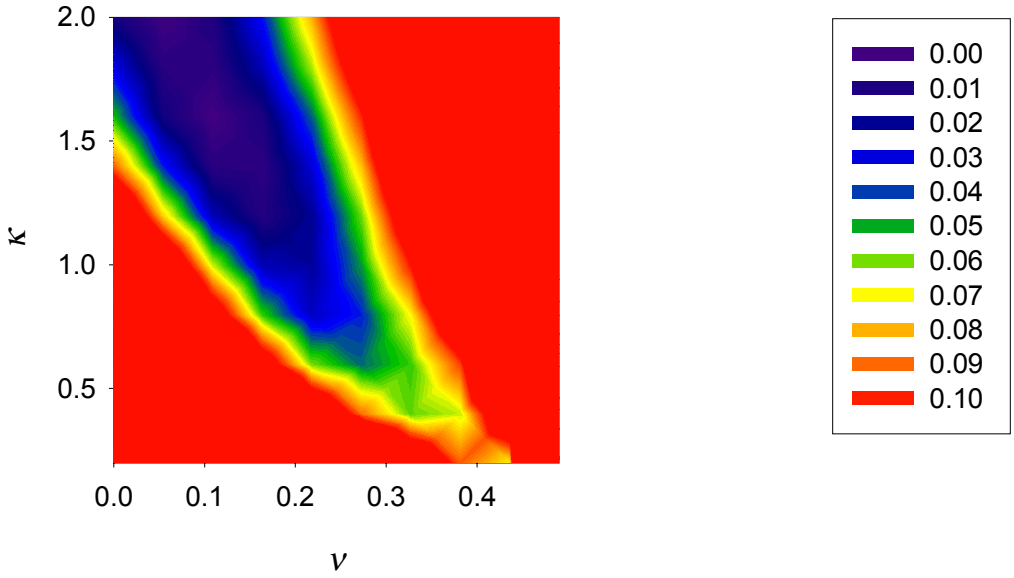

Figure 6.13 Results of sensitivity analysis showing the relative change in the objective function for a change in the elastic material parameters for cane variety Q117 prepared at a shredder speed of 1200 r/min

The analysis of variance for ν found only one significant effect: a main effect for coefficient of friction. The parameter estimation process has not provided any guidance to suggest that ν is dependent on either cane variety or preparation. The median value

for a coefficient of friction of 0.5 was 0.26. The median value for a coefficient of friction of 1.0 was 0.15.

The results of the analysis of variance for M were quite similar to those for ν with the only significant effect being the coefficient of friction. The median value for a coefficient of friction of 0.5 was 2.1. The median value for a coefficient of friction of 1.0 was 2.9.

The results of the analysis of variance for λ_1 show that differences in parameter values resulting from differences in cane variety, preparation and coefficient of friction, are significant, even though the differences are quite small. The λ_1 values shown in Table 6.7 were considered appropriate for use, although only two significant figures were desired.

For reasons discussed in section 6.5.2, a value for M of 3.0 was chosen. This value corresponds quite closely to the value of M estimated for a coefficient of friction of 1.0. Consequently, ν was given a value of 0.15, the value estimated for a coefficient of friction of 1.0. The parameter values chosen as representative of the prepared cane used in the two-roll mill experiment are summarised in Table 6.9.

Table 6.9 Solid phase material parameters selected to be representative of the prepared cane used in the two-roll mill experiment

Cane variety	Shredder speed (r/min)	κ	ν	M	λ_1
Q124	1200	0.7	0.15	3.0	0.28
	2000	0.7	0.15	3.0	0.30
Q117	1200	0.7	0.15	3.0	0.30
	2000	0.7	0.15	3.0	0.31

6.4.3 Material parameters for the fluid phase

The steady state method, described in section 5.3, was used to determine material parameters for the fluid phase.

Six steady-state permeability tests were conducted for each material. The tests were conducted as a 2x3 randomised factorial experiment where the effects of sample mass and void ratio on permeability were assessed. Two sample masses were explored: 0.6 kg and 1.2 kg. Three average void ratios were explored: nominally 30, 10 and 5. The desired void ratio was achieved by the selection of appropriate spacers to control the sample thickness. A complete list of the permeability tests is presented in Appendix D.

For each test, water was pumped through the sample. The inlet pressure was gradually increased from an initial value of about 15 kPa to a final value of about 200 kPa. At about eight pressure settings, the flow rate was measured.

For this test series, the pressure at the outlet of the test cell was not measured and a relatively long hose of small diameter was used to drain the water from the cell. Calculations using theory for steady incompressible flow through pipes (Streeter & Wiley 1981) showed that the pressure loss in the hose could not be neglected in determining the pressure drop across the prepared cane sample. Consequently, the pipe flow theory was used to amend the pressure readings.

The permeability parameters, k_1 and k_2, were derived from a parameter estimation process where predicted flow rates from a model of the test were matched to the experimental results, as described in section 5.3.4. For this process, four of the six tests for each material were analysed together. The remaining two tests corresponding to the average void ratio of 30 were not used in the parameter estimation process because the pressure measurements, after allowing for the hose pressure drop, were small and considered unreliable. The estimated parameters are shown in Table 6.10.

Table 6.10 Results of the permeability parameter estimation process

Cane variety	Shredder speed (r/min)	k_1	k_2
Q124	1200	0.36×10^{-18}	7.12
	2000	13.76×10^{-18}	5.73
Q117	1200	1.10×10^{-18}	3.29
	2000	55.79×10^{-18}	5.37

To assess whether the differences in parameters between the different cane varieties and levels of preparation represent true differences in material behaviour or limitations in the estimation process, the void ratio / permeability relationships defined by the permeability parameters were graphed (Figure 6.14). The spread of the permeability values between the uppermost curve and the lowermost curve is, at most, a factor of seven, less than one order of magnitude. Since the curves in Figure 6.14 cross over at a void ratio of about 15, there is no consistent trend in permeability between the results. Consequently, a single set of permeability parameters was chosen to represent all of the cane variety and preparation combinations.

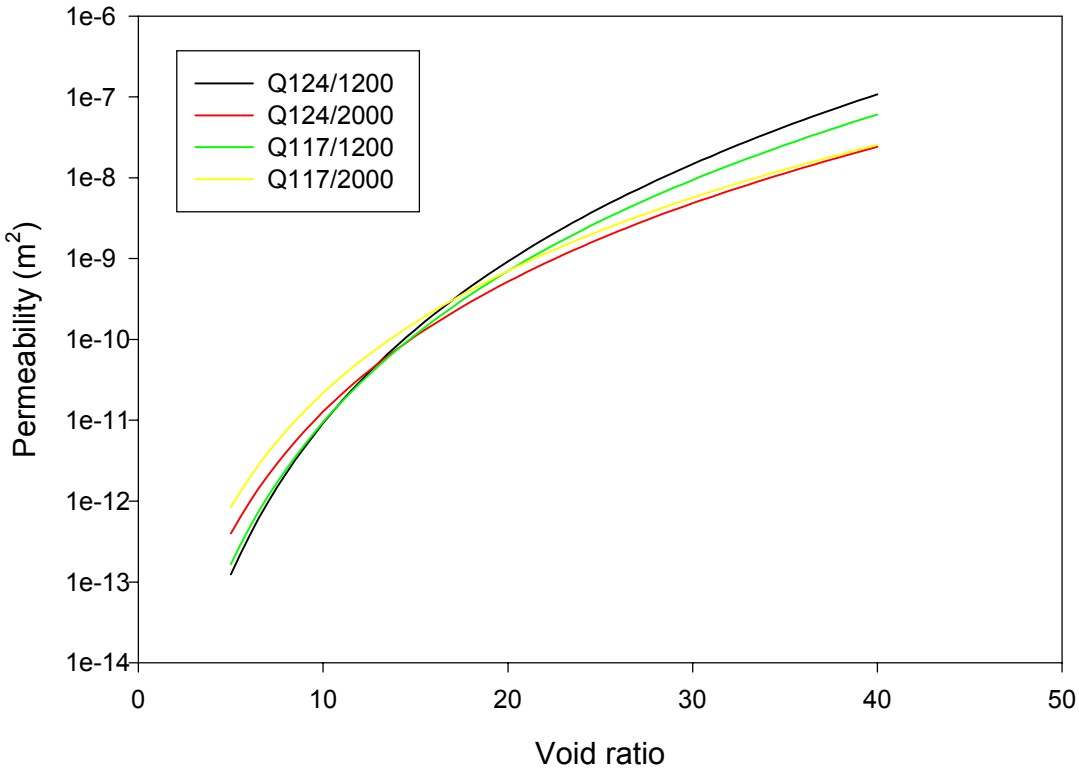

Figure 6.14 Permeability relationships for each cane variety and level of preparation using the estimated parameters

To produce a combined set of permeability parameters, a regression analysis was completed using the data presented in Figure 6.14. The selected permeability parameters were $k_1 = 2.3 \times 10^{-17}$ m^2 and $k_2 = 5.8$.

6.4.4 Concluding remarks

Material parameters for the solid phase and the fluid phase of prepared cane have been determined for use in the new throughput model. Of the four solid phase parameters and two fluid phase parameters estimated, only one parameter (λ_1) was confidently determined to have different values for the two cane varieties and levels of preparation used in the two-roll mill experiment (section 6.3). For the remaining parameters, the same values were assumed suitable for each material.

6.5 Modelling the experiment without juice expression

6.5.1 Introductory remarks

The experiment to measure the effect of mill parameters on throughput (section 6.3) showed that Murry's feed speed ratio was higher with a larger nip setting, a larger contact angle and a larger feed pressure. There was also some evidence to suggest that Murry's feed speed ratio was higher at lower roll speed. Forward slip of the bagasse mat through the nip was observed under large nip setting, small contact angle, larger feed pressure and low roll speed conditions.

Probable causes for the measured behaviour were identified in sections 6.3.6 and 6.3.7. The true contact angle is considered overestimated at high contact angles, resulting in inflated values for Murry's feed speed ratio. Forward shear through the bagasse mat is believed to occur under larger nip setting, larger feed pressure and lower roll speed conditions, resulting in higher values for Murry's feed speed ratio. Forward slip of bagasse mat is believed to occur at high feed pressures where the feed pressure exceeds the frictional resistance forces, at low contact angles and large nip settings where the frictional resistance is less and at low roll speeds where the air pressure resistance is less. The feed pressure at the roll surface is believed to increase throughout a test as the frictional resistance caused by the prepared cane block sliding on the wooden board underneath reduces.

In this section, a model to predict the throughput of a two-roll mill is described and tested against the experimental results presented in section 6.3. The model is capable of quantifying all of the probable causes of the measured behaviour listed above.

6.5.2 Model details

Introductory remarks

The pre-compression and milling components of the test procedure (section 6.3.4) were modelled separately. The pre-compression stage was a low-speed simple uniaxial compression operation that could be adequately modelled as a single element. A simple computer program was developed to model this operation. The two-roll mill was modelled within the ABAQUS finite element analysis software (Hibbitt, Karlsson & Sorensen 2000).

Both models solved the governing equations described in chapter 4.

Material parameters

The material parameters listed in Table 6.9 and in section 6.4.3, with the exception of k_1 (discussed later this section), were used.

The two solid phase material parameters not defined in Table 6.9, p_t^e and p_t were chosen to ensure computational stability of the model. Specifically, p_t^e was chosen to limit the amount of expansion of the prepared cane block after pre-compression and p_t was chosen to limit lateral expansion. These issues are discussed further below. The chosen parameter values were p_t^e = -200 Pa and p_t = -500 Pa.

As mentioned in section 6.4.2, a value of 3.0 was selected for M. This value was chosen to allow the block of prepared cane to be loaded in unconfined uniaxial compression as discussed below. Unconfined uniaxial compression creates a stress condition where one direct stress component is non-zero and all other stress components are zero. Substituting the stress components into equations **(4.15)** and **(4.16)**, it can be shown that unconfined uniaxial compression requires $\eta = \frac{q}{p} = 3$.

Figure 6.15 shows a typical stress loading path in relation to the yield surface during unconfined uniaxial compression. The stress magnitudes in Figure 6.15 are relevant for one of the 7 kPa feed pressure tests. At the start of the test, the stress state is at the origin. The stresses then increase along the loading path as the test progresses. Depending on the maximum feed pressure, the loading path may or may not reach the initial yield surface. If the loading path does reach the initial yield surface, the yield surface will grow until the maximum feed pressure is reached.

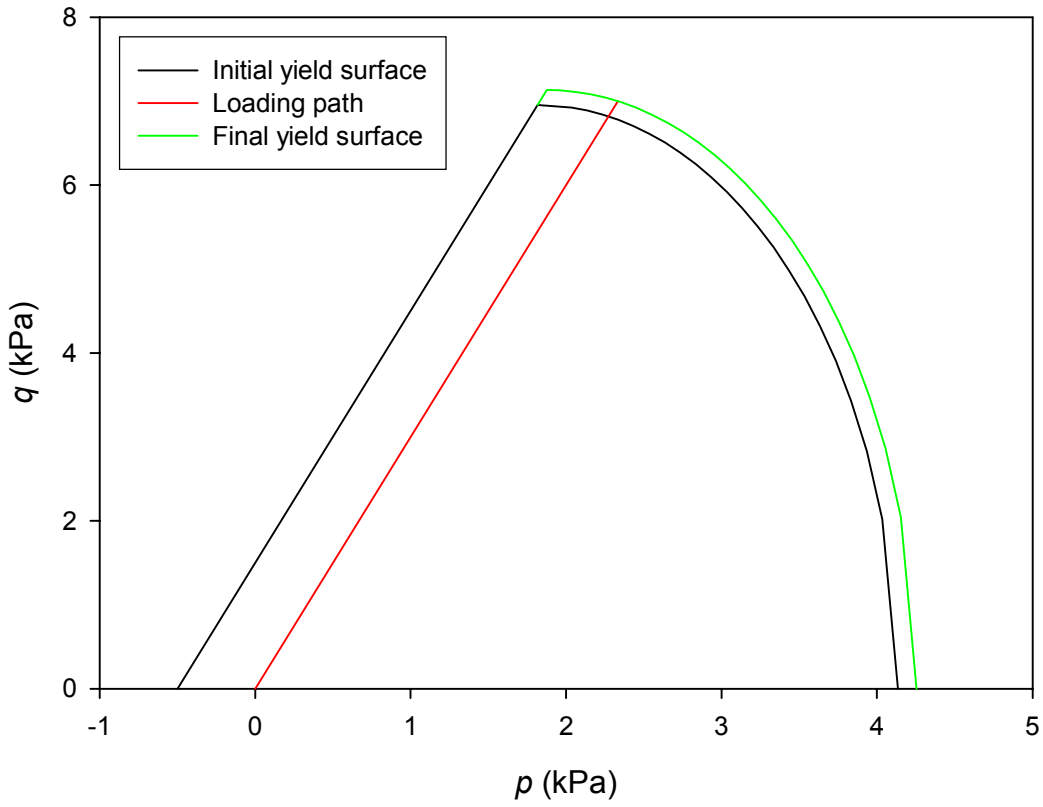

Figure 6.15 Typical unconfined uniaxial compression loading path

Because M = 3.0 in Figure 6.15, the shear failure yield surface (Figure 4.3) is parallel to the loading path. If a lower value for M was chosen, care would be required in the selection of p_t to ensure p_t was sufficiently large so that, at the maximum feed pressure, the loading path did not intersect the shear failure yield surface. By choosing M = 3.0, the loading path can never intersect the shear failure yield surface.

The parameter p_t was assigned the value –500 Pa to ensure that, when the loading path reached the yield surface, the point of contact was sufficiently far from the apex of the cap that the plastic strain vector, perpendicular to the yield surface, was not too close to the q direction. Keeping the plastic strain vector away from the q direction ensured that the model did not expand too greatly in the transverse direction when yielding in unconfined uniaxial compression.

As discussed in section 6.3.6, the appropriate fluid for use in the fluid phase constitutive model was air. While Darcy's law, the constitutive model, was developed for incompressible fluids, the use of Darcy's law for air at low air pressures was considered acceptable. For a perfect gas, pressure is proportional to density at constant temperature. Since atmospheric pressure is typically 100 kPa and the air pressure drops expected in the model are typically 1 kPa, the density of the air is expected to change only 1%, a small amount of compressibility. The air was characterised by an absolute viscosity of 0.02 mPa.s.

Although the analysis of the permeability tests provided an estimate for k_1 of 2.3×10^{-17} m^2, this value had to be reduced by more than two orders of magnitude to 6.0×10^{-20} m^2 in order to reproduce the desired speed trend (shown in section 6.5.3). Considering the permeability values shown in Figure 6.14 span five to six orders of magnitude, this reduction in permeability is not large. It is also possible that the estimated permeability values were somewhat in error. As discussed in section 6.4.3, the permeability parameters were derived from tests conducted at nominal void ratios of 5 and 10. In comparison, the void ratios calculated in the two-roll models were typically above 20, well outside the range of void ratios for which the permeability parameters were estimated. It is also possible that the permeability measurements, conducted under saturated conditions, overestimate the permeability under the unsaturated conditions of this experiment.

Initial conditions for the pre-compressor

As discussed in section 6.3.4, each test involved forming a block of prepared cane in a pre-compressor, removing the block from the pre-compressor and then pushing the

block into the mill. The initial conditions for the ABAQUS model were taken at the point before the block was pushed into the mill. A simple model, described below, was used to determine the ABAQUS model initial conditions based on the predicted behaviour in the pre-compressor. The initial conditions for the simple model were defined at the fully loaded position in the pre-compressor.

The aim of loading in the pre-compressor was to pre-compress the sample to its desired feed pressure (section 6.3.4). Consequently, the initial effective stress in the bagasse flow direction, σ'_{xx}, was assumed to be equal to the feed pressure. The other two effective stress components were determined from:

$$\sigma'_{yy} = \sigma'_{zz} = K_0 \, \sigma'_{xx} \qquad \textbf{(6.5)}$$

Since the pre-compressor compression was a confined uniaxial compression operation, K_0 was calculated from equation **(5.8)** and equation **(5.21)**.

The initial void ratio was defined from the known volume of the pre-compressor in its loaded state, the known sample mass and the measured fibre content:

$$e_0 = \frac{l \, h \, L \, \rho_f}{f \, m} - 1 \qquad \textbf{(6.6)}$$

where l is the length of the bagasse mat, h is the height of the bagasse mat (the feed chute setting), L is the width of the bagasse mat (the roll length), ρ_f is the density of fibre (1530 kg/m^3), f is the fibre content and m is the sample mass.

Modelling relaxation in the pre-compressor

A simple model was used to model the relaxation of the prepared cane block in the pre-compressor as the applied load was removed. The behaviour is uniaxial so equations **(5.3)**, **(5.4)**, **(5.5)** and **(5.6)** applied. The relaxation was elastic, so equation **(5.9)** described the complete behaviour. The relaxation was defined in two stages.

The first relaxation stage consisted of confined uniaxial behaviour. Following the same procedure used to define equation **(5.21)**, equation **(5.9)** was simplified for confined uniaxial relaxation to show:

$$\eta = \frac{3(1-2\nu)}{1+\nu} \qquad \textbf{(6.7)}$$

Equation **(6.7)** defines the proportional amounts that p and q reduce due to a reduction in the applied pressure σ'_{xx}. Equation **(5.9)** was used to determine the decrement in strain that accompanied the pressure reduction. The accompanying increase in void ratio was determined from equation **(4.26)**.

As shown in equation **(6.7)**, the proportional amounts that p and q reduce, and consequently, the amounts that the axial and transverse stress components reduce, is dependent on Poisson's ratio, ν. Consequently, the value of ν determines whether the transverse stress component reaches zero before or after the applied load is completely removed. At the selected value for ν of 0.15, the transverse stress component reaches zero before the applied load is completely removed. Consequently, the final stage of applied load removal occurs under unconfined uniaxial relaxation conditions, since the model predicts the bagasse will separate from the pre-compressor walls after the transverse stress reaches zero. Having bagasse separate from the walls after the transverse stress reaches zero is not consistent with qualitatively observed behaviour where the bagasse generally is wedged into the cell after load removal, meaning that, perhaps, ν should be smaller. Having bagasse separate from the walls, however, is mathematically simpler since it avoids the need to define a negative value for q.

The relaxation under unconfined uniaxial relaxation conditions is the second relaxation stage. As discussed above, unconfined behaviour occurs when $\eta = 3$. Once again, equation **(5.9)** was used to determine the decrement in strain that accompanied the pressure reduction and the accompanying increase in void ratio was determined from equation **(4.26)**.

No attempt was made to model the fluid phase in the pre-compressor model. The void ratios were typically above 25 and the relaxation times were long (in the order of minutes) so fluid pressure was considered unlikely to have any significant impact on the stress state at the end of the pre-compression stage.

Two-roll model geometry

The model was developed within the ABAQUS finite element analysis software using three dimensions, since the plane strain assumption used previously for the two-dimensional model (Adam & Loughran 1998) was not considered valid for the experimental conditions where the nip setting (120 mm to 240 mm) was of the same order of magnitude as the roll length (225 mm). Symmetry assumptions were used to reduce the model to one-quarter of the original geometry. The model was constructed using eight-node linear three-dimensional elements with four degrees of freedom (three displacement and one pore pressure).

The model geometry was determined from the block size in the pre-compressor and the strains calculated in the pre-compressor model. Typical element dimensions were 25 mm to 50 mm.

Two-roll model initial conditions

All stress components, including pore pressure, were assumed to be zero, initially. The initial void ratio was calculated in the pre-compressor model.

Two-roll model boundary conditions

The roll was modelled as a flat contact surface rotating at the desired roll speed. A coefficient of friction between the bagasse mat and the roll surface of 0.36 was chosen to model the forward slip observed in three tests (as discussed in section 6.3.5). The choice of coefficient of friction is discussed further in section 6.5.4). The pneumatic ram head was modelled as a contact surface behind the trailing face of the bagasse mat.

The bagasse mat was attached to the ram head by a soft spring. The spring was used to constrain rigid body motion of the bagasse mat.

To match the experimental procedure, the model was subjected to two load steps. The first load step described the mat moving at a constant speed towards the rolls and the feeding of the mat between the rolls until the desired feed pressure was developed. The second load step described the feeding of the mat between the rolls at constant feed pressure.

The first load step involved applying a velocity equal to 5 $S \cos \alpha$ in the bagasse feed direction to the ram head. The velocity was applied until the target feed pressure was developed at the ram head. The factor of 5 ensured that the ram speed was sufficient for the feed pressure to be developed early in the test simulation.

The second load step involved applying the feed pressure to the ram head until the trailing face of the bagasse mat made contact with the roll surface. As discussed in section 6.3.7, friction between the prepared cane block and the wooden board underneath is believed to have reduced the effective feed pressure at the front of the block. Rather than model the frictional force directly, a fixed feed pressure was applied to the rear of the block. The feed pressure was determined using equation **(6.4)** where m was defined as the total mass of the block. A value of 0.6 was selected for μ_b.

The pore pressure on all external boundaries was defined to be zero.

Calculating feed speed

The feed speed of the bagasse mat, S_F, was calculated from the average speed of the ram head during the second load step.

6.5.3 Model results

From the two-roll mill experiment described in section 6.3, the 29 tests that were assumed not to be affected by forward slip (section 6.3.5) were modelled in a numerical

experiment using the two-roll model described in section 6.5.2. A summary of the mean values of the experiment is presented in Figure 6.16. These results can be directly compared to those in Figure 6.4, the equivalent results from the two-roll mill experiment.

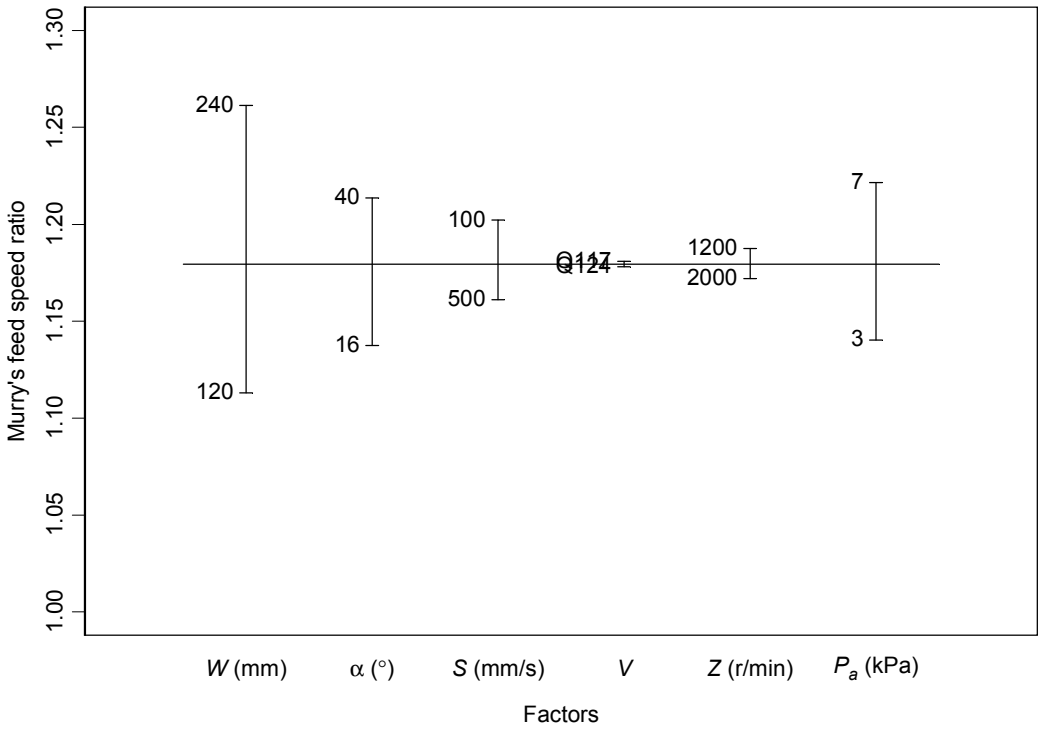

Figure 6.16 Mean values of Murry's feed speed ratio for the two-roll mill numerical experiment

While the two-roll mill results show a grand mean of about 1.10, the numerical results have a grand mean of about 1.18, a 7% difference. The model predicts similar effects to the experiment for all parameters. Table 6.11 shows the difference in Murry's feed speed ratio for each factor between the mean at the high factor level and the mean at the low factor level for both the model and the experiment.

Table 6.11 Main effect of each experimental factor on Murry's feed speed ratio

Factor	Murry's feed speed ratio difference	
	Model	Experiment
Work opening	0.15	0.17
Contact angle	0.08	0.09
Roll speed	0.04	0.06
Variety	small	small
Preparation	small	small
Feed pressure	0.08	0.09

It is no coincidence that the roll speed and feed pressure effects were well estimated. The desired feed pressure trend was achieved by adjusting μ_b, the coefficient of friction between the prepared cane block and the wooden block underneath. The desired roll speed trend was achieved by adjusting k_1, the permeability parameter. Overall, the calculated effects from the two-roll model matched the measured effects from the experiment quite well.

To show the results on a test-by-test comparison, the model results were plotted against the experimental results in Figure 6.17. The figure shows that Murry's feed speed ratio was generally predicted within about 10% of the experimental value with the outliers about 20% from the experimental value.

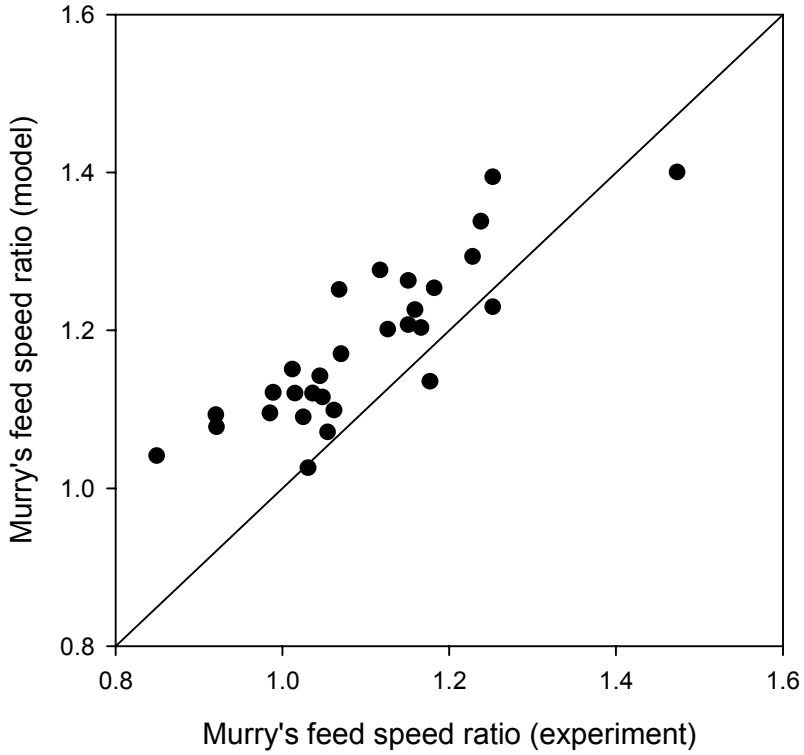

Figure 6.17 Murry's feed speed ratio compared between the two-roll mill model and the two-roll mill experiment

6.5.4 Using the model to explore mill feeding behaviour

Introductory remarks

In section 6.3.6, explanations for the effects found in the two-roll mill experiment were provided. In this section, the model is used to support those explanations.

The true contact angle

In section 6.3.6, it was argued that the prepared cane mat is pulled in towards the nip before it makes contact with the roll, causing the true contact angle to be less than the nominal contact angle and the true speed to be greater than the theoretical $S \cos \alpha$. To support that argument, the model was used to examine the effect of contact angle on Murry's feed speed ratio.

A series of six model runs were undertaken, based on the parameter values used for modelling test 21 of the two-roll mill experiment. The only parameter changed between runs was the contact angle, changed from its original 40° to 35°, 30°, 25°, 20° and 16°, respectively. The nominal element dimension was 25 mm for all runs. To determine typical values for blanket speed and contact angle for each run, a node in the centre of the top of the cane mat, approximately 490 mm from the front of the mat, was examined.

Figure 6.18 shows the predicted deformation of the blanket for the 40° and 16° contact angle runs. For the 40° case, the mesh can be seen compressing slightly in the vertical direction before contacting the roll, indicating that the true contact angle was, indeed, less than the theoretical contact angle. The element on the top of the mesh just making contact with the roll can be seen to be larger than the following element, indicating that the node at the contact point has accelerated forward, as predicted.

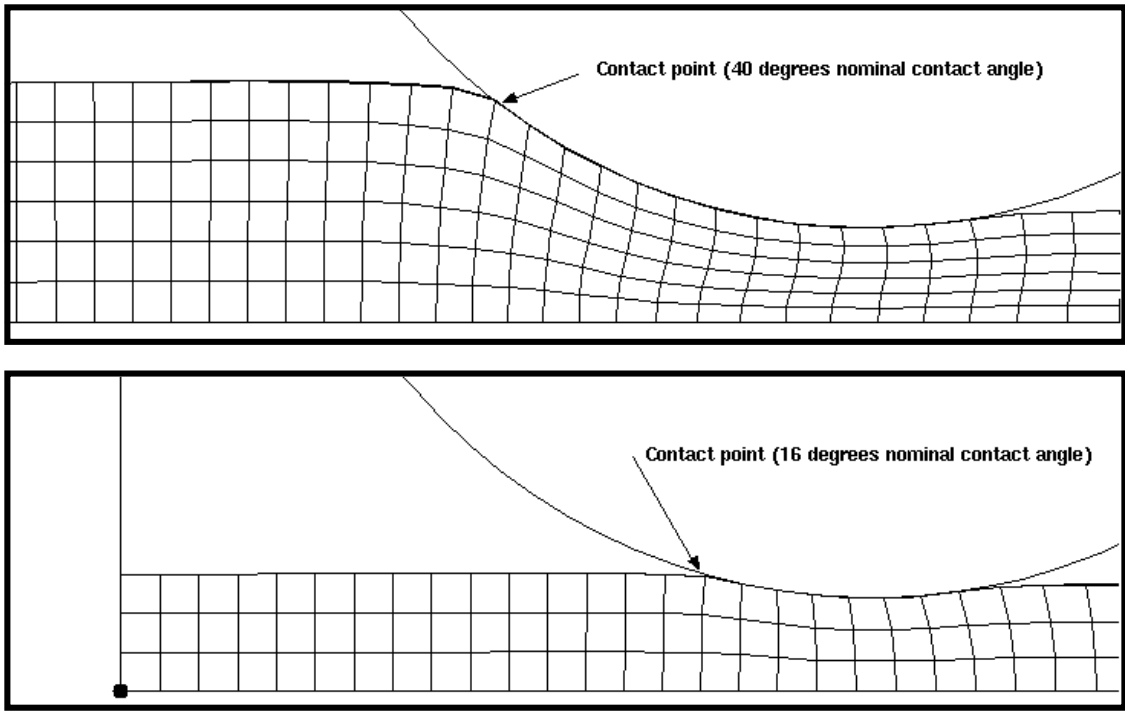

Figure 6.18 Model blanket deformation for 40° and 16° model runs

Based on the height of the blanket at the point of contact, the true contact angle for each run was calculated (using equation **(6.1)** with a modified *h*). For each run, the ratio of the cosine of the true contact angle to the cosine of the theoretical contact angle was calculated. This ratio was then divided by the ratio calculated from the 16° contact angle run (the run where the true contact angle and the theoretical contact angle were assumed to be closest in value) and presented in Figure 6.19. For comparison, the ratio of the feed speed ratio for each run to the feed speed ratio from the 16° contact angle run is also presented. Figure 6.19 shows that correcting the contact angle accounts for less than 20% of the predicted contact angle effect on Murry's feed speed ratio.

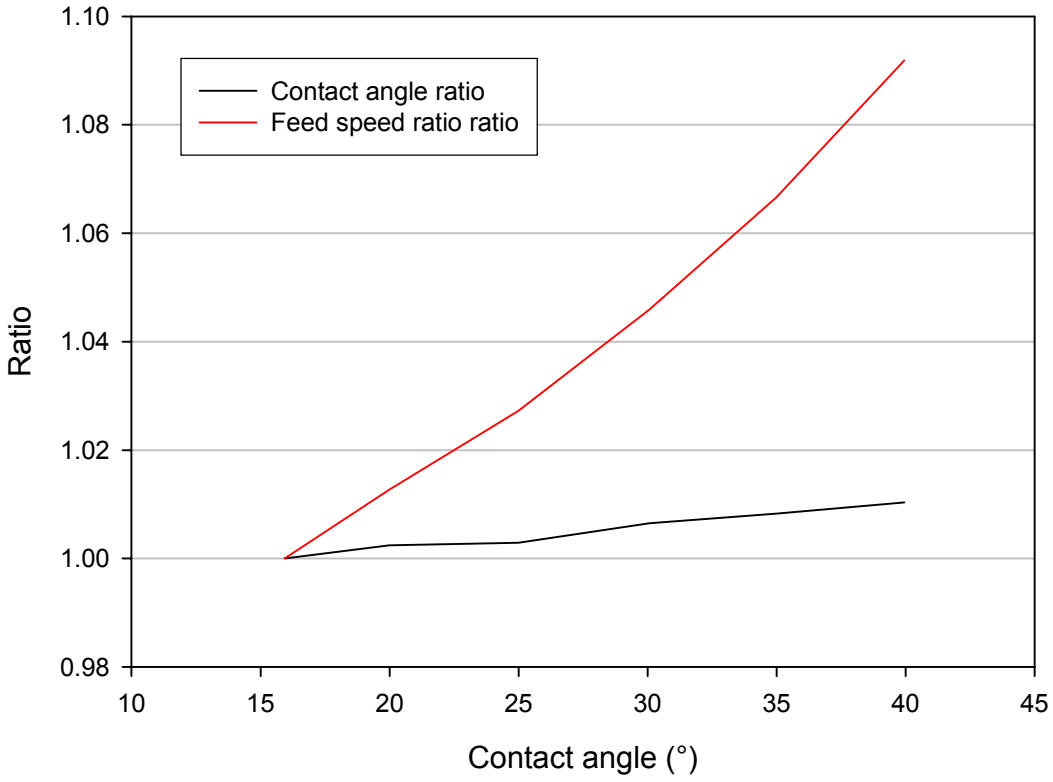

Figure 6.19 Comparing the contact angle effect to the feed speed ratio effect

To examine the effect of contact angle on the speed of the top of the prepared cane mat, the displacement of the selected node was differentiated with respect to time. The speed of the top of the mat for the 40° and 16° contact angle runs is shown in Figure 6.20. The oscillations in the feed speed are related to the individual nodes making contact

with the rolls and do not represent a real effect. While the speed of the mat for the 16° contact angle run changes very little until contact with the roll surface is made (indicated by the smoother curve at the right-hand end of the figure), the speed of the mat for the 40° contact angle run increases about 20% just before contact with the roll surface is made. Figure 6.20 quantifies the effect shown in Figure 6.18 for the 40° contact angle case where the top of the mat has moved forward relative to the centre of the mat at the contact point. This increase in speed is sufficient to explain the 10% increase in feed speed ratio shown in Figure 6.19.

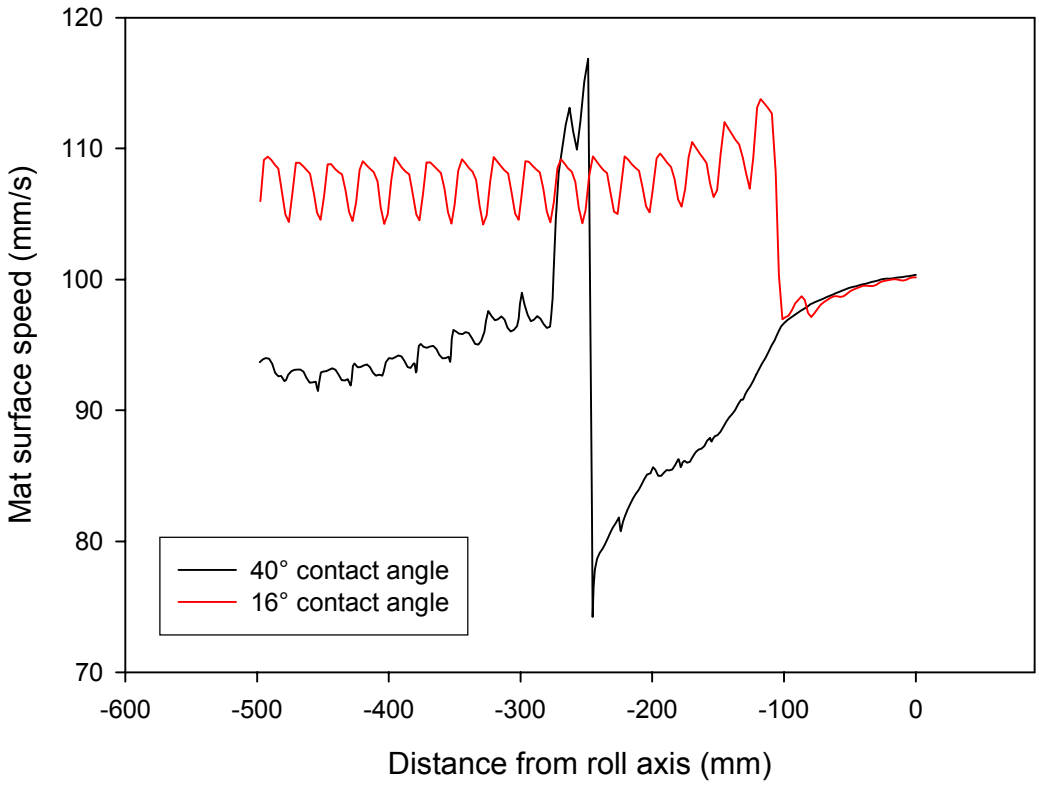

Figure 6.20 Speed of the selected node for 40° and 16° model runs

In summary, the major cause for Murry's feed speed ratio to increase as contact angle increased was the outside of the mat being pulled forward into the rolls due to increasing compression at the contact point. The discrepancy in contact angle has been shown to contribute only a small amount to the increase in Murry's feed speed ratio.

Slip on the roll surface

As stated in section 6.3.5, forward slip was clearly observed in two tests and believed to have occurred in a third test of the two-roll mill experiment. This slip occurred under conditions of low contact angle, high work opening, low roll speed and higher feed pressure. Explanations for this slip were suggested in section 6.3.6 and are examined further in this section. In addition, the likelihood of other tests being affected by slip but not detected is discussed.

As discussed in section 6.5.2, the model used a coefficient of friction between the prepared cane mat and the roll surface of 0.36 to ensure that slip occurred for tests 3, 13 and 19, the three tests observed to have slipped. The value of 0.36 was determined by continually lowering the coefficient of friction until slip was observed in all three tests. Slip was detected by the inability of the solver to reach the desired feed pressure in the first load step (section 6.5.2) or the inability to complete the second load step. With the coefficient of friction set to 0.36, the only tests where slip prevented a solution were tests 3, 13 and 19, providing excellent agreement with the experimental observations.

In section 6.3.6, it was argued that slip on the roll surface was unlikely to have significantly affected Murry's feed speed ratio. To test that argument, the 29 tests for which model solutions were obtained were reprocessed using a coefficient of friction between the prepared cane mat and the roll surface of 1.0. The percentage difference between the results is shown in Figure 6.21. The difference was greater than 2% for only three of the 29 tests. These three tests were tests 4, 29 and 30. All three of these tests were carried out with the 240 mm nip setting and the 16° contact angle and either the 7 kPa feed pressure or the 100 mm/s surface speed. As such, these tests were the next three tests likely to involve forward slip and consequently, the three tests most likely to have a higher value for Murry's feed speed ratio at a coefficient of friction of 0.36 than at a coefficient of friction of 1.00. If the model has incorrectly predicted some forward slip for these three tests, the impact on the overall results shown in Figure 6.16 will still be quite small.

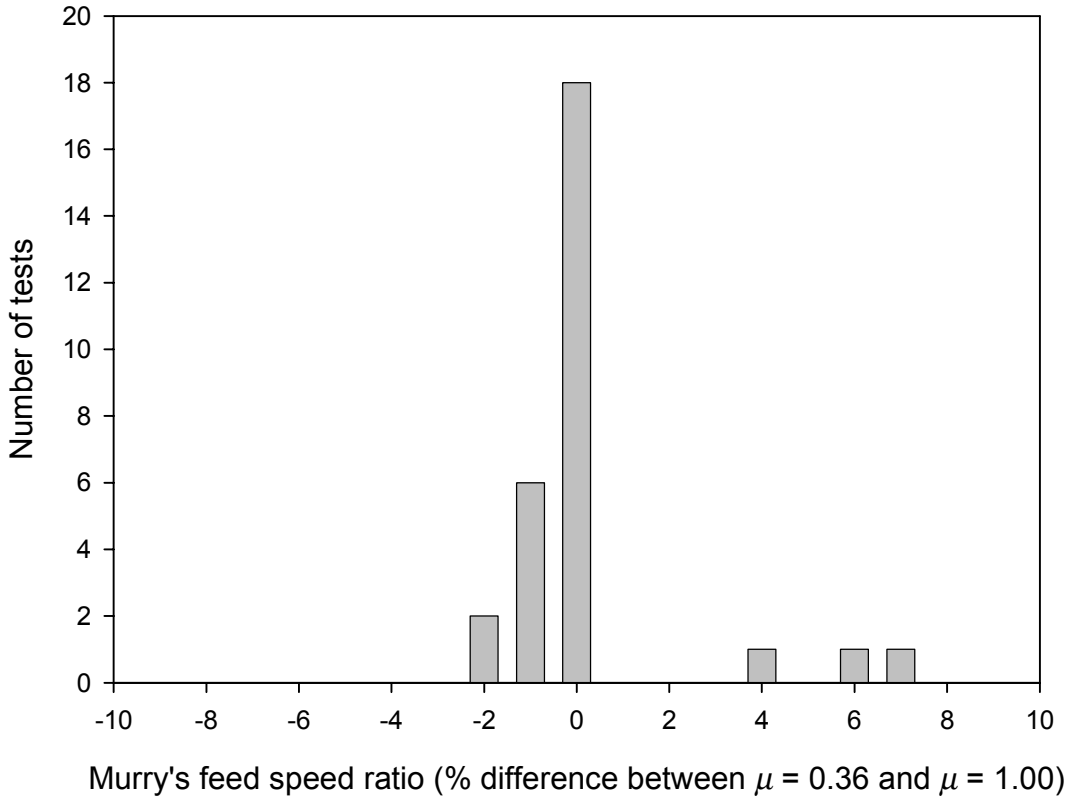

Figure 6.21 Difference in Murry's feed speed ratio between models using coefficient of friction between prepared cane mat and roll surface of 0.36 and 1.00

To gain some further understanding of the effect of slip between the prepared cane mat and the roll surface on the mill feeding behaviour, the ratio of the tangential stress to the normal stress at the roll surface was calculated for one node from each test. As in the previous section, the selected node was approximately 490 mm from the front on the top of the mesh on the plane of symmetry. Figure 6.22 presents the results of the calculations for contact angles of 40°, 30° and 16°.

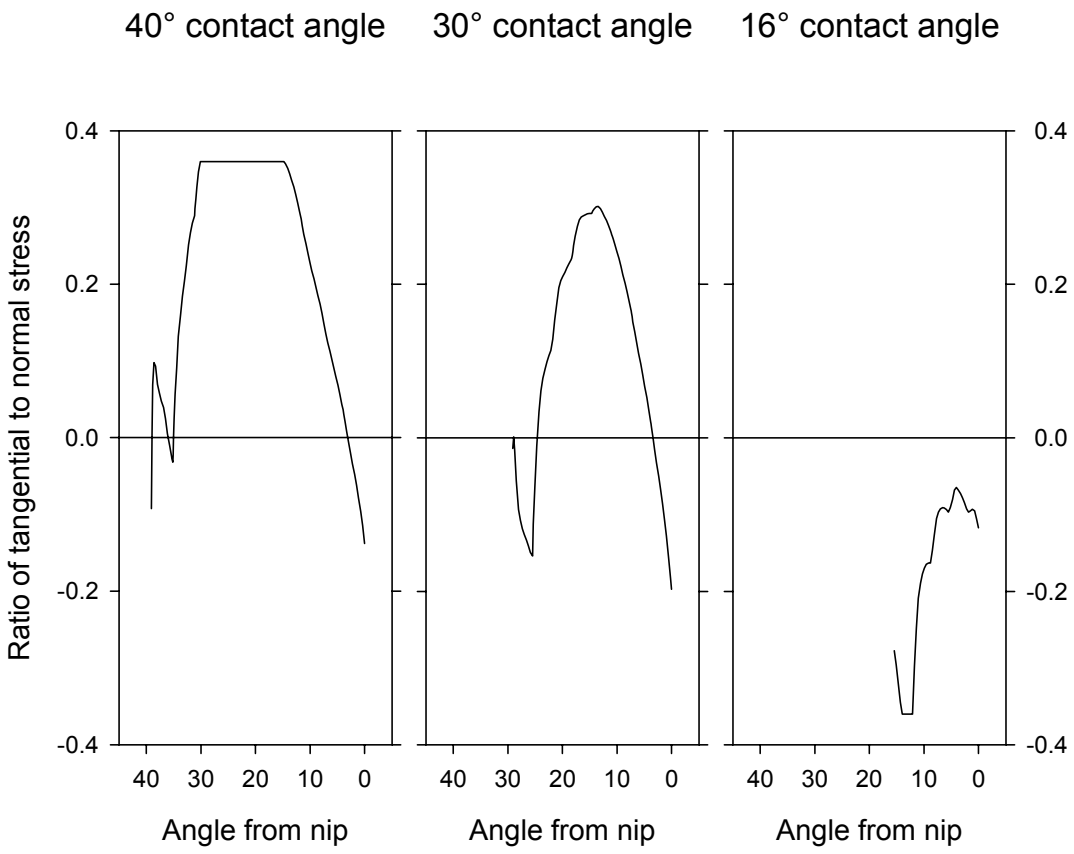

Figure 6.22 Effect of contact angle on the ratio of tangential stress to normal stress

For all contact angles in Figure 6.22, the stress ratios are bounded by ±0.36, the coefficient of friction. For the 40° contact angle case, the stress ratio reaches +0.36, indicating that the ability of the roll surface to pull the mat into the rolls (in other words, to feed) is nearing its limit. For the 16° contact angle case, the stress ratio reaches -0.36, indicating that the ability of the roll surface to prevent forward slip has almost reached its limit. At the intermediate, 30°, contact angle case, the stress ratio did not reach either limit, indicating that no slip occurred in this configuration.

For the 16° contact angle case, the limit of –0.36 was reached at the contact point between the prepared cane mat and the roll surface, the point where the normal stress is lowest. As the material moves towards the nip, the normal stress increases, causing the ratio of tangential to normal stress to reduce and allowing sufficient tangential stress to develop to resist the feed pressure. Because the slip occurs at the contact point, forward slip has the ability to affect the feed speed, as observed with tests 4, 29 and 30 above.

For the 40° contact angle case, on the other hand, slip does not occur at the contact point but further towards the nip. This case provides an explanation for why the coefficient of friction had little effect on the feed speed for the high contact angle cases. If the contact angle increased further or the coefficient of friction reduced further, a situation could arise where the ratio of tangential to normal stress was exceeded at the contact point. Under these conditions, the prepared cane mat would not feed into the nip, giving a zero value for Murry's feed speed ratio.

Non-uniform speed distribution

In section 6.3.6, the reason for the higher values for Murry's feed speed ratio under conditions of higher feed pressure, larger nip setting and lower roll speed was argued to be a higher speed at the centre of the prepared cane mat as opposed to on the surface. In this section, some support for this argument is presented.

As in *the true contact angle* section above, three additional models have been run based on test 21 of the two-roll mill experiment. The three models differed from the test 21 model in one parameter value. The first model was run with a nip setting of 240 mm instead of 120 mm. The second model was run with a feed pressure of 3 kPa instead of 7 kPa. The third model was run with a feed speed of 500 mm/s instead of 100 mm/s. The nominal element dimension was 25 mm for all runs. To determine typical values for blanket speed for each run, two nodes approximately 490 mm from the front of the mesh on the plane of symmetry were examined: one on the surface of the blanket and the other in the centre of the blanket.

Figure 6.23 shows the deformation of the prepared cane mat for test 21 and the three additional models. The examined node at the top of the blanket is the node just making contact with the roll. The examined node at the centre of the blanket is the node at the bottom of the mesh in the same column of nodes. Figure 6.23 shows a similar deformation profile for all models at the point of contact. At the nip, however, the deformation profiles are quite different. While the centre of the blanket remains behind the top of the blanket for test 21 and the other two models with the smaller nip setting, the centre of the blanket has moved ahead of the top of the blanket for the model with

the larger nip setting. For the lower feed pressure and higher roll speed models, the centre of the blanket has fallen further behind the top of the blanket than in the test 21 model. In summary, the centre of the blanket has travelled further forward relative to the top of the blanket under conditions of larger nip setting, higher feed pressure and lower roll speed, as argued using the thick beam analogy in section 6.3.6.

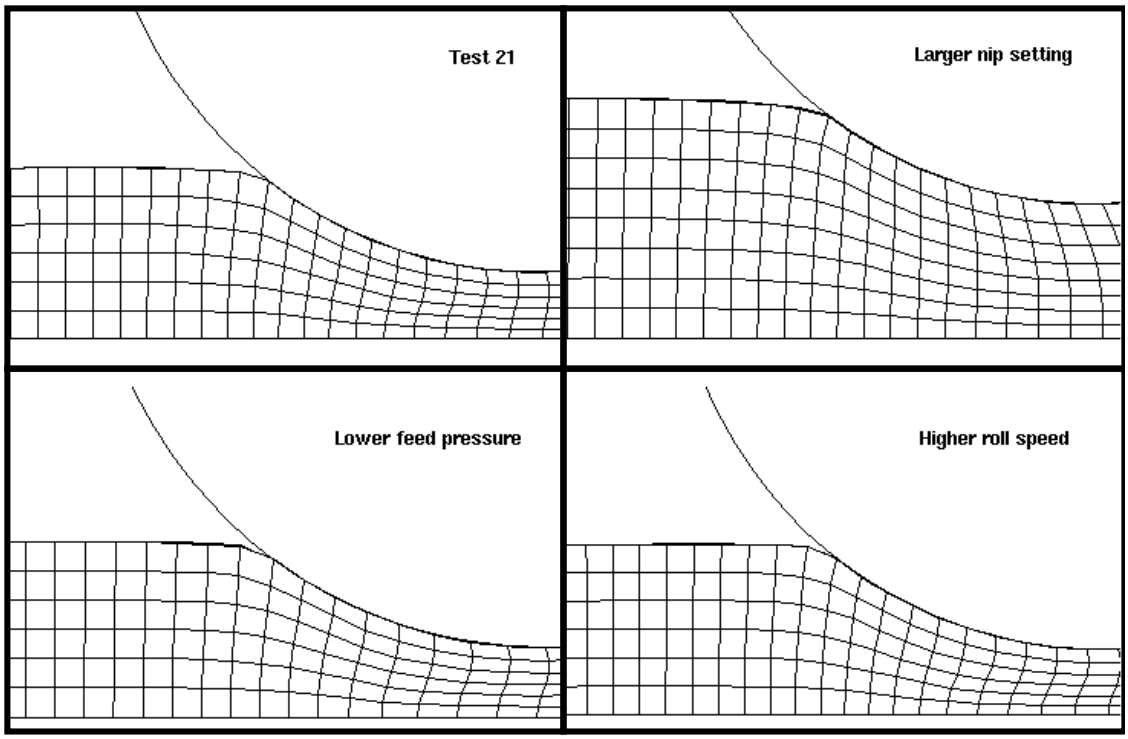

Figure 6.23 The effect of nip setting, feed pressure and roll speed on model blanket deformation

Figure 6.24 presents the speed of the two nodes as they approach the nip for all four models. Speed has been presented as a ratio to roll surface speed. The top node has a speed ratio of 1.0 at the roll axis for all models indicating no slip at the nip. The top node speed was quite similar for all models when in contact with the rolls (distances from about –250 mm to 0). The larger nip setting curve is smoother than that for the other three models when in contact with the roll indicating no slip for the larger nip setting case. While the top node curves are similar, the centre node curves are quite different, again indicating that the behaviour of the centre of the blanket is responsible for the change in Murry's feed speed ratio with nip setting, feed pressure and roll speed.

The speed of the centre of the blanket is greater under conditions of larger nip setting, larger feed pressure and lower roll speed, again in agreement with the discussion presented above.

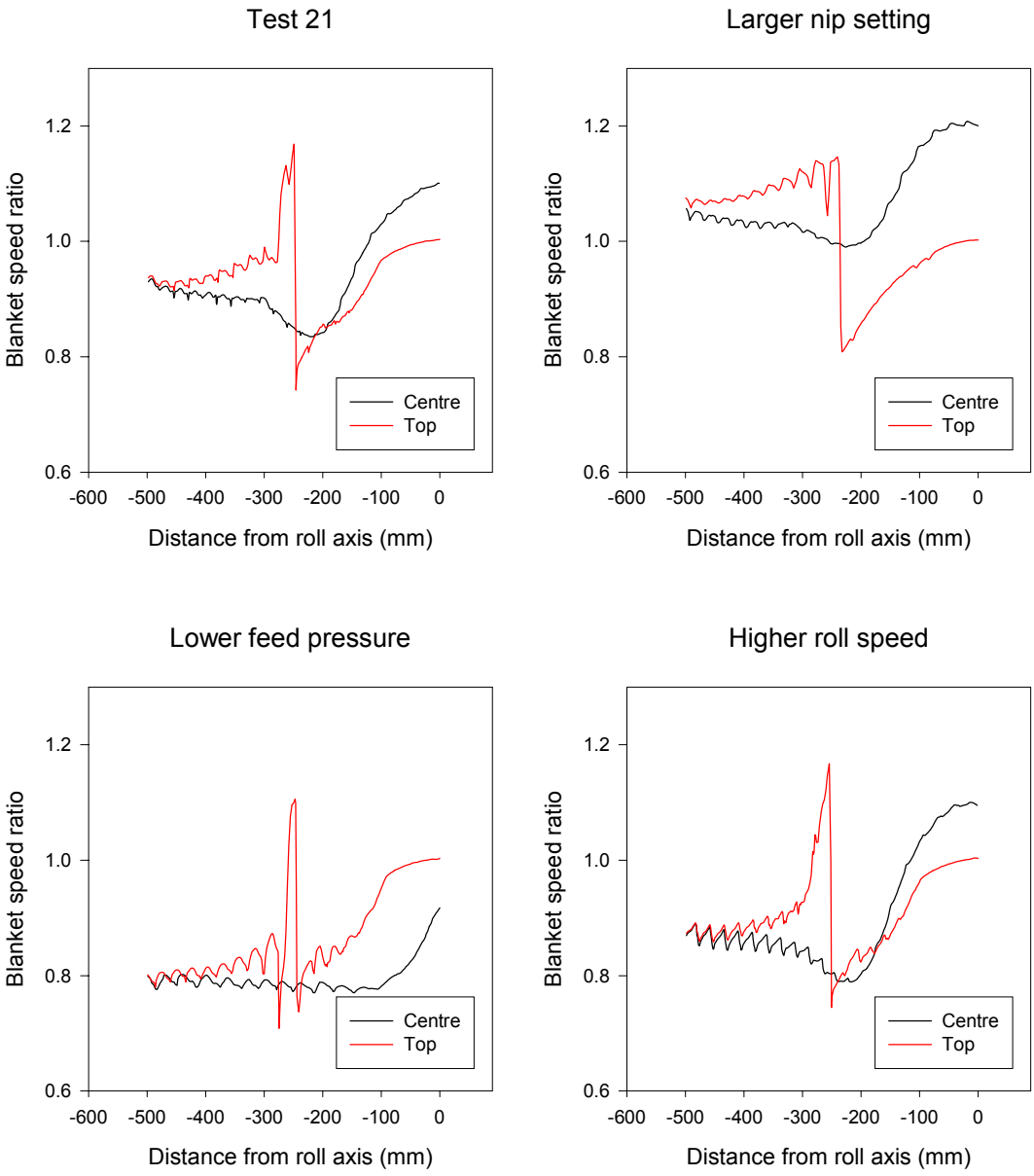

Figure 6.24 The effect of nip setting, feed pressure and roll speed on model blanket speed

In section 6.3.6, it is argued that air pressure is the cause of the difference in Murry's feed speed ratio as roll speed changes. As a result, air pressure effects were included in the model (section 6.5.2). To gain some impression of the size of the air pressure

difference between the 100 mm/s and 500 mm/s surface speeds, the air pressure was plotted in Figure 6.25. The air pressure reached about 4 kPa in the 100 mm/s model and about 7 kPa in the 500 mm/s model, similar sizes to the feed pressure factor levels, indicating that the effect of roll speed on Murry's feed speed ratio, at the 120 mm nip setting and 40° contact angle, at least, is of similar size to the effect of feed pressure. No measurements of air pressure have been undertaken to confirm if pressures of this size are reasonable, but they are at the upper end of expectations.

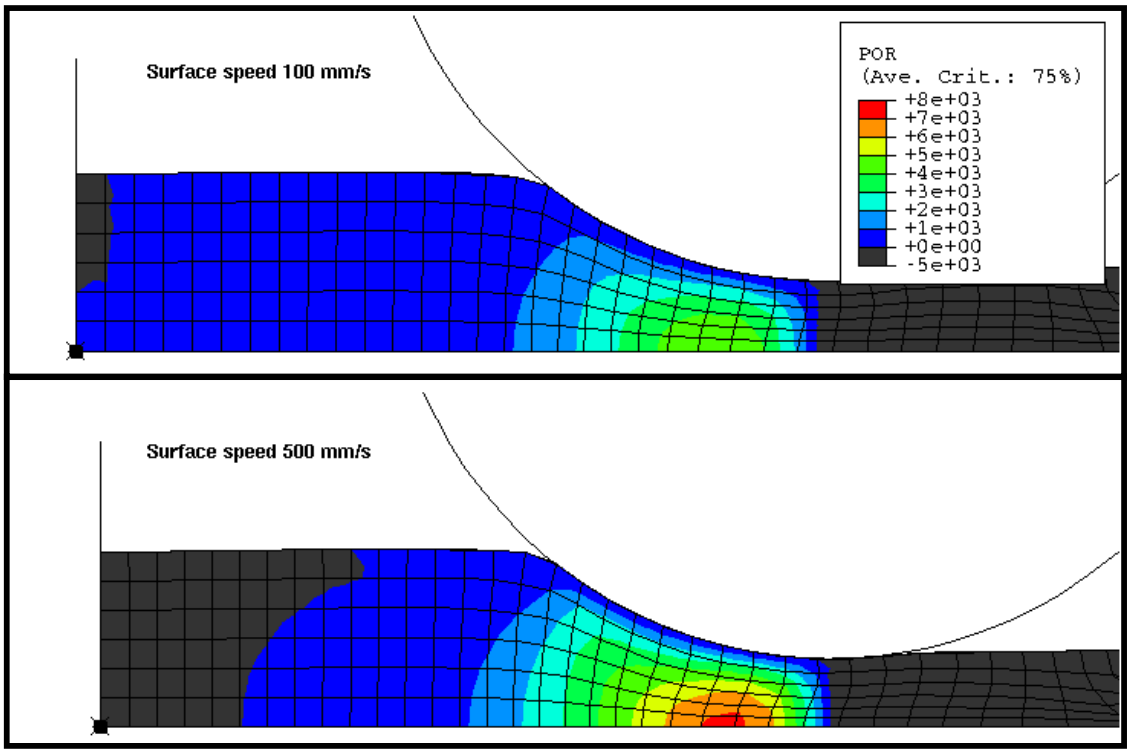

Figure 6.25 Air pressure differences due to surface speed changes (Pa)

Concluding remarks

The two-roll model was used to support the arguments presented in section 6.3.6 to explain the behaviour observed in the two-roll mill experiment described in section 6.3.5.

Deformation occurring at the point of contact between the prepared cane mat and the roll surface causes the top of the mat to accelerate prior to contact with the roll surface.

This effect is greater as contact angle gets greater, resulting in higher values for Murry's feed speed ratio at greater contact angles.

Some slip between the prepared cane blanket and the roll surface is believed to have occurred in most tests, but the slip rarely influenced Murry's feed speed ratio. The only tests for which slip is believed to have affected Murry's feed speed ratio to any extent are those with a nip setting of 240 mm, a contact angle of 40° and either a 7 kPa feed pressure or a 100 mm/s roll speed. In all cases, the blanket has slipped forward, resulting in inflated values of Murry's feed speed ratio.

The model has confirmed that the cause of higher values for Murry's feed speed ratio at larger nip setting, larger feed pressure and lower roll speed is the deformation at the centre of the blanket. Under larger nip setting, larger feed pressure and lower roll speed conditions, the forces pushing the prepared cane mat into the nip produce more deformation in the forwards direction, resulting in higher average blanket speeds.

6.5.5 Concluding remarks

A model of a two-roll mill has been developed. The model predicts all of the trends observed in the two-roll mill experiment (section 6.3.5) and supports the arguments raised to explain the trends (section 6.3.6).

6.6 Concluding remarks

The theory that Murry (1960) developed to predict the throughput of the two-roll mill assumes that mill throughput is influenced by feed compaction, roll speed, nip setting and contact angle. The theory is based on the assumption that the feed speed (S_F) is equal to $S \cos \alpha$ where S is the roll surface speed and α is the contact angle.

In this study, an experiment using a small-scale two-roll mill has explored the factors affecting the throughput of a two-roll mill. Murry's feed speed ratio, $\frac{S_F}{S\cos\alpha}$, assumed by Murry to have a constant value of one, was found to be a function of contact angle, nip setting, feed pressure and roll speed. This experiment is the most comprehensive study into the feeding of a two-roll mill and the first time the contact angle effect has been studied. The results of the experiment showed that Murry's feed speed ratio increases with increasing contact angle, nip setting and feed pressure and with decreasing roll speed.

The new throughput model, described in chapter 4, was used to model the two-roll mill experiment. The model has produced the same trends observed in the experiment and has been used to support explanations for the observed behaviour.

Deformation occurring at the point of contact between the prepared cane mat and the roll surface causes the top of the mat to accelerate prior to contact with the roll surface. This effect is greater as contact angle increases, resulting in higher values for Murry's feed speed ratio at greater contact angles.

Some slip between the prepared cane blanket and the roll surface is believed to have occurred in most tests, but in most cases, the slip has had no influence on Murry's feed speed ratio. The only tests for which slip is believed to have affected Murry's feed speed ratio to any extent are those with a larger nip setting and contact angle of 40° and at least one each of a larger feed pressure and a smaller roll speed. In all cases, the blanket has slipped forward, resulting in inflated values of Murry's feed speed ratio.

The model has confirmed that the cause of higher values for Murry's feed speed ratio at larger nip setting, larger feed pressure and lower roll speed is the deformation at the centre of the blanket. Under larger nip setting, larger feed pressure and lower roll speed conditions, the forces pushing the prepared cane mat into the nip produce more deformation in the forwards direction, resulting in higher average blanket speeds.

7 Mill feeding in a two-roll mill with juice expression

7.1 Introductory remarks

In chapter 6, a throughput model for a two-roll mill was presented, along with evidence that it provided satisfactory agreement with the behaviour observed in a two-roll mill. To simplify the testing and modelling programme, the experiment was conducted at underfeed nip conditions where no juice was expressed. Under these conditions, compression of the prepared cane mat resulted in expression of air, not juice. As discussed in section 6.3.6, the air expression behaviour was considered to be a key feature of the measured throughput behaviour. Since juice is generally expressed in the remaining mill nips, it is necessary to be able to adequately model the expression of juice as well as air.

In this chapter, the behaviour of a two-roll mill with juice expression is discussed. The experiments of Solomon (1967) that were briefly discussed in section 2.2.3 are reviewed here in detail. Solomon's experiments are the only known two-roll mill experiments with juice expression that examined the factors affecting mill throughput. Comparisons are made between the experimentally observed behaviour without juice expression and the experimentally observed behaviour with juice expression. The behaviour is shown to be very similar. Although no modelling of Solomon's experiments was undertaken, the application of the two-roll model described in section 6.5 to Solomon's experiments is discussed.

7.2 Review of Solomon's experiments

7.2.1 Introductory remarks

The experiments of Solomon (1967), briefly mentioned in section 2.2.3, are believed to be the only designed experiments that explored the factors affecting the throughput of a two-roll mill where juice expression was involved. Since they are directly applicable to the aims of this chapter, they are reviewed in some detail.

Solomon aimed to confirm the theory of Murry (1960b), described in section 2.2.3, that the average feed speed of cane at the entry to a mill (S_F) is equal to $S \cos \alpha$. Since this is the only assumption in Murry's theory, confirmation of this result would provide confidence that Murry's theory would adequately describe the throughput of a two-roll mill.

Solomon's experiments were carried out at compression ratios from 1.5 to 3.5, corresponding to conditions from the pressure feeder nip through to the delivery nip.

Solomon carried out four two-roll mill experiments with prepared cane. The layout of the mill was essentially the same as that used for the two-roll mill experiment described in section 6.3 (Figure 6.1). Three of those experiments were quite similar and assessed only the influence of compression ratio (C_0) on feed speed. These series were identified as the initial tests, the compression ratio tests and the photographic measurements. The remaining experiment was a factorial experiment involving five factors: roll surface speed, compression ratio, feed height (h), feed pressure (P_a) and cane preparation (Z). These four experiments are discussed in the following sections. The comparison to the experiment without juice expression (chapter 6) is made in section 7.3.

7.2.2 Comments on experimental design

Considering that Solomon's stated aim was to test the theory that S_F is equal to $S \cos \alpha$, it is surprising that Solomon only varied S in one experiment (the factorial experiment) and did not vary cos α appreciably in any of the experiments. Table 7.1 shows the minimum and maximum values of cos α for each of the experiments. The range is shown as a percentage of the mean value. For the three test series where compression ratio was the only factor, the range of values for cos α was only 3%. Even the factorial experiment only managed a range of 11%.

Table 7.1 Range of values for cos α in Solomon's experiments

Test series	cos α		
	Minimum	Maximum	Range (%)
Initial tests	0.879	0.903	3
Compression ratio tests	0.871	0.895	3
Factorial experiment[1]	0.843	0.940	11
Photographic measurements	0.880	0.903	3

The ideal experimental design would have had S and cos α as factors and any remaining factors independent of these two factors. For the three series where compression ratio was the only factor, cos α did vary with compression ratio but, as shown in Table 7.1, only by a small amount. The roll speed was kept constant. For the factorial experiment, S was varied by 50% independently of the remaining factors but it is believed that cos α varied with compression ratio, feed height, feed pressure and preparation (Appendix E). Figure 7.1 shows the influence of each factor on cos α. The factor with the greatest influence on cos α, h, only provided a 6% variation for cos α.

[1] Solomon only reported contact angles for the initial test series and the compression ratio test series. Estimates for the contact angles for the remaining series are presented in Appendix E.

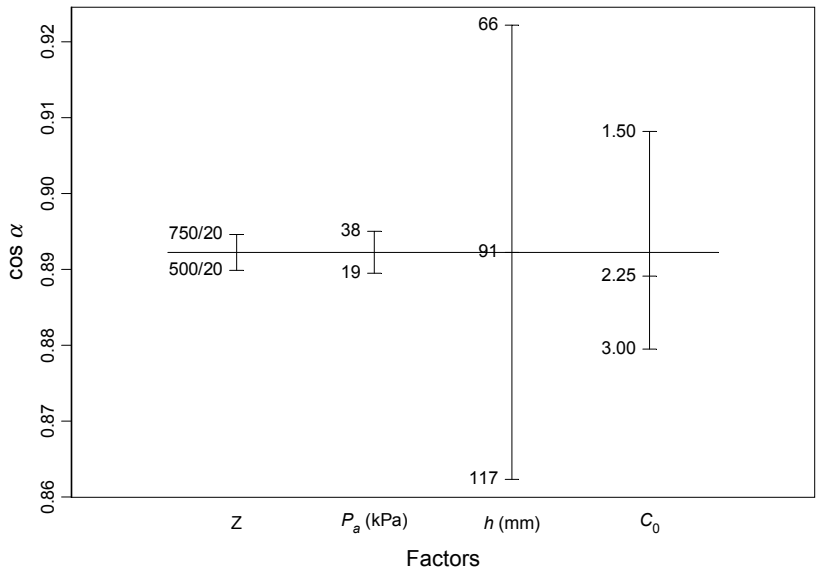

Figure 7.1 Mean values of cos α for each level of each factor for the factorial experiment[1]

While Solomon's experiments do not strictly examine whether $S \cos \alpha$ is an appropriate measure of S_F, they do examine whether other parameters (preparation, feed pressure, feed height and compression ratio) should also be included in the theory. Consequently, they remain valuable experiments for providing information on the factors affecting mill throughput.

7.2.3 Analysis of results

As discussed in section 6.2, Murry's feed speed ratio, $\frac{S_F}{S \cos \alpha}$, is considered the most appropriate quantity to study the throughput behaviour of the two-roll mill. Any variation in Murry's feed speed ratio away from a value of one is an indication of weakness in Murry's theory. Solomon used S_F / S as the dependent variable in his analysis. Since cos α was essentially constant throughout the experiments (section 7.2.2), this difference is unlikely to produce substantial differences between Solomon's

[1] 750/20 refers to preparation in a Waddell hammer mill operating at 750 r/min for 20 s.

conclusions and those made here. The results for Solomon's four test series are represented in Appendix E.

An analysis of variance on the initial test series, the compression ratio test series and the photographic measurement series showed that, in all three experiments, the compression ratio factor had a significant effect on Murry's feed speed ratio. Figure 7.2, Figure 7.3 and Figure 7.4 show the mean values of Murry's feed speed ratio at each compression ratio level in the three experiments. For each experiment, increasing compression ratio caused a decrease in Murry's feed speed ratio. This result is consistent with Solomon's conclusions.

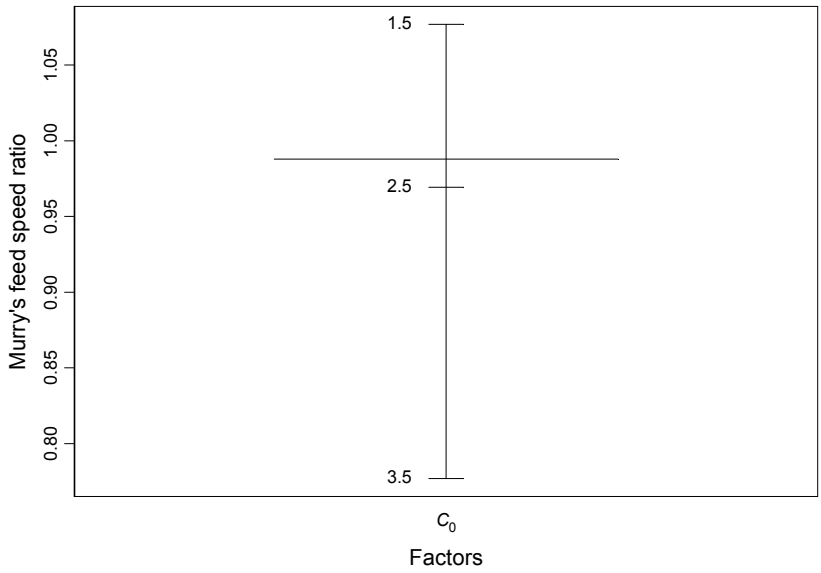

Figure 7.2 Mean values of Murry's feed speed ratio for each level of compression ratio for Solomon's initial test series

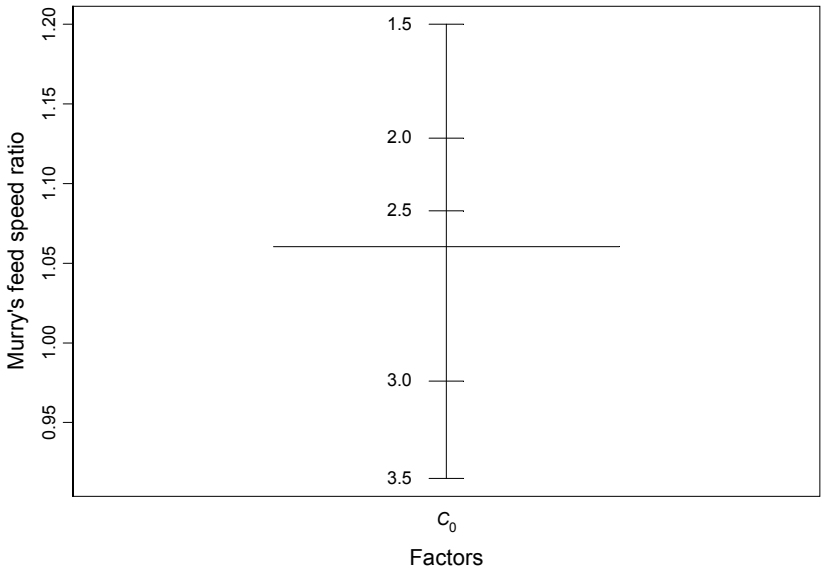

Figure 7.3 Mean values of Murry's feed speed ratio for each level of compression ratio for Solomon's compression ratio test series

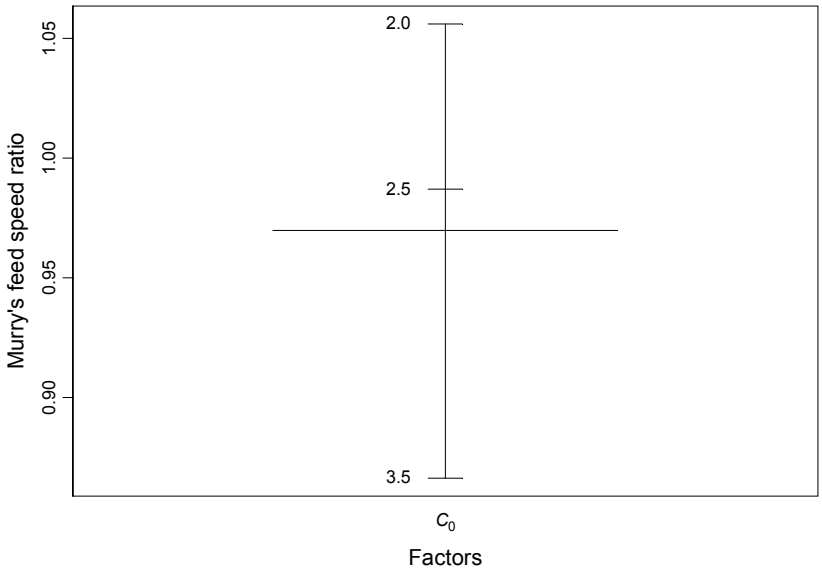

Figure 7.4 Mean values of Murry's feed speed ratio for each level of compression ratio for Solomon's photographic measurement series

Rather than carry out an analysis of variance on the entire factorial experiment, Solomon split his results into four by grouping together the tests with the same preparation and feed pressure. Solomon explained that this separation was carried out because the compression ratio factors were not the same for different preparation and feed pressure combinations. The effect of this separation was that, instead of analysing one large 72-test experiment with the advantages of many degrees of freedom for hypothesis testing in the analysis of variance, Solomon had four 18-test experiments where there were many less degrees of freedom for hypothesis testing. Solomon found that only the compression ratio factor had a significant influence on S_F / S.

Solomon's decision to split his experiment into four is not believed to have been necessary. Hicks (1964) shows that an experiment of this type can be treated as a *nested-factorial experiment*. A roll surface speed, compression ratio and feed height experiment is nested within a preparation and feed pressure experiment.

An analysis of variance table for Murry's feed speed ratio for the factorial experiment, treating it as a nested-factorial experiment, is presented in Table 7.2. The level of significance is only quantified for those terms where the level of significance is less than 0.1. The analysis of variance confirms the significance of the compression ratio factor. It also highlights the significance of roll surface speed, a factor observed significant in three of Solomon's four analyses. It also identifies four interaction terms as being significant.

Table 7.2 Analysis of variance of Murry's feed speed ratio for Solomon's factorial experiment

Source	Degrees of freedom	Mean square	Variance ratio	Significance level
Z	1	0.030	1.4	-
P_a	1	0.028	1.3	-
Residuals	1	0.021		
S	1	0.125	13.4	< 0.001
h	2	0.020	2.2	-
C_0	2	0.252	26.9	< 0.001
Z:S	1	0.040	4.2	0.05
Z:h	2	0.044	4.7	0.01
Z:C_0	2	0.032	3.4	0.04
P_a:S	1	0.012	1.3	-
P_a:h	2	0.018	1.9	-
P_a:C_0	2	0.013	1.3	-
S:h	2	0.026	2.8	0.07
S:C_0	2	0.009	1.0	-
h:C_0	4	0.004	0.4	-
Residuals	45	0.009		

Figure 7.5 shows the mean levels of each of the parameters. As for the initial test series, the compression ratio test series and the photographic measurement series, this series of tests shows that Murry's feed speed ratio is higher at lower compression ratio. Murry's feed speed ratio reduces as the other highly significant factor, roll surface speed, increases.

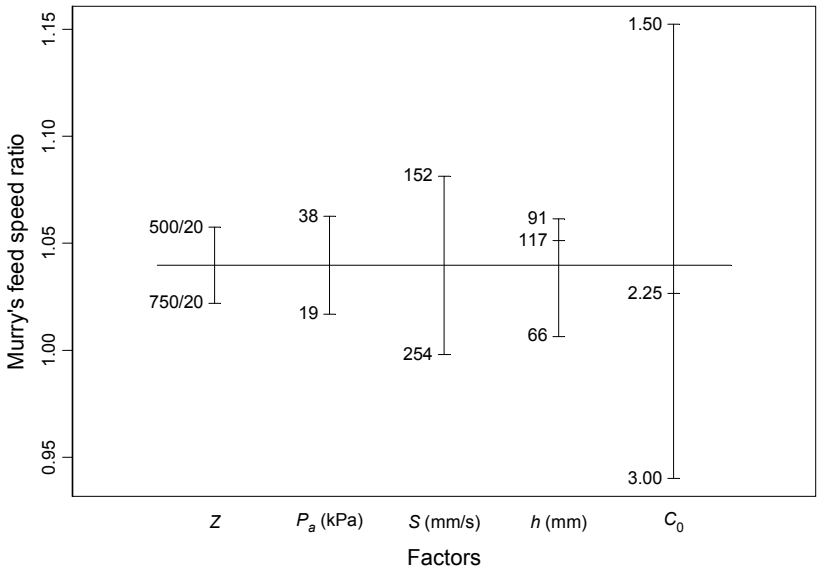

Figure 7.5 Mean values of Murry's feed speed ratio for each level of each factor for Solomon's factorial experiment series

Figure 7.6 shows the effect of each of the significant interaction terms from Table 7.2 on Murry's feed speed ratio.

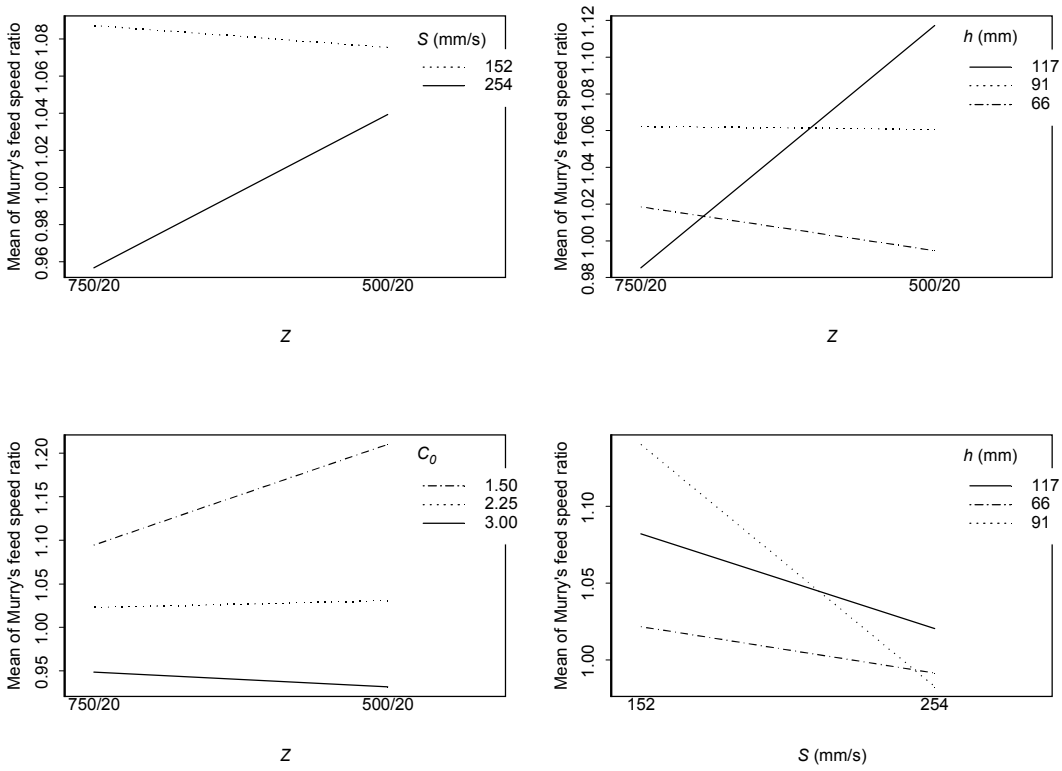

Figure 7.6 Significant interactions identified in the analysis of variance of Murry's feed speed ratio for Solomon's factorial experiment series

Although there is a significant compression ratio / preparation interaction, the trend between compression ratio and Murry's feed speed ratio shown in Figure 7.5 is observed at both levels of preparation. However, the difference in feed speed ratio between the compression ratio levels is greater at the coarser (500/20) preparation.

There are two significant interactions involving roll surface speed: preparation and feed height. In both cases, the trend between roll surface speed and Murry's feed speed ratio shown in Figure 7.5 is observed at all levels of both interacting factors. Speed has a greater effect on Murry's feed speed ratio at the finer preparation (750/20). The interaction with feed height is not as clear. Speed had the largest effect on Murry's feed speed ratio at the middle feed height level (91 mm).

The remaining significant interaction is between preparation and feed height. While Murry's feed speed ratio appears to be largely independent of preparation at the two

lower feed heights, it decreased with increasing preparation at the largest feed height level (117 mm).

In each experiment, the compression ratio factor was identified as the most significant influence on Murry's feed speed ratio. However, it is questionable whether compression ratio, as such, is responsible for the variation. For the initial test series, the compression ratio test series and the photographic measurement series, it is clear that Solomon achieved his compression ratio levels by selecting appropriate work openings. It is conceivable that work opening, rather than compression ratio, was the parameter that caused Murry's feed speed ratio to vary. For the factorial experiment, however, cane preparation, feed pressure and feed height, as well as compression ratio, were taken into account in the selection of work opening. Figure 7.7, however, shows that, once again, compression ratio was the factor mostly responsible for the selected work opening (based on the work openings estimated in the analysis described in Appendix E).

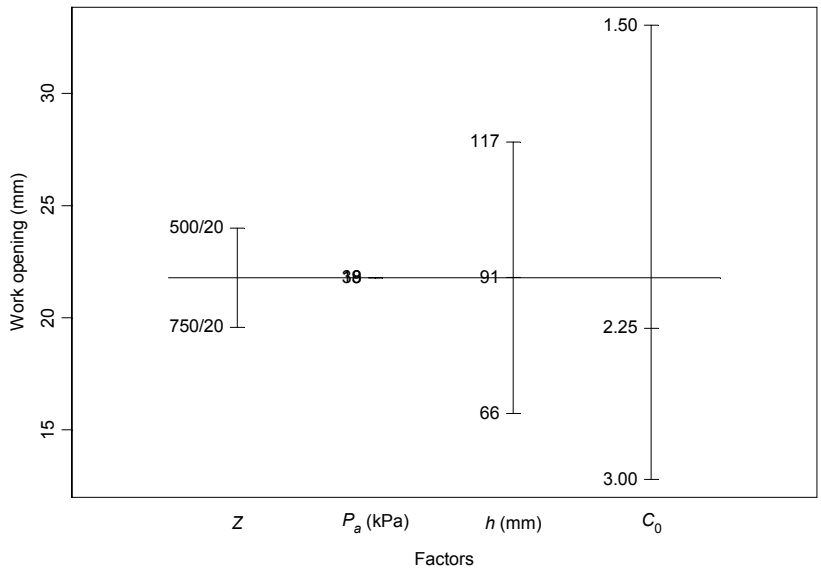

Figure 7.7 Factors from Solomon's factorial experiment that affect work opening

7.2.4 Concluding remarks

The analysis described in section 7.2.3 confirmed Solomon's conclusion that, of the factors he investigated, the compression ratio effect on Murry's feed speed ratio was greatest. The analysis showed that Murry's feed speed ratio was greater when compression ratio was lower. The analysis also showed that the effect of compression ratio was greater at lower preparation.

Compression ratio was the main factor explored in Solomon's experiments. The main parameter used to set compression ratio was work opening (nip setting). In the initial tests, the compression ratio tests and the photographic measurements, compression ratio was adjusted by changing work opening. Work opening could have substituted for compression ratio as the experimental factor and the results would have been identical. In the factorial experiment, work opening was adjusted with cane preparation, feed pressure and feed height in addition to compression ratio so a direct substitution of compression ratio with work opening cannot be done. The change in work opening with compression ratio was, however, significantly greater than with the other factors, indicating that the measured compression ratio effect was largely a work opening effect.

Roll surface speed was the other factor that had a significant influence on Murry's feed speed ratio. The analysis showed that Murry's feed speed ratio was greater at lower roll surface speed. The analysis also showed that the effect of speed was greater at finer preparation.

The effect of feed height on Murry's feed speed ratio was unclear. Figure 7.5 and Figure 7.6 show that the effect of feed height on Murry's feed speed ratio is not consistent. Figure 7.5 shows that Murry's feed speed ratio was highest for the middle level of the feed height factor. The trends showing the effect of feed height on Murry's feed speed ratio in Figure 7.6 are not the same at each feed height level.

Solomon's experiment has shown that Murry's theory that $S_F = S \cos \alpha$ is not sufficient to describe the throughput of a two-roll mill. Roll surface speed has a lesser influence on throughput than Murry's theory suggests. Solomon's experiment provides no

substantial indication of the influence of cos α on throughput. The experiments have also demonstrated the strong influence of compression ratio or work opening on throughput. Throughput also appears to be affected, to a limited extent, by preparation.

7.3 Comparing Solomon's results to the results of the experiment without juice expression

The two-roll mill throughput tests conducted by Solomon (1967) and the two-roll mill underfeed nip throughput tests conducted for this study were quite similar in apparatus and procedure. Apart from the possible effect of juice expression in Solomon's experiment resulting from the higher compactions achieved, the results from the two experiments could be expected to be similar.

For both experiments, nip setting or work opening (or compression ratio) was the factor that had the largest effect on Murry's feed speed ratio. Similar trends were observed in both experiments. In both experiments, Murry's feed speed ratio increased with both larger nip setting and lower roll speed.

Solomon's experiment found that the effect of roll speed on Murry's feed speed ratio was statistically significant. Murry's feed speed ratio decreased at the higher roll speed. This trend was also present in the underfeed nip experiment but was not statistically significant. It was theorised, however, that the roll speed trend was a real effect (section 6.3.6). It was also theorised that fluid flow was responsible for the roll speed effect. Since the fluid in Solomon's experiment was juice, compared to air in the underfeed nip experiment, a greater roll speed effect was expected in Solomon's experiment.

The underfeed nip experiment showed that higher feed pressure increased Murry's feed speed ratio. The feed pressure trend was present in Solomon's experiment as well (Figure 7.5) but the analysis of variance did not identify the effect as significant.

The underfeed nip experiment showed that Murry's feed speed ratio increased at lower contact angle at low roll speed. Unfortunately, Solomon's experiment did not substantially change contact angle (section 7.2.2).

Solomon's experiment showed that coarse cane preparation led to higher values of Murry's feed speed ratio at high roll speed and low compression ratio. Preparation did not appear as a very significant factor in the underfeed nip experiment and, if anything, contradicted Solomon's result. The effect of cane preparation on Murry's feed speed ratio remains unclear.

In summary, the results from Solomon's experiment were in some respects similar to those of the underfeed nip experiment, indicating that similar mechanisms were likely to be involved in producing the observed behaviour.

7.4 Modelling the two-roll mill with juice expression

Although no juice was expressed in the underfeed nip experiment, the compression of the prepared cane mat as it passed between the rolls caused expression of air. It was found necessary to model the expression of air in order to match the experimentally-observed (although not statistically significant) effect of roll speed on Murry's feed speed ratio.

The air expression effect was modelled using the fluid-related equations described in chapter 4. The air constitutive parameters were defined through the permeability parameters, k_1 and k_2, and the absolute viscosity, μ_v. The permeability parameters are properties of the prepared cane mat itself and not the fluid, so the permeability parameters for air are expected to be the same as for juice. A value for viscosity appropriate for air, however, was used. In summary, the only difference between air expression and juice expression, as far as the model is concerned, is the viscosity of the fluid.

7.5 Concluding remarks

The mill feeding experiments of Solomon (1967) have been reviewed in detail. Solomon's experiments are the only known experiments where the throughput of a two-roll mill involving juice expression has been studied.

Solomon's results are in some respects similar to those found from the experiment without juice expression (section 6.3). Solomon's results found decreasing compression ratio to result in increasing values for Murry's feed speed ratio. It is believed compression ratio was changed through changes to nip setting, the same parameter found in the experiment without juice expression to be most significant. Solomon also found that Murry's feed speed ratio increased with decreasing roll speed and increasing feed pressure, the same results obtained in the experiment without juice expression. Solomon did not investigate the effect of contact angle.

The only appreciable difference between Solomon's experiments and the experiment without juice expression is the fluid being expressed. Consequently, it was considered appropriate that the same model be used for juice expression and air expression. The only difference believed required is in the viscosity of the fluid.

Since the same model is believed appropriate for both underfeed nip conditions where no juice is generally expressed and conditions involving juice expression such as the pressure feeder nip or subsequent nips, the same model is considered appropriate for use throughout the milling unit.

8 Modelling mill feeding in a factory milling unit

8.1 Introductory remarks

In chapter 6, a model of a two-roll milling unit was developed that covered the range of compactions present in the first pair of rolls in a factory milling unit (the underfeed nip). In chapter 7, a two-roll mill experiment was reviewed that covered a higher range of compactions, including those present in the second pair of rolls in a factory milling unit (the pressure feeder nip). It was found that the behaviour at the higher compactions was similar to that at lower compactions. Consequently, the model developed for the first pair of rolls in a factory milling unit was also considered suitable for the second pair of rolls in a factory milling unit.

The Jenkins and Murry (1981) model was designed to predict the throughput of the six-roll mill but only addressed the feeding behaviour of the three-roll pressure feeder, assuming that the subsequent three mill rolls, on the other end of the pressure feeder chute, had negligible effect on throughput. In this chapter, the same approach is taken. It is assumed that it is only necessary to model the three-roll pressure feeder, incorporating the underfeed nip and the pressure feeder nip, to satisfactorily model the throughput of the six-roll factory milling unit.

In this chapter, a model of the three-roll pressure feeder is presented. The results of four experiments to validate the model are presented: three originally presented by Jenkins and Murry (1981) and one conducted as part of this project. The model is shown to adequately match the experimental results.

8.2 Features of the factory milling unit

The two-roll mill described in section 6.2 was a simple arrangement. As well as having only two identical rolls, the two-roll mill was set up symmetrically so that the contact angle on each roll was the same. Because this geometry was so simple, the two-roll mill model described in section 6.5.2 could take advantage of symmetry so that only one roll needed to be modelled.

The three-roll pressure feeder of a factory milling unit is somewhat more complex. Symmetry cannot be used to simplify the arrangement. The three rolls generally have different diameters. The position of the three rolls relative to each other must be known. The contact angles between the feed chute and the first two rolls are generally not the same. The feed chute often does not feed the bagasse vertically into the first pair of rolls. To adequately describe a factory pressure feeder, parameters to represent all of these features are required.

Figure 8.1 shows the general layout of a three-roll pressure feeder that will be used throughout this and subsequent chapters to describe the geometry of a factory milling unit. The terminology to describe the pressure feeder was introduced in section 1.2.3. The top and bottom pressure feeder rolls and the underfeed roll are indicated by symbols used for their outside diameters, D'_{pt}, D'_{pb} and D'_{u}, respectively.

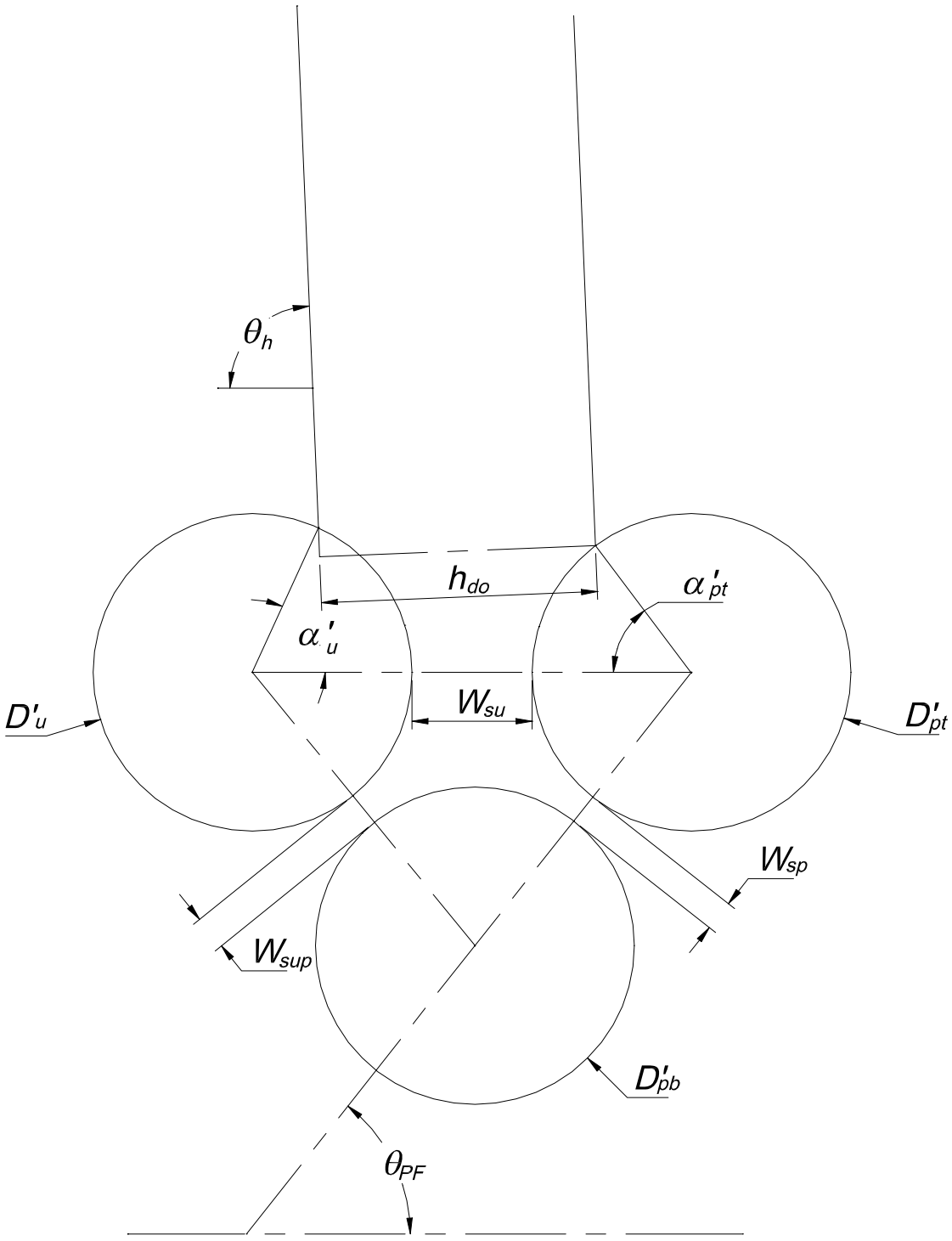

Figure 8.1 Three-roll pressure feeder layout

The feed passes down the feed chute (opening h_{do}) into the underfeed nip (opening W_{su}) and then through the pressure feeder nip (opening W_{sp}). To position the rolls in space,

the pressure feeder angle, θ_{PF}, and the opening between the underfeed roll and the bottom pressure feeder roll, W_{sup}, were defined.

The chute setting, h_{do}, was defined as the shortest distance between the intersection of an extension of the chute wall on the top pressure feeder roll side on to the top pressure feeder roll and an extension of the chute wall on the underfeed roll side. The chute is orientated an angle θ_h from the same datum used to define θ_{PF}. As discussed above, the contact angles between the extensions of the chute walls and the outside diameters of the underfeed roll and top pressure feeder roll are generally not equal and have been defined as α'_u and α'_{pt} respectively. The chute setting, h_{do}, the chute angle, θ_h, and one of the two contact angles, α'_u or α'_{pt}, adequately define the position of the feed chute.

Rather than define one of the two contact angles, the work in this chapter refers to the calculated contact angle, α'_{do}, using the definition in equation **(1.4)** and an angular bias, θ_{pt}, which defines the difference in angle between the calculated contact angle and the actual contact angle on the top pressure feeder roll. The calculated contact angle is defined by:

$$\cos\alpha'_{do} = \frac{\frac{D'_u + D'_{pt}}{2} + W_{su} - h_{do}}{\frac{D'_u + D'_{pt}}{2}} \qquad \textbf{(8.1)}$$

The top pressure feeder roll contact angle, α'_{pt}, is related to the calculated contact angle and the angular bias by:

$$\alpha'_{pt} = \alpha'_{do} + \theta_{pt} \qquad \textbf{(8.2)}$$

8.3 A computational feeding model

8.3.1 Introductory remarks

Using a similar approach to the one used to develop the computational model for a two-roll mill (section 6.5.2), a computational model was developed for the three-roll pressure feeder. As discussed in section 8.1, the three-roll model is considered sufficient to model the feeding behaviour of the Australian six-roll milling unit.

8.3.2 Geometry

The computational model uses 13 parameters to define the geometry of a pressure feeder as follows:

- the three mean roll diameters, D_{pt}, D_{pb} and D_u,
- the three work openings, W_u, W_p and W_{up},
- the angle defining the orientation of the two pressure feeder rolls, θ_{PF},
- the feed chute exit setting, h_{do},
- the contact angle bias, θ_{pt},
- the chute angle, θ_h,
- a height above the top pressure feeder roll to end the feed chute (h_{pt}),
- a factor to define the initial height of bagasse in the chute (this parameter is important for large contact angle bias),
- a mesh size factor to define the initial average element size.

As discussed in section 1.2.4, it is usual to define roll diameter and work opening for the pressure feeder nip in terms of the mean diameter (the outside diameter less the groove depth). For the underfeed nip, however, it is usual to define roll diameter and work opening in terms of the outside diameter. For the computational model that requires a single diameter to represent the top pressure feeder roll, these definitions presented a

conflict. To resolve that conflict, a convention was established to define the roll diameter for the two pressure feeder rolls to be the mean diameter and the roll diameter for the underfeed roll to be the outside diameter. The work opening for each nip was defined as the centre distance between the rolls less half the diameter of each of the rolls. Compared to the usual definitions, the pressure feeder nip is defined the same while the underfeed nip is defined to be larger by half of the groove depth of the top pressure feeder roll. Since the underfeed nip setting is generally large (typically 300 mm to 500 mm) and the groove depth on the top pressure feeder is somewhat smaller (typically 50 mm to 70 mm), the discrepancy will generally be less than 10%.

An example model is shown in Figure 8.2 partway through a run. Note the curved ends at the bottom of the feed chute to ensure a smooth flow out of the chute. There is a plate across the top of the bagasse mat on which the feed pressure is applied and from which the feed speed is calculated.

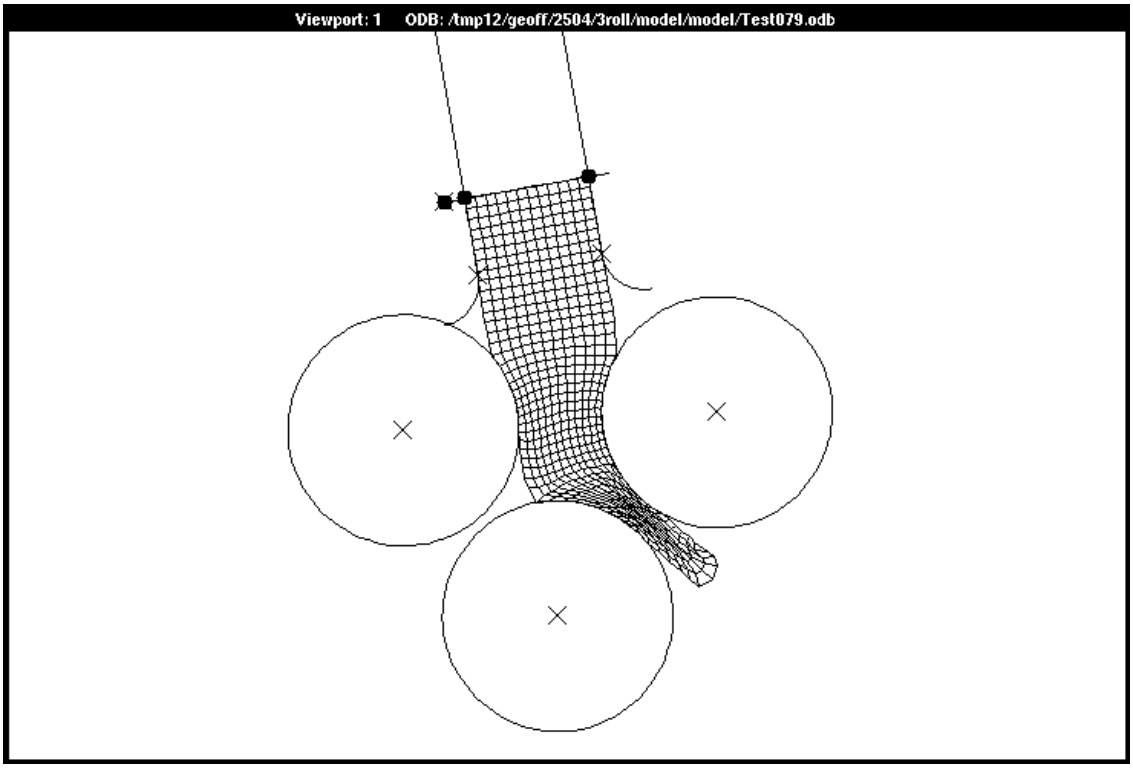

Figure 8.2 Example model geometry

8.3.3 Material parameters

The material parameters for the model were defined in sections 4.7 and 4.8. The parameters are:

- the three elastic parameters, κ, ν and p_t^e ,
- the three plastic parameters, M, p_t and λ_1,
- the two permeability parameters, k_1 and k_2,
- the absolute viscosity for air and water, μ_{va} and μ_{va}, respectively,
- the density of fibre and juice (ρ_f and ρ_j),
- the fibre content (f).

The density of fibre is used in the determination of the initial void ratio from the feed chute exit compaction.

As described in sections 4.5 and 4.8, the fluid behaviour in the model was defined in terms of a single fluid and the volume of voids was assumed to be the same as the volume of fluid (that is, saturated). In bagasse, both air and juice expression takes place. To avoid complicating the model further, the approach of Adam and Loughran (1998) was used where a two-stage permeability equation was used to account for expression of air above a particular void ratio and expression of juice below that void ratio. The void ratio at which the change occurred was calculated as a function of the fibre and juice densities and the fibre content. The permeability changed in proportion to the relative viscosities of the air and juice. A typical permeability curve with a transition at a void ratio of about 7 is presented in Figure 8.3.

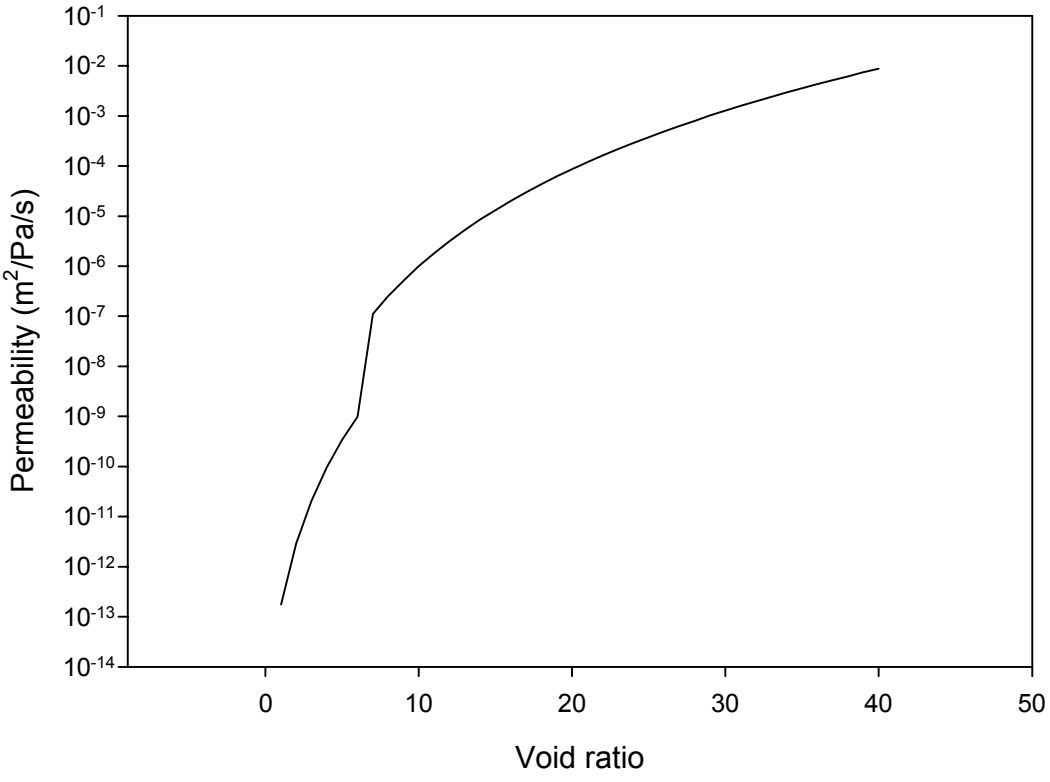

Figure 8.3 Typical relationship between void ratio and permeability $\left(\frac{k}{\mu_v}\right)$

8.3.4 Boundary and initial conditions

The model's boundary conditions are defined by:

- the coefficient of friction on the three rolls (μ_u, μ_{pt} and μ_{pb}),
- the speed of the three rolls (ω_u, ω_{pt} and ω_{pb}),
- a factor defining the initial speed of the bagasse mat (defined by the speed of a plate that initially sits under the bagasse mat in the chute and guides the mat into the first pair of rolls),
- the feed pressure acting on the top of the bagasse in the chute (P_{do}),
- the initial compaction in the chute (γ_{do}).

8.3.5 Feed speed calculation

As discussed in section 8.3.2, the feed speed was calculated from the plate on top of the bagasse mat. The feed speed that was recorded is the average feed speed from the point in time when the bottom node on the underfeed roll side of the mat passes through the pressure feeder nip until the top row of nodes on the bagasse reaches a point near the bottom of the feed chute.

8.3.6 Concluding remarks

The model described in chapter 4 is a general model for defining bagasse behaviour and is independent of the geometry or boundary conditions imposed upon it. There is some empiricism built into the solid and liquid phase constitutive models but this empiricism is far less constraining than the empiricism in the feeding model of Jenkins and Murry (1981).

The parameters described in section 8.3 were found to be sufficient to completely describe the feeding behaviour of any six-roll milling unit in the Australian sugar industry. Having the model completely described by a series of essentially independent parameters made the task of exploring the model over a range of parameter values and of modelling the behaviour of factory milling units a relatively simple process.

8.4 Modelling Jenkins and Murry's small-scale experiments

8.4.1 Introductory remarks

The experiments of Jenkins and Murry (1981) that were briefly discussed in section 2.2.4 are believed to be the only small-scale experiments that explored the factors affecting the throughput of a three-roll feeder.

Jenkins and Murry aimed to understand the flow of bagasse through the feeder in order to be able to determine feeder geometries that would enhance mill throughput.

Jenkins and Murry carried out two experiments as outlined in section 2.2.4. The first series explored the effects of the underfeed nip setting (W_{su}), the offset of the feed chute from a symmetrical position over the underfeed and top pressure feeder rolls (U), the feed chute angle (θ_h), the ratio of underfeed roll surface speed to pressure feeder roll surface speed (S'_u/ S'_p), the pressure feeder roll surface speed (S'_p) and the presence of bars across the surface of the underfeed roll as a feeding aid. The second series explored the effects of the feed chute angle, the underfeed nip setting, the feed chute setting (h_{do}) and the ratio of underfeed roll surface speed to top pressure feeder roll surface speed. The results of these experiments are discussed in section 8.4.2.

8.4.2 Analysis of results

Jenkins and Murry carried out their experiments by varying one factor at a time. Since this experimental design approach does not lend itself to an analysis of variance, a linear regression analysis was carried out in order to identify the significant factors. Like the two-roll mill experiments described in chapters 6 and 7, these experiments were analysed in terms of Murry's feed speed ratio. Here, Murry's feed speed ratio was defined as $\frac{S_F}{S_p' \cos\alpha_{do}'}$ where S_p' is the tip surface speed of the top pressure feeder roll and α_{do}' is the contact angle between the feed chute exit and the underfeed and top pressure feeder roll pair based on the tip diameter of the top pressure feeder roll. The experimental data is reproduced in Appendix F.

The regression equation fitted to the results of the first series of experiments was

$$\frac{S_F}{S_p' \cos\alpha_{co}'} = 1.53 - 0.00402\, W_{su} \qquad \textbf{(8.3)}$$

where W_{su} is the underfeed nip setting. The regression equation is significant at the 0.1% level of significance. Figure 8.4 shows the quality of the fit.

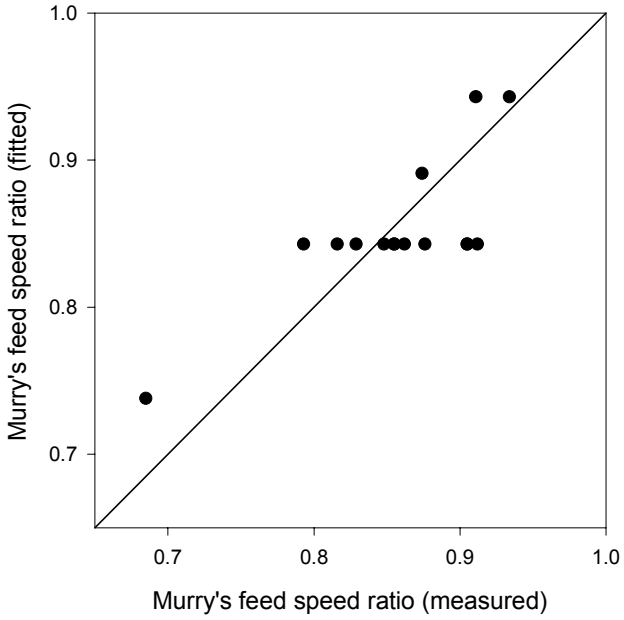

Figure 8.4 Quality of fit for regression equation (8.3)

The regression equation fitted to the results of the second series of tests was:

$$\frac{S_F}{S_p' \cos\alpha_{co}'} = 1.54 - 0.00246\, W_{su} - 0.000845\, h_{co} \qquad \textbf{(8.4)}$$

where h_{co} is the feed chute exit setting. The regression equation is significant at the 0.1% level of significance. Figure 8.5 shows the quality of the fit.

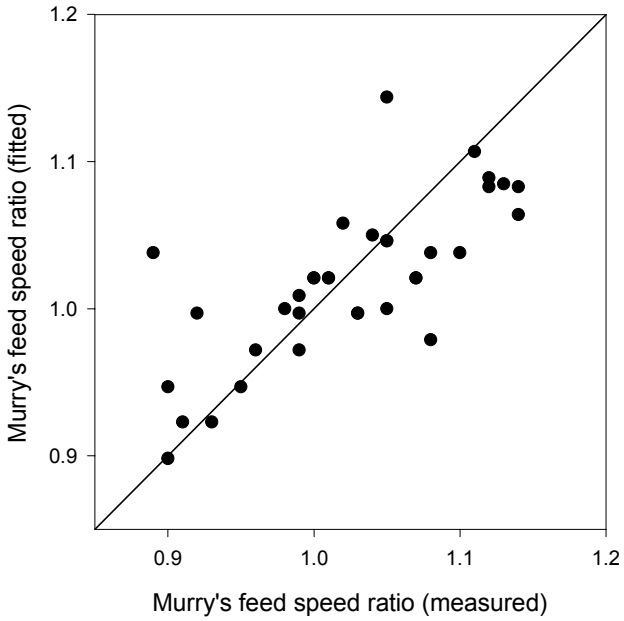

Figure 8.5 Quality of fit for regression equation (8.4)

Equations **(8.3)** and **(8.4)** are consistent with each other. Both equations show that Murry's feed speed ratio reduces as underfeed nip setting increases. Since the feed chute exit setting was constant throughout the first series of tests, feed chute exit setting does not appear in equation **(8.3)**. Equation **(8.4)** shows that Murry's feed speed ratio reduces as feed chute exit setting increases.

In summary, the analysis of the experiments of Jenkins and Murry contained in this section identified two significant trends:

4. Murry's feed speed ratio decreases as underfeed nip setting increases,
5. Murry's feed speed ratio decreases as feed chute exit setting increases.

Although Jenkins and Murry drew additional conclusions from this data, it is not believed that there was sufficient information to be confident of those results.

8.4.3 Modelling Jenkins and Murry's small-scale experiments

Figure 8.6 presents both the experimental results and model predictions for the first experiment. The model predictions were carried out with $k_1 = 5.0 \times 10^{-20}$ m^2 and a coefficient of friction on the underfeed roll of 0.7. The graphs show the mean value of Murry's feed speed ratio for each level of each factor.

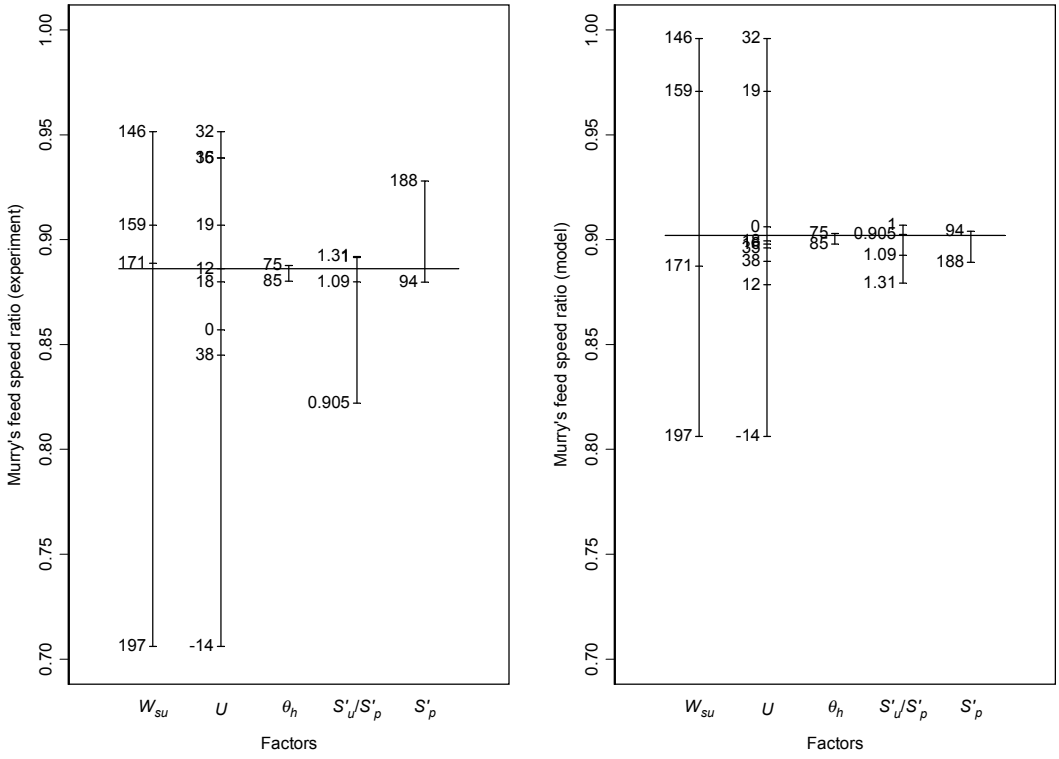

Figure 8.6 Experimental and model results for Murry's feed speed ratio from the first model tests of Jenkins and Murry (1981)

The results show that overall mean values for Murry's feed speed ratio from each experiment were quite close with a value of about 0.88 for the experiment and about 0.90 for the model. These results could have been closer with a further adjustment to the permeability parameter, k_1, but it was felt the results were close enough for a direct comparison without the need for further modelling runs. Figure 8.6 shows that the two factors with the largest influence over the results, underfeed nip setting and tangent

setting were reasonably well matched. The spread of results was similar and the means for each factor level differed by less than 10%. The speed results do not look as good, but the experimental results for the extreme values, underfeed speed to pressure feeder speed ratio of 0.905 and pressure feeder speed of 188 mm/s, were the means of only one and two values, respectively. All in all, the results were very encouraging.

Figure 8.7 presents both the experimental results and model predictions for the second experiment. The model predictions were carried out with the same parameter values as the first model predictions with $k_1 = 5.0 \times 10^{-20}$ m^2 and a coefficient of friction on the underfeed roll of 0.7. Again, there was a good match between the experimental and model results. The spread of the underfeed nip setting results in the model was larger than in the experiment but, again, the extreme values were the mean of only a few tests. There was only one test at underfeed nip settings of 75 mm and 90 mm, for example. Again, the results were very encouraging.

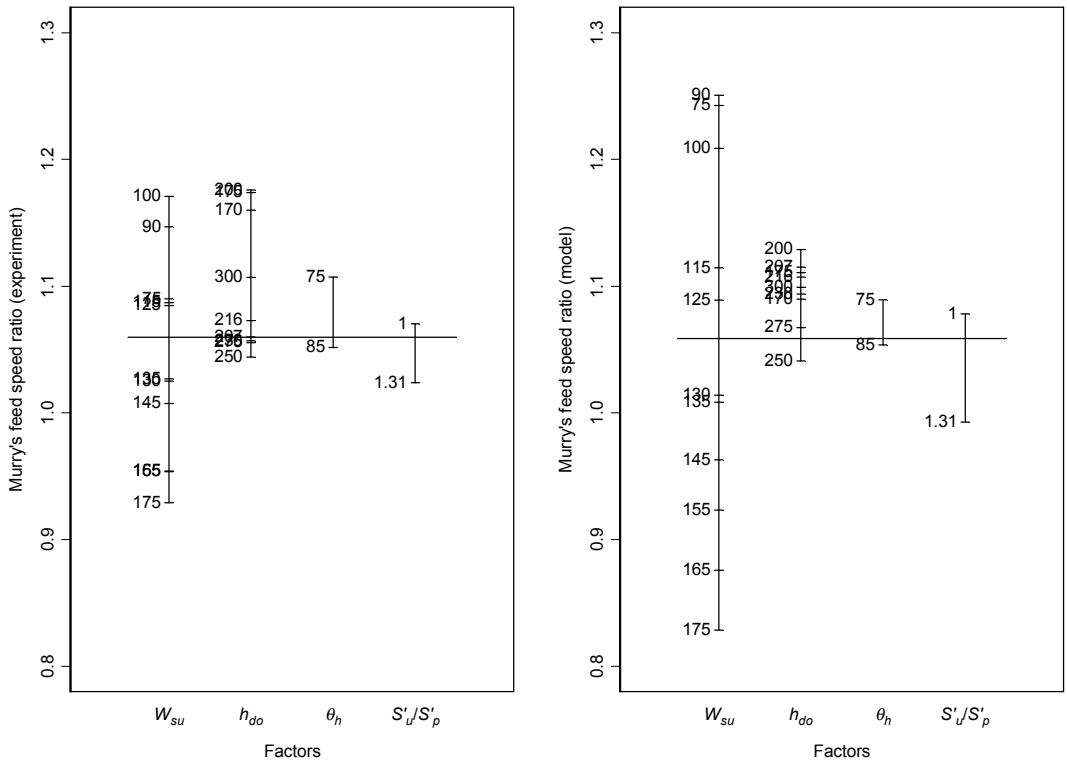

Figure 8.7 Experimental and model results for Murry's feed speed ratio from the second model tests of Jenkins and Murry (1981)

8.4.4 Concluding remarks

From the regression analysis from the experiments, the only parameters for which reliable trend information was obtained were the underfeed nip setting and the feed chute exit setting. Comparing the model predictions to the experimental results, the magnitude and spread of the results for both underfeed nip setting and feed chute exit setting were reasonably consistent, indicating the model provided a satisfactory match to the experimental results.

8.5 Modelling Jenkins and Murry's factory experiment

8.5.1 Introductory remarks

In addition to the model feeder experiments, Jenkins and Murry (1981) carried out feeding experiments on Marian mill's #5 mill in 1978. The experiment was much more limited in scope than the model feeder experiments but was larger in size. A total of 107 tests were carried out. The experiment explored the effect of two parameters on feed speed: underfeed nip setting (W_{su}) and the ratio of the underfeed roll speed to the pressure feeder speed (S'_u/S'_p).

8.5.2 Analysis of results

As for the small-scale experiments (section 8.4), the Jenkins and Murry (1981) factory experiment was conducted by varying one factor at a time, an approach that does not lend itself to an analysis of variance. To have a preliminary look at the experimental data, a linear regression analysis was conducted to identify the significant factors. The best regression equation, containing both underfeed nip setting and the ratio of the underfeed roll speed to the pressure feeder speed, was:

$$\frac{S_F}{S_p' \cos\alpha_{co}'} = 1.98 - 0.0036\, W_{su} + 0.34 \frac{S'_u}{S'_p} \qquad \textbf{(8.5)}$$

Figure 8.8 shows the quality of the fit.

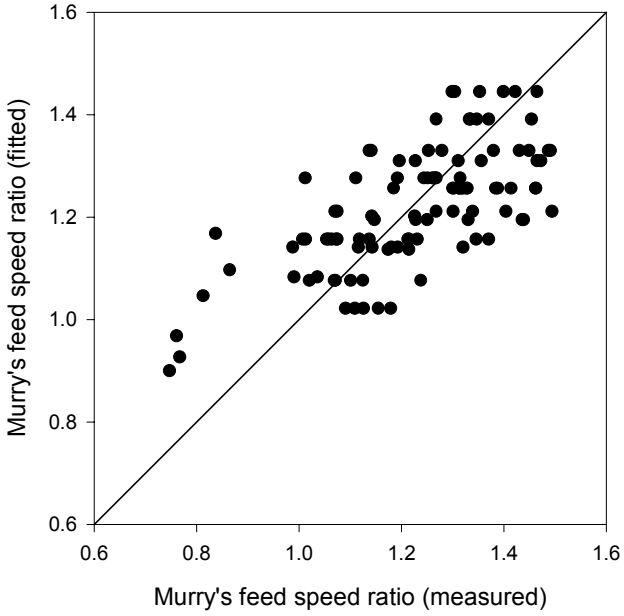

Figure 8.8 Quality of fit for regression equation (8.5)

Equation **(8.5)** is consistent with equation **(8.3)** and equation **(8.4)**. All equations show that Murry's feed speed ratio reduces as the underfeed nip setting increases. Equation **(8.5)** was the only equation of the three to show a significant effect of the ratio of the underfeed roll speed to the pressure feeder speed on Murry's feed speed ratio. It showed that increasing the ratio increased Murry's feed speed ratio.

8.5.3 Modelling the experiment

Figure 8.9 presents both the experimental results and model predictions for the Marian mill experiment. The model predictions were carried out with $k_1 = 1.0 \times 10^{-16}$ m^2 and a coefficient of friction on the underfeed roll of 0.7. This k_1 value is over three orders of magnitude greater than the k_1 value used to model the small-scale feeder experiments (section 8.4.3). The permeability was changed to get the overall mean value for Murry's feed speed ratio in the model to have a value close to the experimental overall mean value. As for the small-scale experiment comparison, a good match was achieved between the experimental and model results with the spread of results for both the underfeed nip setting and the speed ratio being similar.

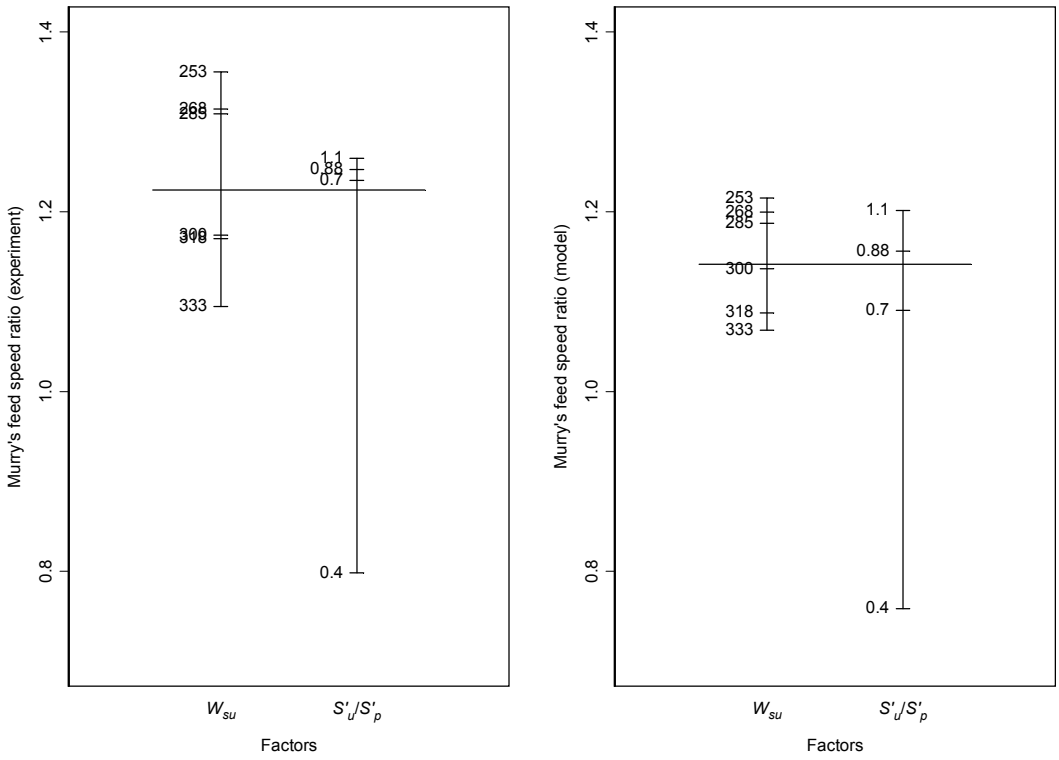

Figure 8.9 Experimental and model results for Murry's feed speed ratio from the Marian mill tests of Jenkins and Murry (1981)

8.5.4 Concluding remarks

The Marian mill experiment showed that the effect of underfeed nip setting on Murry's feed speed ratio, as measured in the small-scale experiment, was also present in the factory milling unit. In addition, the Marian experiment provided significant evidence of the effect of the ratio of the underfeed roll speed to the pressure feeder speed on Murry's feed speed ratio. After a substantial adjustment in the value for the permeability parameter, k_1, the computational model provided good agreement with the experimental results with reasonable predictions of the spread of both the underfeed nip setting and ratio of underfeed roll speed to pressure feeder speed parameters.

8.6 Modelling a new factory experiment

8.6.1 Introductory remarks

In order to collect a consistent data set across a wide range of operating conditions for the purpose of testing a throughput model of a factory milling unit, an experiment was conducted using a factory milling unit. In this section, the experiment and its results are described.

8.6.2 Apparatus

The factory milling unit

The experiment was conducted on the fifth (final) milling unit at Mulgrave Central Mill in north Queensland during the 2001 crushing season. This milling unit was attractive for this experiment because it was fitted with three drives. The two pressure feeder rolls were driven independently of the three-roll mill, allowing changes to mill feeding performance to be made without substantially affecting the performance of the mill. The underfeed roll was driven independently of the pressure feeder rolls by a shaft-mounted hydraulic drive, allowing the underfeed nip setting to be adjusted without the need to adjust the length of a drive chain and allowing the effect of underfeed roll speed on mill throughput to be easily determined.

The pressure feeder rolls were toothed (Farmer 1977) rather than grooved. The toothed rollers were essentially smooth cylinders on which rings of teeth were fitted at an axial pitch of 128 mm. The rings were 30 mm wide with teeth 100 mm high. The underfeed roll surface was grooved with a pitch of about 100 mm, a depth of about 25 mm and very wide flat sections at the base of the grooves between the raised groove flanks. The surface was not roughened. The dimensions of the rolls are presented in Table 8.1. For the pressure feeder rolls, the outside diameter was defined as the diameter of the smooth cylinder (ignoring the rings of teeth). For the underfeed roll, the outside diameter was

defined as the diameter of the smooth flat section at the base of the grooves. For all rolls, a groove depth of zero was assumed.

Table 8.1 Roll dimensions for Mulgrave's #5 mill

Parameter	Value (mm)
Length	2300
Top and bottom pressure feeder roll outside diameter	1180
Underfeed roll outside diameter	990

Modifications to the milling unit were made to enable the underfeed nip setting and feed chute geometry to be changed relatively easily. Figure 8.10 shows the underfeed roll support bracket used to assist in changing the underfeed nip setting. The bracket was designed to slide at an angle that kept the distance between the underfeed roll and the bottom pressure feeder roll relatively constant. Figure 8.11 shows the feed chute. The underfeed roll side of the feed chute is shown at the left of Figure 8.11. That side of the chute was hinged at the top as shown in Figure 8.11. The position of the chute wall was adjusted using a pneumatic cylinder. Two pneumatic cylinders were used to position the top pressure feeder roll side of the feed chute. Using the three pneumatic cylinders, the feed chute exit setting and the angular bias towards the top pressure feeder roll (section 8.2) could be adjusted.

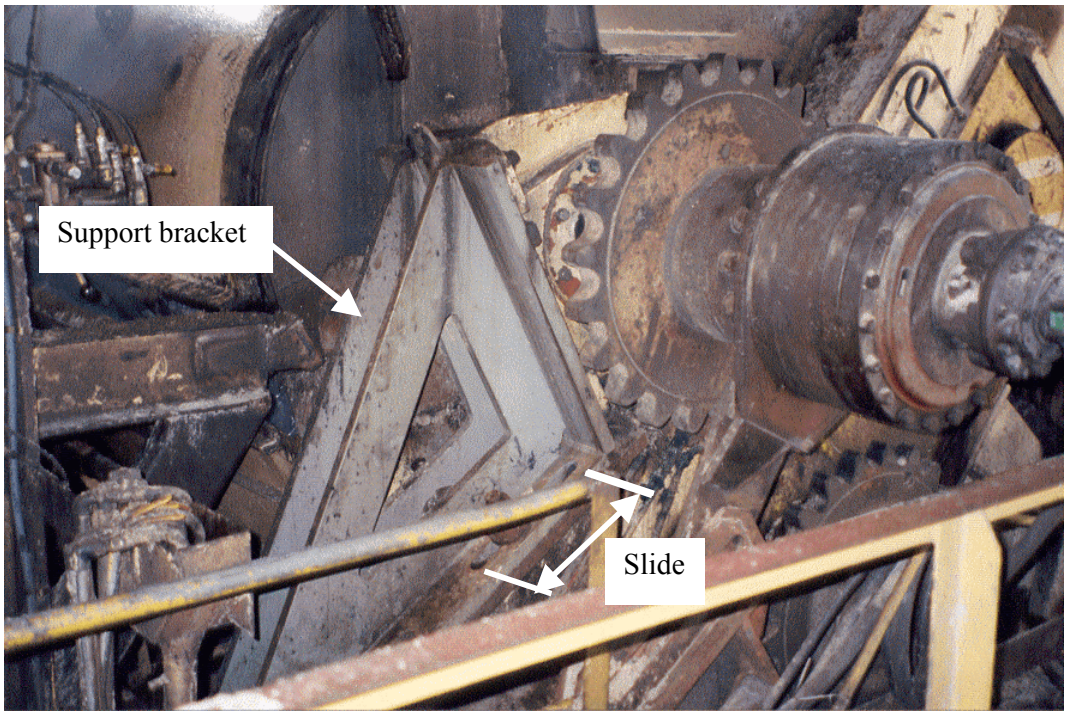

Figure 8.10 The underfeed roll support bracket allowing the underfeed nip setting to be easily adjusted

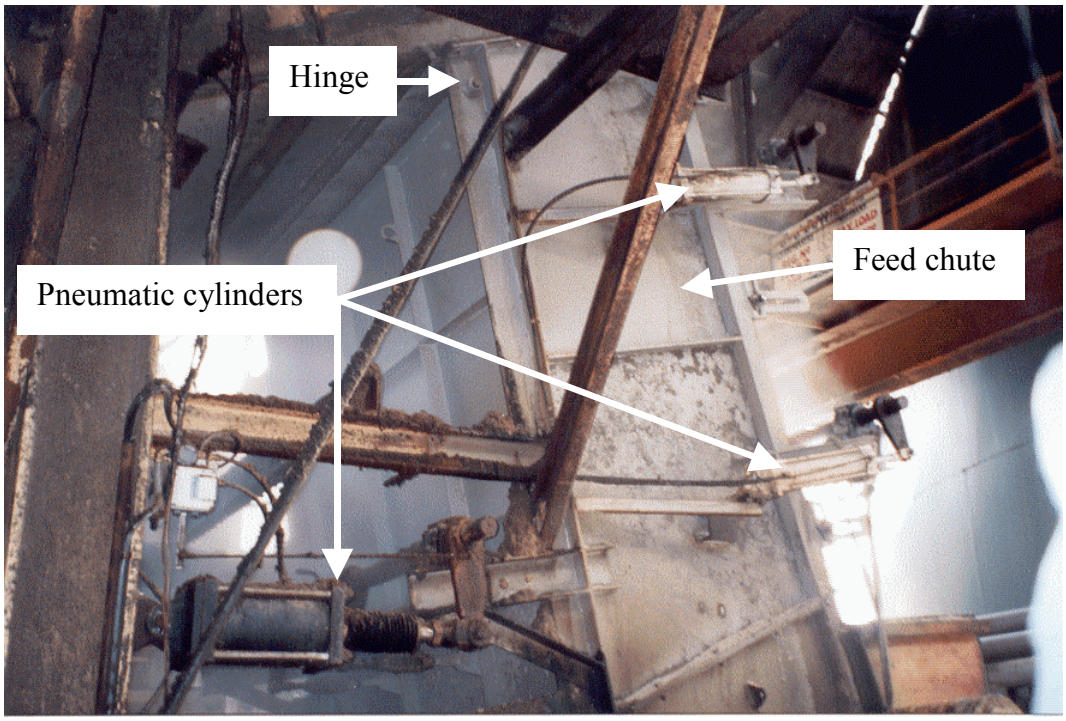

Figure 8.11 The three pneumatic cylinders allowing the feed chute setting and position to be adjusted

Instrumentation

Most of the parameters needed to monitor the operation of the factory milling unit and measure the feed speed were available through the factory's data collection system. The following parameters were relevant to this experiment:

- tonnes of cane crushed,
- cane fibre content,
- added water rate,
- position of the piston in the pneumatic cylinder on the underfeed roll side of the feed chute,
- underfeed roll motor speed,
- pressure feeder motor speed,
- underfeed roll motor hydraulic pressure,
- pressure feeder motor hydraulic pressure,
- chute level.

The tonnes of cane crushed were available from the factory weighbridge records. The crushing rate was determined by dividing the total tonnes of cane crushed by the duration of the test.

The cane fibre content was recorded using the factory's NIR-based *Cane Analysis System* (Staunton et al 1999).

The added water flow rate to the final mill was measured to provide information to determine the mass of bagasse in the mill feed chute, in order to determine the feed chute exit compaction (section 8.6.5).

The pneumatic cylinder on the underfeed roll side of the feed chute (Figure 8.11) was part of the pressure feeder motor torque control system. Although the preferred position of the piston was set at the start of a test, the torque control system increased the piston stroke if the pressure feeder torque set point was exceeded (similar to that described by Paddock & Farrell 1987). This action reduced the feed chute exit setting, causing the

pressure feeder to increase speed, thereby reducing the pressure feeder nip compaction and, hence, the pressure feeder torque. It was necessary to record the piston position in order to determine the average feed chute exit setting and feed chute position for a test.

The drives on both the underfeed roll and pressure feeder were hydraulic motors. Based on manufacturer's specifications, the torque on these drives was calculated from their hydraulic pressure as follows:

$$G_u = 1.76\, P_{su} \qquad \textbf{(8.6)}$$

$$G_p = 11.5\, P_{sp} \qquad \textbf{(8.7)}$$

where P_{su} and P_{sp} are the hydraulic system pressures in the underfeed roll and pressure feeder motor drives, respectively (kPa) and G_u and G_p are the underfeed roll and pressure feeder shaft torques, respectively (N.m).

The feed chute bagasse level was determined using the mill's chute height sensor (Sugar Research Institute 1973) that is based on a series of conductivity sensors positioned along the side wall of the feed chute.

Analysis equipment

As discussed in section 8.6.5, the feed chute exit compaction was estimated in order to calculate Murry's feed speed ratio. The estimation of the feed chute exit compaction required an estimate of the fibre content and the low-pressure compression behaviour of the feed bagasse.

The fibre content of the feed bagasse was determined using a can fibre machine (Bureau of Sugar Experiment Stations 2001, Method 4A).

The compression behaviour of the feed bagasse was determined using a specially constructed confined uniaxial test apparatus. The test cell had a diameter of 350 mm and a height of 260 mm. A pressure up to 50 kPa was applied using a small hydraulic pump through a hydraulic cylinder to a platen that compressed the bagasse. The cell

was instrumented with a load cell to measure the total applied force and a displacement transducer to record the position of the platen.

8.6.3 Experimental design

The experiment was designed to explore the effect of underfeed nip setting, feed chute exit setting, feed chute position over the rolls and underfeed roll speed on mill throughput. Based on the results of the two-roll mill investigations (chapters 6 and 7) and the three-roll feeder and factory milling unit investigations of Jenkins and Murry (1981), underfeed nip setting and feed chute exit setting were expected to influence mill throughput. Jenkins and Murry also investigated the effect of feed chute position and underfeed roll speed on mill throughput but were unable to determine any significant effect. Although the feed chute position and underfeed roll speed had not been found to have a significant effect on mill throughput previously, they were of interest to factory personnel and were included in the experiment at little cost, while having the potential to provide valuable information to test the factory model if a significant effect was found.

A total of 54 tests were conducted in a $2 \times 3^{4-1}$ split-split-plot fractional factorial experimental design to explore the effect of the four factors on mill throughput. The split-split-plot design was chosen because of the difficulty in changing the experimental factors. Changing the underfeed nip setting required a milling train shutdown for several hours, so this factor was changed infrequently. Changing the feed chute setting and the position of the feed chute also required a milling train shutdown, but only for about ten minutes. These factors were changed more frequently than the underfeed nip setting. The underfeed roll speed could be changed during normal crushing operations and so was changed more frequently than the feed chute factors. The specific factors and the levels at which they were tested are presented in Table 8.2.

Table 8.2 Factors and factor levels explored in the experiment

Factor	Level		
	0	1	2
Underfeed nip setting compared to optimum, W_{sua} (mm)	0	-100	100
Feed chute exit setting compared to optimum, h_{doa} (mm)	-200	0	-100
Angular bias of feed chute to top pressure feeder roll, θ_{pt} (º)	2	1	0
Underfeed roll speed compared to pressure feeder speed, ω_u/ω_{pt}	0.4	1.0	1.3

The underfeed nip setting and feed chute exit setting levels were defined relative to their predicted maximum throughput settings, using the theory of Jenkins and Murry (1981), presented in equations **(2.25)** and **(2.26)**. The actual settings were calculated as follows:

$$W_{su} = W_{su}^{*} + W_{sua} \qquad \textbf{(8.8)}$$

$$h_{do} = h_{do}^{*} + h_{doa} \qquad \textbf{(8.9)}$$

where W_{su}^{*} is the underfeed nip setting and h_{do}^{*} is the feed chute exit setting predicted for maximum throughput.

The angular bias towards the top pressure feeder roll, θ_{pt}, was defined using equations **(8.1)** and **(8.2)**.

As discussed in section 8.2, to completely define the geometry of the feed chute, the chute angle was required along with the chute setting and the chute position. Since the chute wall on the underfeed roll side was hinged to a fixed position at the top (Figure 8.11), the chute angle was fixed as a function of the chute setting and the chute position. Over the course of the experiment, the chute angle varied between 76° and 83°, a relatively small range.

The final experimental factor, the underfeed roll speed, was defined as a ratio to the top pressure feeder roll speed, a ratio of angular velocities (not surface speeds). This ratio was necessary since the underfeed roll speed had to be able to vary with the pressure feeder speed as part of the milling unit rate and load control systems.

As in the two-roll mill experiments described in sections 6.3 and 7.2, this experiment was designed to provide information about the feed speed, S_F. Also following the approach taken for the two roll-mill experiments, Murry's feed speed ratio was used, instead of S_F directly. Following the convention established by Jenkins and Murry (1981), Murry's feed speed ratio was defined as $\frac{S_F}{S'_{pt}\cos\alpha'_{do}}$ where S_F is the feed speed at the feed chute exit and S'_{pt} is the surface speed of the top pressure feeder roll.

8.6.4 Procedure

The nominal duration of each test was one hour. In some cases, interruptions to the cane supply caused a test to be halted early. As a general rule, if a test was interrupted before it was halfway through, it was aborted and done again.

During each test, the #4 mill bagasse was continuously sampled (the feed material for #5 mill). Following the completion of a test, the bagasse sample was mixed and subsampled according to Method 5 in Bureau of Sugar Experiment Stations (2001). One of the subsamples was used to determine the fibre content according to Method 4A in Bureau of Sugar Experiment Stations (2001). The other subsample was used to determine the load / displacement characteristics of the bagasse in a low-pressure confined uniaxial test cell (section 8.6.2).

During each test, the feed speed was manually estimated at approximately five-minute intervals by measuring the time for the bagasse to travel between two locations a known distance apart down the side of the feed chute.

During each test, the tonnes of cane crushed, the cane fibre content, the added water rate, the position of the piston in the pneumatic cylinder on the underfeed roll side of the feed chute, the underfeed roll motor speed and hydraulic pressure, the pressure feeder motor speed and hydraulic pressure and the chute level were measured automatically using the factory's data collection system (section 8.6.2).

8.6.5 Results

Analysis of results

As discussed in section 8.6.3, the purpose of each test was to determine the feed speed. Two measures of feed speed were provided by the test procedure: a direct measure and an indirect measure.

As described in section 8.6.4, the feed speed was determined directly from the time for bagasse to travel between two locations down the side of the feed chute.

Following the approach of Jenkins and Murry (1981), the feed speed was also determined indirectly. Rearranging equation **(2.20)**,

$$\frac{S_F}{S_p'} = \frac{E}{\frac{2\,D_p'}{D_p + W_p}\,\frac{2\,h_{do}}{D_p + W_p}} \qquad \textbf{(8.10)}$$

where E is the effectiveness and $D_p + W_p = D_p' + W_{sp}$. The approach used to determine effectiveness was the same as that described in section **(3.2)**.

Feed speed results

Appendix G presents the detailed experimental results. An analysis of variance of the feed speed results was carried out using both measures of feed speed. Table 8.3 presents the analysis of variance from the directly measured feed speed results. Table 8.4 presents the analysis of variance from the indirectly measured feed speed results. The analysis of variance was not particularly successful in identifying significant factors. For the directly measured feed speed results, no factors or interactions with a level of significance less than 10% were identified. For the indirectly measured feed speed results, the underfeed nip setting was identified as a significant factor with a level of significance of 2%. It was noted that, although no significant factors were identified

from the directly measured feed speed results, the underfeed nip setting factor had the highest variance ratio.

Table 8.3 Analysis of variance of Murry's feed speed ratio for the factory mill experiment using the direct measure of feed speed

Source	Degrees of freedom	Mean square	Variance ratio	Significance level
W_{sua}	2	0.180	19.2	-
h_{doa}:θ_{pt}	2	0.003	0.3	-
Residuals	1	0.009		
h_{doa}	2	0.006	0.3	-
θ_{pt}	2	0.000	0.0	-
Residuals	8	0.019		
ω_u/ω_{pt}	2	0.001	0.3	-
W_{sua}:ω_u/ω_{pt}	4	0.004	1.3	-
h_{doa}:ω_u/ω_{pt}	4	0.005	1.5	-
θ_{pt}:ω_u/ω_{pt}	4	0.005	1.4	-
Residuals	22	0.003		

Table 8.4 Analysis of variance of Murry's feed speed ratio for the factory mill experiment using the indirect measure of feed speed

Source	Degrees of freedom	Mean square	Variance ratio	Significance level
W_{sua}	2	0.579	866.4	0.02
h_{doa}:θ_{pt}	2	0.025	37.2	-
Residuals	1	0.001		
h_{doa}	2	0.138	2.8	-
θ_{pt}	2	0.016	0.3	-
Residuals	8	0.050		
ω_u/ω_{pt}	2	0.010	0.8	-
W_{sua}:ω_u/ω_{pt}	4	0.007	0.6	-
h_{doa}:ω_u/ω_{pt}	4	0.013	1.0	-
θ_{pt}:ω_u/ω_{pt}	4	0.016	1.2	-
Residuals	22	0.013		

Figure 8.12 and Figure 8.13 show the mean levels for each of the experimental factors for Murry's feed speed ratio for the directly measured and indirectly measured feed speed results, respectively. Both figures confirm the results of the analysis of variance that the underfeed nip setting was the factor that had most effect on Murry's feed speed ratio. This highest values for Murry's feed speed ratio were observed at the underfeed

nip setting of 100 mm less than the optimum setting estimated using the theory of Jenkins and Murry (1981).

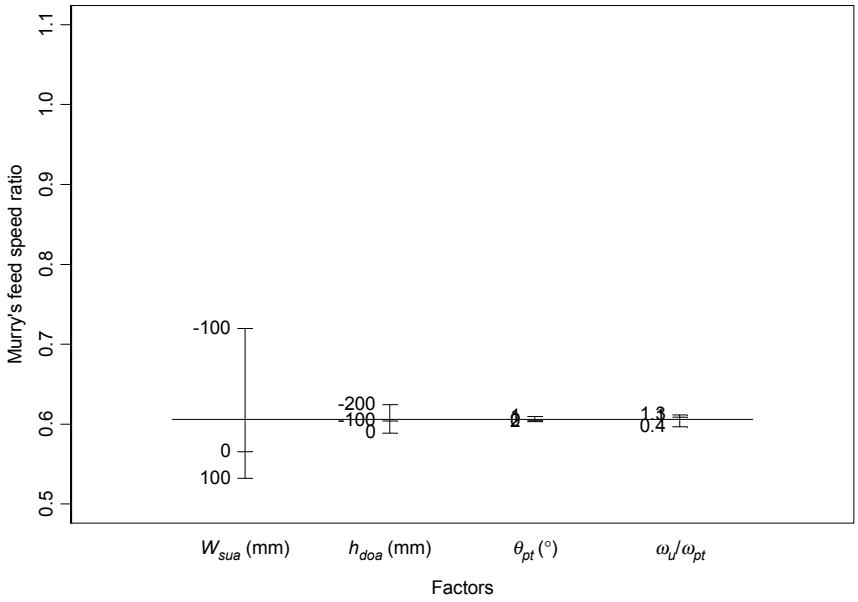

Figure 8.12 Mean levels of Murry's feed speed ratio using directly measured feed speed results

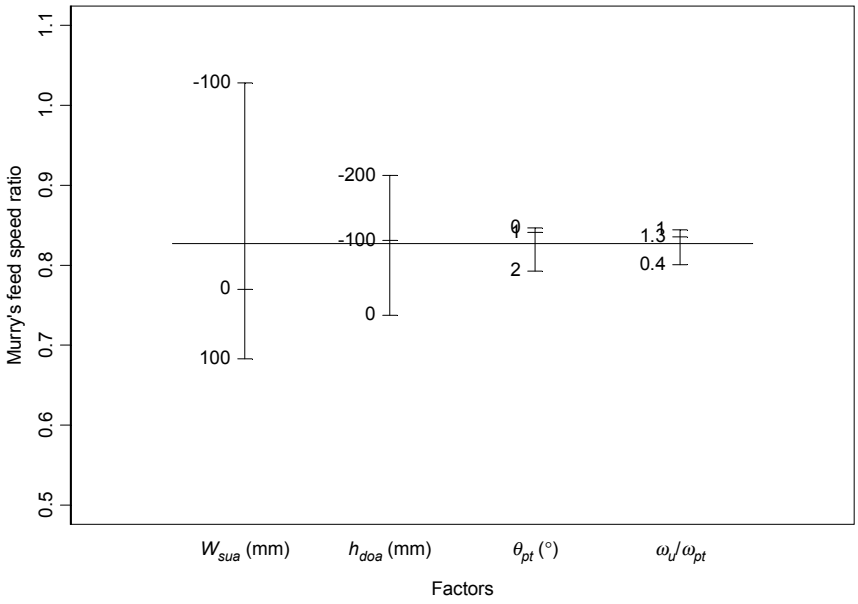

Figure 8.13 Mean levels of Murry's feed speed ratio using indirectly measured feed speed results

Comparison of measures for feed speed ratio

Figure 8.12 and Figure 8.13 show similar trends between the experimental factors and Murry's feed speed ratio. A comparison of the two figures, however, shows that the indirect feed speed results gave a higher mean value and a greater spread for Murry's feed speed ratio. Figure 8.14 shows a test-by-test comparison between the directly and indirectly measured results. While there is clearly a relationship between the two sets of results, the figure supports the observation above that the indirect feed speed results were higher and varied over a greater range. The indirect feed speed measurements, then, were more responsive to changes in the experimental conditions. Consequently, it is not surprising that the indirect feed speed results found the one significant factor in the analysis of variance in Table 8.4.

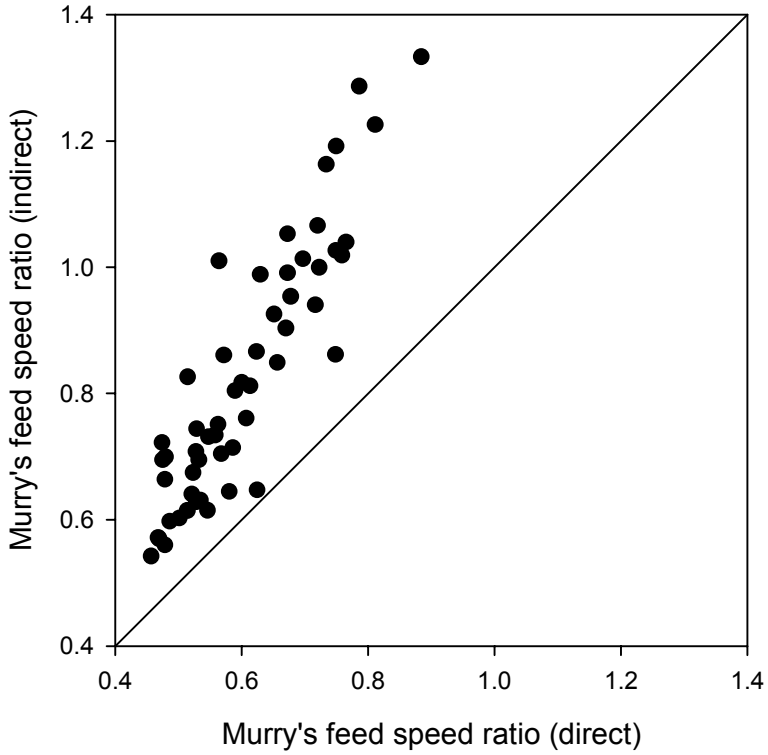

Figure 8.14 Murry's feed speed ratio compared between the values calculated from directly and indirectly measured feed speed results

8.6.6 Discussion of experimental results

In order to assess which of the two measures of Murry's feed speed ratio was more likely to be accurate, the direct measurements were substituted into equation **(2.22)** and then into a rearranged version of equation **(2.18)** to calculate the feed chute exit compaction. The resulting feed chute exit compactions were impossibly large, based on the measured pressure / compaction data and the maximum possible pressure. Consequently, the indirectly measured values were believed to be the more accurate.

8.6.7 Material parameters for modelling the factory experiment

The factory mill feeding experiment was carried out on the fifth (final) mill of a milling train. As such, the feed material to the milling unit was the bagasse from the fourth milling unit, with water added. To determine material parameters for the feed bagasse, some of the bagasse collected during the conduct of the tests (section 8.6.4) was tested in a uniaxial compression test cell and subsequent parameter estimation techniques were used to determine the material parameters for the solid and fluid phases as described in section 5.4. This approach aimed to determine the solid phase material parameter, λ_1, and the fluid phase material parameters, k_1 and k_2.

The test cell was in the configuration shown in Figure 5.2. The test procedure was the same as that described in section 5.4.3. Two series of three tests were undertaken. The results of the parameter estimation process for the two series are presented in Table 8.5. From a comparison of the total pressure and juice pressure graphs from the experiment with the model predictions, the series 1 solution provided a much better fit than the series 2 solution. Consequently, the series 1 material parameter estimates were used in the model predictions presented in section 8.6.8.

Table 8.5 Results of the material parameter estimation process

Series	λ	k_1 (m^2)	k_2
1	0.27	3.3×10^{-18}	6.9
2	0.21	3.0×10^{-19}	7.6

8.6.8 Modelling the factory experiment

Following the same procedure adopted in sections 8.4.3 and 8.5.3, the experiment was modelled using the computational feeding model. Figure 8.15 presents both the experimental results from Figure 8.13 and model predictions for the Mulgrave mill experiment. The model predictions were carried out with $k_1 = 5.0 \times 10^{-19}$ m^2 and a coefficient of friction on the underfeed roll of 0.1. The permeability parameter, k_1, was changed by a factor of about 7 from its estimated value (Table 8.5) to provide a

satisfactory match to the overall experimental mean. As discussed in section 6.5.2, this change is small considering the possible orders of magnitude change in permeability.

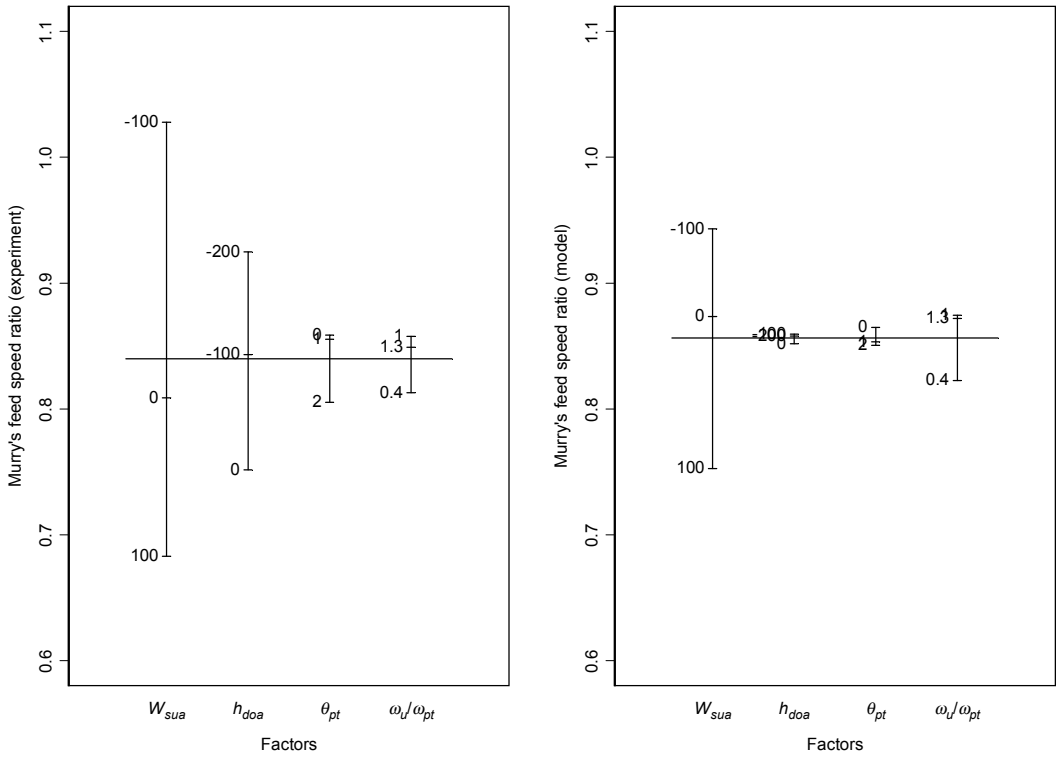

Figure 8.15 Experimental and model results for Murry's feed speed ratio from the Mulgrave mill tests

Since the underfeed nip setting results were the only statistically significant results, these were the more important results to duplicate. The experimental results show a greater spread than the model results although the trend is the same. Although the effect was not statistically significant, there was a sizeable chute setting trend in the experimental results that was completely absent in the model results. The coefficient of friction on the underfeed roll had to be substantially reduced to reduce the size of the underfeed roll speed effect in the model to a similar proportion to the experimentally observed effect. Since the underfeed roll was quite smooth as discussed in section 8.6.2 and was generally quite wet, the low coefficient of friction value was considered realistic.

8.6.9 Concluding remarks

In summary, the Mulgrave mill experiment confirmed the results of previous experiments that the underfeed nip setting has a large effect on Murry's feed speed ratio. The effect of the other parameters; chute setting, contact angle bias and underfeed roll speed; was considerably less.

8.7 Concluding remarks

A general computational model of a factory milling unit has been developed.

Based on the results from modelling four separate feeding experiments, the computational feeding model has been shown to provide quite realistic responses to changes in mill geometry and roll speed. In carrying out this validation, the model was shown to handle three substantially different geometries: one small-scale feeder and two factory milling units, one with a heavy duty pressure feeder and one with a toothed feeder.

One of the validation data sets came from an experimental investigation conducted as part of this study. A factory mill feeding experiment was conducted that explored a greater range of parameter values than previous experimental investigations and confirmed the importance of underfeed nip setting to mill feeding performance.

9 Using the new feeding model

9.1 Introductory remarks

In chapter 8, a computational feeding model is described and shown to adequately reproduce the effects of factors affecting feed speed previously measured in feeding experiments. In this chapter, the computational feeding model is explored. A sensitivity analysis is presented to identify the factors having the largest effect on Murry's feed speed ratio. The ability of the model to reproduce the results of the factory feeding measurements presented in section 3.3, using only the parameters shown in the sensitivity analysis to have a large effect, is tested.

9.2 Sensitivity analysis

9.2.1 Introductory remarks

Due to the large number of parameters in the computational feeding model (section 8.3), the sensitivity analysis was conducted in three stages. Firstly, the response of the model to changes in material parameters was determined across a limited range of geometry and boundary conditions. Secondly the response of the model to changes in the model geometry was determined. Thirdly, a combined sensitivity analysis was conducted with the most influential parameters from each of the first two analyses.

9.2.2 Sensitivity to material parameters and initial and boundary conditions

The first sensitivity analysis determined the response of the model to the following parameters:

- solid phase elastic material parameters κ and p_t^e (the third parameter, v, was chosen to ensure appropriate relaxation behaviour in the model),
- solid phase plastic material parameters M and λ_1 (the third parameter, p_t, was chosen to ensure the ratio of the lateral stress to the normal stress during compression was of suitable magnitude),
- liquid phase material parameter k_1 (the other permeability parameter, k_2, was not used since both parameters affect permeability across the entire void ratio range while the viscosity was believed to be known accurately enough to not be of concern),
- initial conditions f, γ_{do} and P_{do},
- μ_u, the coefficient of friction on the underfeed roll (experience showed that the coefficient of friction on the two pressure feeder rolls needed to be at least 0.7 to ensure feeding into the pressure feeder nip so a value of 0.7 was adopted throughout for these two rolls)
- ω_u/ω_{pb}, ratio of underfeed roll speed to pressure feeder roll speed,
- underfeed nip setting and feed chute exit setting.

While the material parameters and the initial and boundary conditions were the main focus of this sensitivity analysis, the two settings and the roll speed ratio were included to determine if these parameters had any influence on which of the material parameters and the initial and boundary conditions were most important.

The sensitivity analysis was conducted as a 2^{12-4} fractional factorial numerical experiment. The mean results are presented in Figure 9.1. An analysis of variance of the results has shown that the parameters with the greatest influence on the feed speed ratio were:

- the material parameter, k_1 (there was also a significant interaction between the two solid phase elastic parameters),
- the initial conditions, f and γ_{do},
- the coefficient of friction on the underfeed roll, μ_u through interactions with the underfeed nip setting and the roll speed ratio,
- the underfeed nip setting and the roll speed ratio.

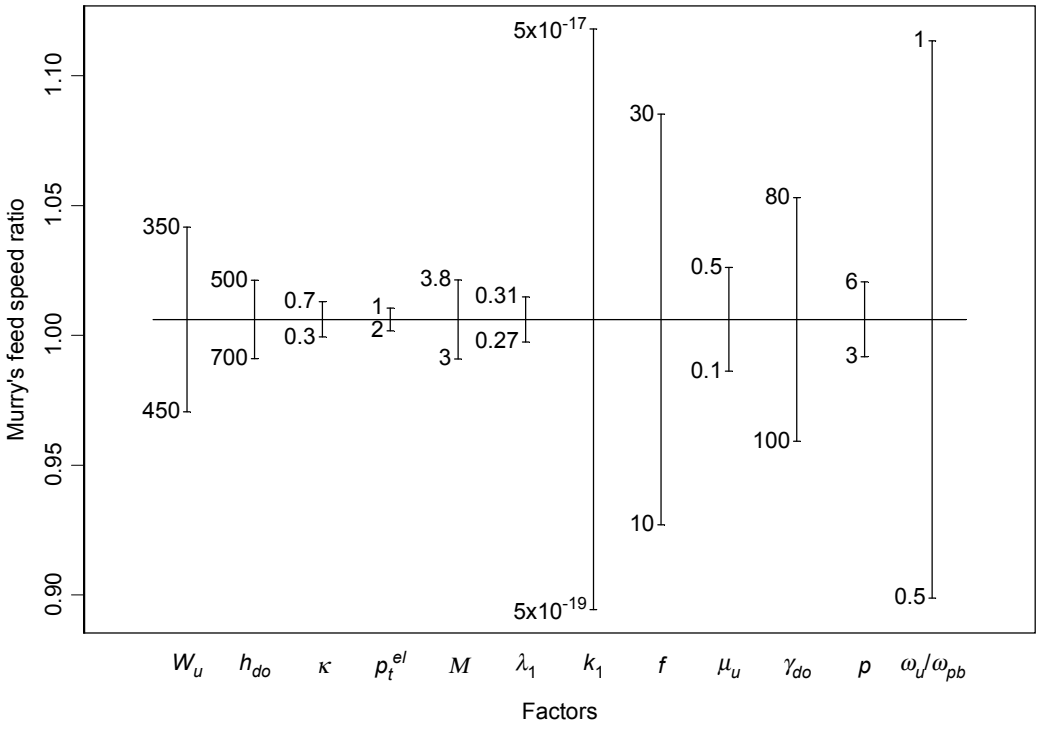

Figure 9.1 Results of the sensitivity analysis of the material parameters and the initial and boundary conditions

The analysis showed that permeability was the most significant material parameter affecting feed speed. The permeability parameter, k_1, the fibre content, f, and the feed chute exit compaction, γ_{do} all affect permeability and it is believed that the effect of these parameters on permeability is the main cause of their influence on feed speed. The interaction between the two elastic parameters is believed to be an indication of the

importance of selecting appropriate combinations of these parameters, rather than an indication of their importance in affecting the feed speed.

The coefficient of friction at the underfeed roll surface was also found to be important at various combinations of the underfeed nip setting and the roll speed ratio.

9.2.3 Sensitivity to geometry

The second sensitivity analysis determined the response of the model to the following geometrical parameters:

- D_{pb}, the diameter of the two pressure feeder rolls,
- D_u/D_{pb}, the ratio of the underfeed roll diameter to the pressure feeder roll diameter,
- W_u/W_p, the ratio of the underfeed nip work opening to the pressure feeder nip work opening,
- W_p/D_{pb}, the ratio of the pressure feeder nip work opening to the pressure feeder roll diameter,
- W_{up}, the work opening between the underfeed roll and the bottom pressure feeder roll,
- h_{do}/h^*_{do}, the ratio of the feed chute exit setting to the *optimum* feed chute exit setting, according to the Jenkins and Murry (1981) theory,
- θ_{pt}, the contact angle bias towards the top pressure feeder roll,
- θ_h, the chute angle,
- S_u/S_{pb}, ratio of underfeed roll surface speed to pressure feeder roll surface speed.

The sensitivity analysis was conducted as a 2^{9-3} fractional factorial numerical experiment. The mean results are presented in Figure 9.2. An analysis of variance of the results has shown that the parameters with the greatest influence on the feed speed ratio were, in order of importance:

- W_u/W_p, the ratio of the underfeed nip work opening to the pressure feeder nip work opening,
- W_p/D_{pb}, the ratio of the pressure feeder nip work opening to the pressure feeder roll diameter,
- D_{pb}, the diameter of the two pressure feeder rolls.

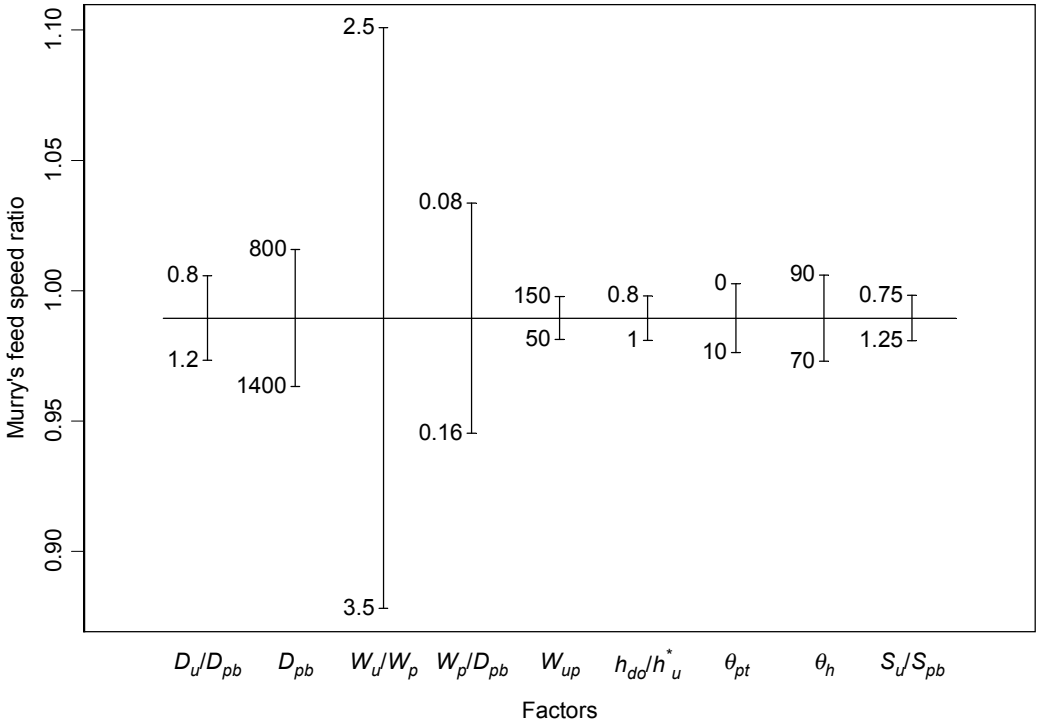

Figure 9.2 Results of the sensitivity analysis of the geometrical parameters

The underfeed roll diameter was not found to be of great importance, provided the surface speed matched the surface speed of the pressure feeder rolls.

9.2.4 A final sensitivity analysis

A final sensitivity analysis was conducted to assess the relative importance of the material parameters and the geometrical parameters. The parameters chosen for this analysis were those identified as most significant in the previous two analyses:

- D_{pb}, the diameter of the two pressure feeder rolls,
- W_u/W_p, the ratio of the underfeed nip work opening to the pressure feeder nip work opening,
- W_p/D_{pb}, the ratio of the pressure feeder nip work opening to the pressure feeder roll diameter,
- k_1, the permeability parameter,
- f, the fibre content,
- γ_{do}, the feed chute exit compaction,
- μ_u, the coefficient of friction on the underfeed roll,
- S_{pb}, the pressure feeder roll surface speed,
- S_u/S_{pb}, the ratio of underfeed roll surface speed to pressure feeder roll surface speed.

The sensitivity analysis was conducted as a $3^2 \times 2^{7-2}$ fractional factorial numerical experiment. From previous experience (Jenkins & Murry 1981), the responses of the ratio of the underfeed nip work opening to the pressure feeder nip work opening and the ratio of the underfeed roll surface speed to the pressure feeder roll surface speed to feed speed were expected to contain a maximum value. These factors were explored at three levels, rather than two, to gain some idea of where that maximum value lay. The other parameters were explored at two levels, as in the previous two analyses.

The mean results are presented in Figure 9.3. Of the parameters explored, the roll diameter was the least influential.

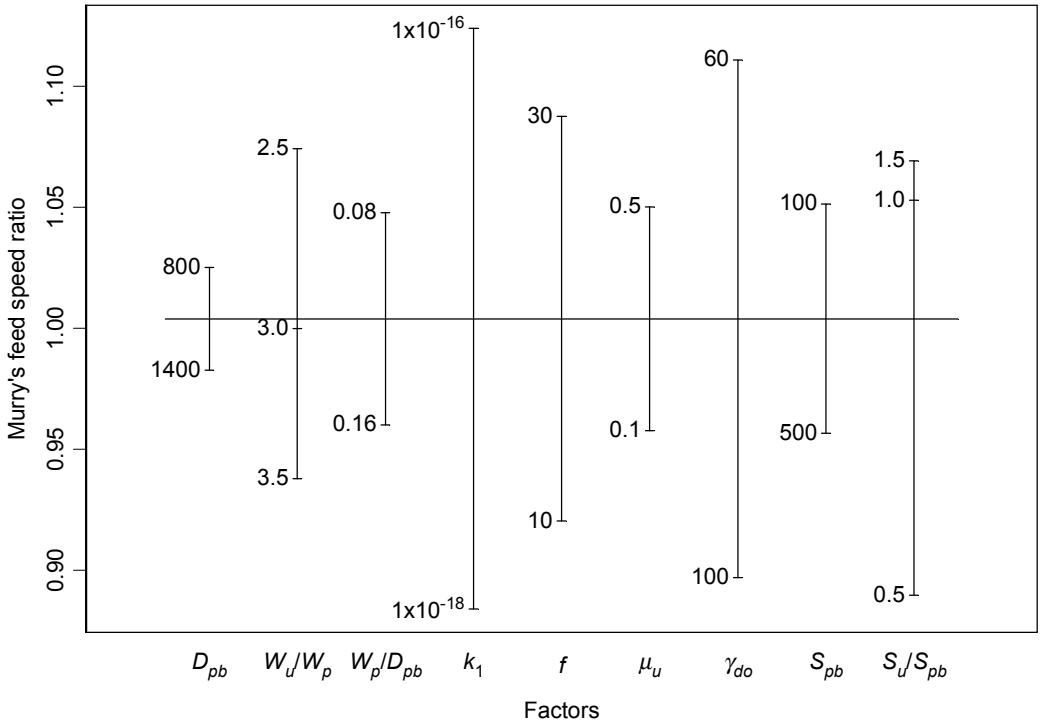

Figure 9.3 Results of the sensitivity analysis of the most influential parameters

9.2.5 Concluding remarks

As discussed in section 9.1, the purpose of the sensitivity analysis was to separate the parameters that were important to measure accurately from those that were not important. The list of important parameters consisted of:

- two geometry parameters, W_u/W_p and W_p/D_{pb},
- two speed parameters, S_{pb} and S_u/S_{pb},
- one material parameter, k_1,
- two initial conditions, f and γ_{do},
- the coefficient of friction on the underfeed roll, μ_u.

Of these parameters, the geometry parameters and the speed parameters are easily measured and are readily available. The two initial conditions are not as easily measured but can be determined. The fibre content can be determined from a mass balance of the milling train and, for practical purposes, the quantities don't change much for a given milling unit. The feed chute exit compaction is less readily available. The only satisfactory measurement technique available is from the use of chute theory that relies on knowing the low pressure compaction characteristics of the feed material. In practice, it is likely that an estimate based on Figure 3.8 of Jenkins and Murry (1981) will be adequate for providing an estimate of feed chute exit compaction. There remain two parameters for which very poor information is available: the permeability parameter and the coefficient of friction parameter.

If only one parameter remained, that parameter could be calculated from known mill operating conditions. Consequently, it was desirable to remove one parameter from the list of important parameters. Since the effect of coefficient of friction on the underfeed roll had a substantially smaller effect than the permeability parameter, the coefficient of friction parameter was removed. The final list of parameters selected to describe the feeding behaviour of a milling unit was:

- two geometry parameters, W_u/W_p and W_p/D_{pb},
- two speed parameters, S_{pb} and S_u/S_{pb},
- one material parameter, k_1,
- two initial conditions, f and γ_{do}.

9.3 Comparison with Jenkins and Murry model

Two substantial sets of measurements of factory mill feeding performance are presented in section 3.3. The computational feeding model was tested against both data sets. While the model outputs in chapter 8 were presented in terms of Murry's feed speed ratio, the outputs are presented in terms of effectiveness in this section. Murry's feed

speed ratio was converted to effectiveness by using a modified version of equation **(2.22)**:

$$E = r_M \cos\alpha_{do} \frac{D_p}{h^*} \frac{h_{do}}{h^*} \qquad \textbf{(9.1)}$$

In modelling each of the tests, only the parameters listed in section 9.2.5 were varied. Standard values were used for all other parameters. These standard values are listed in Appendix H.

As discussed in section 9.2.5, no measurements were available for the permeability parameter, k_1, and a calibration step was needed to determine its value. The approach adopted was to match the measured effectiveness to the model effectiveness by varying k_1 for all of the #1 mill results. The resultant k_1 value was then used in the prediction of effectiveness for the remainder of the milling train. Since insufficient permeability measurements have been made to determine how permeability varies along a milling train, the assumption of constant k_1 was considered adequate.

Figure 9.4 compares the performance of the Jenkins and Murry (1981) empirical model against the new computational feeding model for the Jenkins and Murry (1981) factory survey measurements and the 1997 factory survey measurements. In all cases, the #1 mill results were removed since the process for predicting effectiveness for the new computational feeding model involved matching the #1 mill results exactly. The top two graphs show the comparison of the Jenkins and Murry empirical model against both sets of measurements. In both cases, the measurements do not correlate well with the model predictions. The bottom two graphs, showing the comparison of the computational model predictions against both sets of data, show better correlation. It is also worth noting that the six points of highest predicted effectiveness in the bottom left hand graph all belong to one milling train.

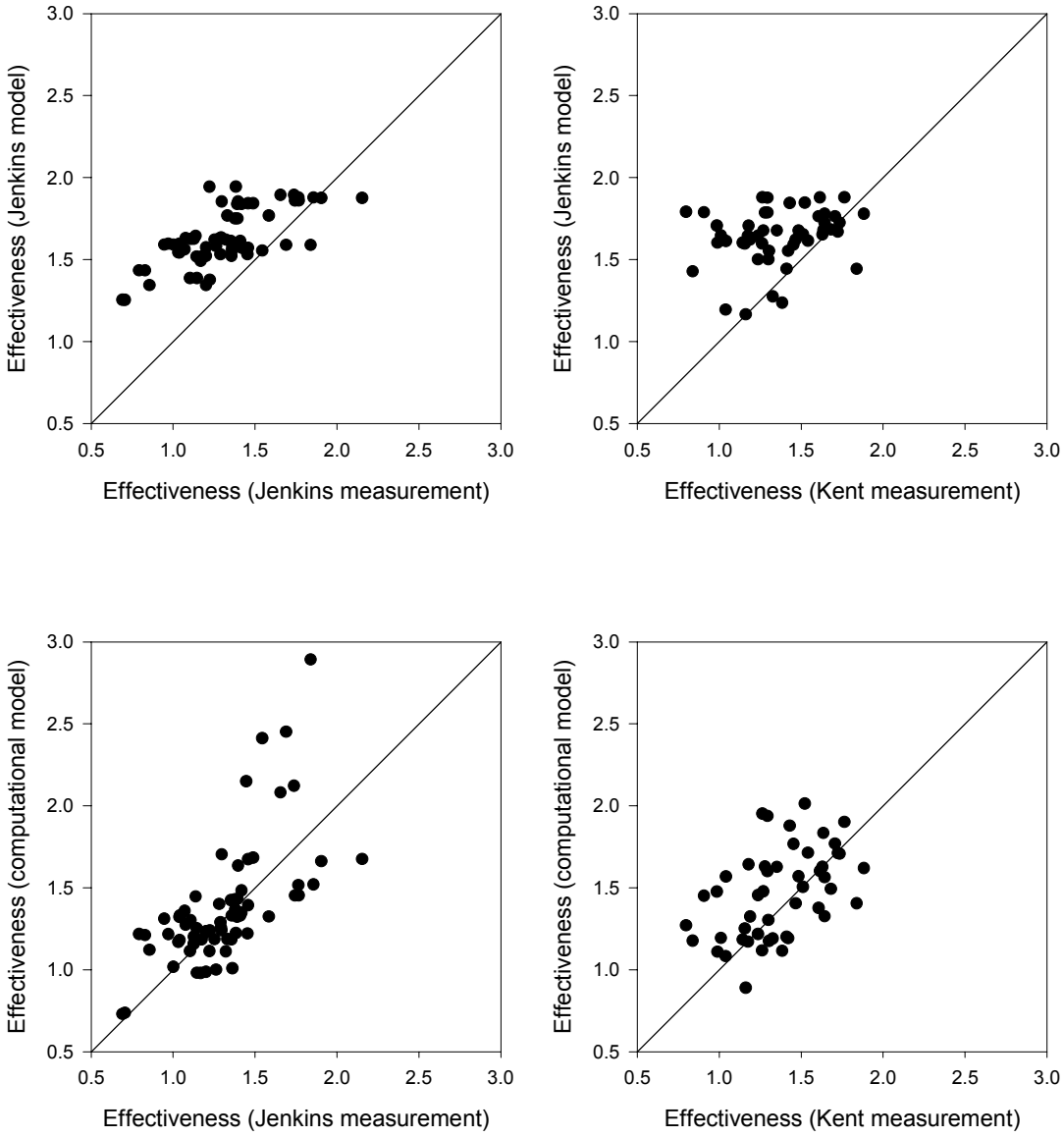

Figure 9.4 Comparison of Jenkins and Murry (1981) empirical model and new computational model predictions of effectiveness against measurements of Jenkins and Murry (1981) and Kent (1998)

Comparing the effectiveness differences of individual milling units in a milling train against the predicted differences provided a more severe test of the computational feeding model. Firstly, multiple comparison tests were carried out using the measured effectiveness values within each milling train for both the Jenkins and Murry and the Kent data sets. From those test results, pairs of milling units with significantly different effectiveness were identified and the difference in effectiveness was calculated. The measured difference in effectiveness was plotted against the predicted difference in

effectiveness using both the Jenkins and Murry empirical model and the computational feeding model in Figure 9.5.

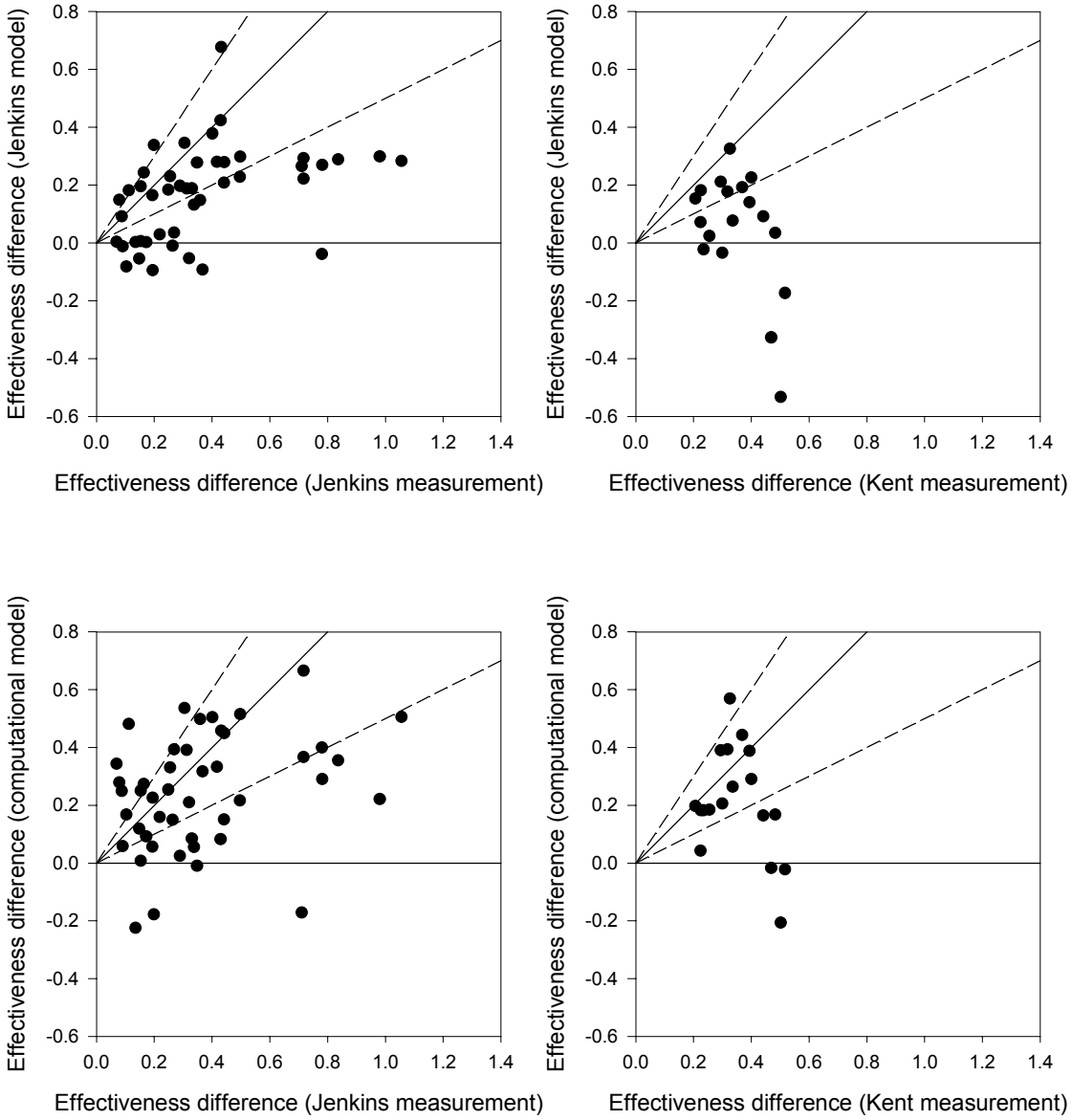

Figure 9.5 Comparison of effectiveness differences using the Jenkins and Murry (1981) empirical model and new computational model predictions of effectiveness against measured effectiveness differences from Jenkins and Murry (1981) and 1997 measurements

In Figure 9.5, points below the horizontal axis represent situations where an increase in effectiveness was measured between two milling units while the model predicted a decrease. The dashed lines represent boundaries where the magnitude of the predicted

difference was 50% different from the magnitude of the measured difference. Table 9.1 shows the percentage of data points below the horizontal axis and within the 50% error bands for all graphs in Figure 9.5. For both data sets, the computational model performed better than the Jenkins and Murry model, although there remains further scope for improvement.

Table 9.1 Comparison of model results from Figure 9.5

Data set	Model	Percentage with wrong sign	Percentage with error less than 50%
Jenkins & Murry	Jenkins & Murry	18	36
	Computational	9	47
Kent	Jenkins & Murry	28	39
	Computational	17	61

9.4 Concluding remarks

The long list of computational model parameters described in section 8.3 has been reduced to a more-manageable list of seven parameters that have a substantial effect on Murry's feed speed ratio. The parameters are:

- two geometry parameters, W_u/W_p and W_p/D_{pb},
- two speed parameters, S_{pb} and S_u/S_{pb},
- one material parameter, k_1,
- two initial conditions, f and γ_{do}.

This list contains one parameter that is generally unknown: the permeability parameter, k_1. A calibration procedure was developed to determine k_1 for a milling train. Use of that parameter value for each mill in a milling train provides a reasonable match between predicted effectiveness and measured effectiveness.

The computational feeding model has been compared against the Jenkins and Murry (1981) empirical feeding model in matching the measured effectiveness of the Jenkins

and Murry (1981) and 1997 factory feeding survey results and found to provide better predictions.

9.5 Concluding remarks

The computational feeding model for the six-roll mill has been explored through the conduct of a sensitivity analysis across the range of parameter values expected to be of use in factory mills. Seven parameters with a substantial effect on Murry's feed speed ratio were identified:

- two geometry parameters, W_u/ W_p and W_p/D_{pb},
- two speed parameters, S_{pb} and S_u/S_{pb},
- one material parameter, k_1,
- two initial conditions, f and γ_{do}.

Another parameter, the coefficient of friction between bagasse and the underfeed roll, was also identified as having a significant effect but has not been used in subsequent work because its value is not well defined.

Using only the seven parameters and setting all other model parameters to fixed values, the computational feeding model was used to predict mill effectiveness for each case presented in the factory feeding measurement surveys of Jenkins and Murry (1981) and the 1997 survey. A calibration procedure was used to change the permeability parameter, k_1, to match the #1 mill results for each milling train. For the remaining results for each milling train, the effectiveness predictions from the computational feeding model were better than those from the Jenkins and Murry feeding model that the computational model was designed to replace.

10 Avenues for increasing the capacity of Australian raw sugar factory milling units

10.1 Introductory remarks

In chapter 8 and chapter 9, the computational feeding model for the Australian six-roll milling unit was shown to adequately reproduce the results of mill feeding experiments and to provide a better estimate of pressure feeder speed than the Jenkins and Murry (1981) model that it was benchmarked against. With the confidence that it adequately matches factory performance measurements and the knowledge that its amount of empiricism is minimal, the computational feeding model is considered a satisfactory tool to explore avenues for increasing the capacity of Australian raw sugar factory milling units.

While the computational feeding model is considered a satisfactory tool to explore avenues for capacity increases, solution times are long and searches for maximum capacity values using the model would be time consuming. To simplify this process, an alternative approach was adopted. Rather than using the computational model directly, the computational model was used to create a data set with which to develop a new empirical feeding model. While the data set itself consisted of discrete points only, the empirical model filled in the gaps with a smooth function, allowing the entire data space to be mapped. Conditions for maximum capacity were then determined by differentiating the equation for the empirical model.

In addition to its uses in determining maximum throughput, the new empirical feeding model is a suitable replacement for the Jenkins and Murry model for routine use by factory milling personnel.

10.2 An empirical feeding model

10.2.1 A data set for developing the new empirical feeding model

To provide a data set for developing the new empirical feeding model, a numerical experiment was conducted using the computational feeding model. The experiment was a second-order composite design with *cube*, *star* and *centre* components as described by Box and Draper (1987).

The parameters included in the empirical model development process were those identified in the sensitivity analysis in section 9.2 as having most influence on Murry's feed speed ratio. Using the argument presented in section 9.3, the coefficient of friction on the underfeed roll was not included. Of the parameters included, six were used in the data set without modification. It was found necessary however, to change the form of the underfeed nip work opening parameter in order to adequately match the range of parameters achieved in the factory data sets presented in section 3.3. Rather than use underfeed nip work opening as a ratio to the pressure feeder nip work opening (W_u/W_p), the parameter was used as a ratio to the pressure feeder roll diameter (W_u/D_{pb}).

The final list of parameters included in the data set were:

- two geometry parameters, W_u/ D_{pb} and W_p/D_{pb},
- two speed parameters, S_{pb} and S_u/S_{pb},
- one material parameter, k_1,
- two initial conditions, f and γ_{do}.

The computational model details and the resulting data set are presented in Appendix H.

10.2.2 The new empirical feeding model

A multiple linear regression analysis was conducted to develop a new empirical model based on the computational model results presented in Appendix H. The resulting model for Murry's feed speed ratio, r_M, was:

$$\begin{aligned} r_M = & -1.686 - 2.759\frac{W_u}{D_{pb}} + 12.92\frac{W_p}{D_{pb}} - 0.04663\ln k_1 + 0.2325 f \\ & - 0.005340\gamma_{do} - 0.0002900 S_{pb} + 2.313\frac{S_u}{S_{pb}} - 4.688\left(\frac{W_p}{D_{pb}}\right)^2 \\ & - 0.2925\left(\frac{S_u}{S_{pb}}\right)^2 - 3.000\frac{W_u}{D_{pb}}\frac{W_p}{D_{pb}} - 0.05944\frac{W_u}{D_{pb}}\ln k_1 \\ & - 0.7000\frac{W_u}{D_{pb}}\frac{S_u}{S_{pb}} + 0.1538\frac{W_p}{D_{pb}}\ln k_1 - 0.1258\frac{W_p}{D_{pb}} f \\ & + 2.213\frac{W_p}{D_{pb}}\frac{S_u}{S_{pb}} + 0.004717\ln k_1\ f + 0.03375\ln k_1\frac{S_u}{S_{pb}} \\ & - 0.004080\gamma_{do}\frac{S_u}{S_{pb}} \end{aligned} \qquad \textbf{(10.1)}$$

Figure 10.1 presents a comparison of the computational model results from Appendix H with predictions from equation **(10.1)**. The new empirical model provides a good fit to the computational model outputs with a residual standard error of 0.05 and a R^2 value of 0.98.

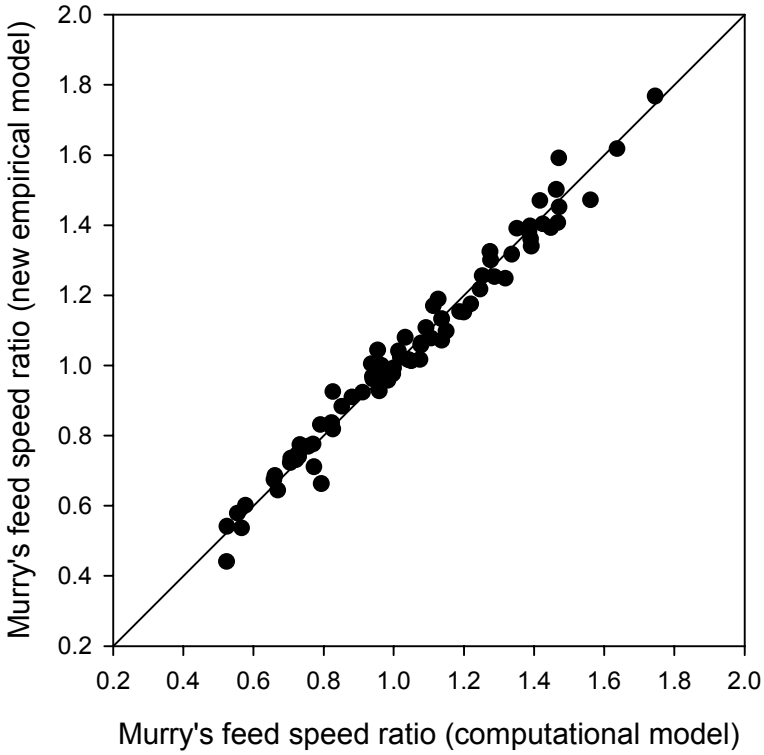

Figure 10.1 Comparison of new empirical model predictions with computational model values

10.2.3 Testing the new empirical feeding model

The new empirical model was tested by subjecting it to the same tests as the computational feeding model presented in section 9.3.

Figure 10.2 compares the new empirical model to the factory survey data sets of Jenkins and Murry (1981) and the 1997 measurements. Figure 10.2 is directly comparable with the predictions of the Jenkins and Murry empirical model and the computational feeding model in Figure 9.4. The predictions from the new empirical model are substantially better than the Jenkins and Murry empirical model predictions and comparable to the computational model predictions.

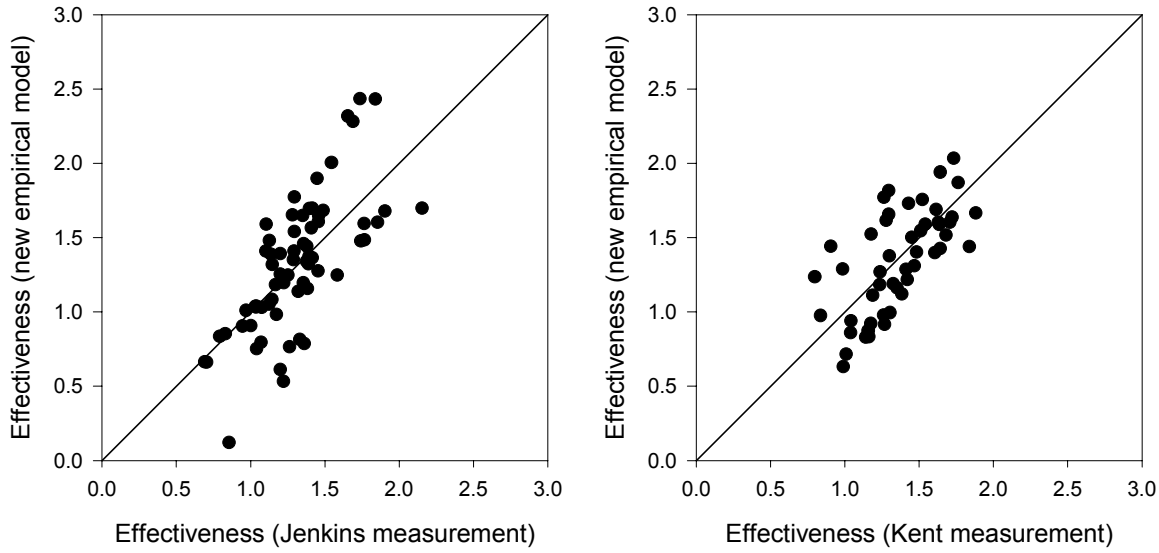

Figure 10.2 Comparison of new empirical model predictions against measurements of Jenkins and Murry (1981) and 1997 measurements

The tests of effectiveness differences within single milling trains presented in 9.3 were reproduced in Figure 10.3 and Table 10.1 for the new empirical model. Again, the new empirical model performed well in comparison to the Jenkins and Murry empirical model. The new empirical model also performed slightly better against the 1997 data set than the computational feeding model although the computational feeding model performed better against the Jenkins and Murry data set. It is unusual for the empirical model prediction to be better than the computational model used to generate it. This improvement is believed to result from the use of k_1, for calibration purposes. The ln k_1 term in the empirical model constrains the model more than the true non-linear relationship in the computational model.

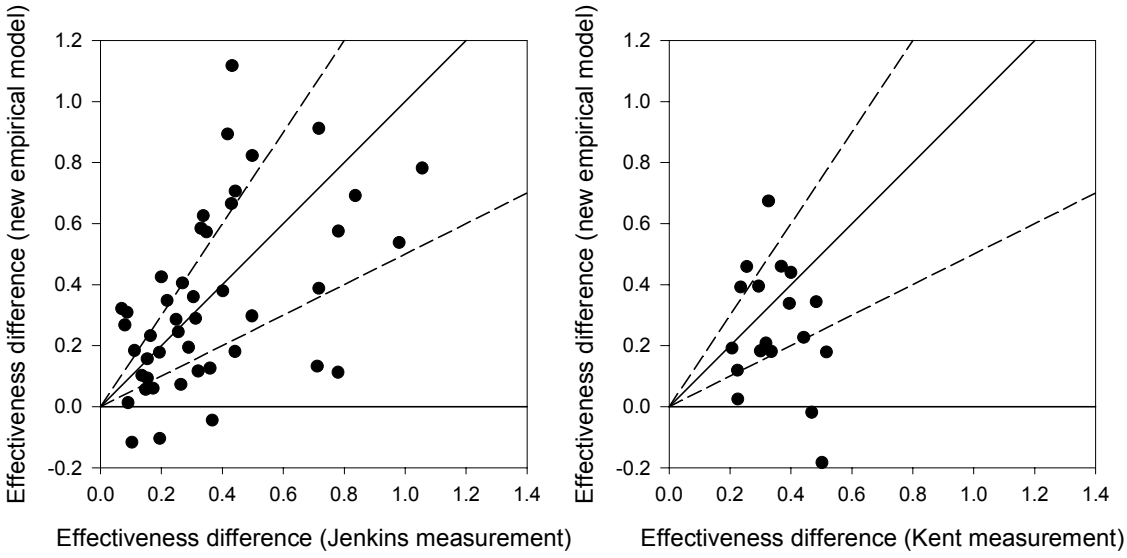

Figure 10.3 Comparison of effectiveness differences using new empirical model predictions against measured effectiveness differences of Jenkins and Murry (1981) and Kent (1998)

Table 10.1 Comparison of model results from Figure 10.3

Data set	Model	Percentage with wrong sign	Percentage with error less than 50%
Jenkins & Murry	New empirical	7	41
Kent	Jenkins & Murry	11	61

10.2.4 Concluding remarks

A new empirical feeding model has been developed for the purpose of identifying conditions for maximum capacity. Tests showed that the new model did achieve comparable performance to the computational feeding model indicating that it should be capable of identifying the conditions for maximum capacity.

The new empirical feeding model is also expected to have application as a replacement for the Jenkins and Murry model for routine use by milling personnel. More work, however, is required to simplify the use of the model through a user-friendly software package.

10.3 Conditions for maximum throughput

10.3.1 Introductory remarks

Generally the simplest means of increasing capacity is to increase the pressure feeder nip setting. While this approach is reliable, it is accompanied by a reduction in pressure feeder nip compaction that results in a reduction of juice expression at the pressure feeder, leading to a need for more juice expression in the feed nip. It is expected that presenting wetter bagasse to the feed nip will lead to poorer juice extraction performance across the milling unit, although there is no experimental evidence to confirm this statement. This section focuses on alternative means of maximising capacity that do not result in a decrease in pressure feeder nip compaction.

For a given pressure feeder nip setting, the throughput is maximised when the effectiveness is maximised (equation **(2.17)**). The empirical feeding model calculates Murry's feed speed ratio. Equation **(9.1)** converts Murry's feed speed ratio into effectiveness.

The sensitivity analysis in Figure 9.2 shows that Murry's feed speed ratio is essentially independent of the chute setting. Consequently, equation **(2.21)**, applied to the underfeed nip, gives the chute setting for minimum pressure feeder speed:

$$h_{do} = \frac{\frac{D_u}{2} + W_u + \frac{D_{pt}}{2}}{2} \qquad \textbf{(10.2)}$$

As discussed in section 10.2, the empirical feeding model contains a total of seven parameters. Of those seven parameters, four can immediately be eliminated from the list of parameters that can maximise capacity:

- pressure feeder nip setting since the aim is to find the maximum capacity at a given pressure feeder nip setting,

- pressure feeder speed since that the task is essentially to find the capacity at a given pressure feeder speed,
- permeability parameter, k_1, and the feed chute exit compaction since they are essentially properties of the bagasse.

The remaining parameters; underfeed nip setting, ratio of underfeed roll speed to pressure feeder speed and fibre content; can potentially be varied to minimise pressure feeder speed and are investigated in this section.

10.3.2 Effect of underfeed nip setting on effectiveness

The Jenkins and Murry (1981) empirical feeding model identified that the underfeed nip setting could be manipulated to maximise throughput (equation **(2.25)**).

The location of the optimum underfeed nip setting can be found by differentiating effectiveness with respect to underfeed nip setting. For the new empirical feeding model, the optimum underfeed nip setting for maximising throughput is:

$$\frac{W_u}{D_{pb}} = \frac{-(2c_1 + c_2)}{3c_2}$$

$$\begin{aligned} c_1 = {} & -1.686 + 12.92\frac{W_p}{D_{pb}} - 0.04663\ln k_1 + 0.2325 f - 0.005340\gamma_{do} \\ & - 0.0002900 S_{pb} + 2.313\frac{S_u}{S_{pb}} - 4.688\left(\frac{W_p}{D_{pb}}\right)^2 - 0.2925\left(\frac{S_u}{S_{pb}}\right)^2 \\ & + 0.1538\frac{W_p}{D_{pb}}\ln k_1 - 0.1258\frac{W_p}{D_{pb}} f + 2.213\frac{W_p}{D_{pb}}\frac{S_u}{S_{pb}} \\ & + 0.004717\ln k_1\, f + 0.03375\ln k_1\frac{S_u}{S_{pb}} - 0.004080\gamma_{do}\frac{S_u}{S_{pb}} \end{aligned} \qquad \textbf{(10.3)}$$

$$c_2 = -2.759 - 3.000\frac{W_p}{D_{pb}} - 0.05944\ln k_1 - 0.7000\frac{S_u}{S_{pb}}$$

According to equation **(10.3)**, the underfeed nip setting to maximise throughput is a function of the other six parameters. To gain an impression of the magnitude of the optimum underfeed nip setting, equation **(10.3)** was applied to the data set used to develop the empirical feeding model (Appendix H). Figure 10.4 summarises the results. The optimum underfeed nip setting was found to be typically 0.3 to 0.4 times the pressure feeder roll diameter. The parameter with the largest effect on the optimum underfeed nip setting was the feed chute exit compaction.

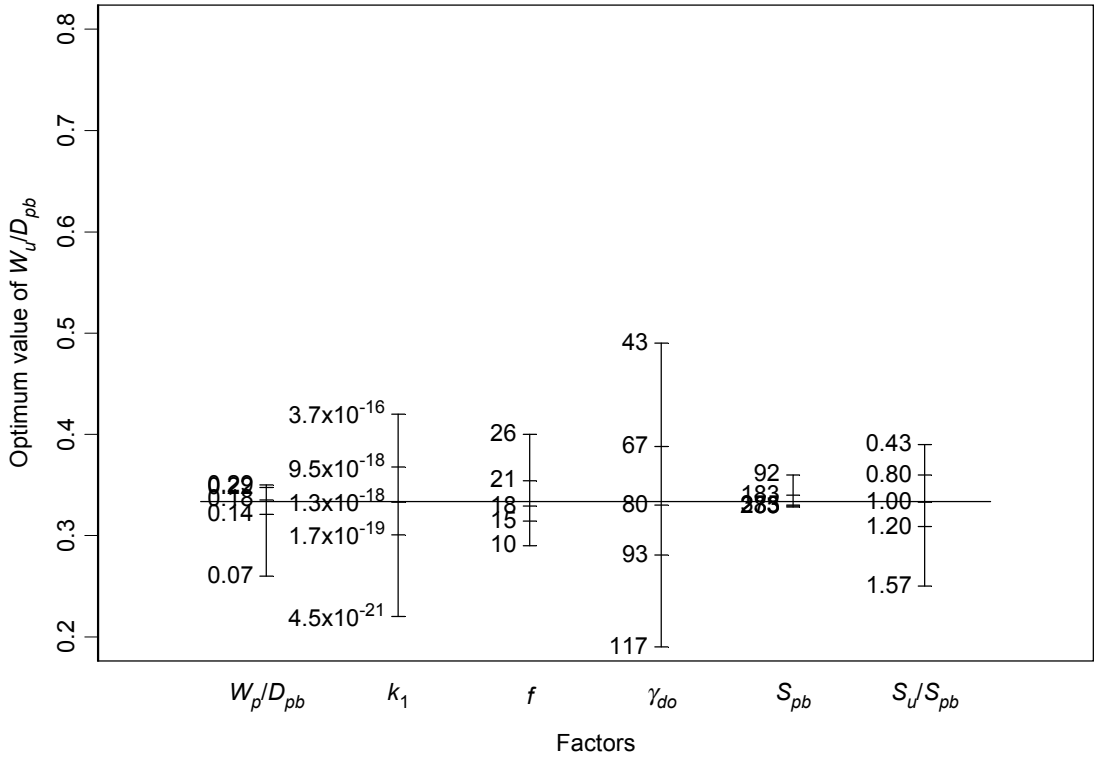

Figure 10.4 Effect of model parameters on the optimum underfeed nip setting (new empirical feeding model)

For comparison, the same approach was used with the Jenkins and Murry (1981) empirical model to determine the optimum underfeed nip setting. According to the Jenkins and Murry model, the only parameter affecting the optimum underfeed nip setting is the pressure feeder nip setting. The optimum underfeed nip setting using the

Jenkins and Murry model is presented in Figure 10.5. According to the Jenkins and Murry model, the optimum underfeed nip model is far more sensitive to the pressure feeder nip setting and is somewhat larger, being typically 0.4 to 0.6 times the pressure feeder roll diameter.

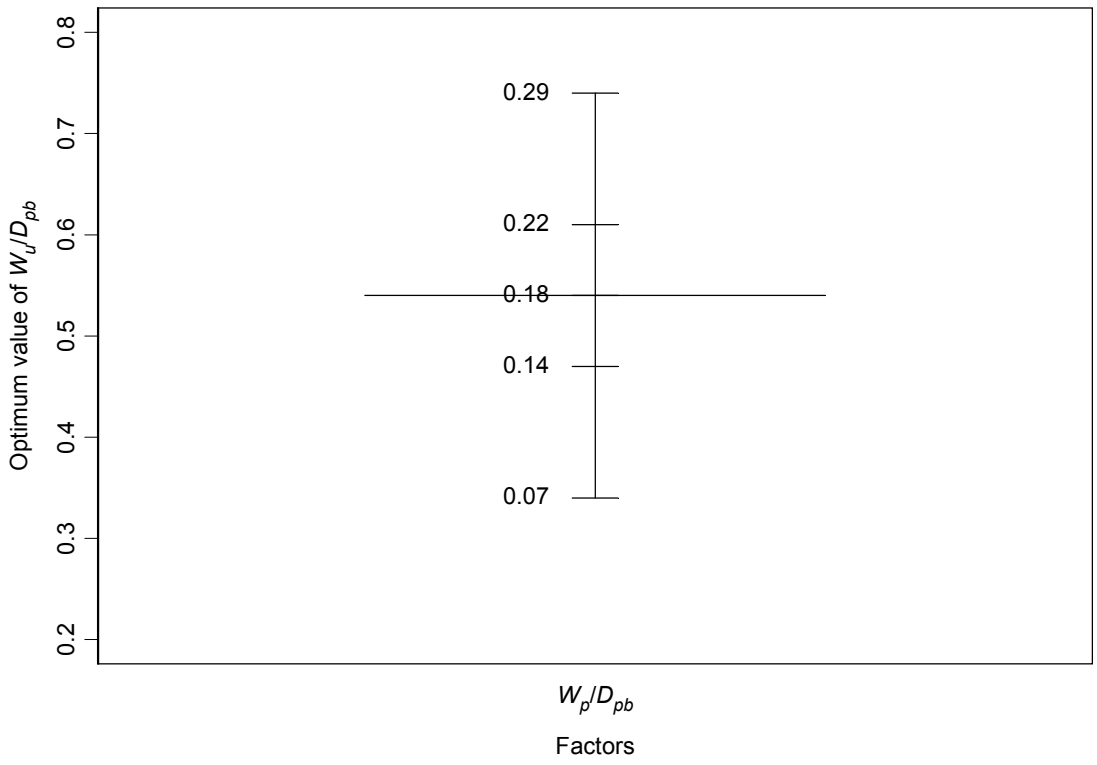

Figure 10.5 Effect of model parameters on the optimum underfeed nip setting (Jenkins and Murry model)

While no effort has been made during this study to test the optimum underfeed nip conditions, it was noted that higher effectiveness results were observed in the Mulgrave mill experiment (section 8.6.5) at underfeed nip settings somewhat less than the optimum underfeed nip setting identified by the Jenkins and Murry model. This result gives some confidence in the predictions of equation **(10.3)**.

10.3.3 Effect of underfeed roll speed on effectiveness

Although the Jenkins and Murry (1981) model was insensitive to the ratio of the underfeed roll speed to the pressure feeder roll speed, Jenkins and Murry (1981) did suggest best results when the underfeed roll surface speed was 1.0 to 1.1 times the pressure feeder roll surface speed.

In the new empirical feeding model, the ratio of the underfeed roll speed to the pressure feeder roll speed is a model parameter. By differentiating the effectiveness (or Murry's feed speed ratio) with respect to the speed ratio, conditions for maximum throughput can be determined. The conditions for maximum throughput are:

$$\frac{S_u}{S_{pb}} = 3.954 - 1.197\frac{W_p}{D_{pb}} + 3.783\frac{W_p}{D_{pb}} + 0.05769\ln k_1 - 0.006974\gamma_{do} \qquad \textbf{(10.4)}$$

Using the procedure adopted in section 10.3.2 to explore the optimum underfeed nip setting, the effect of the parameters on the optimum ratio of underfeed roll speed to pressure feeder roll speed is presented in Figure 10.6. The optimum ratio is typically 1.0 to 1.2, generally higher than the Jenkins and Murry recommendations. The value of the optimum ratio is most strongly affected by the pressure feeder nip setting.

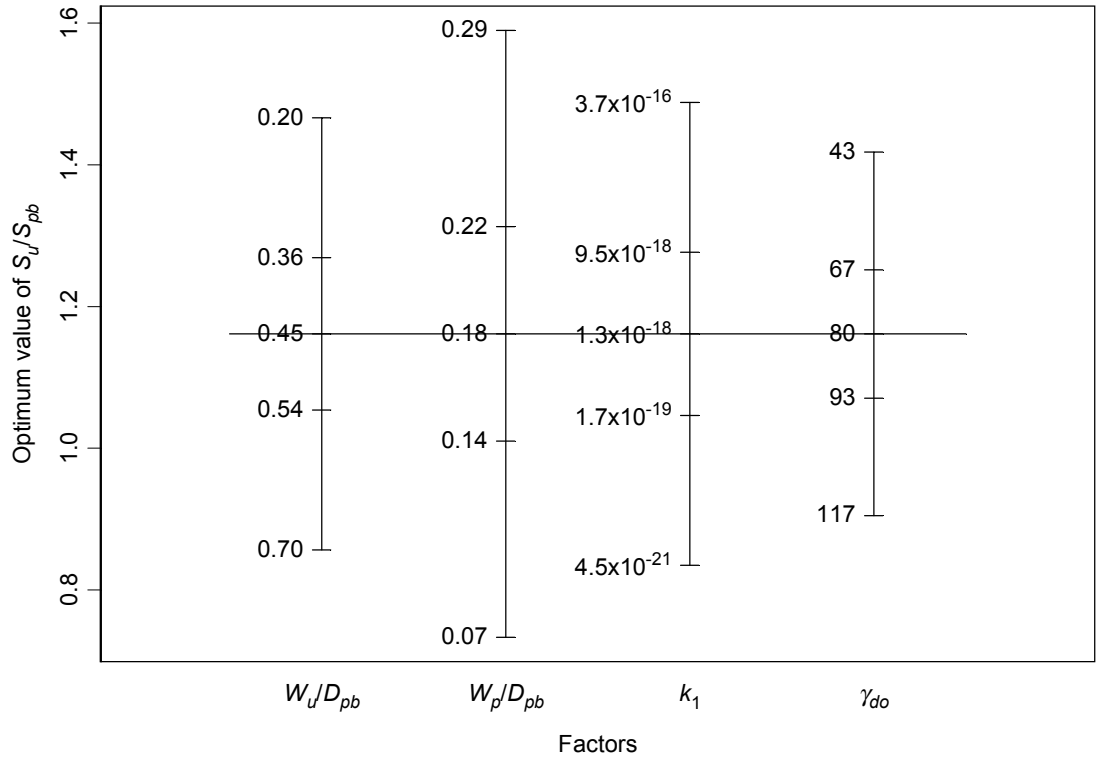

Figure 10.6 Effect of model parameters on the optimum ratio of underfeed roll speed to pressure feeder roll speed (new empirical model)

10.3.4 Effect of fibre content on effectiveness

Under extreme circumstances, there is limited scope to increase throughput by changing the fibre content of the feed bagasse. The fibre content can be increased through the application of less added water or by diverting a proportion of the imbibition stream away from a struggling mill. While these strategies will cause a reduction in extraction, they may cause less reduction in extraction than the alternative of allowing bagasse to bypass the mill because of an overflowing feed chute.

The new empirical feeding model does not predict an *optimum* fibre content and there is no reason to suspect one exists. To gain an impression of the magnitude of the effect of

fibre content on pressure feeder speed, Murry's feed speed ratio is plotted against fibre content in Figure 10.7 for average values of the remaining parameters from Appendix H.

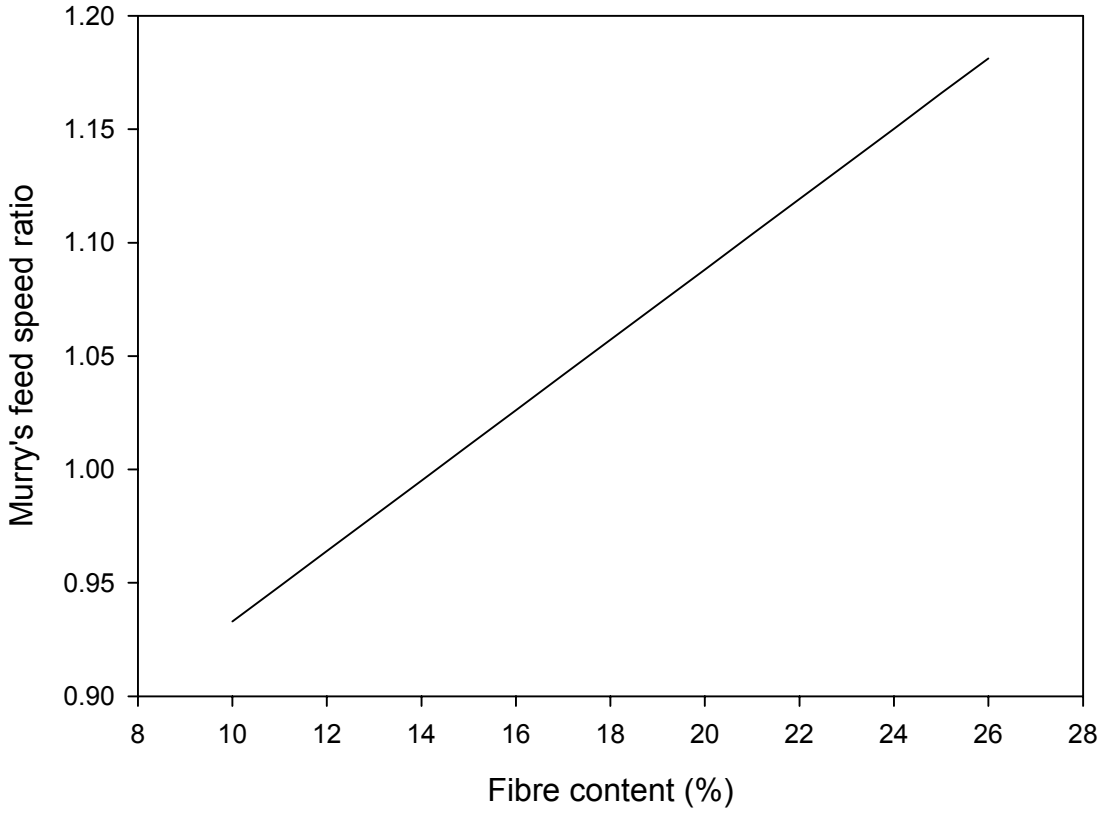

Figure 10.7 Typical effect of fibre content on Murry's feed speed ratio (new empirical model)

10.3.5 Concluding remarks

For a given pressure feeder nip setting, three avenues were identified for increasing capacity:

- adjusting the underfeed nip setting, generally to a lower value than recommended by Jenkins and Murry,

- adjusting the ratio of the underfeed roll speed to the pressure feeder roll speed, generally to a higher value than recommended by Jenkins and Murry,
- increasing the fibre content by diverting imbibition away from the mill (only as a last resort).

10.4 Understanding the conditions for maximum throughput

10.4.1 Introductory remarks

In section 10.3, the conditions for maximum capacity of the six-roll mill were identified. In this section, the reason for those results is discussed.

10.4.2 Comparing laboratory two-roll mill results to factory six-roll mill results

As discussed in section 6.3.6, Murry's feed speed ratio in the laboratory two-roll mill was found to increase with increasing contact angle, nip setting and feed pressure and with decreasing roll speed. These results were quite different to those presented in section 9.2 and section 10.3 for the factory six-roll mill.

Comparing the nip of the laboratory two-roll mill to the underfeed nip of the factory six-roll mill, the main difference between the two-roll mill and the six-roll mill is the presence of the pressure feeder nip following the underfeed nip in the six-roll mill. While the feed pressure is the main force acting on the bagasse mat in the feed direction in a two-roll mill, the pressure feeder nip provides resistance acting in the opposite direction to the feed pressure in the six-roll mill.

Figure 10.8 shows the stresses in the bagasse mat for a typical pressure feeder while Figure 10.9 shows the same stresses where the bottom pressure feeder roll was absent

(in the model, the bottom pressure feeder roll was still included but no contact between the bagasse and the bottom pressure feeder roll was defined). In both cases, the feed pressure was 3 kPa. In Figure 10.8, immediately below the underfeed nip, there remains a compressive stress acting on the mat ranging in size from about zero near the underfeed nip to about 10 kPa near the top pressure feeder roll. In Figure 10.9, immediately below the underfeed nip, the stress drops to zero as expected.

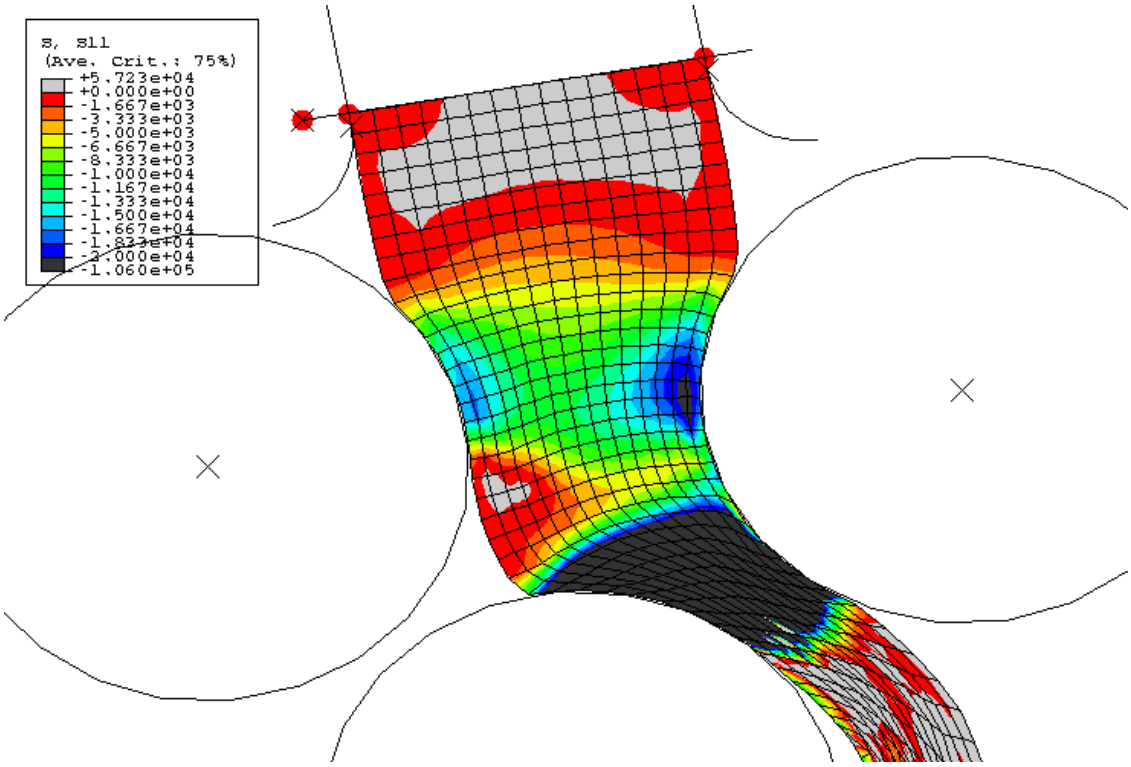

Figure 10.8 Stresses in the feed direction for a typical pressure feeder (in Pa)

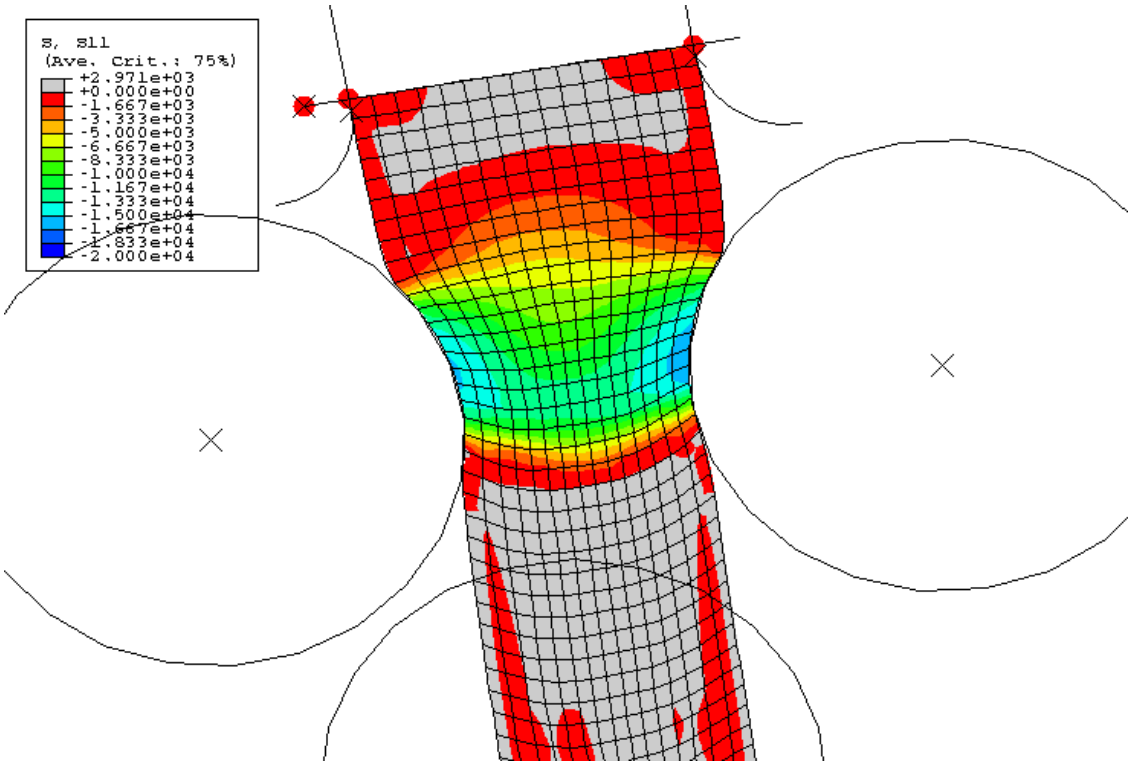

Figure 10.9 Stresses in the feed direction for a pressure feeder without a bottom pressure feeder roll (in Pa)

Since average stress caused by the resistance from the pressure feeder was larger than the feed pressure, the pressure feeder resistance is consequently expected to dominate the feeding behaviour. The mesh distortions in Figure 10.8 and Figure 10.9 support this argument. In Figure 10.9 where the feed pressure dominates, the bagasse mat distorts forwards, increasing the average feed speed. In Figure 10.8 where the pressure feeder resistance dominates, the bagasse mat distorts backwards, reducing the average speed.

While increasing the feed pressure increased Murry's feed speed ratio in the two-roll mill, increasing feed pressure in the six-roll mill had only a small effect (Figure 9.1). No substantial feed pressure result was found for the six-roll mill because the feed pressure effect was small compared to the effect of the resistance offered by the pressure feeder nip.

While increasing the nip setting increased Murry's feed speed ratio in the two-roll mill, decreasing the underfeed nip setting in the six-roll mill increased Murry's feed speed ratio. The pressure feeder nip resistance, again, can explain this effect. In the two-roll

mill, increasing the nip setting allowed the feed pressure to push the centre of the bagasse blanket further forward, increasing Murry's feed speed ratio. In the six-roll mill, reducing the nip setting prevented the pressure feeder resistance from pushing the centre of the bagasse blanket further backward.

Roll speed had a similar effect on Murry's feed speed ratio in both cases. The fluid flow resistance acted against the feed in both cases, causing Murry's feed speed ratio to be lower at higher roll speed. The permeability parameter, fibre content and void ratio effects in the six-roll mill model all affect the fluid flow resistance and so affect Murry's feed speed ratio in the same way as roll speed.

While contact angle had a significant effect on Murry's feed speed ratio in the two-roll mill, it had no substantial effect on the six-roll mill. This difference was not explored in detail since the contact angle effect was as expected for the six-roll mill and no explanation seemed necessary. Again, it seems likely that the pressure feeder nip resistance has prevented the blanket motion necessary for the larger values for Murry's feed speed ratio found at high contact angles in the two-roll mill.

10.4.3 The underfeed roll effect

As discussed in section 10.3.3, the empirical model found an optimum value for the ratio of the underfeed roll speed to the pressure feeder speed where throughput was maximised.

To investigate the effect of underfeed roll speed further, a series of computational models were solved where the ratio of the underfeed roll speed to the pressure feeder speed was varied from 0.6 to 2.0 for a coefficient of friction between the bagasse and the underfeed roll of 0.5. The resultant values for Murry's feed speed ratio are shown in Figure 10.10. For this particular case, there was a large increase in Murry's feed speed ratio between the 0.6 to 0.8 values for the ratio of the underfeed roll speed to the pressure feeder speed, rising to a maximum value at 1.0 and then gradually falling.

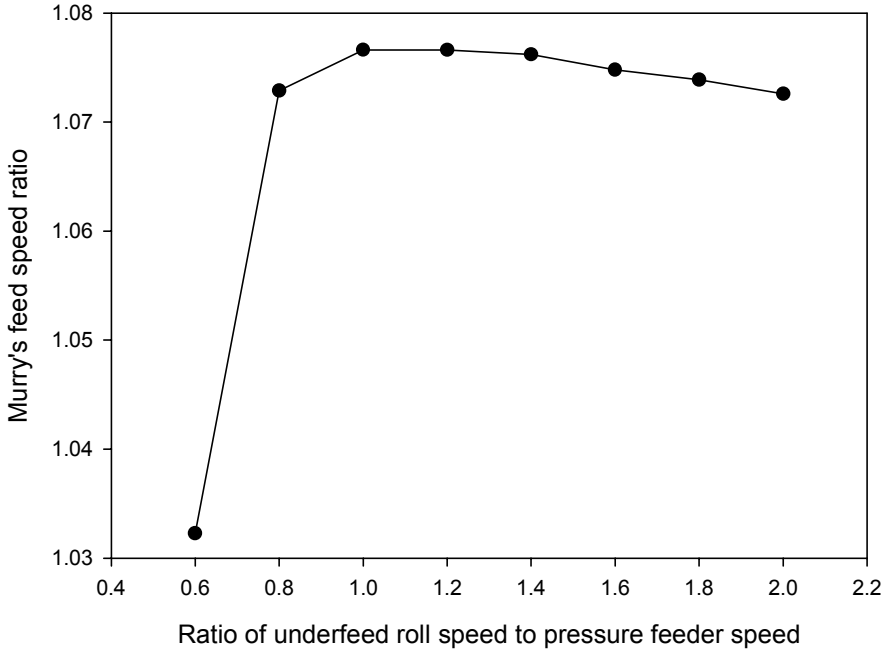

Figure 10.10 The effect of the ratio of the underfeed roll speed to the pressure feeder speed on Murry's feed speed ratio

The reason for the sharp rise and gradual decline in Murry's feed speed ratio shown in Figure 10.10 can be found in Figure 10.11 which shows the ratio of the tangential stress to the normal stress on the underfeed roll for ratios of underfeed roll speed to pressure feeder roll speed from 0.6 to 1.2. For a ratio of 0.6, the ratio of tangential to normal stress was positive for part of the time of contact between the underfeed roll and the bagasse, indicating that the underfeed roll was holding back the bagasse, resulting in a lower value for Murry's feed speed ratio. At an underfeed to pressure feeder speed ratio of 0.8 and 1.0, the ratio of tangential to normal stress was always negative, indicating that the roll was pushing the bagasse forward, resulting in higher values for Murry's feed speed ratio. At an underfeed to pressure feeder speed ratio of 1.2, however, the ratio of tangential to normal stress was at a constant value of 0.5, corresponding to the coefficient of friction and indicating that the underfeed roll slipped on the bagasse continuously. At higher ratios of underfeed roll speed to pressure feeder speed where the underfeed roll slipped on the bagasse continuously, Murry's feed speed ratio gradually declined. The best result occurred at the highest ratio of underfeed to pressure feeder speed for which the underfeed roll was able to provide some grip on the bagasse.

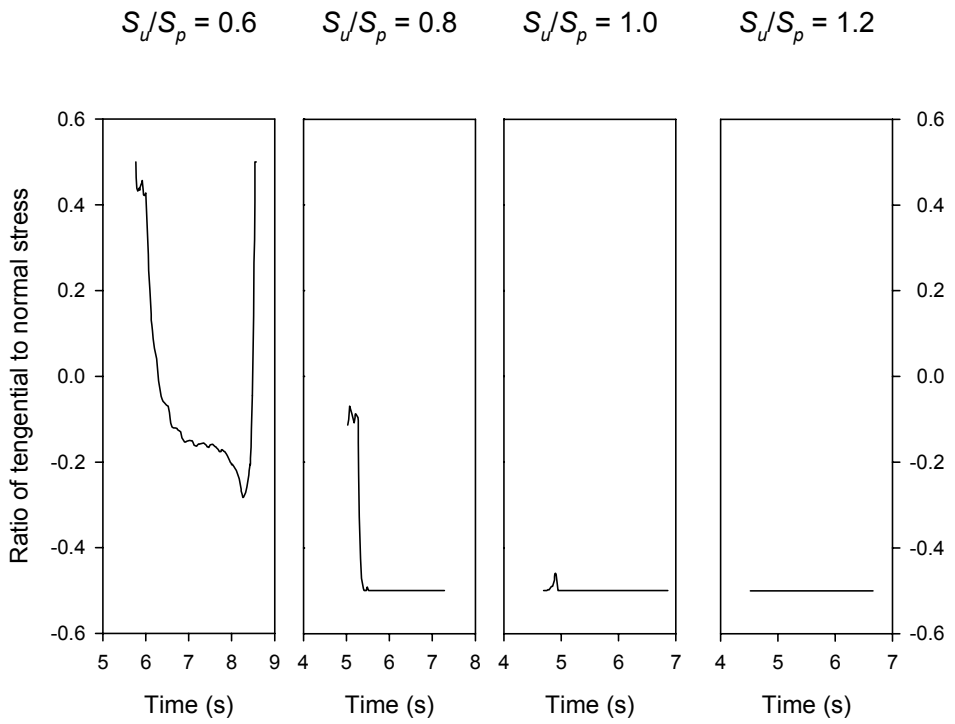

Figure 10.11 The ratio of the tangential pressure to the normal pressure on the underfeed roll for different ratios of the underfeed roll speed to the pressure feeder speed

10.4.4 Concluding remarks

The presence of the pressure feeder nip adds an additional component to the force system acting on the bagasse in the underfeed nip. This additional force component acts in the opposite direction to the feed pressure and is generally larger than the feed pressure.

In the three-roll pressure feeder case, changing feed pressure has minimal effect on Murry's feed speed ratio because it has a lesser effect on the force system in the presence of the pressure feeder resistance.

Because the pressure feeder resistance is greater than the feed pressure, increasing the nip setting allows the resistance to reduce Murry's feed speed ratio. This trend is opposite to the two-roll situation where the feed pressure acted to increase Murry's feed speed ratio.

As in the two-roll mill case, increasing roll speed increases fluid resistance in the three-roll pressure feeder.

No contact angle effect was found in the three-roll pressure feeder and it is hypothesised that this lack is due to the greater restraint on the bagasse blanket because of the pressure feeder nip.

Increasing the ratio of the underfeed roll speed to the pressure feeder roll speed has a beneficial effect on Murry's feed speed ratio, up to the point where the underfeed roll no longer provides any grip on the bagasse.

10.5 Concluding remarks

A new empirical feeding model was developed from a consistent data set produced by the computational feeding model. The empirical feeding model performs in a similar fashion to the computational feeding model and is much simpler and faster to use. The empirical model was used to identify conditions for maximum throughput and is expected to replace the Jenkins and Murry model for routine use by factory milling personnel.

Using the new empirical feeding model, underfeed nip settings and underfeed roll speeds were identified for maximum throughput. The effect of fibre content on throughput was also quantified as a last resort means of increasing throughput.

Comparing the factory model and experimental results to those from the two-roll mill study in chapters 6 and 7, explanations for the differences in behaviour were examined. The resistance offered by the pressure feeder nip is believed responsible for much of the difference. Whereas in the two-roll mill, the feed pressure has a large effect on Murry's feed speed ratio, in the factory mill, the pressure feeder resistance is more dominant and acts in the opposite direction. As a result, feed pressure has little effect on Murry's feed speed ratio and the effect of increasing underfeed nip setting reduces Murry's feed

speed ratio rather than increases it. The roll speed effect, however, is the same. No contact angle effect was found for the factory mill, presumably because of the more constrained nature of the force system on bagasse in the underfeed nip.

Increasing the ratio of the underfeed roll speed to the pressure feeder roll speed has a beneficial effect on Murry's feed speed ratio, up to the point where the underfeed roll no longer provides any grip on the bagasse.

11 General discussion and conclusions

11.1 Introductory remarks

This chapter summarises the research and highlights the main conclusions from the research. The significance of the research for the Australian raw sugar industry is described. Recommendations are made for further work based on the foundations of this research.

11.2 Aim of the research

This research aimed to identify methods to increase the capacity of the Australian raw sugar factory six-roll milling units. The approach taken was to construct a model capable of predicting mill throughput and then use that model to identify ways to increase mill throughput.

11.3 Summary and conclusions of the research

11.3.1 Previous throughput models

Roller mills such as the Australian raw sugar factory milling unit are used in a wide range of applications for processing materials such as steel, plastics, coal, oil shale,

powder, sorghum, wheat, corn, paper and textiles. These applications were reviewed in section 2.3 but few throughput models for these applications were found. The throughput models developed by Sander and Schönert (1999) for grinding quartz materials and by Katrus (1997) for pressing powders were the most advanced models found. Neither of these models had features more desirable than those already in the existing sugarcane roller mill throughput models.

The sugarcane roller mill throughput model of Jenkins and Murry (1981), described in section 2.2.5, was identified as the most advanced throughput model available. It was specifically developed for the Australian raw sugar factory six-roll milling unit. While being essentially a theoretical model, it has an empirical factor known as effectiveness that was designed to account for the performance of the underfeed roll and correct for errors in the model assumptions.

The ability of the Jenkins and Murry throughput model to predict mill throughput was evaluated in chapter 3. The evaluation involved comparing model predictions of effectiveness to measurements of effectiveness from factory milling units. The factory measurements came from a data set collected by Jenkins and Murry (1981) and a data set collected as part of this research. For both data sets, agreement between the model predictions and the factory measurements was poor. To eliminate cane supply differences from the comparison, statistical analyses of the effectiveness measurements within individual milling trains were conducted to identify milling unit pairs with statistically significant effectiveness differences. For each identified milling unit pair, the effectiveness difference was calculated and compared to the predicted effectiveness difference using the Jenkins and Murry theory. Over 60% of the Jenkins and Murry model effectiveness differences differed from the measured effectiveness differences by more than 50%. In summary, the empirical effectiveness factor did not match the measured behaviour well.

11.3.2 The new feeding model

The development and testing of a new (computational) feeding model was the primary focus of the research. The new feeding model was based on the computational model described by Adam and Loughran (1998). While the Jenkins and Murry (1981) feeding model had considerable empiricism in the effectiveness factor relating to the mill geometry, the empiricism in the computational model of Adam and Loughran is less restricting and limited to the material description of the bagasse. Consequently, the new feeding model applies to a wider range of parameter values than the Jenkins and Murry model.

In the Adam and Loughran model, bagasse is assumed to consist of a deformable solid structure containing voids. Both the solid particles making up the structure (the fibre) and the fluid filling the voids (juice and air) are assumed incompressible (for the range of pressures involved with the air component, the incompressible assumption was considered adequate). The model is based on the laws of force equilibrium and fluid continuity. The principle of effective stress is used to describe the relationship between stress on the solid structure and pressure on the fluid. The specific equations of the model are described in chapter 4.

The model uses the porous elasticity and Drucker-Prager cap plasticity models available in the ABAQUS finite element software (Hibbitt, Karlsson & Sorensen 2000) to describe the constitutive behaviour of the solid structure. The porous elasticity model was chosen instead of the linear elasticity model used by Adam and Loughran because its behaviour more closely reproduces the measured expansion behaviour of bagasse (Loughran & Adam 1998; Downing, Loughran & Domanti 1999). While Adam and Loughran used the Drucker-Prager cap plasticity model, this research has improved the definition of the hardening rule over the approach described by Downing, Loughran and Domanti (1999). A hardening parameter, λ_1, was used to describe the size of the yield and plastic potential surfaces (section 4.7.5). This hardening parameter was adopted from Butterfield (1979) who argued that it was appropriate for highly compressible soils. Unlike the regression constants used by Downing, Loughran and Domanti (1999),

λ_1, is a single material parameter that defines the hardening rule. The specific definition of the hardening rule was presented in equation **(4.46)**.

Adam and Loughran's definitions for the constitutive behaviour of the fluid phase were adopted. The constitutive behaviour is based on Darcy's law. A relationship between void ratio and permeability involving two constants, k_1 and k_2, was adopted from Adam and Loughran's model. Adam and Loughran's approach for handling the two fluids (juice and air) through changes in the void ratio and permeability relationship was also adopted (section 8.6.8). The approach assumed that air was expressed first and, when no air remained, juice was expressed. The transition was assumed to occur at a specific void ratio determined from the initial conditions. The permeability change was related to the absolute viscosity of the air and juice components.

As part of this research, improved methods for estimating the material parameters, λ_1, k_1 and k_2, were developed. A special uniaxial test cell was constructed and found to provide a suitable means of estimating all three parameters. The developed procedure involved three compression tests at different speeds and the continuous measurement of total pressure, pore pressure at the bottom of the cell and sample height. A one-dimensional version of the computational model was developed to simulate the compression tests more efficiently than the ABAQUS software. Parameter estimation software called PEST (Watermark Numerical Computing 2000) was used to estimate the material parameters based on matching the simulation results to the measured data. The procedure was described in detail in section 5.4.

Two other approaches were also used to estimate material parameters. Low speed and low pressure compression tests were carried out to measure the solid phase material parameters (section 5.2). While estimates were made for four of the material parameters, only λ_1 was particularly well defined. An alternative and more conventional steady-state approach was also used to measure the permeability parameters (section 5.3). While an experiment showed that the compression test approach and the steady-state approach both gave similar estimates for the permeability parameters (section 5.5), the compression test approach is preferred because of the simplicity of the physical testing.

Two specific versions of the computational model were developed. The first model was constructed to reproduce the observed behaviour of a throughput experiment carried out in a small-scale two-roll mill (section 6.5). The second model was constructed to reproduce the observed throughput behaviour of the six-roll milling unit (section 8.6.8). The only differences between these models were in the definition of geometry and boundary conditions.

11.3.3 Testing the new feeding model

A two-stage approach was used to test the new computational feeding model. Firstly, a two-roll model was constructed and tested against experimental results. Once sufficient confidence was obtained in the two-roll mill model, a more complex three-roll model was constructed to represent the feeding behaviour of a six-roll mill. The three-roll model was tested against both experimental results and factory measurements.

As part of this research, an experiment to explore low-pressure conditions similar to those in the first pair of rolls of a factory six-roll mill was conducted in a small-scale two-roll mill (section 6.3). The experiment explored the effect of nip setting, contact angle, roll speed, feed pressure, cane variety and cane preparation on feed speed using a dimensionless parameter called Murry's feed speed ratio. Good agreement was observed between the model and experimental results (section 6.5).

Since juice expression is known to occur in a factory milling unit, it was also desirable to explore two-roll mill behaviour at higher nip compactions involving juice expression. The experiments of Solomon (1967) were reviewed in detail in chapter 7. The observed trends were quite similar to those observed in the low-pressure experiment. Since the model used to handle the juice expression for this experiment was identical to the model used to handle the air expression in the low-pressure experiment apart from the viscosity change, no modelling of this experiment was undertaken.

The three-roll model of a factory milling unit was tested against the results of four experiments. Jenkins and Murry (1981) carried out three of the experiments. Two of

the experiments were conducted on a small-scale three-roll feeder (section 8.4). The other experiment was conducted on a factory milling unit (section 8.5). As part of this research a fourth experiment was conducted on a factory milling unit using a wider range of parameter values than explored previously (section 8.4). These experiments explored the effect of underfeed nip setting, feed chute exit setting, contact angle bias, chute angle, pressure feeder speed and ratio of the underfeed roll speed to the pressure feeder speed on Murry's feed speed ratio. To match the observed results, modification of two parameters was required. The permeability parameter, k_1, was modified to match the overall mean of Murry's feed speed ratio for the experiment. The coefficient of friction on the underfeed roll was modified to match the observed trends for the ratio of the underfeed roll speed to the pressure feeder speed. Satisfactory matches between the experimental and model results were obtained.

To determine whether the computational feeding model was better than the Jenkins and Murry (1981) empirical feeding model, the computational feeding model was tested against the data sets of factory measurements from Jenkins and Murry (1981) and from this research (section 9.3): the same tests used to evaluate the Jenkins and Murry model. To use the computational feeding model, a calibration step was required to determine the appropriate permeability parameter, k_1. For each #1 mill, the model effectiveness was matched to the measured effectiveness by adjusting k_1. The adjusted k_1 values were then used for the remainder of the milling train. The computational model results were shown to be better than the Jenkins and Murry model results for both data sets. While over 60% of the Jenkins and Murry model effectiveness differences differed from the measured effectiveness differences by more than 50%, approximately 50% of the computational model effectiveness differences differed by more than 50%.

11.3.4 Insights into the feeding process

Murry's feed speed ratio is a valuable parameter for assessing mill feeding performance because it accounts for two major factors affecting feed speed: roll speed and contact angle. A Murry's feed speed ratio of 1.0 implies that the simple theory of Murry (1960b) provides an adequate match to the measured behaviour and that the

assumptions in the theory (no slip on the roll surface and a constant velocity profile across the blanket) are satisfied.

For the simple two-roll mill studied in chapter 6, Murry's feed speed ratio was found to increase with increasing contact angle, nip setting and feed pressure and with decreasing roll speed. Deformation occurring at the point of contact between the prepared cane mat and the roll surface causes the top of the mat to accelerate prior to contact with the roll surface. This effect is greater as contact angle increases, resulting in higher values for Murry's feed speed ratio at greater contact angles. Under larger nip setting, larger feed pressure and lower roll speed conditions, the forces acting on the bagasse cause the centre of the bagasse mat to deform in the direction of the feed, causing the speed of the centre of the mat to increase. In all cases, it is the constant velocity profile assumption that is invalid. While some slip on the roll surface was observed in the models, the slip generally had no influence on Murry's feed speed ratio (forward slip was observed in several tests in relatively unrealistic conditions where the nip setting was only slightly less than the chute setting and insufficient frictional force was generated to counteract the feed pressure).

From the exploration of the three-roll factory model described in chapter 9 and chapter 10, the factors affecting Murry's feed speed ratio in the factory milling unit were found to be somewhat different to those affecting Murry's feed speed ratio in the two-roll mill. The difference in behaviour is caused by the resistance to flow caused by the pressure feeder nip in the three-roll pressure feeder.

Unlike the two-roll mill case, contact angle and feed pressure had only minimal effect on Murry's feed speed ratio for the factory mill case.

While the two-roll mill case found that increasing work opening increased Murry's feed speed ratio, the factory mill case found that decreasing work opening increased Murry's feed speed ratio. In the two-roll mill case, the feed pressure was the main force acting on the bagasse in the feed direction and increasing the work opening enabled the feed pressure to push the bagasse in the centre of the blanket further forward, increasing Murry's feed speed ratio. In the factory mill case, the resistance offered by the pressure

feeder nip is more substantial than the feed pressure and acts in the opposite direction. Closing the underfeed nip work opening reduces the effect of the resistance on the centre of the bagasse blanket, preventing it from being pushed back as far.

The effect of speed and permeability on both the two-roll mill and the factory mill was the same with lower speed and higher permeability resulting in higher values for Murry's feed speed ratio. These effects are both caused by the resistance to flow offered by the juice and air in the bagasse blanket.

The more complex geometry of the factory mill also provided further avenues for increasing Murry's feed speed ratio. The speed of the underfeed roll and the coefficient of friction between the underfeed roll and the bagasse also affect Murry's feed speed ratio. The effect of underfeed roll speed is greater when the coefficient of friction is higher. There is a maximum speed beyond which the bagasse slips on the roll surface and increasing the speed further has no benefit.

11.3.5 Increasing milling unit capacity

While the modelling work focussed on predicting Murry's feed speed ratio, milling unit throughput is a function of more than just Murry's feed speed ratio. It is also a function of feed chute exit compaction, chute setting, roll speed and contact angle.

The conditions for maximum throughput were determined in section 10.3 based on an empirical feeding model developed from the computational feeding model (section 10.2). These conditions were determined assuming a constant pressure feeder nip setting. While increasing pressure feeder nip setting increases capacity, it also reduces the pressure feeder nip compaction and consequently the amount of juice expression in the pressure feeder nip that is expected to lead to lower juice extraction in the mill, an undesirable result.

There is an optimum underfeed nip setting that maximises capacity. While decreasing underfeed nip setting increases Murry's feed speed ratio, it also results in a decrease in

the cosine of the contact angle that decreases throughput. There is also an optimum underfeed roll speed as discussed in section 11.3.4. While not a preferred option, reducing the amount of imbibition to increase the fibre content of bagasse can also increase capacity.

11.4 Significance of the research

11.4.1 Introductory remarks

The benefits to be gained from the application of the mill feeding models developed in this project come from being able to be predict pressure feeder speed more accurately and from being able to predict the feed chute and pressure feeder settings and the ratio of the underfeed roll speed to pressure feeder speed that will minimise the pressure feeder speed by maximising throughput. These benefits will be realised through increased extraction of sugar from cane and through the deferral of capital expenditure.

11.4.2 Extraction benefits

Being able to predict pressure feeder speed more accurately allows the pressure feeder speed range to be chosen to reduce the likelihood of the feed chute overflowing or emptying. It also allows the mill settings to be chosen to reduce the likelihood of the load control system exceeding its control range. The avoidance of all of these conditions has benefits in terms of increased extraction and reduced bagasse moisture content.

The use of settings and speeds to minimise pressure feeder speed allows the throughput of a milling unit to be maximised with minimal decrease in pressure feeder nip compaction. As pressure feeder nip compaction decreases, less juice expression occurs in the pressure feeder and more juice expression is required in the mill. While there is

no conclusive evidence, it is believed likely that lower pressure feeder nip compactions result in lower extraction and higher bagasse moisture content.

It is difficult to predict the benefits in extraction to be gained. If a factory producing 150 000 t of sugar achieved a 0.1 unit increase in extraction (a conservative estimate) through improvements in rate and load control or through a higher pressure feeder nip compaction, and half of that extraction improvement resulted in extra sugar production (again, a conservative estimate), an extra 75 t of sugar would be produced. At $300 a tonne, a gain of $22 500 would be made.

11.4.3 Deferral of capital expenditure

If a significant increase in throughput is required beyond the calculated capacity of a milling unit, it is possible that the milling unit will be replaced. By allowing lower pressure feeder speeds to be used by maximising mill feeding performance, the replacement of a milling unit may be deferred, resulting in significant savings.

Assuming a new milling unit to cost $4 million and money can be invested at 10%, if a milling unit purchase can be deferred by one year, a saving of $400 000 would be made. This saving may be offset by a loss in extraction costing $22 500 for each 0.1 unit of extraction as discussed in section 11.4.2.

11.5 Recommendations for future research

While the research described in this thesis is considered comprehensive, there remain several tasks required to complete the work.

While both the computational feeding model and the new empirical feeding model were both adequately tested against factory measurements to validate their ability to predict pressure feeder speed, no such validation has been undertaken to test their ability to predict the conditions for maximum throughput. There remains a need to make use of

the empirical feeding model for specific factory milling units and confirm that the predicted conditions for maximum throughput (or minimum speed) match the results from factory performance.

The new model makes use of the permeability parameter, k_1, to calibrate the model to match factory throughput. There is a need to determine how permeability changes throughout a milling train (the validation carried out in chapter 9 assumed that k_1 remained constant throughout the milling train). Permeability measurements should be made throughout several milling trains to quantify the change in permeability for use in milling train throughput predictions.

While the three-roll computational model has been shown to reproduce feed speed well, it was found to perform poorly at reproducing roll torques, a subject not discussed in this thesis but was the subject of Plaza (2003). Roll torque predictions remain a problem for all mill situations (Kannapiran 2002). Further model development work is required to address this issue.

11.6 Concluding remarks

In conclusion, this study has contributed to knowledge through the following discoveries:

- The introduction of a new hardening parameter, λ_1, to define the size of the yield and plastic potential surfaces for bagasse in the computational feeding model,
- The development of improved methods for measuring λ_1 and the two permeability parameters, k_1 and k_2,
- Showing that both steady state and transient permeability measurement techniques can be used to derive the same permeability parameter values,
- Showing that permeability is essentially not dependent on fluid velocity and that Darcy's law is applicable across a wide range of fluid velocities,

- Measurements of the effect of various parameters on Murry's feed speed ratio in a laboratory two-roll mill and a factory milling unit,
- Development of computational feeding models for the laboratory two-roll mill and a factory milling unit,
- Identifying the causes of the effects of the various parameters on Murry's feed speed ratio in both the laboratory two-roll mill and a factory milling unit,
- Development of a new empirical feeding model for a factory milling unit,
- Determining the conditions for maximum throughput in the factory milling unit.

References

Adam, C.J. 1997, Application of computational porous media mechanics to the rolling of prepared sugar cane, PhD thesis, James Cook University of North Queensland.

Adam, C.J. & Loughran, J.G. 1998, 'Application of computational mechanics to rolling of a saturated porous media', in *Simulation of Material Processing: Theory, Methods and Applications*, Huétink & Baaijens (eds), Balkema, Rotterdam, pp. 503-8.

Adamski, T. 1964, 'New two-roll grinding mill', *Chemical and Process Engineering*, July, pp. 343-7.

Alexander, A.G. 1973, *Sugarcane physiology*, Elsevier Scientific Publishing Company, Amsterdam, The Netherlands.

Alonso, S.P. 1949, 'Grinding capacity of sugar mills. A rational formula', *Proceedings of the XXIII annual meeting*, Asociacion de Tecnicos Azucareros de Cuba, pp. 273-80.

Australian sugar year book 2002 c. 2002, Rural Press Limited, Brisbane, Australia.

Banks, P.J. 1984, 'Theory of constant-rate expression and subsequent relaxation', *Proceedings Fourth International Drying Symposium*, Vol. 1, pp. 112-8.

Bernhardt, H.W. 1996, A study of the phenomenon of bridging of sugarcane bagasse, PhD thesis, University of Natal.

Box, G.E.P. & Draper, N.R. 1987, *Empirical model-building and response surfaces*, John Wiley & Sons, New York.

Bryan, W.L., Monroe, G.E. & Gascho, G.J. 1985, 'Juice expression from sweet sorghum cultivars of different fiber content', *Transactions of the ASAE*, vol. 28, no. 3, pp. 980-5.

Bullock, K.J. 1955, 'The effect of speed, preparation and compression ratio on the performance of the experimental sugar mill in the University of Queensland',

Proceedings of the Queensland Society of Sugar Cane Technologists, 22nd Conference, pp. 201-18.

Bullock, K.J. 1957, An investigation into the crushing and physical properties of sugar cane and bagasse, PhD thesis, University of Queensland.

Bullock, K.J. 1958, 'The capacity of sugar cane mills. Part III: Theoretical analysis of mill feeding', *Sugar Journal*, vol. 21, no. 7, pp. 13-20.

Bullock, K.J. & Murry, C.R. 1957, 'Coefficient of friction of bagasse on iron surfaces', *Proceedings of the Queensland Society of Sugar Cane Technologists*, 24th conference, pp. 81-8.

Bureau of Sugar Experiment Stations 1984, *The standard laboratory manual for Australian sugar mills: volume 1: principles and practices*, Brisbane, Australia.

Bureau of Sugar Experiment Stations 2001, *The standard laboratory manual for Australian sugar mills: volume 2: analytical methods and tables*, Brisbane, Australia.

Bureau of Sugar Experiment Stations 2003, *Approved variety list*, viewed 20 May 2003, http://www.bses.org.au/Information/pdf/ApprovedVarList2003.pdf.

Butterfield, R. 1979, 'A natural compression law for soils (an advance on *e*-log *p′*), *Géotechnique*, Vol. 29, No. 4, pp. 469-80.

Chauhan, M.K. 1988, 'Some theoretical aspects of mill capacity – a new look', *Proceedings of the 51st Annual Convention of The Sugar Technologists' Association of India*, pp. E1-9.

Crawford, W.R. 1955, 'Mill feeding – the basic factor in efficient cane milling', *Proceedings of the Queensland Society of Sugar Cane Technologists*, 22nd Conference, pp. 167-79.

Cullen, R.N. 1965, An investigation of the shear strength of bagasse, MEngSc thesis, University of Queensland.

de Boer, A.T. 1972, 'Two-roller cane mills. A reappraisal in the light of value engineering of milling. Part II', *International Sugar Journal*, vol. 74, no. 881, pp. 136-40.

Donnelly, H.D. 1958, 'Milling and mill feeding', *Proceedings of the Queensland Society of Sugar Cane Technologists*, 25th conference, pp. 83-91.

Downing, C.M. 1999a, 'Rate dependence of permeability in clean and soil contaminated prepared cane', *Proceedings of the Australian Society of Sugar Cane Technologists*, 21st Conference, pp. 313-9.

Downing, C.M. 1999b, Investigation of the effects of soil contamination on the crushing of comminuted sugar cane, PhD thesis, James Cook University.

Downing, C.M., Loughran, J.G. & Domanti, S.A. 1999, 'Parameter estimation for highly deformable porous media', in *Computational mechanics for the next millennium. Volume 2. Geomechanics, models and techniques*, eds C.M. Wang, K.H. Lee & K.K. Ang, Elsevier, Amsterdam.

Farmer, N.C. 1977, 'The toothed roller continuous pressure feeder', *Proceedings of the International Society of Sugar Cane Technologists*, 16th congress, pp. 2241-9.

Fry, J. 1997, 'A global perspective of the sugar industry', in *Intensive sugarcane production: meeting the challenges beyond 2000*, eds B.A. Keating & J.R. Wilson, CAB International, Wallingford, United Kingdom, pp. 1-16.

Hibbitt, Karlsson & Sorensen 1998, *ABAQUS theory manual*, Pawtucket, U.S.A.

Hibbitt, Karlsson & Sorensen 2000, *ABAQUS/Standard user's manual*, Pawtucket, U.S.A.

Hildebrand, C. 2002, *Independent assessment of the sugar industry*, viewed 20 May 2003, http://www.affa.gov.au/content/output.cfm?ObjectID=CE264379-360F-47F2-9120DDA17BC39936

Hicks, C.R. 1964, *Fundamental concepts in the design of experiments*, Holt, Rinehart and Winston, New York.

Holt, J.E. 1960, 'Permeability of prepared cane', *Proceedings of the Queensland Society of Sugar Cane Technologists*, 27th conference, pp. 249-57.

Holt, J.E. 1961, 'The effect of fineness on the permeability of prepared cane', *Proceedings of the Queensland Society of Sugar Cane Technologists*, 28th conference, pp. 147-9.

Hugot, E. 1986, *Handbook of cane sugar engineering*, 3rd edn, trans. G.H. Jenkins, Elsevier, Amsterdam.

Jenkins, D.M. & Murry, C.R. 1981, *Investigations of mill feeding*, Technical Report No. 159, Sugar Research Institute.

Jenkins, G.H. 1953, 'Some factors involved in the feeding of cane mills', *Proceedings of the Queensland Society of Sugar Cane Technologists*, 20th Conference, pp. 169-74.

Julien, M.H.R., Irvine, J.E. & Benda, G.T.A. 1989, 'Sugarcane anatomy, morphology and physiology', in *Diseases of sugarcane: major diseases*, eds C. Ricaud, B.T. Egan, A.G. Gillaspie, Jr & C.G. Hughes, Elsevier Science Publishers, Amsterdam, The Netherlands, pp. 1-17.

Júnior, M.S. & Delfini, P. de T. 1988, 'Regulagem de moendas e máxima alimentação', *Boletim Tecnico Copersucar*, no. 40, pp. 48-51.

Kannapiran, A. 2002, Computational and experimental modelling of the crushing of prepared sugar cane, PhD thesis, James Cook University (submitted).

Katrus, O.A. 1997, 'Production of semifinished items with set sizes and density on rolling powders', *Powder Metallurgy and Metal Ceramics*, vol. 36, nos 3-4, pp. 164-9.

Kent, G.A. 1998, *Factory mill feeding performance*, Syndicated Project Report 10/98, Sugar Research Institute.

Kent, G.A. 2001, 'Estimating material parameters for a critical state model from a uniaxial compression test', in *Computational mechanics: New frontiers for the new millennium*, eds S. Valliappan & N. Khalili, Elsevier Science Ltd, Oxford, United Kingdom, vol. 2, pp. 1141-6.

Kent, G.A. 2003, 'A better material parameter for describing the strain hardening behaviour of bagasse', *Proc. Aust. Soc. Sugar Cane Technol.*, vol. 25.

Kent, G.A. & McKenzie, N.J. 2000, *A laboratory investigation into feeding a pair of rolls*, Syndicated Project Report 1/00, Sugar Research Institute.

Kent, G.A., McKenzie, N.J. & Downing, C.M. 2000, *Predicting milling train extraction performance*, Technical Report 4/00, Sugar Research Institute.

Leitch, C.J. 1996, An experimental investigation into the constitutive behaviour of prepared sugar cane, MEngSc thesis, James Cook University of North Queensland.

Loughran, J.G. & Adam, C.J. 1998, 'Properties of prepared cane for computational crushing models', *Proceedings of the Australian Society of Sugar Cane Technologists*, 20th Conference, pp. 307-12.

Loughran, J.G. & Kannapiran, A. 2002, 'Finite element modelling of the crushing of prepared cane and bagasse', *Proceedings of the Australian Society of Sugar Cane Technologists*, 21st conference, pp. 329-33.

Loughran, J.G. & Kauppila, D. 1999, 'Development of an advanced experimental crushing facility', *Proceedings of the Australian Society of Sugar Cane Technologists*, 24th conference, pp. 339-46.

Loughran, J.G. & Murry, C.R. 1984, *The varietal effects on predicted no. 1 mill performance – an interim report*, Technical Report No. 181, Sugar Research Institute.

Mackay Institute of Milling Engineers 1937, 'Mill settings and feed hoppers', *Proceedings of the Queensland Society of Sugar Cane Technologists*, Eighth Conference, pp. 17-28.

Mathsoft, 1999, *S-Plus 2000. Guide to statistics, volume I*, Seattle, Washington.

McMaster, I. 2003, 'High performance industry strategies', *Proc. Aust. Soc. Sugar Cane Technol.*, Vol. 25.

Mittal, B.L. 1969, 'Critical survey of formulae for assessing cane milling capacity and cane milling efficiency', *International Sugar Journal*, vol. 71, no. 841, pp. 9-15.

Muir Wood, D. 1990, *Soil behaviour and critical state soil mechanics*, Cambridge University Press.

Murry, C.R. 1960a, A theoretical and experimental investigation into the mechanics of crushing prepared sugar cane, PhD thesis, University of Queenland.

Murry, C.R. 1960b, 'The pressure required to feed cane mills. Part I – theoretical considerations', *International Sugar Journal*, vol. 62, no. 744, pp. 346-9.

Murry, C.R. 1998, 'Low pressure compression characteristics of prepared cane: a review', *Proceedings of the Australian Society of Sugar Cane Technologists*, 20th Conference, pp. 413-20.

Murry, C.R. & Hutchinson, R. 1958, 'Movement of bagasse in long chutes', *Proceedings of the Queensland Society of Sugar Cane Technologists*, 25th Conference, pp. 75-81.

Murry, C.R. & Russell, G.E. 1969, *Prediction of the extraction performance of crushing trains*, Technical Report No. 104, Sugar Research Institute.

Murry, C.R. & Shann, D.S. 1969, 'Crushing mill feeding: a review of Queensland practice', *Sugar Technology Reviews*, vol. 1, pp. 43-60.

Neill, S.W., McKinnon, S.A. & Garson, C.A. 1996, *A library of cane transport and sugar factory images*, Internal Report 1/96, Sugar Research Institute, Mackay, Australia.

Owen, D.R.J., de Souza Neto, E.A., Zhao, S.Y., Perić, D. & Loughran, J.G. 'Finite element simulation of the rolling and extrusion of multi-phase materials', *Comput. Methods Appl. Mech. Engrg.*, Vol. 151, pp. 479-95.

Owen, D.R.J., Zhao, S.Y. & Loughran, J.G. 1995, 'Application of porous media mechanics to the numerical simulation of the rolling of sugar cane', *Engineering Computations*, vol. 12, pp. 281-302.

Paddock, D.R. & Farrell, R.M. 1987, 'Control of a fixed mill top roll load using a load cell and variable speed pressure feed roller drives', *Proceedings of the Australian Society of Sugar Cane Technologists*, 9th conference, pp. 129-36.

Payne, J.H. 1968, 'Cane diffusion – the displacement process in principle and practice', *Proceedings of the International Society of Sugar Cane Technologists*, 13th congress, pp. 103-21.

Perk, C.G.M. 1957, 'Capacity ratings of milling trains', *Quarterly Bulletin*, no. 4, Sugar Milling Research Institute, pp. 35-8.

Pidduck, J. 1955, 'Physical properties of bagasse', *Proceedings of the Queensland Society of Sugar Cane Technologists*, 22nd conference, pp. 147-55.

Plaza, F. 2003, 'Finite element modelling of a pressure feeder using direct shear test measurements', *Proc. Aust. Soc. Sugar Cane Technol.*, vol. 25.

Plaza, F., Harris, H.D. & Kirby, J.M. 2001, 'Modelling the compression, shear and volume behaviour of final bagasse', *Proceedings of the Australian Society of Sugar Cane Technologists*, 23rd conference, pp. 428-36.

Plaza, F. & Kent, G.A. 1998, 'A soil shear test to investigate feeding at the pressure feeder', *Proceedings of the Australian Society of Sugar Cane Technologists*, 20th conference, pp. 327-33.

Roux, J.C. & Vincent, J.P. 1991, 'A proposed model in the analysis of wet pressing', *Tappi Journal*, vol. 74, no. 2, pp. 189-96.

Russell, G.E. 1968, An investigation of the extraction performance of sugar cane crushing trains, PhD thesis, University of Queensland.

Sander, U. & Schönert, K. 1999, 'Operational conditions of a screw-feeder-equipped high-pressure roller mill', *Powder Technology*, vol. 105, pp. 282-7.

Scriven, H.E.B. 1941, 'The continuous pressure feeder', *Proceedings of the Queensland Society of Sugar Cane Technologists*, 12th conference, pp. 159-63.

Shann, D.S. 1962, *Milling studies - general*, Technical Report No. 72, Sugar Research Institute.

Solomon, T.J. 1967, Theoretical and experimental studies in the mechanics of crushing sugar cane, PhD thesis, University of Queensland.

Staunton, S.P., Lethbridge, P.J., Grimley, S.C., Streamer, R.W., Rogers, J. & Mackintosh, D.L. 1999, 'On-line cane analysis by near infra-red spectroscopy', *Proceedings of the Australian Society of Sugar Cane Technologists*, 21st conference, pp. 20-7.

Streeter, V.L. & Wylie, E.B. 1981, *Fluid mechanics*, McGraw-Hill Ryerston Limited, Toronto.

Sugar Research Institute 1957, *Milling studies. Experimental mill. 1. The influence of roller speed on no. 1 mill performance*, Technical Report No. 37.

Sugar Research Institute 1973, 'Conductivity sensing circuits', in *Technical Circular*, No. 32.

United States Department of Agriculture 2002, *Sugar: World markets and trade*, November 2002, viewed 20 May 2003, http://www.fas.usda.gov/htp/sugar/2002/November/complete%20circular.pdf

Waddell, C.W. 1953, 'Effective fibre determination in sugar cane', *Proceedings of the International Society of Sugar Cane Technologists*, 8th congress, pp. 828-41.

Watermark Numerical Computing 2000, *PEST*.

Znidarčić, D., Schiffman, R.L., Pane, V., Croce, P., Ko, H.-Y. and Olsen, H.W. 1986, 'The theory of one-dimensional consolidation of saturated clays: part V, constant rate of deformation testing and analysis', *Géotechnique*, Vol. 36, No. 2, pp. 227-37

Jenkins and Murry's factory measurements of effectiveness

Table A.1 represents the measurements of effectiveness reported by Jenkins and Murry (1981, app. II). Only the measurements from milling units with underfeed rolls are presented. The measurements are described in section 3.3.

Table A.1 Jenkins and Murry's factory measurements of effectiveness

Factory number	Mill number	Test number	D_p' / h^*	h_{co} / h^*	W_{us} / h^*	E
1	1	1	1.86	1.119	0.865	1.669
1	1	2	1.86	1.119	0.865	1.733
2	1	1	1.95	1.188	0.786	1.504
2	1	2	1.95	1.188	0.786	1.784
3	2	1	1.71	0.829	0.787	1.341
3	2	2	1.71	0.829	0.787	1.236
4	1	1	1.76	1.453	0.874	2.431
4	2	1	1.74	1.242	0.753	1.655
4	3	1	1.93	1.621	0.609	1.448
4	4	1	1.93	1.457	0.443	1.691
4	1	2	1.76	1.453	0.874	2.523
4	2	2	1.74	1.242	0.753	1.738
4	3	2	1.93	1.621	0.609	1.545
4	4	2	1.93	1.457	0.443	1.840
5	1	1	1.90	0.769	0.545	1.235
5	2	1	1.92	1.114	0.818	1.380
5	3	1	1.95	1.206	0.830	1.359
5	4	1	1.94	1.153	0.680	1.293
5	5	1	1.95	0.983	0.766	1.169
6	1	1	1.98	1.095	0.444	1.327
6	2	1	1.95	1.142	0.591	1.138
6	4	1	1.93	0.902	0.501	1.201
6	5	1	1.99	0.765	0.511	1.225
7	1	1	1.99	0.838	0.534	0.947
7	2	1	1.92	0.988	0.542	1.076
7	3	1	1.96	1.029	0.557	0.971
7	4	1	2.01	0.905	0.592	0.793
7	5	1	1.99	0.742	0.708	0.706
7	1	2	1.99	0.838	0.534	0.948
7	2	2	1.92	0.988	0.542	1.126
7	3	2	1.96	1.029	0.557	1.038
7	4	2	2.01	0.905	0.592	0.829
7	5	2	1.99	0.742	0.708	0.692
8	1	1	1.88	1.037	0.606	1.383
8	2	1	1.76	1.095	0.665	1.459
8	3	1	1.85	1.097	0.575	1.378
8	4	1	1.77	1.113	0.689	1.391
8	5	1	1.97	0.979	0.543	1.041
8	1	2	1.88	1.037	0.606	1.405
8	2	2	1.76	1.095	0.665	1.489
8	3	2	1.85	1.097	0.575	1.394
8	4	2	1.77	1.113	0.689	1.417
8	5	2	1.97	0.979	0.543	1.071
9	2	1	1.93	0.949	0.556	2.115

Factory number	Mill number	Test number	D_p' / h^*	h_{co} / h^*	W_{us} / h^*	E
9	3	1	1.94	0.938	0.529	2.129
9	4	1	1.93	0.971	0.578	1.769
9	5	1	1.95	0.979	0.576	1.804
9	2	2	1.93	0.949	0.556	2.173
9	3	2	1.94	0.938	0.529	2.216
9	4	2	1.93	0.971	0.578	1.872
9	5	2	1.95	0.979	0.576	1.865
10	1	1	1.94	1.099	0.831	1.522
10	2	1	1.95	1.031	0.546	1.410
10	3	1	1.96	0.973	0.542	1.458
10	4	1	1.93	1.186	0.759	1.296
10	5	1	1.93	1.167	0.750	1.127
10	6	1	1.93	0.747	0.642	1.146
10	1	2	1.94	1.099	0.831	1.447
10	2	2	1.95	1.031	0.546	1.352
10	3	2	1.96	0.973	0.542	1.417
10	4	2	1.93	1.186	0.759	1.283
10	5	2	1.93	1.167	0.750	1.107
10	6	2	1.93	0.747	0.642	1.104
11	1	1	1.94	1.124	0.593	1.319
11	2	1	1.59	1.237	0.599	1.906
11	3	1	1.66	1.093	0.584	1.765
11	4	1	1.66	1.242	0.585	1.743
11	5	1	1.92	1.065	0.786	1.363
11	6	1	1.93	1.000	0.657	0.946
11	1	2	1.94	1.124	0.593	1.308
11	2	2	1.59	1.237	0.599	2.155
11	3	2	1.66	1.093	0.584	1.857
11	4	2	1.66	1.242	0.585	1.768
11	5	2	1.92	1.065	0.786	1.263
11	6	2	1.93	1.000	0.657	1.002
12	1	1	1.98	0.943	0.762	1.607
12	1	2	1.98	0.943	0.762	1.744
13	1	1	1.91	1.110	0.902	1.367
13	4	1	1.91	1.170	0.970	1.175
13	5	1	1.89	1.158	0.882	1.322
13	1	2	1.91	1.110	0.902	1.392
13	4	2	1.91	1.170	0.970	1.145
13	5	2	1.89	1.158	0.882	1.253
14	1	1	1.91	1.110	0.902	1.472
14	2	1	1.69	1.026	0.976	1.396
14	3	1	1.92	1.101	0.902	1.356
14	4	1	1.91	1.158	0.948	1.455
14	1	2	1.91	1.110	0.902	1.532
14	2	2	1.69	1.026	0.976	1.297

Factory number	Mill number	Test number	D_p' / h^*	h_{co} / h^*	W_{us} / h^*	E
14	3	2	1.92	1.101	0.902	1.201
14	4	2	1.91	1.158	0.948	1.290
15	1	1	1.96	1.053	0.710	1.195
15	2	1	1.93	0.925	0.655	1.040
15	3	1	1.97	1.048	0.670	1.144
15	4	1	2.00	1.058	0.766	0.933
15	5	1	1.96	0.970	0.888	1.197
15	1	2	1.96	1.053	0.710	1.185
15	2	2	1.93	0.925	0.655	1.033
15	3	2	1.97	1.048	0.670	1.167
15	4	2	2.00	1.058	0.766	0.989
15	5	2	1.96	0.970	0.888	1.222
16	1	1	1.60	1.209	0.816	1.238
16	2	1	1.69	0.865	0.608	1.333
16	3	1	1.68	1.151	0.784	1.222
16	4	1	1.94	0.688	0.540	0.857
16	1	2	1.60	1.209	0.816	1.684
16	2	2	1.69	0.865	0.608	1.585
16	3	2	1.68	1.151	0.784	1.384
16	4	2	1.94	0.688	0.540	1.201

1997 factory measurements of effectiveness

Table B.1 presents the measurements of effectiveness made in Australian raw sugar factories in 1997 as part of this project (section 3.3).

Table B.1 Factory measurements of effectiveness

Factory number	Mill number	Test number	D_p' / h^*	h_{co} / h^*	W_{us} / h^*	E
1	1	1	1.92	0.781	0.562	1.328
1	1	2	1.92	0.781	0.562	1.315
1	2	1	1.95	0.684	0.742	1.384
1	2	2	1.95	0.717	0.742	1.327
1	4	1	1.70	0.633	0.913	0.838
1	5	1	1.74	0.948	0.736	0.798
1	5	2	1.74	0.947	0.736	0.907
2	1	1	1.71	1.109	0.845	1.227
2	1	2	1.71	1.029	0.845	1.218
2	2	1	1.71	0.900	0.722	1.278
2	2	2	1.71	0.900	0.722	1.296
2	3	1	1.71	1.094	0.635	1.264
2	3	2	1.71	1.092	0.635	1.296
2	4	1	1.91	1.311	0.594	0.986
2	4	2	1.91	1.311	0.594	1.179
2	5	1	1.71	1.088	0.554	1.523
2	5	2	1.71	1.075	0.554	1.431
3	1	1	1.91	1.106	0.595	1.207
3	1	2	1.91	1.106	0.595	1.436
3	2	1	1.83	1.181	0.760	1.643
3	2	2	1.83	1.181	0.760	1.883
3	3	1	1.70	1.028	0.797	1.615
3	3	2	1.70	1.028	0.797	1.764
3	4	1	1.86	1.218	0.660	1.608
3	4	2	1.86	1.218	0.660	1.707
3	5	1	1.96	0.971	0.580	1.305
3	5	2	1.96	0.971	0.580	1.422
4	1	1	1.92	0.824	0.383	1.263
4	1	2	1.92	0.812	0.383	1.287
4	2	1	1.96	0.809	0.541	1.412
4	2	2	1.96	0.809	0.541	1.839
4	3	1	1.87	1.086	0.551	1.644
4	3	2	1.87	1.086	0.551	1.734
4	4	1	1.96	0.856	0.500	1.238
4	4	2	1.96	0.856	0.500	1.301
4	5	1	1.98	0.559	0.425	1.163
4	5	2	1.98	0.579	0.425	1.041
5	1	1	1.92	0.818	0.502	1.089
5	1	2	1.92	0.844	0.502	1.333
5	1	3	1.92	0.739	0.502	1.335
5	2	1	1.93	1.041	0.507	1.237
5	2	2	1.93	1.062	0.507	1.630
5	2	3	1.93	1.069	0.507	1.512
5	3	1	1.91	1.452	0.642	1.269

Factory number	Mill number	Test number	D_p' / h^*	h_{co} / h^*	W_{us} / h^*	E
5	3	2	1.91	1.436	0.642	1.683
5	3	3	1.91	1.452	0.642	1.484
5	4	1	1.94	1.195	0.488	1.352
5	4	2	1.94	1.126	0.488	1.723
5	4	3	1.94	1.199	0.488	1.636
5	5	1	1.98	1.365	0.464	1.042
5	5	2	1.98	1.361	0.464	1.542
5	5	3	1.98	1.421	0.464	1.453
6	1	1	1.94	1.184	0.618	0.974
6	1	2	1.94	1.171	0.618	1.082
6	2	1	1.89	0.923	0.582	1.189
6	2	2	1.89	0.923	0.582	1.468
6	3	1	1.96	1.054	0.570	1.143
6	3	2	1.96	1.043	0.570	1.262
6	4	1	1.95	1.113	0.557	1.010
6	4	2	1.95	1.110	0.557	1.176
6	5	1	1.94	0.965	0.506	0.990
6	5	2	1.94	0.954	0.506	1.157

Permeability measurements for comparing measurement techniques

This appendix presents the data from the permeability experiments described in section 5.5.

Table C.1 presents the experimental design for the direct permeability experiment described in section 5.5.3. The results and calculated void ratio and permeability are presented in Table C.2. Table C.3 presents the parameter values used in the void ratio and permeability calculations.

Table C.1 Experimental design for the direct permeability experiment

Test	Preparation	Sample height (mm)	Nominal void ratio
1	750/10	43	5
2	750/30	43	9
3	750/30	104	5
4	750/10	104	5
5	750/30	43	5
6	750/30	104	7
7	750/10	104	9
8	750/10	43	9
9	750/10	104	7
10	750/10	43	7
11	750/30	104	9
12	750/30	43	7

Table C.2 Results and calculated void ratio and permeability for the direct permeability experiment

Test	Fibre content (%)	Sample mass (kg)	$\frac{Q}{\Delta P}$ (L/min/kPa)	Void ratio	Permeability (m^2)
1	11.9	2.20	0.00102	4.7	1.02×10^{-13}
2	11.3	1.32	0.00329	9.0	3.27×10^{-13}
3	11.3	5.19	0.00021	5.2	4.93×10^{-14}
4	11.9	5.19	0.00037	4.9	8.95×10^{-14}
5	11.3	2.20	0.00104	5.0	1.03×10^{-13}
6	11.3	4.15	0.00074	6.7	1.78×10^{-13}
7	11.9	3.11	0.00164	8.8	3.95×10^{-13}
8	10.8	1.32	0.00442	9.5	4.40×10^{-13}
9	10.8	4.14	0.00090	7.1	2.15×10^{-13}
10	10.8	1.76	0.00164	6.8	1.63×10^{-13}
11	10.1	3.11	0.00196	10.4	4.72×10^{-13}
12	10.1	1.76	0.00209	7.3	2.08×10^{-13}

Table C.3 Parameter values used in the void ratio and permeability calculations

Parameter	Value
Total cell area	22 650 mm^2
Density of fibre	1530 kg/m^3
Absolute viscosity of water	0.894 mPa.s
Flow area	6439 mm^2

Table C.4 presents the experimental design for the indirect permeability experiment described in section 5.5.4. For each of the 8 kg tests, the initial sample height was assumed to be 800 mm. For each of the 4 kg tests, the initial sample height was assumed to be 400 mm. The initial axial stress in the sample was assumed to be 1 kPa. The fibre content was assumed to be 11% for all tests.

Table C.4 Experimental design for the indirect permeability experiment

Test	Preparation	Sample mass (kg)	Platen speed (mm/s)
1	750/30	4	100
2	750/10	8	100
3	750/30	4	1
4	750/10	4	1
5	750/10	8	20
6	750/10	4	20
7	750/30	8	20
8	750/30	8	1
9	750/10	8	1
10	750/30	8	100
11	750/30	4	20
12	750/10	4	100

A two-roll mill experiment at underfeed nip conditions

Introductory remarks

This appendix presents the data from the two-roll mill experiment described in sections 6.3 and 6.4.

The experiment

Table D.1 presents the experimental design. The results are presented in Table D.2.

Table D.1 Order of tests for the two-roll mill experiment

Test	Nominal nip setting (mm)	Cane variety	Cane preparation (r/min)	Nominal feed pressure (kPa)	Nominal roll speed (mm/s)	Nominal contact angle (°)
1	240	Q124	2000	7	100	40
2	240	Q117	2000	3	500	40
3	240	Q124	1200	3	100	16
4	240	Q117	1200	7	500	16
5	120	Q117	2000	3	500	16
6	120	Q124	2000	7	100	16
7	120	Q117	1200	7	500	40
8	120	Q124	1200	3	100	40
9	120	Q117	2000	3	100	40
10	120	Q124	2000	7	500	40
11	120	Q124	1200	3	500	16
12	120	Q117	1200	7	100	16
13	240	Q124	1200	7	100	16
14	240	Q117	1200	3	500	16
15	240	Q117	2000	7	500	40
16	240	Q124	2000	3	100	40
17	240	Q117	1200	3	100	40
18	240	Q124	1200	7	500	40
19	240	Q117	2000	7	100	16
20	240	Q124	2000	3	500	16
21	120	Q124	1200	7	100	40
22	120	Q117	1200	3	500	40
23	120	Q117	2000	7	500	16
24	120	Q124	2000	3	100	16
25	120	Q124	2000	3	500	40
26	120	Q117	2000	7	100	40
27	120	Q117	1200	3	100	16
28	120	Q124	1200	7	500	16
29	240	Q124	2000	7	500	16
30	240	Q117	2000	3	100	16
31	240	Q124	1200	3	500	40
32	240	Q117	1200	7	100	40

Table D.2 Results from the two-roll mill experiment

Test	Nip setting (mm)	Chute setting (mm)	Feed mass (kg)	Feed pressure (kPa)	Roll speed (mm/s)	Feed speed (mm/s)	Feed speed ratio
1	240	427	36.9	7.3	100	95	1.252
2	240	427	31.9	3.1	498	436	1.151
3	240	275	20.5	4.5	102	130	1.339
4	240	275	23.7	7.4	500	550	1.151
5	120	150	11.2	2.9	496	405	0.849
6	120	150	13.0	7.1	98	99	1.048
7	120	302	26.1	7.0	496	407	1.070
8	120	302	22.6	3.1	102	79	1.015
9	120	302	22.6	3.1	99	81	1.062
10	120	302	26.1	7.0	498	399	1.045
11	120	150	11.2	3.4	490	434	0.921
12	120	150	13.0	7.0	100	100	1.036
13	244	275	23.7	7.0	101	177	1.825
14	244	275	20.5	3.4	498	484	1.012
15	244	427	36.9	6.8	498	468	1.228
16	244	427	31.9	3.0	99	90	1.182
17	244	427	31.9	2.9	100	82	1.068
18	244	427	36.9	6.9	498	472	1.238
19	244	275	23.7	7.0	100	224	2.333
20	244	275	20.5	3.3	490	554	1.177
21	120	302	26.1	7.1	100	89	1.159
22	120	302	22.6	3.3	483	341	0.920
23	120	150	13.0	7.0	499	506	1.054
24	120	150	11.2	3.5	100	95	0.985
25	120	302	22.6	3.0	496	392	1.031
26	120	302	26.1	7.0	100	86	1.126
27	120	150	11.2	3.8	99	94	0.989
28	120	150	13.0	6.8	496	489	1.025
29	240	275	23.7	7.8	494	527	1.117
30	240	275	20.5	3.9	99	119	1.252
31	240	427	31.9	2.9	503	446	1.166
32	240	427	36.9	7.1	102	114	1.473

Material parameters for the solid phase

Table D.3 lists the tests undertaken to determine the solid phase material parameters for the cane varieties and levels of preparation used in the two-roll mill throughput experiment. The *compression* test type in Table D.3 refers to a simple compression test at nominally constant speed. The *expansion* test type in Table D.3 refers to a test similar to the compression test type but where the platen movement was reversed during

the test to provide some data with which to assess the elastic parameters. Only thirteen of the eighteen tests are shown in Table D.3. The remaining five tests were unsuitable for material parameter estimation because of instrumentation failures.

Table D.3 Compression tests undertaken to determine solid phase material parameters

Test	Cane variety	Shredder speed (r/min)	Test type
1	Q117	2000	Compression
2			Compression
3			Expansion
4			Expansion
5	Q124	2000	Compression
6			Compression
7			Expansion
8			Expansion
13	Q117	1200	Compression
14			Compression
16			Expansion
17	Q124	1200	Compression
18			Expansion

Material parameters for the fluid phase

Table D.4 lists the tests undertaken to determine the permeability parameters for the cane varieties and levels of preparation used in the two-roll mill throughput experiment. Table D.5 presents the parameter values used in the void ratio and permeability calculations.

Table D.4 Steady-state permeability tests undertaken to determine fluid phase material parameters

Test	Cane variety	Shredder speed (r/min)	Sample mass (kg)	Nominal void ratio
1	Q117	2000	0.6	10
2			0.6	5
3			0.6	30
4			1.2	10
5			1.2	30
6			1.2	5
7	Q124	2000	0.6	10
8			1.2	5
9			0.6	5
10			1.2	30
11			1.2	10
12			0.6	30
13	Q124	1200	1.2	10
14			0.6	30
15			0.6	10
16			0.6	5
17			1.2	5
18			1.2	30
19	Q117	1200	1.2	5
20			0.6	5
21			0.6	30
22			1.2	30
23			0.6	10
24			1.2	10

Table F.5 Parameter values used in the permeability calculations

Parameter	Value
Total cell area	22 650 mm^2
Density of fibre	1530 kg/m^3
Absolute viscosity of water	0.894 mPa.s
Flow area	6439 mm^2

Results of Solomon's two-roll mill feeding experiments

Introductory remarks

Solomon (1967) carried out experiments to determine the factors affecting the throughput of a two-roll mill with the aim of investigating the assumption of Murry (1960) that the feed speed (S_F) was equal to $S \cos \alpha$ where S is the roll surface speed and α is the contact angle. Solomon's results are represented here. His results are reviewed in detail in section 7.2.

While Solomon used S_F / S to analyse his experiments, $\frac{S_F}{S \cos \alpha}$ is believed to be a better ratio for this analysis. Unfortunately Solomon did not report the contact angles for all of his experiments. In this appendix, contact angle estimates are made for those experiments where the contact angle was not reported.

Results of the initial test series

Table E.1 presents the results of the initial test series.

Table E.1 Results of the initial test series

Nominal compression ratio	Roll speed (in/s)	cos α	Feed speed (in/s)
1.5	5.73	0.903	5.61
1.5	5.77	0.903	5.71
1.5	5.92	0.903	5.60
2.5	5.93	0.886	5.15
2.5	6.11	0.886	5.34
2.5	5.95	0.886	4.96
3.5	5.64	0.879	3.85

Results of the compression ratio test series

Table E.2 presents the results of the compression ratio test series.

Table E.2 Results of the compression ratio test series

Nominal compression ratio	Roll speed (in/s)	cos α	Feed speed (in/s)
1.5	6.17	0.895	6.75
1.5	6.36	0.895	6.70
2.0	5.94	0.884	6.05
2.0	5.75	0.884	5.60
2.5	6.17	0.878	5.75
2.5	5.94	0.878	5.75
3.0	6.17	0.874	5.15
3.0	6.17	0.874	5.35
3.5	6.17	0.871	4.80
3.5	6.17	0.871	5.05

Contact angle calculations for initial test series and compression ratio test series

For both the initial test series and the compression ratio test series, Solomon reported the contact angles for his tests (shown in Table E.1 and Table E.2). These test series were analysed in order to determine Solomon's method of calculating the contact angle.

cos α was calculated from equation **(1.4)**:

$$\cos\alpha = \frac{D + W - h}{D} \qquad \textbf{(E.1)}$$

D and h were known for each test. W needed to be estimated.

From equation **(1.9)**:

$$C_0 = \frac{V_0}{V_E} \qquad \textbf{(E.2)}$$

Now:

$$V_0 = \frac{Q}{\rho_0} \qquad \textbf{(E.3)}$$

where ρ_0 is the density of cane at the no-void volume. ρ_0 is nominally constant for a particular sample of cane and so was assumed constant for each experiment.

The crushing rate is a function of the feed speed:

$$Q = \rho_a \, L \, h \, S_F \qquad \textbf{(E.4)}$$

From equation **(1.6)**, the escribed volume at the nip is:

$$V_E = L \, W \, S \qquad \textbf{(E.5)}$$

Substituting equations **(E.3)**, **(E.4)** and **(E.5)** into equation **(E.2)**, compression ratio is defined:

$$C_0 = \frac{\rho_a \, h \, S_F}{\rho_0 \, W \, S} \qquad \textbf{(E.6)}$$

Since the cane supply for an experiment undoubtedly came from a single cane block, ρ_0 could be assumed constant for an experiment. For a particular test, C_0, ρ_a, h and S were known. To determine the work opening only an estimate for S_F was required.

If S_F was assumed to be equal to $S \cos \alpha$, then $C_0 W / \cos \alpha$ would be a constant for an experiment where only compression ratio was varied. Both the initial test series and the compression ratio test series fit into this category. Using equation **(E.1)** to calculate W for each test in the initial test series and the compression ratio test series, $C_0 W / \cos \alpha$ is plotted for each compression ratio in Figure E.1. From Figure E.1, it appears that S_F was assumed to be equal to $S \cos \alpha$ in the initial test series but not in the compression ratio test series.

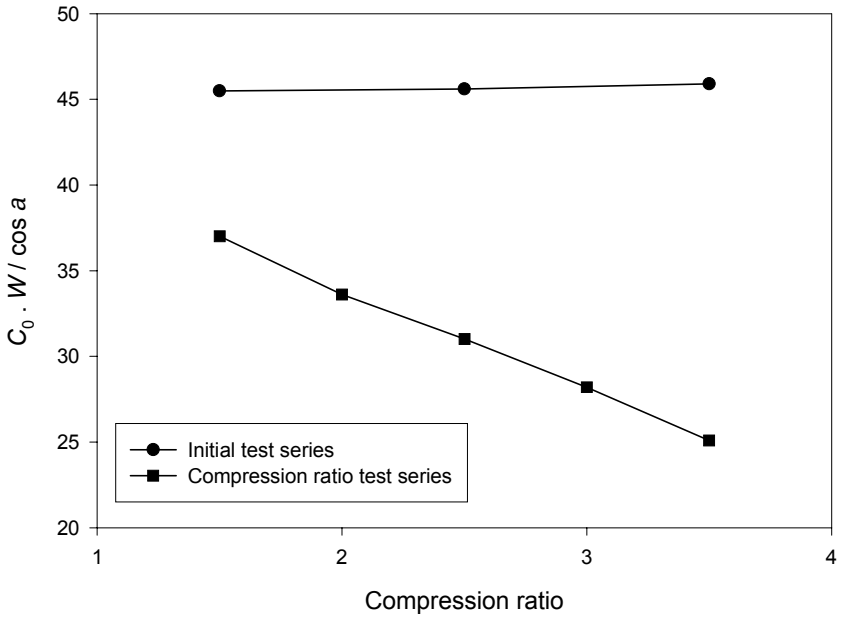

Figure E.1 **$C_0 W / \cos \alpha$ for the initial test series and the compression ratio test series.**

It is possible that Solomon used the results of the initial test series to estimate S_F for the compression test series. A relationship for S_F/S as a function of compression ratio for the initial test series was developed. The first step was to calculate the actual compression ratio achieved in each test from equation **(E.6)**. In order to use this equation, ρ_a had to be calculated. Solomon (1967, sec. 9.2) provided a relationship

between feed pressure (P_a) and compression ratio in the feed (C_{0a}) that is considered appropriate for this experiment:

$$P_a = c_2 \left(C_{0a} - c_1\right)^2 \qquad \textbf{(E.7)}$$

where c_1 and c_2 are constants for a sample of cane (Solomon 1967, table 9.1). Now:

$$C_{0a} = \frac{\rho_a}{\rho_0} \qquad \textbf{(E.8)}$$

Substituting equations **(E.7)** and **(E.8)** into equation **(E.6)**:

$$C_0 = C_{0a} \frac{h}{W} \frac{S_F}{S} \qquad \textbf{(E.7)}$$

Using the calculated compression ratios from equation **(E.7)** and the S_F/S results from the initial test series, a linear regression analysis was carried out to determine S_F/S as a function of compression ratio. The relationship is shown in Figure E.2.

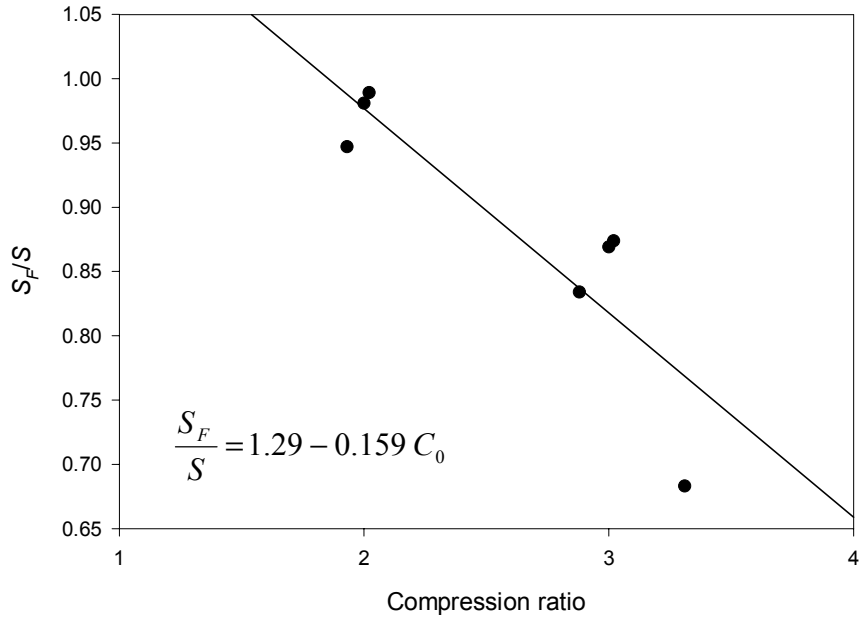

Figure E.2 Relationship between compression ratio and speed ratio for the initial test series

If Solomon did use a regression relationship like the one in Figure E.2 to determine the work opening for the compression ratio test series, then $C_0\ W\ S\ /\ S_F$ would be a constant for an experiment. This hypothesis is checked in Figure E.3. From Figure E.3, it is plausible that Solomon used the technique described above.

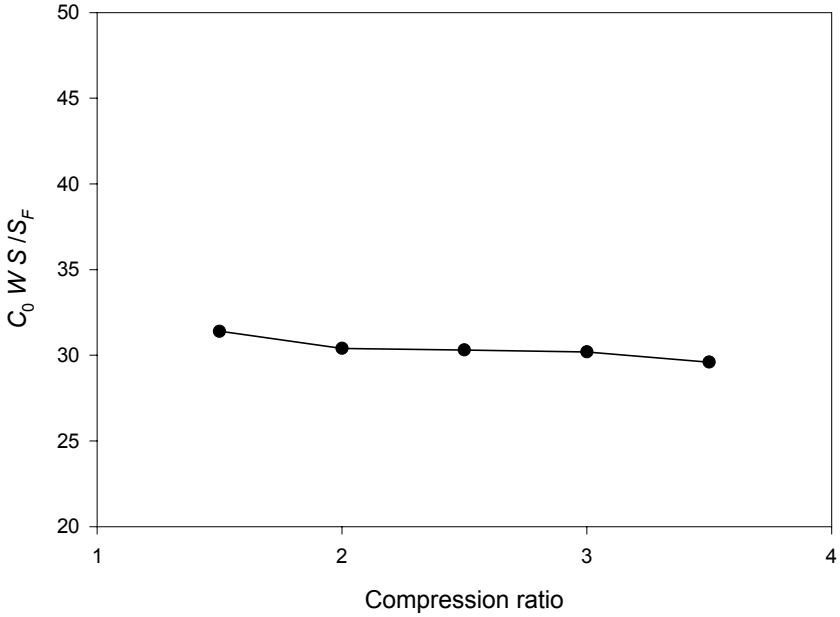

Figure E.3 $C_0 W S / S_F$ **for the initial test series and the compression ratio test series.**

While the technique described above appears to be the approach taken by Solomon to determine work opening and contact angle, there is an inconsistency in his published data. The cos α values he has reported for the compression ratio test series appear to be too low and result in work openings that suggest compression ratios well in excess of those intended. Either the wrong contact angles were reported or the work openings used in the experiment were incorrectly selected.

Table E.3 shows the cos α values that would be calculated if the approach described above was used and compares the results to those reported by Solomon. Even if the compression ratios were considerably in error, Table E.3 shows that cos α is still estimated within 3%. Consequently, the technique used to estimate cos α is not of great importance.

Table E.3 Comparison of contact angles calculated from the S_F / S regression to Solomon's reported values

Compression ratio	cos α		% difference
	Regression approach	Solomon's values	
1.5	0.921	0.895	3
2.0	0.903	0.884	2
2.5	0.892	0.878	2
3.0	0.884	0.874	1
3.5	0.879	0.871	1

Results of the factorial experiment series

Table E.4 presents the results of the factorial experiment series. As discussed in section E.4, Solomon did not report contact angle values for the factorial experiment series. The values presented in Table E.4 were calculated using the regression equation described in section E.4.

Table E.4 Results of the factorial experiment series

Nominal preparation	Nominal feed pressure (lb/ft^2)	Nominal roll speed (ft/min)	Nominal feed height (in)	Nominal compression ratio	Roll speed (ft/min)	cos α	Feed speed (ft/min)
750/20	400	30	2.6	1.50	33.11	0.932	33.36
750/20	400	30	2.6	2.25	33.11	0.919	32.92
750/20	400	30	2.6	3.00	26.95	0.913	24.32
750/20	400	30	3.6	1.50	34.08	0.907	35.60
750/20	400	30	3.6	2.25	34.08	0.888	29.39
750/20	400	30	3.6	3.00	31.75	0.879	33.48
750/20	400	30	4.6	1.50	33.59	0.881	34.44
750/20	400	30	4.6	2.25	34.33	0.857	33.12
750/20	400	30	4.6	3.00	29.43	0.845	25.65
750/20	400	50	2.6	1.50	54.21	0.932	53.64
750/20	400	50	2.6	2.25	56.87	0.919	49.49
750/20	400	50	2.6	3.00	53.89	0.913	46.39
750/20	400	50	3.6	1.50	48.03	0.907	41.22
750/20	400	50	3.6	2.25	56.87	0.888	46.15
750/20	400	50	3.6	3.00	57.22	0.879	42.79
750/20	400	50	4.6	1.50	45.66	0.881	44.20
750/20	400	50	4.6	2.25	51.50	0.857	36.37
750/20	400	50	4.6	3.00	49.31	0.845	38.28
750/20	800	30	2.6	1.50	28.43	0.940	26.02
750/20	800	30	2.6	2.25	32.18	0.924	31.13
750/20	800	30	2.6	3.00	31.53	0.915	27.77
750/20	800	30	3.6	1.50	31.98	0.917	39.92
750/20	800	30	3.6	2.25	29.34	0.894	33.14
750/20	800	30	3.6	3.00	34.98	0.883	36.78
750/20	800	30	4.6	1.50	28.96	0.894	26.83
750/20	800	30	4.6	2.25	30.29	0.865	27.39
750/20	800	30	4.6	3.00	31.22	0.850	22.15
750/20	800	50	2.6	1.50	46.82	0.940	44.09
750/20	800	50	2.6	2.25	49.31	0.924	51.44
750/20	800	50	2.6	3.00	56.52	0.915	51.08
750/20	800	50	3.6	1.50	43.31	0.917	41.30
750/20	800	50	3.6	2.25	54.21	0.894	48.83
750/20	800	50	3.6	3.00	53.28	0.883	38.16
750/20	800	50	4.6	1.50	51.50	0.894	50.80
750/20	800	50	4.6	2.25	54.21	0.865	42.08
750/20	800	50	4.6	3.00	52.67	0.850	31.02
500/20	400	30	2.6	1.50	32.75	0.929	38.46
500/20	400	30	2.6	2.25	30.09	0.917	27.05
500/20	400	30	2.6	3.00	33.47	0.911	29.30
500/20	400	30	3.6	1.50	33.34	0.901	36.75
500/20	400	30	3.6	2.25	33.70	0.885	31.04
500/20	400	30	3.6	3.00	34.98	0.877	25.57
500/20	400	30	4.6	1.50	34.33	0.874	35.63

Nominal preparation	Nominal feed pressure (lb/ft^2)	Nominal roll speed (ft/min)	Nominal feed height (in)	Nominal compression ratio	Roll speed (ft/min)	cos α	Feed speed (ft/min)
500/20	400	30	4.6	2.25	34.33	0.853	29.64
500/20	400	30	4.6	3.00	32.53	0.843	28.65
500/20	400	50	2.6	1.50	50.38	0.929	53.95
500/20	400	50	2.6	2.25	54.21	0.917	44.35
500/20	400	50	2.6	3.00	60.19	0.911	39.74
500/20	400	50	3.6	1.50	49.84	0.901	55.17
500/20	400	50	3.6	2.25	55.51	0.885	47.35
500/20	400	50	3.6	3.00	58.67	0.877	41.09
500/20	400	50	4.6	1.50	57.94	0.874	54.32
500/20	400	50	4.6	2.25	52.37	0.853	46.28
500/20	400	50	4.6	3.00	46.35	0.843	39.42
500/20	800	30	2.6	1.50	33.70	0.933	32.46
500/20	800	30	2.6	2.25	31.11	0.920	25.91
500/20	800	30	2.6	3.00	32.87	0.913	29.58
500/20	800	30	3.6	1.50	27.59	0.908	29.87
500/20	800	30	3.6	2.25	31.63	0.889	35.45
500/20	800	30	3.6	3.00	34.59	0.879	30.10
500/20	800	30	4.6	1.50	32.18	0.882	38.07
500/20	800	30	4.6	2.25	31.85	0.858	31.29
500/20	800	30	4.6	3.00	31.85	0.846	27.33
500/20	800	50	2.6	1.50	52.97	0.933	60.79
500/20	800	50	2.6	2.25	64.37	0.920	53.05
500/20	800	50	2.6	3.00	51.50	0.913	43.91
500/20	800	50	3.6	1.50	47.54	0.908	56.46
500/20	800	50	3.6	2.25	51.79	0.889	50.15
500/20	800	50	3.6	3.00	54.53	0.879	39.80
500/20	800	50	4.6	1.50	52.97	0.882	59.95
500/20	800	50	4.6	2.25	48.28	0.858	49.20
500/20	800	50	4.6	3.00	48.78	0.846	46.06

Results of the photographic measurement series

Table E.5 presents the results of the factorial experiment series. Like the factorial experiment series, Solomon did not report contact angle values for the photographic measurement series. Once again, the calculation procedure using the regression equation described in section E.4 was used to estimate cos α.

Table E.5 Results of the photographic measurement series

Nominal compression ratio	Roll speed (ft/min)	cos α	Feed speed (ft/min)
3.5	29.7	0.880	24.3
3.5	31.7	0.880	23.0
3.5	31.1	0.880	23.0
2.5	31.7	0.892	26.8
2.5	31.7	0.892	27.8
2.5	30.4	0.892	27.3
2.0	31.1	0.903	29.1
2.0	30.4	0.903	28.6
2.0	29.7	0.903	28.1

Concluding remarks

The method presented in section E.4 to estimate S_F / S is not a general method since it relies on a regression equation developed under specific conditions and only considers the effects of one parameter, compression ratio.

While there is some doubt about the actual work openings used by Solomon, the contact angles presented in Table E.4 and Table E.5 are expected to be reasonably accurate (within 3%) and so are expected to be adequate for the analysis described in section 7.2.

Appendix F *Results of Jenkins and Murry's feeding experiments*

A.1 Introductory remarks

This appendix represents the results of feeding experiments originally presented by Jenkins and Murry (1981). Section F.2 presents the results for the first experiment using a small-scale three-roll feeder. Section F.3 presents the results for the second experiment using the same feeder. Section F.4 presents the results for an experiment conducted on the #5 mill at Marian factory.

A.2 The first model experiment

The feeder was constructed with pressure feeder rolls with an outside diameter of 457 mm and a length of 305 mm. The rolls had 25 mm pitch grooving with a groove depth of 30 mm. The underfeed roll had a diameter of 457 mm and no grooving. For the first experiment, the pressure feeder nip setting was 32 mm and the feed chute exit setting was 225 mm. The parameters explored in the experiment are presented in Table F.1. The tangent setting was defined as the largest distance perpendicular to the chute wall on the underfeed roll side of the chute between an extension of the chute wall and the surface of the underfeed roll. The results of the experiment (Murry's feed speed ratio, r_M) are presented in Table F.2.

Table F.1 Parameters explored in the first small-scale experiment

Parameter	Symbol
Underfeed nip setting	W_{su}
Tangent setting	U
Feed chute angle	θ_h
Ratio of underfeed roll speed to pressure feeder speed	S'_u / S'_p
Pressure feeder speed	S'_p

Table F.2 Results of the first small-scale experiment

Test	W_{su} (mm)	U (mm)	θ_h (°)	S'_u / S'_p	S'_p (mm/s)	r_M
1	171	12	75	1.00	94	0.939
2	197	-14	75	1.00	94	0.706
3	159	19	75	1.00	94	0.907
4	146	32	75	1.00	94	0.939
5	146	32	75	1.00	188	0.964
6	171	12	75	1.00	188	0.892
7	171	12	75	0.91	94	0.822
8	171	12	75	1.09	94	0.880
9	171	12	75	1.31	94	0.880
10	171	16	85	1.00	94	0.939
11	171	38	85	1.00	94	0.845
12	171	0	85	1.00	94	0.857
13	171	18	75	1.00	94	0.880
14	171	35	75	1.00	94	0.939
15	171	12	75	1.31	94	0.904

A.3 The second model experiment

The second experiment was conducted using the same small-scale feeder as the first experiment. For this experiment, however, the pressure feeder nip setting was 25 mm and the feed chute exit setting (h_{do}) was included as an experimental factor. The chute was positioned to achieve symmetrical feeding so the tangent setting was not used as a factor. The pressure feeder speed was fixed at 94 mm/s. The results of the experiment are presented in Table F.3.

Table F.3 Results of the second small-scale experiment

Test	W_{su} (mm)	h_{do} (mm)	θ_h (°)	S'_u / S'_p	r_M
1	125	230	75	1.00	1.129
2	125	200	75	1.00	1.176
3	125	175	75	1.00	1.174
4	125	250	75	1.00	1.040
5	125	275	75	1.00	1.017
6	125	170	85	1.00	1.160
7	125	216	85	1.00	1.073
8	125	207	85	1.00	1.060
9	125	230	85	1.00	0.927
10	125	230	85	1.00	1.115
11	125	250	85	1.00	1.054
12	125	275	85	1.00	1.094
13	125	300	85	1.00	1.107
14	125	250	85	1.00	1.111
15	135	250	85	1.00	0.954
16	145	250	85	1.00	0.994
17	155	250	85	1.00	0.928
18	165	250	85	1.00	0.966
19	175	250	85	1.00	0.929
20	100	250	85	1.00	1.186
21	75	250	85	1.00	1.090
22	90	250	85	1.00	1.147
23	115	250	85	1.00	1.087
24	115	250	85	1.00	1.087
25	125	250	85	1.00	1.111
26	100	250	85	1.00	1.156
27	135	250	85	1.00	1.024
28	135	250	85	1.31	1.065
29	165	250	85	1.31	0.941
30	155	250	85	1.31	0.980
31	145	250	85	1.31	1.021
32	125	250	85	1.31	1.040
33	125	250	85	1.31	1.054
34	130	250	85	1.31	1.025
35	135	250	85	1.31	1.065

A.4 The factory experiment

The factory experiment was conducted on the #5 mill at Marian factory. The mill rolls were 1981 mm long. The mill had 813 mm outside diameter pressure feeder rolls and a 766 mm outside diameter underfeed roll. The pressure feeder groove depth was 45 mm.

The pressure feeder nip setting was 33 mm. The feed chute exit setting was fixed at 451 mm. The feed chute angle was also fixed at about 79°. The experiment explored the effect of underfeed nip setting and ratio of underfeed roll speed to pressure feeder speed. The results are shown in Table F.4.

Table F.4 Results of the Marian #5 mill experiment

Test	W_{su} (mm)	S'_u / S'_p	S'_p	r_M
1	333	1.10	205	1.213
2	333	1.10	242	1.058
3	333	1.10	251	1.007
4	333	1.10	265	1.064
5	333	1.10	227	1.013
6	333	1.10	241	1.073
7	333	1.10	199	1.370
8	333	1.10	273	1.054
9	318	1.10	261	1.075
10	300	1.10	252	1.111
11	285	1.10	250	1.449
12	285	1.10	223	1.380
13	300	1.10	234	1.263
14	300	1.10	254	1.251
16	318	1.10	256	1.070
19	318	1.10	219	1.404
21	333	1.10	271	1.075
22	333	1.10	264	1.137
23	285	1.10	266	1.279
24	285	1.10	256	1.491
25	300	1.10	246	1.192
26	300	1.10	252	1.267
27	300	1.10	243	1.260
28	285	1.10	259	1.137
29	285	0.88	212	1.462
30	285	0.88	264	1.185
31	300	0.88	250	1.142
32	300	0.88	240	1.226
33	318	0.88	240	1.174
34	318	0.88	239	1.215
35	333	0.88	247	0.990
36	333	0.88	263	1.036
37	285	0.88	247	1.313
38	285	0.88	237	1.313
39	285	0.88	244	1.384
40	285	0.88	244	1.388
41	285	0.88	238	1.302
42	285	0.88	247	1.327
43	285	0.70	255	1.330
44	285	0.70	244	1.147
45	285	0.70	260	1.250
46	285	0.70	247	1.436
47	285	0.70	261	1.228
48	285	0.70	255	1.438

Test	W_{su} (mm)	S'_u / S'_p	S'_p	r_M
49	268	0.70	266	1.328
50	268	0.70	249	1.320
51	268	0.70	257	1.317
52	268	0.70	253	1.462
53	268	0.70	275	1.414
54	268	0.70	259	1.300
55	253	0.70	264	1.465
56	253	0.70	251	1.356
57	253	0.70	272	1.227
58	253	0.70	253	1.311
59	253	0.70	244	1.472
60	253	0.70	258	1.196
61	300	0.70	247	1.193
62	300	0.70	244	1.143
63	300	0.70	267	1.180
64	300	0.70	251	1.116
65	300	0.70	254	1.320
66	300	0.70	277	0.988
67	318	0.70	271	1.125
68	318	0.70	269	1.020
69	318	0.70	270	1.069
70	318	0.70	261	1.238
71	318	0.70	229	1.101
72	318	0.70	240	1.071
73A	333	0.34	317	0.747
73B	333	0.42	309	0.767
73C	318	0.38	326	0.761
73D	300	0.42	322	0.813
73E	285	0.41	317	0.865
73F	268	0.44	346	0.837
74	333	0.70	287	1.091
75	333	0.70	256	1.109
76	333	0.70	265	1.126
77	333	0.70	281	1.179
78	333	0.70	266	1.155
80	333	1.10	237	1.231
81	333	1.10	229	1.346
82	333	1.10	245	1.118
83	333	1.10	233	1.215
84	318	1.10	213	1.301
85	318	1.10	214	1.339
86	318	1.10	209	1.494
87	318	1.10	214	1.268
88	300	1.10	223	1.315
89	300	1.10	237	1.244
90	300	1.10	231	1.012

Test	W_{su} (mm)	S'_u / S'_p	S'_p	r_M
91	300	1.10	236	1.268
92	285	1.10	235	1.253
93	285	1.10	224	1.141
94	285	1.10	237	1.487
95	285	1.10	224	1.430
96	268	1.10	244	1.347
97	268	1.10	259	1.454
98	268	1.10	251	1.335
99	268	1.10	243	1.370
100	268	1.10	252	1.268
101	268	1.10	226	1.333
102	253	1.10	263	1.465
103	253	1.10	254	1.304
104	253	1.10	241	1.353
105	253	1.10	257	1.299
106	253	1.10	252	1.422
107	253	1.10	259	1.399

A factory mill experiment

Introductory remarks

This appendix presents the data from the factory mill experiment undertaken as part of this study and described in sections 8.4 and 8.6.7.

The experiment

Table G.1 presents the experimental design. Table G.2 presents the actual operating parameters that were achieved. The results are presented in Table G.3. The parameters appearing in the headings were described in sections 8.2, 8.6.2 and 8.6.3.

Table G.1 Order of tests for the factory mill experiment

Test	W_{sua} (mm)	Replicate	h_{doa} (mm)	θ_{pt} (°)	ω_u/ω_{pt}
1	0	1	0	1	0.4
2	0	1	0	1	1.3
3	0	1	0	1	1.0
4	0	1	-200	2	0.4
5	0	1	-200	2	1.0
6	0	1	-200	2	1.3
7	0	1	-100	0	0.4
8	0	1	-100	0	1.3
9	0	1	-100	0	1.0
10	100	2	0	2	0.4
11	100	2	0	2	1.0
12	100	2	0	2	1.3
13	100	2	-100	1	0.4
14	100	2	-100	1	1.0
15	100	2	-100	1	1.3
16	100	2	-200	0	0.4
17	100	2	-200	0	1.0
18	100	2	-200	0	1.3
19	100	1	0	0	1.3
20	100	1	0	0	1.0
21	100	1	0	0	0.4
22	100	1	-100	2	1.0
23	100	1	-100	2	0.4
24	100	1	-100	2	1.3
25	100	1	-200	1	1.0
26	100	1	-200	1	0.4
27	100	1	-200	1	1.3
28	-100	2	-100	0	0.4
29	-100	2	-100	0	1.0
30	-100	2	-100	0	1.3
31	-100	2	-200	2	0.4
32	-100	2	-200	2	1.3
33	-100	2	-200	2	1.0
34	-100	2	0	1	0.4
35	-100	2	0	1	1.0
36	-100	2	0	1	1.3
37	-100	1	-200	0	1.3
38	-100	1	-200	0	1.0
39	-100	1	-200	0	0.4
40	-100	1	-100	1	1.3
41	-100	1	-100	1	1.0
42	-100	1	-100	1	0.4
43	-100	1	0	2	1.3
44	-100	1	0	2	0.4
45	-100	1	0	2	1.0
46	0	2	-200	1	0.4
47	0	2	-200	1	1.0
48	0	2	-200	1	1.3

Test	W_{sua} (mm)	Replicate	h_{doa} (mm)	θ_{pt} (°)	ω_u/ω_{pt}
49	0	2	0	0	1.0
50	0	2	0	0	1.3
51	0	2	0	0	0.4
52	0	2	-100	2	1.0
53	0	2	-100	2	0.4
54	0	2	-100	2	1.3

Table G.2 Operating parameters from the factory mill experiment

Test	W_{su} (mm)	h_{do} (mm)	θ_{pt} (°)	θ_h (°)	ω_u (r/min)	ω_{pt} (r/min)
1	450	770	2.8	78	1.43	3.58
2	450	660	3.3	77	3.69	2.81
3	450	780	2.7	78	3.84	3.82
4	450	560	1.8	78	1.43	3.60
5	450	550	1.8	78	3.29	3.25
6	450	550	1.8	78	5.01	3.88
7	450	670	0.1	80	1.68	4.21
8	450	620	0.4	79	4.97	3.83
9	450	650	0.2	80	4.06	4.02
10	550	730	1.9	80	1.57	3.92
11	550	780	1.8	81	3.61	3.57
12	550	770	1.8	81	5.18	3.98
13	550	740	2.3	80	1.57	3.86
14	550	740	2.3	80	4.20	4.17
15	550	740	2.3	80	5.70	4.40
16	550	620	0.6	81	1.48	3.69
17	550	620	0.6	81	3.99	3.95
18	550	620	0.6	81	3.96	3.04
19	550	830	1.1	82	4.35	3.34
20	550	830	1.1	82	3.91	3.94
21	550	840	1.1	82	1.50	3.79
22	550	720	2.5	80	3.76	3.76
23	550	720	2.5	80	1.33	3.30
24	550	720	2.5	80	4.91	3.73
25	550	620	1.5	80	3.39	3.42
26	550	620	1.5	80	1.26	3.18
27	550	620	1.5	80	4.77	3.67
28	370	630	0.9	78	1.35	3.37
29	370	590	1.1	77	3.50	3.44
30	370	570	1.2	77	3.31	2.59
31	370	520	3.1	75	1.34	3.39
32	370	520	3.1	75	4.36	3.32
33	370	520	3.1	75	3.06	3.06
34	370	710	1.9	77	1.46	3.65
35	370	710	2.0	77	3.62	3.61
36	370	710	2.0	77	4.06	3.11
37	370	530	1.1	77	4.21	3.28
38	370	520	1.2	77	2.57	2.58
39	370	520	1.2	77	1.16	2.95
40	370	620	2.4	76	4.23	3.25
41	370	620	2.4	76	3.58	3.71
42	370	630	2.3	76	1.26	3.19
43	370	670	2.4	77	5.45	4.18
44	370	680	2.4	77	1.76	4.36
45	370	680	2.4	77	3.36	3.35
46	450	540	1.3	78	1.30	3.30
47	450	560	1.2	78	3.83	3.85
48	450	560	1.2	78	5.77	4.44

Test	W_{su} (mm)	h_{do} (mm)	θ_{pt} (°)	θ_h (°)	ω_u (r/min)	ω_{pt} (r/min)
49	450	740	0.2	81	3.22	3.24
50	450	750	0.2	81	5.99	4.58
51	450	750	0.2	81	1.83	4.52
52	450	640	2.3	78	3.69	3.71
53	450	650	2.3	78	1.76	4.51
54	450	660	2.3	78	4.24	3.26

Table G.3 Results from the factory mill experiment

Test	S_F direct (mm/s)	S_F indirect (mm/s)	G_u (kN.m)	G_{pt} (kN.m)
1	0.59	0.71	16	191
2	0.72	0.94	21	209
3	0.58	0.64	20	183
4	0.59	0.80	11	182
5	0.67	0.90	17	191
6	0.53	0.71	17	167
7	0.51	0.61	15	194
8	0.56	0.75	18	211
9	0.52	0.67	17	214
10	0.53	0.63	11	203
11	0.55	0.61	13	195
12	0.48	0.56	13	191
13	0.50	0.60	10	184
14	0.47	0.57	14	187
15	0.46	0.54	15	187
16	0.53	0.70	9	188
17	0.48	0.70	13	183
18	0.60	0.82	13	180
19	0.52	0.64	18	181
20	0.49	0.60	16	180
21	0.53	0.63	13	179
22	0.56	0.73	15	172
23	0.61	0.76	11	176
24	0.55	0.73	16	175
25	0.57	0.86	13	175
26	0.62	0.87	9	183
27	0.53	0.74	14	175
28	0.72	1.07	4	175
29	0.63	0.99	13	208
30	0.79	1.29	15	218
31	0.70	1.01	6	176
32	0.73	1.16	16	194
33	0.77	1.04	14	196
34	0.72	1.00	11	183
35	0.68	0.95	16	189
36	0.75	0.86	17	193
37	0.75	1.19	16	192
38	0.88	1.33	14	200
39	0.75	1.03	5	174
40	0.81	1.23	16	213
41	0.67	1.05	16	213
42	0.76	1.02	9	196
43	0.62	0.65	20	197
44	0.57	0.70	13	181
45	0.65	0.93	15	195
46	0.56	1.01	5	214
47	0.51	0.83	10	190

Test	S_F direct (mm/s)	S_F indirect (mm/s)	G_u (kN.m)	G_{pt} (kN.m)
48	0.47	0.72	12	180
49	0.67	0.99	12	202
50	0.48	0.66	15	174
51	0.47	0.57	10	194
52	0.61	0.81	15	212
53	0.48	0.69	10	191
54	0.66	0.85	13	194

Appendix H ***Data set used for the development of the new empirical feeding model***

The parameters common to all of the computational model tests are presented in Table H.1. The parameters varied in the model and the Murry's feed speed ratio results are presented in Table H.2.

Table H.1 Fixed parameters in computational model

Underfeed roll diameter	D_u (mm)	1100
Top pressure feeder roll diameter	D_{pt} (mm)	1100
Bottom pressure feeder roll diameter	D_{pb} (mm)	1100
Work opening between underfeed roll and bottom pressure feeder roll	W_{up} (mm)	50
Pressure feeder angle	θ_{PF} (°)	52
Feed chute exit setting	h_{do}	$\frac{D_u}{2}+W_u+\frac{D_{pt}}{2}$
Contact angle bias	θ_{pt} (°)	0
Feed chute angle	θ_h (°)	80
Height of bottom of feed chute above top pressure feeder roll	h_{pt} (mm)	200
Length factor (related to initial height of bagasse in chute)		1.2
Mesh size	(mm)	50
Logarithmic bulk modulus	κ	0.7
Poisson's ratio	v	0.03
Elastic tensile limit	p_t^{el} (kPa)	1
Slope of critical state line	M	3
Tensile strength	p_t (kPa)	0.5
Hardening rule size parameter	λ_1	0.3
Permeability parameter	k_2	6.9
Viscosity of air	μ_{va} (Pa.s)	$2.00\text{x}10^{-5}$
Viscosity of juice	μ_{vj} (Pa.s)	$8.94\text{x}10^{-4}$
Density of fibre	ρ_f (kg/m^3)	1530
Density of juice	ρ_j (kg/m^3)	1080
Coefficient of friction on underfeed roll	μ_u	0.5
Coefficient of friction on top pressure feeder roll	μ_{pt}	0.7
Coefficient of friction on bottom pressure feeder roll	μ_{pb}	0.7
Feed pressure	P_a (kPa)	3
Maximum distance (parameter relating to time step)		0.2
Time factor (parameter relating to time step)		1
Ratio of top pressure feeder roll speed to bottom pressure feeder roll speed	$\omega_{pt}/\ \omega_{pb}$	1
Speed factor (relating to initial speed of feed in chute		2.5

Table H.2 The factors in the numerical experiment and the experimental results

$\frac{W_u}{D_{pb}}$	$\frac{W_p}{D_{pb}}$	k_1 (m^2)	f(%)	γ_{do} (kg/m^3)	S_{pb} (mm/s)	$\frac{S_u}{S_{pb}}$	r_M
0.36	0.14	$1.7x10^{-19}$	15	67	183	0.80	0.997
0.36	0.14	$1.7x10^{-19}$	15	67	283	1.20	0.940
0.36	0.14	$1.7x10^{-19}$	15	93	183	1.20	0.722
0.36	0.14	$1.7x10^{-19}$	15	93	283	0.80	0.706
0.36	0.14	$1.7x10^{-19}$	21	67	183	1.20	1.079
0.36	0.14	$1.7x10^{-19}$	21	67	283	0.80	1.050
0.36	0.14	$1.7x10^{-19}$	21	93	183	0.80	0.826
0.36	0.14	$1.7x10^{-19}$	21	93	283	1.20	0.737
0.36	0.14	$9.5x10^{-18}$	15	67	183	1.20	1.253
0.36	0.14	$9.5x10^{-18}$	15	67	283	0.80	1.200
0.36	0.14	$9.5x10^{-18}$	15	93	183	0.80	0.984
0.36	0.14	$9.5x10^{-18}$	15	93	283	1.20	0.940
0.36	0.14	$9.5x10^{-18}$	21	67	183	0.80	1.390
0.36	0.14	$9.5x10^{-18}$	21	67	283	1.20	1.468
0.36	0.14	$9.5x10^{-18}$	21	93	183	1.20	1.113
0.36	0.14	$9.5x10^{-18}$	21	93	283	0.80	1.093
0.36	0.22	$1.7x10^{-19}$	15	67	183	1.20	1.393
0.36	0.22	$1.7x10^{-19}$	15	67	283	0.80	1.246
0.36	0.22	$1.7x10^{-19}$	15	93	183	0.80	1.019
0.36	0.22	$1.7x10^{-19}$	15	93	283	1.20	0.955
0.36	0.22	$1.7x10^{-19}$	21	67	183	0.80	1.288
0.36	0.22	$1.7x10^{-19}$	21	67	283	1.20	1.336
0.36	0.22	$1.7x10^{-19}$	21	93	183	1.20	1.033
0.36	0.22	$1.7x10^{-19}$	21	93	283	0.80	0.965
0.36	0.22	$9.5x10^{-18}$	15	67	183	0.80	1.464
0.36	0.22	$9.5x10^{-18}$	15	67	283	1.20	1.636
0.36	0.22	$9.5x10^{-18}$	15	93	183	1.20	1.386
0.36	0.22	$9.5x10^{-18}$	15	93	283	0.80	1.319
0.36	0.22	$9.5x10^{-18}$	21	67	183	1.20	1.745
0.36	0.22	$9.5x10^{-18}$	21	67	283	0.80	1.471
0.36	0.22	$9.5x10^{-18}$	21	93	183	0.80	1.389
0.36	0.22	$9.5x10^{-18}$	21	93	283	1.20	1.561
0.54	0.14	$1.7x10^{-19}$	15	67	183	1.20	0.712
0.54	0.14	$1.7x10^{-19}$	15	67	283	0.80	0.707
0.54	0.14	$1.7x10^{-19}$	15	93	183	0.80	0.524
0.54	0.14	$1.7x10^{-19}$	15	93	283	1.20	0.524
0.54	0.14	$1.7x10^{-19}$	21	67	183	0.80	0.790
0.54	0.14	$1.7x10^{-19}$	21	67	283	1.20	0.733
0.54	0.14	$1.7x10^{-19}$	21	93	183	1.20	0.567
0.54	0.14	$1.7x10^{-19}$	21	93	283	0.80	0.555
0.54	0.14	$9.5x10^{-18}$	15	67	183	0.80	0.960
0.54	0.14	$9.5x10^{-18}$	15	67	283	1.20	0.912
0.54	0.14	$9.5x10^{-18}$	15	93	183	1.20	0.661
0.54	0.14	$9.5x10^{-18}$	15	93	283	0.80	0.658

$\frac{W_u}{D_{pb}}$	$\frac{W_p}{D_{pb}}$	k_1 (m^2)	f (%)	γ_{do} (kg/m^3)	S_{pb} (mm/s)	$\frac{S_u}{S_{pb}}$	r_M
0.54	0.14	$9.5\text{x}10^{-18}$	21	67	183	1.20	1.137
0.54	0.14	$9.5\text{x}10^{-18}$	21	67	283	0.80	1.106
0.54	0.14	$9.5\text{x}10^{-18}$	21	93	183	0.80	0.852
0.54	0.14	$9.5\text{x}10^{-18}$	21	93	283	1.20	0.823
0.54	0.22	$1.7\text{x}10^{-19}$	15	67	183	0.80	1.000
0.54	0.22	$1.7\text{x}10^{-19}$	15	67	283	1.20	0.955
0.54	0.22	$1.7\text{x}10^{-19}$	15	93	183	1.20	0.756
0.54	0.22	$1.7\text{x}10^{-19}$	15	93	283	0.80	0.729
0.54	0.22	$1.7\text{x}10^{-19}$	21	67	183	1.20	1.014
0.54	0.22	$1.7\text{x}10^{-19}$	21	67	283	0.80	0.949
0.54	0.22	$1.7\text{x}10^{-19}$	21	93	183	0.80	0.770
0.54	0.22	$1.7\text{x}10^{-19}$	21	93	283	1.20	0.727
0.54	0.22	$9.5\text{x}10^{-18}$	15	67	183	1.20	1.277
0.54	0.22	$9.5\text{x}10^{-18}$	15	67	283	0.80	1.220
0.54	0.22	$9.5\text{x}10^{-18}$	15	93	183	0.80	0.952
0.54	0.22	$9.5\text{x}10^{-18}$	15	93	283	1.20	0.936
0.54	0.22	$9.5\text{x}10^{-18}$	21	67	183	0.80	1.275
0.54	0.22	$9.5\text{x}10^{-18}$	21	67	283	1.20	1.352
0.54	0.22	$9.5\text{x}10^{-18}$	21	93	183	1.20	1.188
0.54	0.22	$9.5\text{x}10^{-18}$	21	93	283	0.80	1.137
0.20	0.18	$1.3\text{x}10^{-18}$	18	80	233	1.00	1.471
0.70	0.18	$1.3\text{x}10^{-18}$	18	80	233	1.00	0.794
0.45	0.07	$1.3\text{x}10^{-18}$	18	80	233	1.00	0.577
0.45	0.29	$1.3\text{x}10^{-18}$	18	80	233	1.00	1.448
0.45	0.18	$4.5\text{x}10^{-21}$	18	80	233	1.00	0.669
0.45	0.18	$3.7\text{x}10^{-16}$	18	80	233	1.00	1.417
0.45	0.18	$1.3\text{x}10^{-18}$	10	80	233	1.00	0.827
0.45	0.18	$1.3\text{x}10^{-18}$	26	80	233	1.00	1.127
0.45	0.18	$1.3\text{x}10^{-18}$	18	43	233	1.00	1.425
0.45	0.18	$1.3\text{x}10^{-18}$	18	117	233	1.00	0.772
0.45	0.18	$1.3\text{x}10^{-18}$	18	80	92	1.00	1.150
0.45	0.18	$1.3\text{x}10^{-18}$	18	80	375	1.00	1.041
0.45	0.18	$1.3\text{x}10^{-18}$	18	80	233	0.43	0.882
0.45	0.18	$1.3\text{x}10^{-18}$	18	80	233	1.57	1.075
0.45	0.18	$1.3\text{x}10^{-18}$	18	80	233	1.00	1.077
0.45	0.18	$1.3\text{x}10^{-18}$	18	80	233	1.00	1.077
0.45	0.18	$1.3\text{x}10^{-18}$	18	80	233	1.00	1.077